Understanding the anti-cancer efficacy of cyclin-dependent kinase inhibitors

Karla Vuina

Supervisor:

Professor Rob de Bruin

UCL

Doctor of Philosophy

I, Karla Vuina, confirm that the work presented in my thesis is my own. Where information has been derived from outer sources, I confirm that this has been indicated in the thesis.

Abstract

Tumour growth is driven by sustained cellular growth and proliferation. The key regulator of cellular proliferation is the activity of cyclin-dependent kinases (CDKs). An increased CDK activity has been widely reported in cancer. Therefore, CDK inhibitors (CDKis) carry great potential as pan-cancer therapies.

Multiple CDKis have been in development, with three CDK4/6is being the most successful and already in clinical use for treating advanced breast cancer. Moreover, a selective CDK7i, samuraciclib, has been fast-tracked for clinical approval in treating CDK4/6i-resistant cancers. CDK4/6 have an important role in promoting the G1-to-S transition, and CDK7 has a central role in activating all mitotic CDKs and regulating RNA polymerase II-mediated transcription. However, the exact mechanisms underlying cancer cell sensitivity to these CDKis are not well understood.

Here I show that samuraciclib, the most clinically advanced CDK7i, as well as the CDK4/6i palbociclib, induce senescent phenotypes without promoting cell death. My work reveals that active growth signalling, via mTOR pathway, increases cell size during a CDKi arrest, which is an important driver of senescence. Even when cells do not permanently arrest during a CDKi arrest, an excessive increase in cell size causes replication-acquired damage and subsequent cell cycle exit. Since enhanced growth signalling is a hallmark of cancer, this could help explain the anti-cancer efficacy of these CDKis.

Moreover, I show that samuraciclib induces a more robust cell cycle exit and a more rapid accumulation of p21 compared to palbociclib. I show that samuraciclib-induced cell cycle arrest and the induction of a senescent state relies on active p53-dependent upregulation of p21. However, samuraciclib sensitivity does not depend on the tumour suppressor Rb, whereas palbociclib sensitivity does. This work therefore gives insight into mechanisms by which these two clinically relevant CDKis achieve their anti-cancer efficacy and reveals differences in their sensitivity and resistance mechanisms.

Impact Statement

Cancer constitutes one of the leading global health issues. According to the World Health Organization, around 10 million people die from cancer each year and this number is estimated to grow in the future. Despite a rising number of available anti-cancer therapies, more often than not, treatment resistance mechanisms lead to cancer relapse at later stages. Therefore, a better understanding of sensitivity and resistance mechanisms can help with patient stratification and expand their clinical use.

Breast cancer is one of the three main cancer type diagnosis. Less than 10 years ago, a first CDK4/6 inhibitor palbociclib was FDA approved for treating advanced breast cancer, and today three CDK4/6 inhibitors are being used as standard of care treatments for metastatic HR+, HER2- breast cancer in combination with endocrine therapy. Although patients initially respond well to these therapies, they frequently acquire resistance, which leads to disease progression. CDK4/6 have an important role in promoting G1-to-S phase transition, but CDK7 acts as the CDK-activating kinase and is required to carry out the activating phosphorylation in the T loop of all mitotic CDKs. In addition, CDK7 also mediates RNA polymerase II transcriptional cycle. A selective CDK7 inhibitor samuraciclib displayed anti-tumour efficacy in pre-clinical models and has entered clinical trials. It was recently fast-tracked for treating CDK4/6 inhibitor-resistant advanced breast cancers. However, the mechanisms of action of both the CDK4/6 and CDK7 inhibitor remain unclear. The aim of my PhD project was to explore what makes cancer cells sensitive to CDK7 and CDK4/6 inhibitors and identify their common and distinct mechanisms of anti-cancer efficacy.

I demonstrated that active mTOR-dependent growth signalling, driving cellular hypertrophy, has an important role in driving a permanent cell cycle exit during CDK inhibitor treatment. Whilst this is mainly via inducing senescence during the arrest, large cells that do re-enter the cell cycle upon inhibitor removal, undergo replication-acquired damage. This work indicates that samuraciclib and palbociclib might be more effective in cancers with hyperactive cellular growth and that inhibiting growth as a concurrent treatment could lead to resistance or relapse.

Moreover, a genome-wide CRISPR knock-out chemogenetic screen revealed distinct roles of other cell cycle regulators commonly mutated in cancer in sensitivity to samuraciclib and palbociclib. I show that samuraciclib induces a more robust and persistent cell cycle arrest than palbociclib and that they have several distinct sensitivity mechanisms. Samuraciclib induces p21 more rapidly and its initial arrest relies on p53-dependent p21 accumulation. However, unlike palbociclib, samuraciclib does not require Rb for its efficacy.

Currently, the use of CDK4/6 and CDK7 inhibitors is restricted to breast cancer and lack of clear biomarkers restricts their use in other cancer types. The work in this thesis establishes multiple sensitivity and resistance mechanisms of these two clinically relevant CDK inhibitors that might guide their clinical use, both for disease positioning and patient stratification.

Acknowledgments

I would firstly like to thank my supervisor, Professor Rob de Bruin for giving me an opportunity to work on such an exciting project and for his continued guidance. Many helpful discussions have really shaped this project. I am grateful for all the expertise and knowledge he shared with me, as well as always providing great advice. I would also like to thank him for constant support, patience while I figured out things in the lab and creating such a positive working environment.

Next, I would like to thank all the other lab members, past and present. Dr. Cosetta Bertoli has always provided very helpful advice on experimental set-ups and results, and I am very grateful for what she has taught me. Many thanks to Gemma for great discussions, advice on protocols and for always being very responsive to my many questions long after she finished her PhD and left the lab. I started my project by finishing her story, which in the end developed into a longer project that we published together last year. I would also like to thank Silvia who has supervised me and taught me most of the techniques when I joined the lab. I would particularly like to thank Leticia and Milk for being such wonderful friends and colleagues, and who have helped me a lot throughout my PhD project. They have given me huge support and made this journey so much more enjoyable. I am really grateful to have gained amazing friends through this journey.

Big thanks to all the current lab members, Milk, Leticia and Sazia, and all the past members, Cosetta, Silvia, Gemma, Biswajit, Koshiro, Joe, Sophie and Elena for all their help and for creating such a nice working environment. It has also been great having joint lab meetings with the High-content Biology lab at the UCL, and thanks to all the members, Denise, Janos, Christin and Niyaz for great discussions and their help, especially Janos with his help on analysing live-cell imaging. I am also thankful to Alex Upperton, whose data I have not shown in this thesis, but has made helpful contributions to my project during his undergraduate project.

Thanks to the MRC LMCB graduate programme for funding my PhD, which allowed me to join this amazing institute and the de Bruin lab. I would also like to thank the whole LMCB, which has been a wonderful institute to do my PhD. Everyone has been

approachable and helpful, creating a very collaborative environment. Thanks to all the core staff for their amazing work with keeping the institute running, and thanks also to Andrew and Ki who taught and helped me with setting up live-cell imaging. I also want to thank my thesis committee, Robin Ketteler, Alison Lloyd and Luigi Aloia, for their helpful discussions and guidance during my committee meetings.

I am thankful to all our collaborators who have contributed to this project. Professor Simak Ali has approached the de Bruin lab with this exciting novel CDK7 inhibitor that ended up being Gemma's project and continued as the main focus of my PhD as well. Postdoc from the Ali lab, Dr. Georgina Sava, generated data that has contributed greatly to my project, which I incorporated into my thesis. Professor Mike Tyers and his lab members, particularly Dr. Thierry Bertomeu, Dr. Caroline Huard and Dr. Jasmin Coulombe-Huntington, carried out the genome-wide CRISPR knock-out chemogenetic screens and provided us with the initial analysis. These screens have been essential for this project, so I am very grateful for their help and contribution.

I would also like to thank all my friends outside the LMCB and a special thanks to my family, my parents and my brothers, for their huge support and encouragement in every step of this journey as well as before my PhD that has led to this moment and has been a constant source of motivation.

Table of Contents

List of Figures

List of Tables

List of Abbreviations

APC/C	Anaphase-promoting complex/cyclosome
ATM	Ataxia telangiectasia mutated
ATR	Ataxia telangiectasia and Rad3 related
C_{12}FDG	5-dodecanoylaminofluorescein di-β-D-galactopyranoside
CAK	CDK-activating kinase
CDK	Cyclin-dependent kinase
CDKi	Cyclin-dependent kinase inhibitor
CPT	Camptothecin
CRISPR	Clustered Regularly Interspaced Short Palindromic Repeats
CHK1	Checkpoint kinase 1
CHK2	Checkpoint kinase 2
CIdU	5-Chloro-2'-deoxyuridine
CTD	C-terminal domain
DDR	DNA damage response
DMSO	Dimethyl sulfoxide
EdU	5-Ethynyl-2'-deoxyuridine
EKO	Extended-knockout
ET	Endocrine therapy
FBS	Fetal bovine serum
FDR	False discovery rate
FUCCI	Fluorescent Ubiquitination-based Cell Cycle Indicator
GAPDH	Glyceraldehyde-3-phosphate dehydrogenase
GO	Gene Ontology
HER2	Human epidermal growth factor 2
HR	Hormone receptor
IC_{50}	Half-maximal inhibitory concentration
IdU	5-Iodo-2'-deoxyuridine
KO	Knock-out
MAPK	Mitogen-activated protein kinase
MDM2	Mouse Double Minute

mTOR	Mammalian target of rapamycin
mTORC	Mammalian target of rapamycin complex
PI3K	Phosphatidylinositol 3-kinase
P-TEFb	Positive transcription elongation factor b
RANKS	Robust Analytics and Normalization for Knock-out Screens
Rb	Retinoblastoma protein
RNAPII	RNA polymerase II
ROS	Reactive oxygen species
RPA	Replication Protein A
RPE1	Retinal Pigment Epithelial 1
RT-qPCR	Reverse Transcriptase quantitative Polymerase Chain Reaction
SA β-gal	Senescence-associated β-galactosidase
SAC	Spindle assembly checkpoint
SAHF	Senescence-associated heterochromatin foci
SASP	Senescence-associated secretory phenotype
SD	Standard deviation
sgRNA	Single-guide RNA
ssDNA	Single-stranded DNA
TF	Transcription factor
TIS	Therapy-induced senescence
TNBC	Triple negative breast cancer
WT	Wild-type

1. Introduction

1.1. Cell cycle progression and regulation

The mitotic cell cycle is required to faithfully duplicate the cell's genetic material and then segregate it equally to produce two genetically identical daughter cells. It is composed of four consecutive phases: G1 (gap 1), S (synthesis), G2 (gap 2) and M (mitosis) phase. G1, S and G2 are collectively referred to as interphase during which genomic DNA is replicated in S phase. Chromosomal segregation and cell division occur during M phase. The two gap phases, G1 and G2, separate these two key cell cycle events and are important growth phases during which the decision is made to enter the cell cycle by initiating S phase and to enter mitosis, respectively (Matthews, Bertoli and de Bruin, 2022).

One of the main drivers of cell cycle progression is the activity of cyclin-dependent kinases (CDKs), which is dependent on their corresponding partner cyclins. The role of a CDK in cell cycle regulation was first identified in yeast and cyclin proteins were first discovered in the eggs of sea urchin *Arbacia punctulate* (Hartwell, Culotti and Reid, 1970; Hartwell *et al.*, 1973, 1974; Nurse, Thuriaux and Nasmyth, 1976; Nurse and Thuriaux, 1980; Nurse and Bissett, 1981; Beach, Durkacz and Nurse, 1982; Evans *et al.*, 1983). Whilst in yeast, only one CDK regulates cell cycle progression, Cdc2 in *Schizosaccharomyces pombe* and Cdc28 in *Saccharomyces cerevisiae*, the mammalian cell cycle depends on the activity of multiple CDKs, responsible for the regulation of different cell cycle phases. Protein levels of mitotic CDKs are constant during the cell cycle; however, their activities are regulated by binding of their partner cyclins, which accumulate at different stages of the cell cycle. This accumulation of cyclins at specific stages is guided by waves of cell cycle-regulated transcription as well as inhibition or initiation of protein degradation, ensuring correct and timely activation of mitotic CDKs that can then phosphorylate numerous proteins required to drive the cell through the cell cycle (Figure 1.1) (Malumbres and Barbacid, 2009).

Here I will discuss the role of CDKs in controlling the mammalian cell cycle. In the G1 phase of the cell cycle, the cell has an option to either enter a new cell cycle or exit it

into a temporary arrest state termed quiescence or G0. Once exited, the cell can, however, re-enter the cell cycle upon appropriate stimuli, such as growth factors. The choice to enter the cell cycle is driven by active cyclin D-CDK4/6 complex. Its activity is driven by growth factors which increase the expression of D-type cyclins (D1, D2 and D3). D-type cyclins then bind to CDK4 and CDK6 (Pennycook and Barr, 2020). Active cyclin D-CDK4/6 complex therefore prevents cell cycle exit and promotes a proliferative G1 state by priming the cell for a G1-to-S transition, which is driven by E2F-dependent transcription. E2F inhibitor and a tumour suppressor, Retinoblastoma protein (Rb) plays a key role in the cell cycle entry decision (Bertoli, Skotheim and de Bruin, 2013; Matthews, Bertoli and de Bruin, 2022). During a quiescent state (G0), Rb is unphosphorylated and keeps E2F transcription factor inactive. According to a new model, an increase in activity of cyclin D-CDK4/6 complex leads to a mono-phosphorylation of Rb at one of the 14 CDK phosphorylation sites (Bertoli and de Bruin, 2014; Narasimha *et al.*, 2014). In the classical model, hypo-phosphorylated Rb by cyclin D-CDK4/6 complex was believed to partially release and inactivate E2F to allow transcription initiation and expression of cyclin E, which in turn activates CDK2 leading to further phosphorylation of Rb and full E2F activation (Mittnacht *et al.*, 1994; Lundberg and Weinberg, 1998; Henley and Dick, 2012; Bertoli and de Bruin, 2014). However, this model was recently challenged, where no hypo-phosphorylated version of Rb was found and the mono-phosphorylated Rb was still able to bind and fully inactivate E2F (Narasimha *et al.*, 2014). This suggested that cyclin D-CDK4/6 does not partially inactivate Rb and initiate E2F-dependent transcription but primes the cell for entering a new cell cycle. In this state, accumulation of E-type cyclins, by an undefined event, results in the formation of cyclin E-CDK2 complex, which then hyper-phosphorylates Rb and therefore inactivates it (Pennycook and Barr, 2020). This activates E2F-dependent transcription and leads to expression of E2F target genes, such as cyclin E and A. This results in the accumulation of these cyclins and initiates a positive feedback loop where cyclin E-CDK2 complex further activates E2F-dependent transcription by inactivating Rb. This allows for an increase in cyclin A-CDK2 activity, which is crucial for commitment to the new cell cycle, S phase entry and DNA replication (Matthews, Bertoli and de Bruin, 2022). An increase in cyclin A-CDK2 activity is not only dependent on the hyperaccumulation of cyclin A but also on the inactivation of anaphase-promoting complex/cyclosome (APC/C^{Cdh1}), which is a G1-specific E3 ubiquitin ligase that degrades cyclin A. This inactivation of APC/C^{Cdh1}

is another crucial step for the irreversible commitment to a new cell cycle and is carried out by its inhibitor EMI1 (early mitotic inhibitor 1), which is also a product of E2F transcriptional program (Barr *et al.*, 2016; Cappell *et al.*, 2016, 2018).

Once DNA replication is completed, CDK1 activity is required to enter M phase. The binding cyclin partners of CDK1 are cyclin A and B, which make the complex active. Cyclin A-CDK1 complex is required for G2 progression whereas cyclin B-CDK1 complex is required for mitotic entry. However, during interphase, CDK1 is inactivated through phosphorylation by WEE1 and MYT1 kinases at tyrosine residue 15 and threonine residue 14 respectively. This allows for cyclin-CDK1 complexes to accumulate without increasing their activity. Once their levels rise above the threshold of WEE1 and MYT1-directed CDK1 inhibitory phosphorylation, the active cyclin-CDK1 complexes initiate positive feedback loops. CDK1 is able to phosphorylate and in turn inactivate WEE1 and MYT1 kinases. However, the activation of the inactive pool of cyclin-CDK1 complexes requires a dephosphorylation of the inhibitory phosphorylation sites, which is carried out by the CDC25 phosphatases. Activation of CDC25 phosphatases is also CDK-dependent, and so these positive feedback loops result in a robust activation of CDK1 activity (O'Farrell, 2001; Potapova *et al.*, 2009; Crncec and Hochegger, 2019; Matthews, Bertoli and de Bruin, 2022). When CDK1 is active, it phosphorylates numerous proteins which triggers the mitotic entry and structural re-organisation essential for DNA segregation (Blethrow *et al.*, 2008; Dephoure *et al.*, 2008; Crncec and Hochegger, 2019). Cyclin A degradation is triggered by the APC/C during prometaphase whereas cyclin B during metaphase which ultimately leads to CDK1 inactivation. However, proteolytic degradation of cyclin B is delayed by the spindle assembly checkpoint (SAC) which ensures all kinetochores are correctly attached and chromosomes are aligned at the metaphase plate to avoid any incorrect segregation of chromosomes (Crncec and Hochegger, 2019). Once CDK1 activity is lost, APC/C triggers a series of events, including the separation of sister chromatids, that leads to mitotic exit and cellular division. APC/C-mediated destruction of cyclins reduces all CDK activity, and the two daughter cells enter a new interphase, more precisely a new G1 phase (Crncec and Hochegger, 2019; Matthews, Bertoli and de Bruin, 2022).

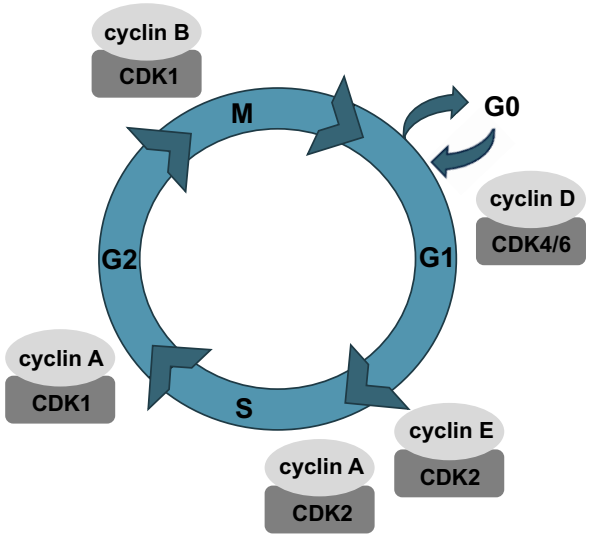

Figure 1.1: CDK activity is the key driver of cell cycle progression.
The mammalian cell cycle is composed of four consecutive phases: G1, S, G2 and M phase. The progression through the cell cycle is driven by the activity of CDKs, which is dependent on the accumulation of their partner cyclins. CDK4/6 in complex with D-type cyclins is important for the cell cycle entry decision and preventing cell cycle exit into G0 inactive state. CDK2 in complex with cyclin E is required for the G1-to-S phase transition and CDK2 in complex with cyclin A drives S phase initiation and progression. CDK1 in complex with cyclin A and subsequently with cyclin B are important for M phase entry and progression. APC/C-directed destruction of cyclins, results in loss of CDK activity upon return to interphase.

1.2. Cell cycle checkpoints

To warrant a correct and complete genome duplication and segregation to form two identical daughter cells, the mammalian cell cycle is tightly controlled by multiple regulatory pathways. Cell cycle checkpoints act as surveillance mechanisms which are required to ensure each phase of the cell cycle is complete before the next one is initiated, in order to prevent any genetic errors being inherited by the two daughter cells. The three main checkpoints respond to DNA damage, DNA replication stress or spindle assembly errors by either arresting or stalling cell cycle progression at different stages via inhibiting the activity of CDKs or the APC/C (Figure 1.2) (Matthews, Bertoli and de Bruin, 2022).

The DNA damage checkpoint is active during interphase, and it monitors for presence of DNA lesions, such as double-strand breaks, which can occur due to a variety of

endogenous and exogenous factors. Some of the endogenous cellular sources include the replication machinery stalling and collapsing during DNA replication or reactive oxygen species (ROS) from cellular metabolism. Exogenous sources comprise different environmental pollutants, chemical agents, irradiation and more (Timmins, 2023). The DNA damage checkpoint is therefore necessary to arrest the progression of the cell cycle and allow for the activation of DNA repair pathways, such as homologous recombination or non-homologous end joining, to resolve these errors ensuring no DNA mutations are passed on to the daughter cells (Huang and Zhou, 2021).

The presence of DNA breaks can lead to different cell cycle outcomes, which depend on both the DNA damage levels and the cell cycle stage. During G1 phase, upon the detection of DNA damage, the cell can exit the cell cycle and enter the temporary arrest, quiescent state (G0 phase). Once the DNA damage is resolved, the cell can re-enter the G1 phase and commit to a new cell cycle. However, higher levels of DNA damage can lead to a permanent exit from the cell cycle known as senescence. Senescence can also occur during the G2 phase of the cell cycle in order to prevent mitosis of damaged cells. Moreover, if the DNA damage levels are too high, the cell can undergo programmed cell death or apoptosis. Apoptosis can occur during any phase of the cell cycle due to a prolonged cell cycle arrest and unresolved DNA damage (Matthews, Bertoli and de Bruin, 2022).

The DNA damage checkpoint is activated by DNA double-strand breaks, which activate the kinase ataxia telangiectasia mutated (ATM). One of its key targets are a downstream kinase Chk2 and transcription factor p53 (Shiloh and Ziv, 2013). This cascade of events results in the stabilisation of p53, which in turn increases transcription of p21 and activates it (Chehab *et al.*, 2000; Hirao *et al.*, 2000). p21 is a CDK2 and CDK4/6 inhibitor. It therefore mainly arrests cells in the G1 phase of the cell cycle. During S and G2 phases, Chk2 inhibits CDC25 phosphatase by marking it for proteasomal degradation. This reinforces inhibitory action of WEE1 kinase towards CDK1 and as a result prevents mitotic entry (Figure 1.2) (Reinhardt and Yaffe, 2009; Matthews, Bertoli and de Bruin, 2022).

Furthermore, the DNA replication stress checkpoint is active during S phase in response to exposure of single-stranded DNA (ssDNA). This occurs as a result of

replication stress, which is slowing down or stalling of replication forks, leaving ssDNA exposed and susceptible to DNA damage (Zeman and Cimprich, 2014). This checkpoint activates the kinase ataxia telangiectasia and Rad3-related protein (ATR) and downstream kinase Chk1, which phosphorylates and activates WEE1. This results in inhibitory phosphorylation of CDK1 and prevents mitotic entry. Similarly to Chk2, Chk1 can phosphorylate CDC25 and target it for proteasomal degradation, which reinforces WEE1 inhibitory effect on CDK1 (Figure 1.2) (Zhang and Hunter, 2014). Therefore, the DNA replication stress checkpoint strengthens the DNA damage checkpoint during S phase. However, it's important to note that replication stress checkpoint does not respond to DNA damage but to ssDNA in order to prevent replication stress-induced DNA damage.

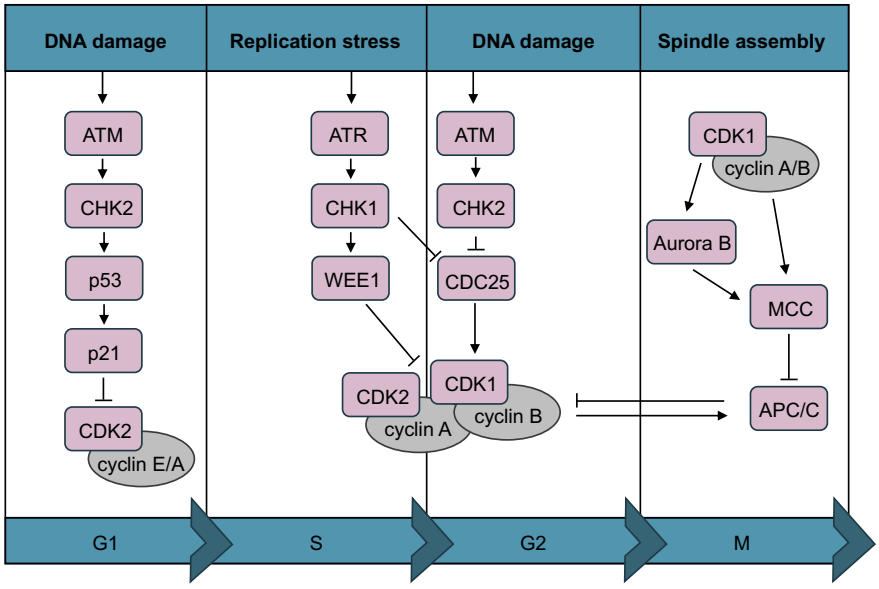

Figure 1.2: Cell cycle checkpoints ensure cell cycle phases are correctly completed.
Three main cell cycle checkpoints act as surveillance mechanisms for DNA damage during interphase, DNA replication stress during S phase and spindle assembly errors during M phase. These regulatory mechanisms arrest or slow down the cell cycle progression by inhibition of CDK or APC/C activity to ensure each phase of the cell cycle is correctly completed before the next one begins. Figure adapted from (Matthews, Bertoli and de Bruin, 2022).

Lastly, the third cell cycle checkpoint, known as the spindle assembly checkpoint (SAC), is active during M phase warranting correct segregation of chromosomes. The SAC is triggered in response to errors in spindle assembly and incorrect chromosomal attachment to the spindles. This response depends on the formation of mitotic checkpoint complex (MCC) at incompletely assembled spindles at kinetochores, which inhibits APC/C activity and therefore blocking mitotic exit (Figure 1.2) (Alfieri *et al.*, 2016). Once all sister chromatid pairs are attached to the bipolar mitotic spindle, the APC/C becomes active and triggers a series of events that lead to nuclear and cellular division (Musacchio and Salmon, 2007).

Cell cycle checkpoints are crucial for maintaining genomic integrity. However, one of the hallmarks of cancer is sustained proliferation and so cancer cells obtain mutations to avoid cell cycle exit and promote cell cycle entry. As a result, cancer-associated mutations are often found in proteins involved in the DNA damage checkpoint as well as those involved in the restriction or commitment point driving S phase entry. On the other hand, DNA replication stress checkpoint and SAC are rarely mutated as they are essential for preventing catastrophic genome instability and therefore cancer cell survival and further proliferation (Hanahan and Weinberg, 2011; Matthews, Bertoli and de Bruin, 2022).

1.3. Senescence, a permanent cell cycle arrest state

Senescence is a process by which cells lose their proliferative ability, exiting the cell cycle irreversibly, without undergoing cell death. It acts as a tumour suppressor mechanism by preventing propagation of damaged cells. The senescence phenomenon was originally described by Hayflick and Moorhead where a limited number of divisions was observed in human fibroblasts grown in culture, but they remained metabolically active (Hayflick and Moorhead, 1961). This was later termed replicative senescence and is known to be caused by shortening of the telomeres. Telomeres are ends of chromosomes composed of highly repetitive DNA sequences (Campisi, 1997). These structures shorten with each cell cycle, in turn increasing amount of DNA lesions, and so when they become too short, this activates the DNA damage response, which causes an irreversible arrest (Manohar and Neurohr, 2023).

It was later shown that cellular senescence can be triggered prematurely due to a variety of stress stimuli, such as oncogene activation, tumour suppressor loss, replication stress, DNA damage, mitochondrial dysfunction, hypoxia, oxidative stress, and other stressors (Roger, Tomas and Gire, 2021). A form of premature senescence is oncogene-induced senescence (OIS). This can be induced by hyperproliferation caused by either an oncogene hyperactivation, such as RAS (Serrano *et al.*, 1997; Sarkisian *et al.*, 2007), or loss of tumour suppressors, such as PTEN (Chen *et al.*, 2005). The OIS is thought to be induced by hyper-replication and DNA fork progression alterations, which leads to replication stress-induced DNA damage, activating the DNA damage response (DDR) (Di Micco *et al.*, 2006; Liu, Ding and Meng, 2018; Manohar and Neurohr, 2023).

Senescence has also been observed as a response to some chemotherapy and radiotherapy. This subtype of senescence is referred to as therapy-induced senescence (TIS). Most anti-cancer agents have been traditionally designed with the aim to induce cytotoxicity, by producing high levels of DNA damage and causing apoptosis of cancer cells. However, these high doses of treatments can have severe side effects, affecting healthy cells as well, and could in some cases lead to acquired treatment resistance or relapse. Cytostatic cancer treatments, and therefore TIS, have also been of increasing interest. Some of the traditional chemotherapeutic genotoxic agents, such as doxorubicin, etoposide and cisplatin, were found to induce senescence in some tumours along with their cytotoxic effects (Ewald *et al.*, 2010; Faheem *et al.*, 2020; Wang, Lankhorst and Bernards, 2022). Moreover, it was shown in cultured cells that varying doses of these agents can lead to different cell cycle exit outcomes. For instance, lower doses of doxorubicin, a topoisomerase II inhibitor and a genotoxic agent, were found to induce TIS in prostate cancer cells, yet higher doses led to apoptosis (Ewald *et al.*, 2009). This could be explained by different levels of DNA damage induced by different doses of these genotoxic agents. Furthermore, TIS has been observed in treatments that do not induce DNA damage, such as CDK4/6 inhibitors (Rader *et al.*, 2013; Yoshida, Lee and Diehl, 2016) or DNA replication kinase CDC7 inhibitor (Wang *et al.*, 2019). Therefore, as senescent cells permanently lose their proliferative ability and cannot be stimulated to proliferate, this would be a favourable outcome of cytostatic cancer therapy as upon drug removal, these cells would be unable to re-enter the cell cycle. However, senescent cells, although unable

to proliferate, are still viable and metabolically active. Therefore, to understand their potential effect on the surrounding cells as well as to be able to study and identify them, it is important to understand senescent cell phenotypes (Figure 1.3).

1.4. Features and identification of senescent cells

Senescent cells have several features by which they can be characterised and studied. The main feature is the irreversible cell cycle arrest and loss of proliferative potential. It is mediated by tumour suppressor proteins p53, p16 and Rb. These are often found mutated in a wide range of cancer types. p53, which is activated through the DDR, induces transcription of a CDK inhibitor p21 that inhibits CDK2 and CDK4/6, leading to an activated Rb by preventing its hyper-phosphorylation. This represses E2F-dependent transcription and causes a G1 phase arrest. Further stress stimuli can activate another CDK inhibitor, p16, which specifically inhibits CDK4 and CDK6 and leads to unphosphorylated Rb, which drives cells out of the cell cycle (Herranz and Gil, 2018). It has been suggested that p53 and p21 are important for senescence induction, whereas p16 is required for maintaining the senescent state (Kumari and Jat, 2021).

Senescent cells, which are permanently arrested, are resistant to apoptosis. They often have an enhanced activation of the pro-survival pathways, referred to as senescent cell anti-apoptotic pathways (SCAPs). Different anti-apoptotic members of the Bcl-2 family are commonly upregulated. These mechanisms protect the senescent cells from inducing cell death (Wang, 1995; Herranz and Gil, 2018; Gasek *et al.*, 2021).

Apart from the stable proliferation arrest and resistance to apoptosis, senescent cells display morphological changes. They are flattened if adherent and have a larger cell size and volume compared to healthy cycling cells (Huang *et al.*, 2022). They also expand their nuclear size (Mitsui and Schneider, 1976). Moreover, senescent cells have also been found to downregulate Lamin B1, an intermediate filament protein encoded by the *LMNB1* gene (Freund *et al.*, 2012; Wang *et al.*, 2017). It is a constituent of the nuclear lamina, which contributes to the nuclear integrity and its shape. Its mRNA and protein loss has been linked to reduced nuclear stability and an increase in cytoplasmic chromatin fragments (CCFs), which can trigger immune responses (Gorgoulis *et al.*, 2019).

Another senescence marker, which is most commonly used for *in vitro* and *in vivo* identification of senescent cells, is senescence-associated β-galactosidase (SA β-gal). β-galactosidase is an acidic lysosomal protein; however, since senescent cells have an increased lysosomal content, SA β-gal can be experimentally detected at pH 6, rather than pH 4, due to its high expression (Dimri *et al.*, 1995; Kurz *et al.*, 2000; Campisi, 2013). Whilst this is commonly used as a marker of senescence, increased SA β-gal activity can be detected in some circumstances which are non-senescence related, such as high confluency or serum starvation (Yang and Hu, 2005). Therefore, it is important to avoid these conditions when identifying senescent cells in cultured cells.

Senescent cells also display chromatin reorganisation, specifically senescence-associated heterochromatin foci (SAHF). It describes condensed heterochromatin regions which are believed to contribute to permanent silencing of proliferation genes, such as E2F target genes which is directed by Rb (Narita *et al.*, 2003; Aird and Zhang, 2013). Moreover, continuous DNA damage causes nuclear DNA damage foci associated with DDR proteins referred to as DNA segments with chromatin alterations reinforcing senescence (DNA-SCARS). They differ to transiently formed DNA damage foci and are persistently present and were found to be important for a permanent proliferative arrest (Rodier *et al.*, 2011; Campisi, 2013).

Although senescent cells are permanently arrested, they are viable and metabolically active. They secrete a number of signalling molecules referred to as the senescence-associated secretory phenotype (SASP). These include cytokines (such as IL-6), chemokines (IL-8), growth factors (VEGF), proteases (MMP3) and other soluble and insoluble molecules (IFN-γ). The composition of this phenotype is very heterogeneous, and it depends on both cell type and senescence inducer. The SASP is thought to only occur in cells that become senescent due to accumulated genomic damage. Therefore, potential roles of the SASP may be to activate the immune system to eliminate these damaged cells or act as a signal for tissue repair by promoting proliferation in neighbouring cells. Whilst having beneficial roles, the SASP can also have pro-tumorigenic effects. These secreted molecules can alter the tumour microenvironment. For instance, increased secretion of proteases can degrade the extracellular matrix allowing tumour cells to metastasise (Coppé *et al.*, 2010; Kumari and Jat, 2021). It is therefore essential to explore the effects of the SASP when

investigating anti-cancer therapies inducing senescence. An approach to avoid harmful effects of the SASP is by clearing senescent cells with compounds termed senolytics, which are currently in development, and some have reached clinical trials, such as dasatinib and quercetin combination or navitoclax, a Bcl-2 family inhibitor. Senolytic drugs are an attractive candidate for cancer therapy by being used in a "one-two punch" approach to selectively eliminate senescent cancer cells that formed in response to a TIS agent (Prasanna *et al.*, 2021).

The aforementioned features are markers that can be used to study senescence (Figure 1.3). However, not all senescent cells will have all the listed features. Both SASP and SAHF, for instance, are dependent on the cell or tissue type, senescence stimulus as well as the duration of the senescent state. There is currently no single marker of senescence (Kumari and Jat, 2021). Therefore, when identifying senescence and studying the ability of anti-cancer therapies to induce a permanent cell cycle arrest, it is important to investigate several senescence characteristics. A more detailed guideline of experimentally assessing senescence was recently published (Kohli *et al.*, 2021).

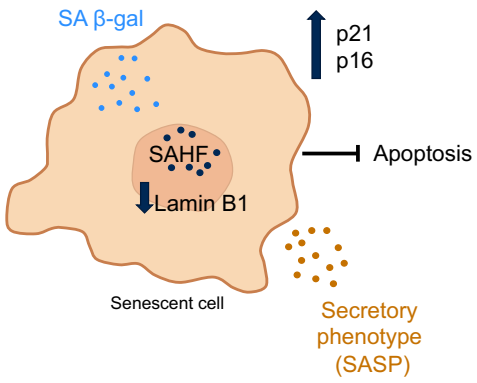

Figure 1.3: Features of a senescent cell.
Senescent cells are in a permanent arrest state but remain viable and resistant to apoptosis. The cell cycle arrest is most commonly regulated by CDK inhibitors, p21 and p16. These cells are metabolically active and secrete a number of signalling molecules, which are collectively termed the senescence-associated secretory phenotype (SASP). Among other features are an increase in cell size, downregulation of Lamin B1, increased activity of senescence-associated β-galactosidase (SA β-gal) and presence of senescence-associated heterochromatin foci (SAHF). The features of senescent cells vary and are dependent on the senescence stimulus, cell type and duration of the senescent state. Figure adapted from (Zhang *et al.*, 2022).

1.5. Increase in cell size: a driver or a consequence of senescence?

One of the key features of senescent cells is the substantial increase in cell size. Under healthy conditions, a specific cell type maintains its cell size in a very narrow range, demonstrating the importance of the regulation of an accurate cell size to preserve its function (Ginzberg, Kafri and Kirschner, 2015). In a proliferating cell, the correct cell size depends on two processes which are coupled, cellular growth (biomass accumulation) and proliferation (cell division) (Lloyd, 2013).

In a permanent form of a cell cycle arrest, senescence, it was observed that these two processes are decoupled as these cells become excessively enlarged. This increase in cell size has been mainly perceived as an outcome of a continued growth during the prolonged cell cycle arrest, therefore being a consequence of a senescent state (Hernandez-Segura, Nehme and Demaria, 2018). More than 15 years ago, a more direct link was made between the need for growth stimulation and senescence induction (Demidenko and Blagosklonny, 2008; Blagosklonny, 2012). A major regulator of cellular growth is the mTOR signalling pathway. It was shown that blocking cellular growth by serum starvation, or treatment with the mTOR inhibitor rapamycin, during a cell cycle arrest caused by different senescence-inducing stimuli, p21 or p53, prevented the expression of senescence markers and allowed cells to preserve their proliferative potential (Demidenko and Blagosklonny, 2008; Demidenko *et al.*, 2009). This reversible cell cycle arrest upon mTOR inhibition was also observed with lower concentrations of genotoxic agents, doxorubicin and etoposide (Leontieva and Blagosklonny, 2010). The process where the initial cell cycle arrest is converted into the irreversible arrested state of senescence, due to the active growth signalling, is termed geroconversion, which can be delayed or hindered by growth inhibition (Figure 1.4) (Blagosklonny, 2012, 2014).

What could be at the basis of geroconversion remains unknown, but recent work suggests it could be linked to limitation in gene expression scaling with size. In a healthy proliferating cell, its total RNA and protein amounts increase and scale with volume as the cell grows, which keeps their concentration constant (Xie, Swaffer and Skotheim, 2022). It was later shown in budding yeast that during a cell cycle arrest, when cell volume continues to increase, DNA becomes limiting. When cells increase their size beyond a certain point, RNA and protein biosynthesis begin to fail to scale with cellular volume, leading to a reduced cytoplasmic density and in turn cytoplasmic

dilution, which contributes to a reduced cell fitness and a stable cell cycle arrest (Neurohr *et al.*, 2019). Similarly, their work in human fibroblasts suggested that an increase in cell size and a reduction in macromolecular crowding contribute to senescence (Neurohr *et al.*, 2019). Other evidence that the limiting DNA abundance in relation to cell size (low DNA-to-cytoplasm ratio) can drive cells into a senescent state was demonstrated by rescuing senescent phenotypes with increasing cellular ploidy (Neurohr *et al.*, 2019; Lanz *et al.*, 2022).

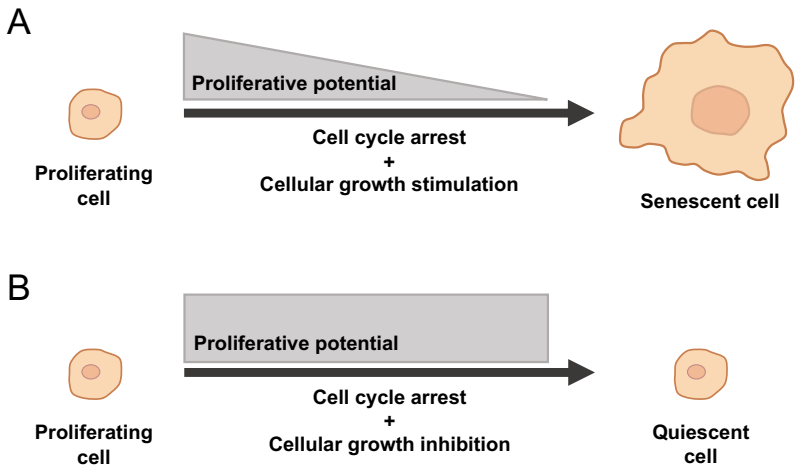

Figure 1.4: Cellular growth stimulation is necessary during cell cycle arrest for induction of a senescent state.
A) A cell is driven out of the cell cycle upon different cell cycle inhibitors. Cellular growth stimulation during this arrest causes an increase in biomass and cell size. This uncoupling of proliferation and cellular growth ultimately leads to a reduced proliferative potential and a senescent state. **B)** If cellular growth is inhibited during the cell cycle arrest, the cell maintains its biomass and its proliferative potential and is able to restart proliferation after cell cycle inhibitor removal. This is a temporary arrest state, quiescence. Figure adapted from (Manohar and Neurohr, 2023).

Multiple studies have further validated the important role of cellular growth and hypertrophy in the induction of a permanent cell cycle exit (Lanz *et al.*, 2022; Crozier *et al.*, 2023; Foy *et al.*, 2023; Manohar *et al.*, 2023; Wilson *et al.*, 2023). One study demonstrated that an increased cell size *per se* might directly affect the fitness of the cell and lead to senescence induction (Lanz *et al.*, 2022). They sorted cycling cells into different size bins and observed that the larger cells have proteome changes that are similar to those of a senescent cell. For instance, they detected an increase in lysosomal proteins, SA β-gal and SASP proteins as well as a decrease in Lamin B1

and Ki67 (a marker of actively dividing cells). These cells were found to become senescent at an earlier passage than smaller cycling cells. Furthermore, these proteome changes were observed in single cells as well (Lanz *et al.*, 2023). Lastly, recently there was evidence of the role of increased cell size in hematopoietic stem cell (HSC) fitness reduction *in vivo* (Lengefeld *et al.*, 2021). They found that enlargement of HSCs leads to a decreased stem cell potential and contributes to their functional decline. Moreover, they observed that reducing the cell size of large non-functional HSCs restored their fitness. This altogether suggests that continued cellular growth itself during a cell cycle arrest can promote senescence induction.

1.6. mTOR: a key regulator of cellular growth

One of the key, and most well-studied, regulators of cellular growth is the mechanistic target of rapamycin (mTOR) signalling pathway. mTOR is a serine/threonine kinase, which interacts with several proteins forming mTOR complex 1 (mTORC1) and mTOR complex 2 (mTORC2) (Saxton and Sabatini, 2017). Although these two large complexes have the same catalytic subunit, they vary in the proteins that are assembled in these complexes as well as their substrates and signalling roles (Liu and Sabatini, 2020). mTORC1 activation responds to growth factors, energy, oxygen, amino acids and stress (Figure 1.5). It controls cellular growth by upregulating anabolic processes, such as macromolecular biosynthesis (proteins, lipids and nucleotides), and downregulating catabolic processes, such as autophagy. mTORC2, on the other hand, responds mainly to insulin and is associated with cytoskeletal regulation and cell survival (Laplante and Sabatini, 2012; Kim and Guan, 2019).

One of the cancer hallmarks is an increase in cellular growth to fuel continued proliferation. As mTOR signalling pathway is crucial in promoting cellular growth, different pathway nodes are commonly mutated in cancer, rendering it hyperactive, which promotes cancer cell proliferation and survival. Growth-promoting mutations often occur in the signalling pathway components upstream of mTOR. For instance, PI3K and Akt commonly harbour activating mutations whereas inactivating mutations occur in negative regulators of the mTOR pathway, such as PTEN, TSC1 and TSC2 (Figure 1.5) (Saxton and Sabatini, 2017). To exploit this dependence of cancer, different PI3K, Akt and mTOR inhibitors have been in development as anti-cancer

therapy, with several already in clinical use (Paplomata and O'Regan, 2014; Kim and Guan, 2019).

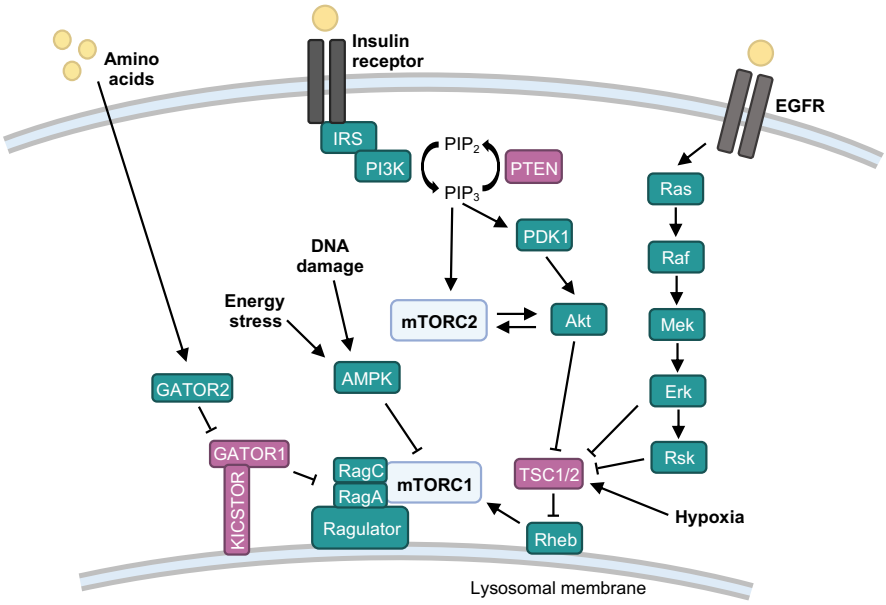

Figure 1.5: mTOR signalling pathway.
Simplified signalling pathways upstream of mTORC1 and mTORC2. Positive regulators of mTORC1 are highlighted in green and negative regulators in magenta. Figure adapted from (Saxton and Sabatini, 2017).

1.7. Cyclin-dependent kinases as cytostatic drug targets

An accumulation of CDK inhibitors, p21 and p16, as previously mentioned, is implicated in cell cycle arrest, and can drive the cells into a senescent state (Herranz and Gil, 2018). With CDKs being the key regulators of the cell cycle progression, their activity is often increased in cancer, with D-type cyclin-CDK4/6 and E-type cyclin-CDK2, promoting a proliferative state and cell cycle entry respectively, being the most prominent (Deshpande, Sicinski and Hinds, 2005; Choi and Anders, 2014; Matthews, Bertoli and de Bruin, 2022). Therefore, there has been great interest in pharmacologically inhibiting cell cycle CDKs to induce cell cycle arrest as anti-cancer therapy. Pharmacological CDK inhibitors have been in development for around 30 years (Zhang *et al.*, 2021). The first generation were non-specific pan-CDK inhibitors. One such example is Roscovitine (CYC202 or seliciclib) that inhibits CDK1, CDK2, CDK5, CDK7 and CDK9. It has not been approved for clinical use as a monotherapy;

however, it might lead to better results in a combinatorial treatment (Cicenas *et al.*, 2015). There have been many other pan-CDK inhibitors developed and some are currently in clinical trials. However, their poor CDK selectivity and toxicity creates difficulty in their accurate use for cancer treatment (Zhang *et al.*, 2021).

To improve the efficacy of CDK inhibitors as potential anti-cancer treatments, more specific CDK inhibitors have been developed. The most successful of these are three CDK4/6 inhibitors: palbociclib (Ibrance, PD-0332991; Pfizer), ribociclib (Kisqali, LEE011; Novartis) and abemaciclib (Verzenois, LY2835219; Eli Lilly). They have been approved by the US Food and Drug Administration (FDA) for the treatment of metastatic hormone receptor-positive (HR+), human epidermal growth factor receptor 2-negative (HER2-) breast cancer in combination with endocrine therapy (ET) (Beaver *et al.*, 2015; US Food and Drug Administration, 2017; Shah *et al.*, 2018; Morrison, Loibl and Turner, 2024). These inhibitors are generally well-tolerated, and they require an intact D-type cyclin-CDK4/6-Rb signalling axis in order to successfully inhibit cellular proliferation. Palbociclib is the most commonly used CDK4/6 inhibitor in pre-clinical studies demonstrating cytostatic effects by mainly inducing senescence (Leontieva and Blagosklonny, 2013; Wagner and Gil, 2020; Maskey *et al.*, 2021; Wang *et al.*, 2022). Mutations that result in, for instance, cyclin E amplification or Rb loss, often lead to CDK4/6 inhibitor resistance as they render cells non-dependent on cyclin D-CDK4/6-Rb signalling axis. These cells enter the cell cycle regardless, due to the loss of restriction or commitment checkpoint mainly due to increased cyclin E-CDK2 activity (Herrera-Abreu *et al.*, 2016; Turner *et al.*, 2019). In line with this, cells that develop CDK4/6 inhibitor acquired resistance were found to be sensitive to CDK2 knock-down (Herrera-Abreu *et al.*, 2016), and CDK2 and CDK4/6 combinatorial inhibition enhances the senescent phenotype in cancer cell lines (Pandey *et al.*, 2020). To potentially overcome CDK4/6 inhibitor acquired resistance and cancer progression, a CDK2/4/6 inhibitor, PF-06873600, was developed (K. D. Freeman-Cook *et al.*, 2021; K. Freeman-Cook *et al.*, 2021).

CDK2 inhibitors, however, have not been approved for cancer treatment mainly due to their non-specificity and therefore increased toxicity. However, several selective CDK2 inhibitors are in development, and a few entered clinical trials, such as PF-07104091 (Yap *et al.*, 2023) and INX-315 (Dietrich *et al.*, 2024).

1.8. CDK7: the CDK-Activating Kinase (CAK)

Another strategy to inhibit the activity of the mitotic CDKs is through targeting the CDK-activating kinase (CAK) CDK7, with several selective inhibitors currently in pre-clinical development or clinical trials. Whilst CDK1, 2, 4 and 6 play specific roles in cell cycle progression, CDK7 has a role in activating all these mitotic CDKs. CDK7 forms a CAK complex with cyclin H and an assembly factor MAT1 (Schachter and Fisher, 2013). Cyclin H binds to the N-terminal region of CDK7 and is required for its activity whereas MAT1 binds to its C-terminal region, interacts with both proteins and in turn stabilises the complex (Tassan *et al.*, 1995; Sava *et al.*, 2020).

In addition to the requirement of binding to specific cyclins, CDKs require phosphorylation at their T loop for full activation. This activating phosphorylation at threonine residues 161, 160, 172 and 177 of CDK1, 2, 4 and 6 respectively, is one of the roles of CDK7 as the only known metazoan CAK. CDK7 activity is low in quiescence and increases upon mitogen stimulation and G1 phase entry and progression (Schachter *et al.*, 2013). However, CDK7 activity levels remain constant throughout the cell cycle. It was therefore unclear how the inhibition of this kinase does not lead to inactivation of all CDKs simultaneously. Studies using chemical genetics were able to answer these questions and further test substrate specificities supporting CDK7 as the cell cycle CAK (Larochelle *et al.*, 2007; Merrick *et al.*, 2008; Schachter *et al.*, 2013). These studies were carried out by mutating the wild-type CDK7 in HCT116 human colon cancer cell line to an analogue-sensitive CDK7 that can be inhibited by bulky adenine analogues. CDK7's ATP binding pocket was expanded by mutating the phenylalanine residue 91 to a glycine residue. This mutation causes this kinase selective for analogue binding, allowing for its selective inhibition (Shah *et al.*, 1997; Larochelle *et al.*, 2006).

It was observed that CDK2 and CDK1 are activated by different mechanisms (Larochelle *et al.*, 2007). When CDK7 was inhibited during the G1 phase, they observed that this blocks cyclin-CDK2 complex activation which in turn causes an S phase delay. However, this does not prevent cyclin-CDK2 complex from assembling, suggesting that CDK7 is not required for the formation and stabilisation of this complex but only for its activation by T loop phosphorylation. On the other hand, inhibiting CDK7 during the G2 phase hinders the formation of cyclin B-CDK1 complex and therefore

prevents M phase entry. This suggested that both cyclin B binding and CDK1 T loop phosphorylation occur simultaneously (Larochelle *et al.*, 2007; Merrick *et al.*, 2008). This could explain how CDK7 is able to activate CDK2 prior to CDK1 despite the two kinases being structurally similar (Schachter and Fisher, 2013).

CDK4 and CDK6 prime the cell for cell cycle entry and are important for preventing cell cycle exit (Bertoli and de Bruin, 2014). It was confirmed that CDK7 phosphorylates and activates CDK4 and CDK6 (Schachter *et al.*, 2013). Interestingly, CDK4/6 phosphorylation appears to be distinct to CDK2 and CDK1 phosphorylation. Upon CDK7 inhibition, phosphorylated CDK2 threonine residue 160 and CDK1 threonine residue 161 remain present for hours. On the contrary, CDK4/6 T loop phosphorylation is reduced immediately after CDK7 activity is lost (Schachter *et al.*, 2013), which likely depends on the activity of a yet to be identified phosphatase. This suggests that CDK7 is required for maintaining CDK4 and CDK6 activities, which is not the case for CDK2 and CDK1 (Sava *et al.*, 2020).

Apart from having a crucial role in activating cell cycle CDKs, CDK7 has a second role in transcriptional regulation, through activating CDK9 and as part of the transcription factor IIH (TFIIH). It plays a role in different phases of the RNA polymerase II (RNAPII) transcription cycle. Transcription is divided into initiation, elongation, and termination stages. Progression through RNAPII-mediated transcription is dependent on a specific pattern of multiple residue phosphorylation events in the C-terminal domain (CTD) of RNAPII, which is composed of the repeats of a heptad sequence, $Y_1S_2P_3T_4S_5P_6S_7$ (Chapman *et al.*, 2008; Fisher, 2019; Sava *et al.*, 2020). When RNAPII CTD is unphosphorylated, the polymerase is found in a preinitiation complex (PIC) together with general transcription factors, one of which is TFIIH, on active RNAPII gene promoters. In order for transcription to initiate, RNAPII must be released from the PIC, a step that is dependent on CTD phosphorylation by the kinase CDK7. CDK7 phosphorylates RNAPII CTD directly at serine residues 5 and 7. This releases RNAPII from PIC and initiates the transcriptional cycle. CDK7 is then, by yet an undetermined mechanism, involved in promoter-proximal pause, a step important for co-transcriptional processing, including 5’ RNA capping to protect it from degradation. Afterwards, it is necessary for pause release and the elongation step of the capped transcript. This step is regulated by CDK7 phosphorylating the T loop of CDK9. This

activates the cyclin T-CDK9 complex, known as positive transcription elongation factor b (P-TEFb), which then phosphorylates serine residue 2 at RNAPII CTD, a step necessary for transcription elongation. Termination steps of the RNAPII-mediated transcriptional cycle are guided by cyclin K-CDK12/13, which could also be mediated by CDK7 through its CAK role, but this requires further investigation (Core and Adelman, 2019; Fisher, 2019; Parua and Fisher, 2020; Sava *et al.*, 2020).

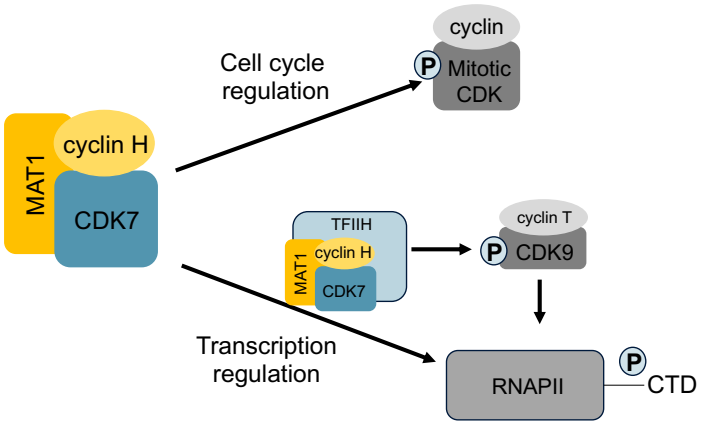

Figure 1.6: CDK7 has both a cell cycle and transcriptional regulation role. CDK7 forms a complex with cyclin H and MAT1, together known as the CDK-activating kinase (CAK). It has a dual function, where it is required for the activation of cell cycle CDKs and for progression through the transcriptional cycle of RNA polymerase II (RNAPII). In its cell cycle regulation role, it is required to phosphorylate and in turn activate mitotic CDKs (CDK1, 2, 4, 6) in their T loop. In its transcriptional regulation role, it is required at different stages of the transcription cycle, by either direct or indirect phosphorylation of C-terminal domain (CTD) of RNAPII via CDK9 activation. Figure adapted from (Sava *et al.*, 2020).

The interest to develop specific CDK7 inhibitors as a cancer therapeutic has increased due to several reasons. Firstly, it has been shown that the expression of CDK7 is increased in cancer cells suggesting an increased dependence on CDK7 activity (Bartkova, Zemanova and Bartek, 1996; Patel *et al.*, 2016; Jiang *et al.*, 2019). Moreover, many cancers develop addiction to transcriptional programs. For instance, one of the most deregulated oncogenes in cancer is the transcription factor Myc, which drives transcriptional programs required for cancer cell proliferation and survival (Beroukhim *et al.*, 2010). With CDK7's dual role in mitotic CDK activity and transcription, it makes it an attractive cancer therapeutic target. Lastly, as previously mentioned, increased cyclin E expression was identified as a likely resistance

mechanism in CDK4/6 inhibitor palbociclib treatment (Turner *et al.*, 2019). This points to a potential compensatory role for cyclin E-CDK2 activity to drive the cell cycle entry without cyclin D-CDK4/6 activity. In fact, a combination of CDK2 and CDK4/6 inhibitors inhibited proliferation of palbociclib-resistant cells (Pandey *et al.*, 2020). Therefore, as CDK7 is required for activating all cell cycle CDKs, inhibiting its activity could prevent cell cycle progression more robustly than single mitotic CDK inhibitor treatments. A recent pre-clinical study demonstrated this, where selective CDK7 inhibition is able to overcome CDK4/6 inhibitor resistance in breast cancer cells (Guarducci *et al.*, 2024). Although this requires further investigation, it supports the increasing interest in developing selective CDK7 inhibitors for cancer treatment.

1.9. CDK7 inhibitor, samuraciclib

Several covalent and non-covalent CDK7 inhibitors have been developed. From the covalent inhibitors, THZ1 has been most commonly used to investigate the role of CDK7, especially in transcription (Kwiatkowski *et al.*, 2014; Nilson *et al.*, 2015; Ebmeier *et al.*, 2017). However, it was shown that THZ1 inhibits the transcriptional kinases CDK12 and CDK13 as well as CDK7 (Kwiatkowski *et al.*, 2014). More selective covalent CDK7 inhibitors were developed: YKL-5-124 (Olson *et al.*, 2019) and SY-1365 (Hu *et al.*, 2019). From the non-covalent CDK7 inhibitors, the first highly selective small molecule inhibitor was BS-181; however, it did not pass absorption, distribution, metabolism, and excretion (ADME) assays to further advance to clinical trials (Ali *et al.*, 2009; Patel *et al.*, 2018). Refining its properties has guided the development of ICEC0942 (CT7001) or currently under clinical name samuraciclib (Patel *et al.*, 2018).

Samuraciclib is the first orally bioavailable non-covalent, ATP-competitive, CDK7 inhibitor. *in vitro* kinase assays show high selectivity towards CDK7 as the IC_{50} values for other CDKs are 15-fold or higher than the value for CDK7, with CDK2 having a 15-fold and CDK9 30-fold higher IC_{50} value. Screening kinases of different classes revealed IC_{50} values which are also around 15-fold or higher than the one for CDK7 (Patel *et al.*, 2018). Further investigation in a prostate cancer cell line confirmed preferential binding and selectivity to CDK7. However, the study also showed some

degree of binding to CDK2 and CDK9 at higher concentrations (Constantin *et al.*, 2023), which is in line with the *in vitro* kinase data (Patel *et al.*, 2018).

Selective sensitivity to samuraciclib treatment has been shown for a variety of cancer cell lines and samuraciclib has been shown to inhibit tumour growth in xenografts of both breast and colorectal cancer (Patel *et al.*, 2018). This small molecule CDK7 inhibitor is the most clinically advanced CDK7 inhibitor. It was developed with CRUK funding and was licensed to Carrick Therapeutics in 2016, and in 2021 the FDA allowed its fast tracking in combination with fulvestrant (hormonal therapy to block estrogen receptors) for CDK4/6 inhibitor resistant HR+, HER2- advanced breast cancer and also in combination with chemotherapy for treating locally advanced or metastatic triple negative breast cancer (TNBC) (Carrick Therapeutics, 2021).

The first results from an in-human clinical trial, a modular phase I study (NCT03363893), evaluating safety as well as preliminary effectiveness of samuraciclib were published last year (Coombes *et al.*, 2023). The study demonstrated satisfactory safety profile as well as an initial indication of clinical efficacy, especially towards TNBC and HR+, HER2- breast cancer. Moreover, wild-type *TP53* was found as a potential treatment response marker, whereas a mutation in *TP53* correlated with poorer partial response to samuraciclib. Currently, there is a great medical need for a treatment of breast cancers that have advanced on CDK4/6 inhibitors. Therefore, this initial evidence of clinical efficacy of samuraciclib towards CDK4/6 inhibitor acquired resistance needs to be investigated in future clinical trials (Coombes *et al.*, 2023). Several phase I/II clinical trials for treating advanced breast cancer using samuraciclib are currently recruiting patients (NCT05963984, NCT06125522, NCT05963997 and NCT04802759). Even though this drug reached and is successfully progressing through clinical trials, the mechanism by which samuraciclib inhibits tumour growth and reduces cell number remains largely unknown.

1.10. Project aim: Understanding the anti-cancer efficacy of cyclin-dependent kinase inhibitors

The use of CDK inhibitors is currently restricted to breast cancer and lack of clear biomarkers restricts their use in other cancer types. In addition, despite CDK4/6 inhibitors being well-tolerated and inducing an effective initial response, patients commonly acquire resistance leading to cancer progression. In order to guide and expand their use in the clinic, a better fundamental understanding is required on how these inhibitors achieve anti-cancer efficacy. The aim of my thesis is to explore what makes cancer cells sensitive to CDK inhibitors using both CDK4/6 and CDK7 inhibitors to identify common and specific mechanism of their anti-cancer efficacy. A better understanding of their mechanisms of action can help guide their clinical use for more accurate patient stratification.

My project has expanded from the work of a previous PhD student in the lab, Gemma Wilson, who studied the mechanism by which the selective CDK7 inhibitor samuraciclib inhibits cellular proliferation (Wilson, 2020). This small molecule inhibitor shows promising anti-cancer efficacy in pre-clinical models, but it remained unclear if this is through cytostatic or cytotoxic effects. An apoptotic effect was observed in cancer cell lines; however, this was detected at concentrations higher than the IC_{50} value (Patel *et al.*, 2018). Gemma Wilson observed that samuraciclib induces senescence phenotypes in both a non-transformed retinal pigment epithelial 1 (RPE1) cell line and a breast cancer MCF7 cell line at their IC_{50} values, and that the inhibition of active cellular growth via mTOR signalling pathway suppresses this effect (Wilson, 2020).

Studies have demonstrated that a CDK4/6 inhibitor palbociclib also has cytostatic effects and induces senescence phenotypes and long-term withdrawal from the cell cycle (Wagner and Gil, 2020; Maskey *et al.*, 2021; Barr and McClelland, 2022; Crozier *et al.*, 2022; Wang *et al.*, 2022). Similarly to samuraciclib, conversion of a prolonged G1 arrest to a senescent state in response to palbociclib is directed by active cellular growth (Leontieva and Blagosklonny, 2013; Neurohr *et al.*, 2019; Lanz *et al.*, 2022; Crozier *et al.*, 2023; Manohar *et al.*, 2023). Therefore, to understand better how a long-lasting response in patients can be achieved by these anti-proliferative drugs, I

investigate the fundamental cellular processes that underlie the sensitivity of cancer cells to CDK inhibitors.

In chapter 3, I explore the role of active growth signalling and an increase in cell size in samuraciclib-induced senescence. We have recently published this story (Wilson *et al.*, 2023), which included a part of the findings presented in this chapter, as well as Gemma Wilson's PhD work (Wilson, 2020). In chapter 4, I compare the long-term loss of proliferative potential between samuraciclib and palbociclib and the role that mTOR signalling and biomass accumulation have on the reduction of proliferative potential. My data from these two chapters show that active cellular growth has a significant role in driving a permanent cell cycle exit during a CDK inhibitor treatment. Whilst this is mainly via inducing senescence during the arrest, even when cells do not permanently arrest initially, they do so upon a return to a proliferative state, most likely due to replication-acquired damage. I established that a prolonged G1 arrest causes mild replication stress upon inhibitor wash-out (Manohar *et al.*, 2023). Since enhanced growth signalling is common in cancers, this work could help explain anti-cancer efficacy of CDK inhibitors, where cellular growth and proliferation processes become uncoupled. It also demonstrates that CDK7 inhibitor treatment causes a more robust permanent cell cycle arrest compared to CDK4/6 inhibitor.

In chapter 5, I explore other non-growth cellular processes that are required for CDK inhibitor sensitivity and those that can lead to resistance. I further analyse the results from the genome-wide CRISPR knock-out chemogenetic screen, carried out by our collaborators from the laboratory of Mike Tyers, which initially identified active mTOR signalling as a mechanism required for samuraciclib sensitivity. I explore the effect of p53-p21 pathway, Rb loss and cyclin E overexpression, all common alterations in cancer, on both samuraciclib and palbociclib sensitivity.

2. Materials and Methods

2.1. Cell culture

Table 2.1: List of cell lines used throughout this research thesis.

Cell line	Media	Media supplements	Source/ reference
hTERT-RPE1	DMEM/F12 (Thermo Fisher Scientific, 33131028)	10% fetal bovine serum (FBS) (Sigma Aldrich, F7524), 1% penicillin/streptomycin (Gibco, 15140122), 3.5% sodium bicarbonate (Gibco, 25080060)	ATCC CRL-4000
hTERT-RPE1-FUCCI	DMEM/F12 (Thermo Fisher Scientific, 33131028)	10% FBS, 1% penicillin/streptomycin, 3.5% sodium bicarbonate	Gift from Buzz Baum, MRC LMB, Cambridge, UK
hTERT-RPE1-p53 KO	DMEM/F12 (Thermo Fisher Scientific, 33131028)	10% FBS, 1% penicillin/streptomycin, 3.5% sodium bicarbonate	(Crozier *et al.*, 2022)
hTERT-RPE1-mRuby PCNA-p21 KO	DMEM/F12 (Thermo Fisher Scientific, 33131028)	10% FBS, 1% penicillin/streptomycin, 3.5% sodium bicarbonate	(Barr *et al.*, 2016; Pennycook and Barr, 2021)
hTERT-RPE1 TetON Cyclin E	DMEM/F12 (Thermo Fisher Scientific, 33131028)	10% FBS, 1% penicillin/streptomycin, 3.5% sodium bicarbonate	(Zeng *et al.*, 2023)
MCF7	DMEM (Thermo Fisher Scientific, 41965039)	10% FBS, 1% penicillin/streptomycin	ATCC HTB-22 (Patel *et al.*, 2018)
T47D	RPMI (Thermo Fisher Scientific, 21875034)	10% FBS, 1% penicillin/streptomycin	ATCC HTB-133
BT549	RPMI (Thermo Fisher Scientific, 21875034)	10% FBS, 1% penicillin/streptomycin	ATCC HTB-122
MCF7 parental (*PIK3CA*^{mut})	DMEM (Thermo Fisher Scientific, 41965039)	10% FBS, 1% penicillin/streptomycin	(Beaver *et al.*, 2013)

Table 2.1: (continued)

Cell line	Media	Media supplements	Source/ reference
MCF7 *PIK3CA*^{wt}	DMEM (Thermo Fisher Scientific, 41965039)	10% FBS, 1% penicillin/streptomycin	(Beaver *et al.*, 2013)
NALM-6	RPMI (Thermo Fisher Scientific, 21875034)	10% FBS, 1% penicillin/streptomycin	(Bertomeu *et al.*, 2018)

All cell lines were cultured at 37°C in the presence of 5% CO_2.

The pair of isogenic MCF7 cell lines, with and without *PIK3CA* mutation, were published previously and created by somatic gene targeting to correct the native E545K mutation in *PIK3CA* as previously described (Beaver *et al.*, 2013). This pair of isogenic cell lines were made to stably express nuclear EGFP, by lentiviral transduction of pTRIP-SFFV-EGFP-NLS (Addgene, #86677) packaged in HEK293T cells, to allow for accurate quantification of cell number via IncuCyte Zoom. This work was carried out by the laboratory of Simak Ali at Imperial College London.

2.2. Drug treatments

Cells were treated with samuraciclib (laboratory of Simak Ali, Imperial College London, UK) at specified concentrations, with palbociclib (Selleckchem, S1116) at specified concentrations, with etoposide (Sigma Aldrich, E1383) (0.5 μg/ml), with camptothecin (Sigma Aldrich, 208925) at specified concentrations, with Torin1 (Merck Millipore, 475991) at specified concentrations, with doxycycline (Sigma Aldrich, D9891) (1 μg/ml). DMSO (Sigma Aldrich, D8418) was the vehicle control in each experiment.

2.3. siRNA transfections

For siRNA transfections, Lipofectamine RNAiMAX (Thermo Fisher Scientific, 13778075) was used in OptiMEM (Gibco, 51985-026) following manufacturer's reverse transfection protocol. Transfection mix per well (for 6-well plate) contained 500 μl OptiMEM, 1.5 μl siRNA (stock concentration 20 μM) and 2.5 μl Lipofectamine

RNAiMAX. Cells were plated on top of a transfection mix in penicillin/streptomycin-free media and left in culture overnight. The following morning, the cells were washed once with PBS and fresh media containing all the necessary supplements, including penicillin/streptomycin, was added. ON-TARGETplus non-targeting control siRNA (Dharmacon, Horizon Discovery, D-001810-01-20), referred to as siCONT, was used as a control in all experiments. Other siRNAs used were ON-TARGETplus SMARTpool human CDKN1A siRNA (sip21) (Dharmacon, Horizon Discovery, L-003471-00-0005), ON-TARGETplus SMARTpool human CDK7 siRNA (siCDK7) (Dharmacon, Horizon Discovery, L-003241-00-005) and custom siRNA oligonucleotides for human Rb (siRb) (duplex sequences: 5'-AAUAAGUUCACAUGUCCUUUC-3' and 5'-GAAAGGACAUGUGAACUUAUU) synthesised by IDT.

2.4. SDS-PAGE and western blot

Cells were harvested by scraping using Falcon cell scraper (Corning, 353086). Whole-cell extracts were prepared in RIPA buffer (Tris pH 7.5 20 mM, NaCl 150 mM, EDTA 1 mM, EGTA 1 mM, NP-40 1%, NaDoc 1%), phosphatase inhibitor cocktails 2 and 3 (Sigma Aldrich, P5726 and P0044 respectively) 1:1000 and protease inhibitor cocktail (Sigma Aldrich, P8340) 1:1000. Protein concentrations were measured using Bradford assay (Bio-Rad 500-0006) following manufacturer's instructions. Whole-cell protein extracts were mixed with Laemmli sample buffer (Tris-HCl pH 6.8, SDS, Bromophenol blue and glycerol) and boiled at 95°C for 2 min. Equal concentrations of protein were loaded onto NuPAGE Novex 4-12% Bis-Tris protein gels (Invitrogen, NP0322) in 1X MOPS running buffer (Invitrogen, NP0001). Protein was transferred onto nitrocellulose membrane (Sigma Aldrich, GE10600001) by wet transfer in transfer buffer (25 mM Tris base, 250 mM glycine, 10% ethanol). Membranes were blocked in 5% milk dissolved in PBS/0.2% Tween or in Immobilon Block-CH reagent (Merck Millipore, WBAVDCH01) for phospho-proteins for 1 hour at room temperature. Membranes were then incubated in primary antibodies diluted in 5% milk or 5% BSA PBS/0.2% Tween for phospho-proteins overnight at 4°C. Primary antibodies and their dilutions are listed in Table 2.2. Following PBS/0.2% Tween washes, membranes were incubated in secondary HRP antibodies diluted in 5% milk or 5% BSA PBS/0.2% Tween for phospho-proteins for 1-2 hours at room temperature. Secondary antibodies and their

dilutions are listed in Table 2.3. HRP was visualised using Immobilon Crescendo Western HRP substrate (Merck Millipore, WBLUR0100). Membranes were developed using Amersham Hyperfilm ECL (GE Healthcare Life Sciences, 28906836) with a XOGRAF Compact X4 film processor or using an Uvitec Alliance Q9 imaging system.

2.5. Antibodies

Table 2.2: Primary antibodies used throughout this research thesis.

Protein	Host	Supplier	Catalogue number	WB dilution	IF dilution
$p21^{Waf1/Cip1}$	Rabbit	Cell Signaling Technology	CST 2947	1:5000	-
p53	Rabbit	Cell Signaling Technology	CST 9282	1:500	-
Phospho-Rb (Ser807/811)	Rabbit	Cell Signaling Technology	CST 8516	1:1000	-
Rb	Mouse	Cell Signaling Technology	CST 9309	1:500	-
Cyclin A2	Rabbit	Abcam	ab181591	1:2000	-
Lamin B1	Rabbit	Abcam	ab16048	1:5000	-
Phospho-p70 S6 kinase (Thr389)	Rabbit	Cell Signaling Technology	CST 9234	1:1000	-
p70 S6 kinase	Rabbit	Cell Signaling Technology	CST 2708	1:1000	-
Phospho-S6 ribosomal protein (Ser235/236)	Rabbit	Cell Signaling Technology	CST 2211	1:1000	-
Phospho-Chk1 (Ser345)	Rabbit	Cell Signaling Technology	CST 2341	1:1000	-
Phopho-RPA32 (Ser4/Ser8)	Rabbit	Bethyl Laboratories	A300-245A	1:2000	-
Phospho-H2A.X (Ser139) (γH2AX)	Rabbit	Cell Signaling Technology	CST 9718	1:250	1:1000
Phospho-Chk2 (Thr68)	Rabbit	Cell Signaling Technology	CST 2661	1:500	-
MDM2	Rabbit	Cell Signaling Technology	CST 86934	1:1000	-
Phospho-CDK1 (Thr161)	Rabbit	Cell Signaling Technology	CST 9114	1:1000	-
BrdU (recognises CIdU)	Rat	Abcam	ab6326	-	1:250
BrdU (recognises IdU)	Mouse	BD Biosciences	347580	-	1:100
GAPDH	Mouse	GeneTex	GTX627408	1:5000	-
Vinculin	Rabbit	Abcam	ab129002	1:10000	-

Table 2.3: Secondary antibodies used throughout this research thesis.

Antibody	Host	Supplier	Catalogue number	WB dilution	IF dilution
anti-rabbit IgG HRP conjugate	Goat	Thermo Fisher Scientific	31460	1:4000	-
anti-mouse IgG HRP conjugate	Goat	Thermo Fisher Scientific	PA1-74421	1:4000	-
Alexa Fluor 647 anti-rabbit IgG	Goat	Life Technologies	A21244	-	1:2000
Alexa Fluor 488 anti-mouse IgG	Goat	Life Technologies	A11029	-	1:500
Alexa Fluor 555 anti-rat IgG	Goat	Life Technologies	A21434	-	1:500

2.6. RNA extraction and reverse transcriptase qPCR

Cells were harvested by trypsinisation and resuspended in PBS. RNA was extracted using a RNeasy Plus Mini Kit (Qiagen, 74136) following manufacturer's instructions. Prior to RNA extraction protocol via column purification, cell pellets were vortexed with RLT buffer with 1% β-mercaptoethanol for 30 seconds and transferred to gDNA eliminator spin column. After centrifuging for 30 seconds at > 8000xg, the flow-through was kept and the protocol was continued according to manufacturer's instructions.

Mesa Blue qPCR MasterMix (Eurogentec, RT-SY2X-03 +NRWOUB) and Euroscript Reverse Transcriptase/RNase inhibitor (Eurogentec, RT-0125-ER) were used for the reverse transcriptase quantitative polymerase chain reaction (RT-qPCR) SRB assays. Total reaction volume used per well was 14 μl. This contained 7 μl of Mesa Blue MasterMix, supplemented with 0.035 μl Euroscript Reverse Transcriptase/RNase inhibitor, 1.5 μl of 5 μM forward primer, 1.5 μl of 5 μM reverse primer and 4 μl of 20 ng/μl RNA product. The primers used are listed in Table 2.4. Samples were loaded in triplicates. *GAPDH* was used as a normalisation control in each experiment. BioRad CTX Connect qPCR machine was used for running RT-qPCR reactions. The programme used is detailed in Table 2.5.

Table 2.4: Primers used for RT-qPCR throughout this research thesis.

Gene	Forward/Reverse	Sequence 5'→ 3'
GAPDH	Forward	GAAATCCCATCACCATCTTCCAGG
	Reverse	GAGCCCCAGCCTTCTCCATG
LMNB1	Forward	GAAAAAGACAACTCTCGTCGCA
	Reverse	GTAAGCACTGATTTCCATGTCCA
CDKN1A	Forward	TCACTGTCTTGTACCCTTGTGC
	Reverse	GGCGTTTGGAGTGGTAGAAA
CCNA2	Forward	CTTCACCAGACCTACCTCAAAG
	Reverse	GGTGGGTTGAGGAGAGAAAC
CCND1	Forward	CAATGACCCCGCACGATTTC
	Reverse	ATGAACTTCACATCTGTGGCA
CCNE1	Forward	GCCAGCCTTGGGACAATAA
	Reverse	GCCTCTGGATGGTGCAATAA

Table 2.5: Programme used for RT-qPCR reactions.

Temperature (°C)	Time	Number of cycles
48	30 minutes	1
95	5 minutes	1
95	30 seconds	40
60	45 seconds	
Measure		
65-85	10 seconds at each temperature	Melt curve

2.7. Flow cytometry

2.7.1. EdU incorporation assay

For proliferation analysis, 5-ethynyl-2'-deoxyuridine (EdU) was added to the cell culture media at the final concentration of 10 μM and cells were incubated for 1 hour at 37°C with 5% CO_2. Cells were trypsinised and resuspended in PBS and then fixed in 4% formaldehyde (Sigma Aldrich, 252549) for 15 minutes at room temperature. EdU detection was then performed using Click-iT EdU Alexa Fluor 647 Flow Cytometry Assay Kit (Thermo Fisher, C10424) following manufacturer's instructions. Prior to EdU detection, cells were counted and diluted to the same number in each sample. Cells were washed in 1 mg/ml BSA in PBS and resuspended in saponin-based permeabilization and wash reagent at room temperature for 15 minutes. Cells were

then resuspended in Click-iT reaction cocktail and incubated at room temperature for 30 minutes protected from light. After this, cells were incubated in 2 μg/ml DAPI (Sigma Aldrich, D9564) for at least 15 minutes at room temperature. Sample measurements were then acquired on a BD LSRII flow cytometer using DIVA software (BD) and analysed using FlowJo software.

2.7.2. Senescence-associated β-galactosidase assay

For the analysis of senescence-associated β-galactosidase (SA β-gal) activity, flow cytometry was carried out as previously described (Debacq-Chainiaux *et al.*, 2009; Cahu and Sola, 2013). Before harvesting the cells, they were incubated with Bafilomycin A1 at a final concentration of 100 nM for 1 hour at 37°C and 5% CO_2. Cells were then incubated with C_{12}FDG (Invitrogen, D2893) at a final concentration of 33 μM for 2 hours at 37°C and 5% CO_2. Cells were then washed twice with PBS, trypsinised, resuspended in PBS and centrifuged at 300xg for 5 minutes at 4°C. Cells were then resuspended in 500 μl of ice-cold PBS and analysed by flow cytometry. Sample measurements were acquired on a BD LSRII flow cytometer using DIVA software (BD) and analysed using FlowJo software.

2.8. Colony formation assay

Following the treatment, cells were washed five times with PBS to remove the drugs. Cells were then harvested by trypisinisation and counted. 1000 cells were plated in 6-well plates for each treatment (~105 cells/cm^2) in triplicates. Cells were allowed to grow for 9-11 days at 37°C with 5% CO_2. When colonies formed at the end of the assay, cells were washed once with PBS and then fixed in 70% ethanol and stained with 1% Methylene Blue (Sigma, M4159) for 20 minutes at room temperature. Cells were washed thoroughly with DI water to remove any excess stain and left to dry overnight. Plates were then scanned and analysed using the ColonyArea macro in Fiji to measure % area of the plate covered by colonies (Guzmán *et al.*, 2014).

2.9. Cell size measurements

For analysis of cell volume, cells were harvested by trypsinisation and resuspended in culture media. They were then diluted 1:10 in Coulter Isoton II diluent (Beckman Coulter, 8546719) and cell volumes were determined using a particle sizing and counting analyser (Multisizer 4 Coulter counter, Beckman Coulter) with Multisizer 4 software. The software exports the data using cell diameter for size bins measurements. To convert these to cell volume measurements, assuming cells to be spheres, the following formula was used: $V=4r^3\pi/3$

2.10. Immunofluorescence

Cells were plated on coverslips pre-coated with fibronectin (Sigma Aldrich, F1141). Cells were fixed in 4% formaldehyde (Sigma Aldrich, 252549) for 20 minutes at room temperature and then permeabilised with 0.2% Triton X-100 (Sigma Aldrich, T8787) in 1x PBS for 5 minutes at room temperature. Cells were blocked in 1% BSA 0.2% Tween in PBS for 1 hour at room temperature and incubated in primary antibody overnight at 4°C. Primary antibodies and their dilutions are listed in Table 2.2. Coverslips were incubated the following day in secondary antibody for 2 hours at room temperature. Secondary antibodies and their dilutions are listed in Table 2.3. Coverslips were stained with Hoechst (Invitrogen, H3570), 1:10000 in 1x PBS and mounted on slides with Fluoroshield (Sigma Aldrich, F6182). Images were acquired with Leica SPE2 confocal microscope using a 40x objective lens and processed with Fiji. 100 cells were analysed per sample.

2.11. DNA fibre assay

Fibre labelling and spreading was carried out as previously described (Petermann, Woodcock and Helleday, 2010). Cells were labelled with 25 μM CIdU (Sigma, C6891) for 15 min at 37°C and then with 250 μM CO_2-equilibrated IdU (Sigma, 17125) for 15 min at 37°C. After labelling, cells were washed in ice-cold PBS, trypsinised and resuspended in PBS at a $100x10^4$ cells/ml for untreated and palbociclib+Torin1 samples and at a $150x10^4$ cells/ml for palbociclib sample. 2.5 μl of the sample was placed on a glass slide and allowed to slightly dry at room temperature for 5 min, after

which spreading buffer (200 mM Tris pH 7.4, 50 mM EDTA, 0.5% SDS) was mixed with the sample and left to incubate for 2 min at room temperature. Slides were then tilted to allow DNA to spread and left to air-dry for 2 min. Slides were then incubated in 3:1 methanol/acetic acid in a coplin jar for 10 min, after which they were air-dried and stored in the fridge until immunostaining.

Slides were washed twice with water, after which they were denatured in 2.5 M HCl for 1 hour 15 min. Slides were then rinsed twice with PBS and blocked for 1 hour in blocking solution (1% BSA, PBS/0.1% Tween). Slides were then stained overnight with primary antibodies (rat anti-BrdU Abcam ab6326 1:250, mouse anti-BrdU BD Biosciences 347580 1:100). The next day slides were rinsed three times in PBS, followed by a 10 min incubation in 4% formaldehyde. Slides were then rinsed three times in PBS and stained with secondary antibodies (Alexa Fluor 555 goat anti-rat 1:500, Alexa Fluor 488 goat anti-mouse 1:500) for 1 hour 30 min at room temperature in the dark. Slides were washed twice in PBS and coverslips were mounted using Fluoroshield. Images were obtained with Leica SPE2 63x objective lens and processed with Fiji. 85-200 fibres were counted for each experiment. Maximum projections of the composite images were constructed to visualise red and green channels. The 'line' tool in Fiji was used to measure the length of ongoing fibres, represented by consecutive red and green tracks. Total amount of fibres (ongoing fibres, replication origins and terminations) was counted to quantify the percentage of origin firing.

2.12. Live-cell imaging

hTERT-RPE1- FUCCI cells were used for live-cell imaging. For samuraciclib treatment experiment, hTERT-RPE1-FUCCI cells were plated in a 6-well plate one day prior to the start of the experiment. The following day cells were treated with vehicle control (DMSO) or samuraciclib and imaging was started for 48 hours. For samuraciclib wash-out/release experiment, hTERT-RPE1-FUCCI cells were treated with DMSO or samuraciclib for 72 hours. Cells were then washed five times with PBS and fresh media was added after which imaging was started for 72 hours.

Live-cell imaging was performed on a Nikon Ti inverted microscope stand with a Nikon DS-Qi2 high sensitivity scientific CMOS camera using a 20x objective lens.

Fluorescence filter sets were Nikon GFP HQ and Texas Red cubes. Fluorescence light source was a CoolLED pE-300. The Nikon DS-Qi2 camera acquisition was binned 3x to enhance sensitivity. Phase contrast and fluorescence images were taken every 10 minutes. Cells were maintained at 37°C with 5% CO_2.

2.13. Image analysis

2.13.1. Quantification of fluorescence intensity

Quantification of nuclear fluorescence intensity was carried out using Fiji. Maximum projections of composite images were constructed. Nuclei were segmented using global thresholding. Mean fluorescence intensity was then measured for each segmented nucleus.

2.13.2. Measurement of DNA fibre length

The measurements of DNA fibre lengths were carried out using Fiji. Maximum projections of the composite images were constructed to visualise red and green channels. The 'line' tool in Fiji was used to measure the length of ongoing fibres, represented by consecutive red and green tracks. Total amount of fibres (ongoing fibres, replication origins and terminations) and replication origins (represented by red track between two green tracks or single green tracks, marking replication origin in both first and second pulse respectively) was counted to quantify the percentage of origin firing. Terminations were represented by single red tracks or green track between two red tracks, marking terminations in both first and second pulse respectively.

2.13.3. Analysis of live-cell imaging timelapse movies

Time-lapse movies were analysed manually by single cell tracking and determining the time of colour changes between red, yellow, green and loss of colour of FUCCI cells. Manual analysis could have resulted in slight differences in colour switch timings. Gaussian Blur filter was used to remove background noise from the green GFP channel. Only cells that were in the field of view throughout the entire movie were included in the analysis and the daughter cells inherited the mother's track history.

Therefore, a mother cell that divided once was presented as two single cell cycle FUCCI profile tracks and was counted as two cell cycle states. For the wash-out/release experiment, red cells were marked at the first time-point and tracked. Cell cycle entry after samuraciclib wash-out was determined by a yellow colour switch. Nuclear area was calculated in Fiji after nuclear segmentation using Bernsen local thresholding.

2.14. Genome-wide CRISPR knock-out chemogenetic screen

This work was carried out by the members of the laboratory of Mike Tyers at Montreal University, Canada. Members included Caroline Huard, Jasmin Coulombe-Huntington and Thierry Bertomeu.

2.14.1. sgRNAs pooled library generation

The pooled library of 278754 different sgRNAs called EKO (extended-knockout) was inserted within the pLX-sgRNA plasmid (Addgene #50662) and lentivirus was generated in HEK-293T cells as previously described (Bertomeu *et al.*, 2018). A doxycycline-inducible Cas9 clonal cell line of NALM-6 (using plasmid pCW-Cas9, Addgene #50661) was generated, infected with the pooled lentivirus libraries and underwent blasticidin selection as previously described (Bertomeu *et al.*, 2018).

2.14.2. Proliferation assay

To determine the IC_{30} concentration of samuraciclib in NALM-6 cells, a Beckman Coulter BioMek FX robot was used to mix NALM-6 cells with 11 different concentrations of the drugs (1:3 dilutions) and they were then loaded into 384-well plates, keeping solvent concentration constant (0.1%) across all wells (IRIC's HTS platform, Montreal, Canada). Plates were kept for 3 days in a high humidity chamber installed in a 37°C, 5% CO_2 incubator. 50 µl of CellTiter-Glo reagent (Promega, G7570) was then added, plates were shaken for 2 minutes, and luminescence read on a BioTek Synergy/Neo microplate reader.

2.14.3. Chemogenetic screen

A NALM-6 doxycycline-inducible Cas9 clone previously infected and blasticidin-selected following lentiviral infection with EKO lentivirus (MOI of 0.3 and a representation of at least 500 cells per sgRNA) was thawed (representation of at least 250 cells per sgRNA) and treated with 2 mg/ml doxycycline to induce Cas9 expression 7 days before samuraciclib or palbociclib were added. Prior to drug addition, a minimum of 70 million cells were collected as samples that had had doxycycline added but had not been treated with drugs. The remaining cells were diluted to 400 000 cells per mL. 28 million cells (100 cells per sgRNA) were treated with 180 nM, 350 nM (the IC_{30} concentration) and 501 nM of samuraciclib, or 335 nM and 1000 nM of palbociclib, and 70 million cells were treated with 0.1% DMSO. A minimum of 70 million cells were left untreated as control. Cell concentration was monitored every 2 days by diluting 1 ml of the cells 1:10 in Isoton II diluent and using a Beckman Coulter Z2 particle count and size analyser. The cells were diluted accordingly to prevent cells from arresting and compounds or DMSO added to maintain initial concentration. After 8 days, the different populations of cells were pelleted, washed with PBS and frozen.

2.14.4. Next Generation Sequencing

Genomic DNA extractions were done using the Gentra Puregene Cell kit (Qiagen, 158745). sgRNA sequences were amplified by PCR using 462 μg of genomic DNA (corresponding to 70 million cells), 575 μL 10X reaction buffer, 115 μl 10 μM dNTPs, 23 μl 100 μM primer Outer 1, 23 μl 100 mM primer Outer 2, 115 μl DMSO and 145 units of GenScript Green Taq DNA polymerase in a total volume of 5.75 mL or 185 μg (28 million cells; same PCR recipe in 2.5X smaller volumes) as templates. Whenever DNA quantities requirements were not met, everything was used and a corresponding few more cycles performed. Multiple 100 μl reactions were set up in 96-well formats on a BioRad T100 thermal cycler and the steps were as follows: 95°C 5 minutes, 25 cycles of 35 seconds at 94°C, 35 seconds at 52°C and 36 seconds at 72°C, final step of 10 minutes at 72°C after the last cycle. Completed 100 μl reaction mixes were combined into one tube and vortexed and 1.5 mL aliquots were concentrated to 100 μl by ethanol-precipitation. A second PCR reaction was performed to add Illumina sequencing adapters and 6 bp indexing primers, using 10 μl of 1:20 dilution of

unpurified PCR1 product, 10 μl 5X buffer Kapa, 5 μl 2,5 mM dNTPs, 1 μl of PAGE-purified equimolar premix 100 μM TruSeq Universal Adapter 0, 1 μl of 100 μM PAGE-purified TruSeq Adapter with appropriate index, 1 μl DMSO and 5 units Kapa HiFi HotStart DNA polymerase and volumes brought to 50 μl total volume. The steps of the PCR reaction were as follows: 5 minutes at 95°C, 5 cycles of 15 seconds at 95°C, 30 seconds at 50°C and 30 seconds at 72°C, 5 cycles of 15 seconds at 95°C, 30 seconds at 56°C and 30 seconds at 72°C, followed by 5 minutes final step at 72°C after the last cycle. A 238-239 bp amplicon was purified using a 1:1 ratio of Spry beads (AxyPrep Mag FragmentSelect-I, Axygen) and 45 bp was read on an Illumina NextSeq 500 with the 23 first bp read in dark cycles (IRIC's genomic platform, Montreal, Canada). Sequencing coverage was close to 20 samples per lane.

2.15. Statistical analysis

GraphPad Prism was used to carry out statistical analysis. Statistical details for each analysis can be found in the figure legends and figures. Statistical tests used are indicated in figure legends. Statistical significance is represented by * in graphs.

Key for statistical analysis used throughout: ns = $P > 0.05$, * = $P < 0.05$, ** = $P < 0.01$, *** = $P < 0.001$, **** = $P < 0.0001$.

For the chemogenetic screen, reads were aligned using Bowtie2.2.5 (Langmead and Salzberg, 2012) in the forward direction only (-norc option) with otherwise default parameters and total read counts per sgRNA tabulated. Read counts from the different time-points of the control screens were summed, including untreated, 0.1% DMSO-treated and 0.1% ethanol-treated samples, to generate a single reference sgRNA distribution. Gene scores were calculated using the RANKS tool (Bertomeu *et al.*, 2018), with a minimal read threshold of 200 and otherwise default settings. Statistical analysis of the chemogenetic screen was carried out by the laboratory of Mike Tyers.

Statistical analysis of Gene Ontology (GO) enrichment was carried out using GOrilla, a web-based GO analysis tool (Eden *et al.*, 2007, 2009). The REVIGO web server was used to produce a representative subset of GO terms (Supek *et al.*, 2011). The FDR

q-value is the corrected p-value using the Benjamini and Hochberg method (Benjamini and Hochberg, 1995; Eden *et al.*, 2007, 2009).

The enrichment value is defined as enrichment = (b/n) / (B/N) where:

- N=the total number of genes
- B=the total number of genes associated with a specific GO term
- n=the number of genes in the target set
- b=the number of genes in the intersection (Eden *et al.*, 2007, 2009)

3. Active growth signalling is required for sensitivity to the CDK7 inhibitor samuraciclib

Samuraciclib is a non-covalent, ATP-competitive CDK7 inhibitor. It was shown to be selective for CDK7 as the IC_{50} values for other CDKs are 15-fold or higher than the value for CDK7 (Patel *et al.*, 2018). Although it was shown that cancer cells are more sensitive to samuraciclib treatment *in vitro* compared to non-transformed cell lines and the drug reached clinical trials, the mechanism by which this small molecule inhibitor prevents tumour growth was still unknown. The work of a previous PhD student in the lab, Gemma Wilson, focused on exploring the mechanism by which samuraciclib inhibits cell proliferation (Wilson, 2020). She found that this selective CDK7 inhibitor induces a cell cycle arrest predominantly with a G1 DNA content, and moreover that this arrest is persistent, which suggested that samuraciclib induces senescence. A genome-wide CRISPR knock-out (KO) chemogenetic screen revealed a potential role for active growth signalling in samuraciclib-induced senescence, which was then validated using an mTOR inhibitor, Torin1. Samuraciclib sensitivity and senescence phenotypes were significantly reduced during a concurrent treatment with Torin1. Overall, Gemma Wilson's PhD research revealed an important role for active cellular growth through mTOR signalling in samuraciclib-induced senescence (Wilson, 2020). Since growth signalling is often upregulated in cancer, this could explain the anti-cancer efficacy of CDK7 inhibitor sensitivity.

In this chapter I further characterise the role of active growth signalling in samuraciclib sensitivity and cell cycle exit induction via senescence. As a model cell line, I use hTERT-immortalised but non-transformed, retinal pigment epithelial (RPE1) cells as they retain intact cell cycle checkpoints and are therefore suitable for delineating a drug's mechanism of action. I use both pharmacological inhibition of mTOR via Torin1 and serum depletion to modulate the levels of mTOR signalling. I also explore samuraciclib sensitivity in breast cancer cell lines. Data presented in this chapter, with that generated by Gemma Wilson during her PhD, was recently published (Wilson *et al.*, 2023).

3.1. Samuraciclib induces a cell cycle arrest predominantly in a G1 state

DNA content analysis by flow cytometry showed that samuraciclib arrests RPE1 cells predominantly with a G1 DNA content and a reduced G2 population (Wilson *et al.*, 2023). Since this was a snapshot analysis of cell populations, I wanted to further analyse the effect of samuraciclib on cell cycle progression in single cells using timelapse imaging of RPE1 FUCCI cells. The FUCCI (Fluorescent Ubiquitination-based Cell Cycle Indicator) reporter was introduced in 2008, which allows for distinguishing at the single-cell level if a cell is in a G0/G1 state, undergoing a G1-to-S transition, in S/G2 or undergoing mitosis (Sakaue-Sawano *et al.*, 2008). It relies on a reciprocal activity of two E3 ubiquitin ligases, APC/C^{Cdh1} complex active in late M/throughout G1, and SCF^{Skp2} complex, which is active during S/G2 phases. This cell cycle reporter further uses the targeted sequences of the DNA replication origin licencing factor Cdt1 and its inhibitor Geminin, which are substrates of SCF^{Skp2} and APC/C^{Cdh1} respectively, and their reciprocal expression can be visualised using fluorescent probes. Cdt1 levels are highest during the G1 phase, which can be visualised by red-labelled nuclei, and Geminin accumulates during S/G2/M phases, which can be visualised by green-labelled nuclei. During the G1-to-S transition, when Cdt1 levels are decreasing and Geminin levels are increasing, the overlap of red and green colours results in a yellow-labelled nucleus. During late M phase, when the Geminin probe is targeted for degradation, there is a short loss of fluorescent signal until early G1 when the Cdt1 probe becomes detectable (Sakaue-Sawano *et al.*, 2008). A brief schematic of the FUCCI reporter system is described in Figure 3.1A.

To explore the effect on cell cycle progression in real-time, I treated RPE1 FUCCI cells with either DMSO as a vehicle control or samuraciclib and initiated live-cell imaging for 48 hours. By tracking individual cells during the 48 hours of imaging, I observed that the majority of DMSO-treated control cells progress through the cell cycle 2 or 3 times (Figure 3.1B) (Wilson *et al.*, 2023). On the contrary, most of the samuraciclib-treated cells complete the first cell cycle and then remain arrested in a G1 state, marked by red nuclei (Figure 3.1B and 3.1C). This supports the flow cytometry analysis (Wilson, 2020; Wilson *et al.*, 2023). Interestingly, a small number of the FUCCI reporter red-labelled cells had undergone mitotic bypass during the

samuraciclib treatment (Figure 3.1C). This is described as green-labelled S/G2 cells that skip the M/G1 transition (colourless) and enter directly a G1 phase (red). The lack of a mitotic entry in this case is noted by no cell rounding and division. Since these cells have not divided before entering the G1 state and therefore still have the G2 DNA content and are thus tetraploid, this could explain why we consistently observe a small population of G2 cells after samuraciclib treatment using DNA content analysis by flow cytometry. FUCCI reporter analysis revealed that the G2 population (green) is around 5%, which is lower than observed previously (Wilson, 2020; Wilson *et al.*, 2023).

I further validated these results by analysing proliferative markers using western blotting. Retinoblastoma protein (Rb) is a cell cycle inhibitor as it inhibits E2F-dependent transcription and prevents G1-to-S transition. Its phosphorylation marks the activation of E2F-dependent transcription and cell cycle entry and can therefore be used as a marker of proliferation. I observe a reduction in phosphorylated Rb at serine residues 807 and 811 during samuraciclib treatment after 24 hours (Figure 3.1D). This reduction in phosphorylated Rb is accompanied by a reduction in total protein levels of Rb (Figure 3.1D) (Wilson *et al.*, 2023). This is expected as Rb protein levels have been found to dilute with an increase in cell size during G1 phase in order to trigger cell cycle entry and ultimately division (Zatulovskiy *et al.*, 2020). Moreover, a marker that is commonly used for a G1 cell cycle arrest is p21, which is a CDK2/4/6 inhibitor preventing cell cycle entry. I observe an increase in p21 levels that correlate with decreased levels of phosphorylated Rb (Figure 3.1D). I also tested levels of cyclin E1 and cyclin A2, which accumulate due to E2F-dependent transcription and therefore mark cell cycle entry and progression. Cyclin A2 levels, in particular, remain high during S/G2/M phases after which it is targeted for degradation at mitotic exit and so its levels are low in G0/G1 phase. Consequently, expression of cyclin A2 signifies these cells are in a proliferative state. I observed a reduction in mRNA levels of both cyclin E1 encoding gene (*CCNE1*) and cyclin A2 encoding gene (*CCNA2*) (Figure 3.1E). Reduction in *CCNA2* mRNA levels is supported by a reduction in cyclin A2 protein levels (Figure 3.1D). This data altogether further supports that samuraciclib induces a G1 arrest. This G1-dominated arrest could be due to CDK7 being required for maintaining CDK4 and CDK6 activities, and not CDK2 and CDK1 (Schachter *et al.*, 2013). This could explain why cells, following CDK7 inhibition, still progress through S-G2-M phases and arrest in the subsequent G1 phase.

Moreover, FUCCI data shows that samuraciclib acts mainly as a cytostatic drug rather than cytotoxic as almost no RPE1 cells undergo mitotic catastrophe and cell death after 48 hours of treatment (Figure 3.1C). This confirms previous work, using annexin V/propidium iodide, showing a non-significant increase in cells undergoing apoptosis after 96 hours of samuraciclib treatment and the absence of cleaved caspase-3, an apoptotic marker (Wilson, 2020; Wilson *et al.*, 2023). Therefore, cell death cannot account for the reduction in cell number.

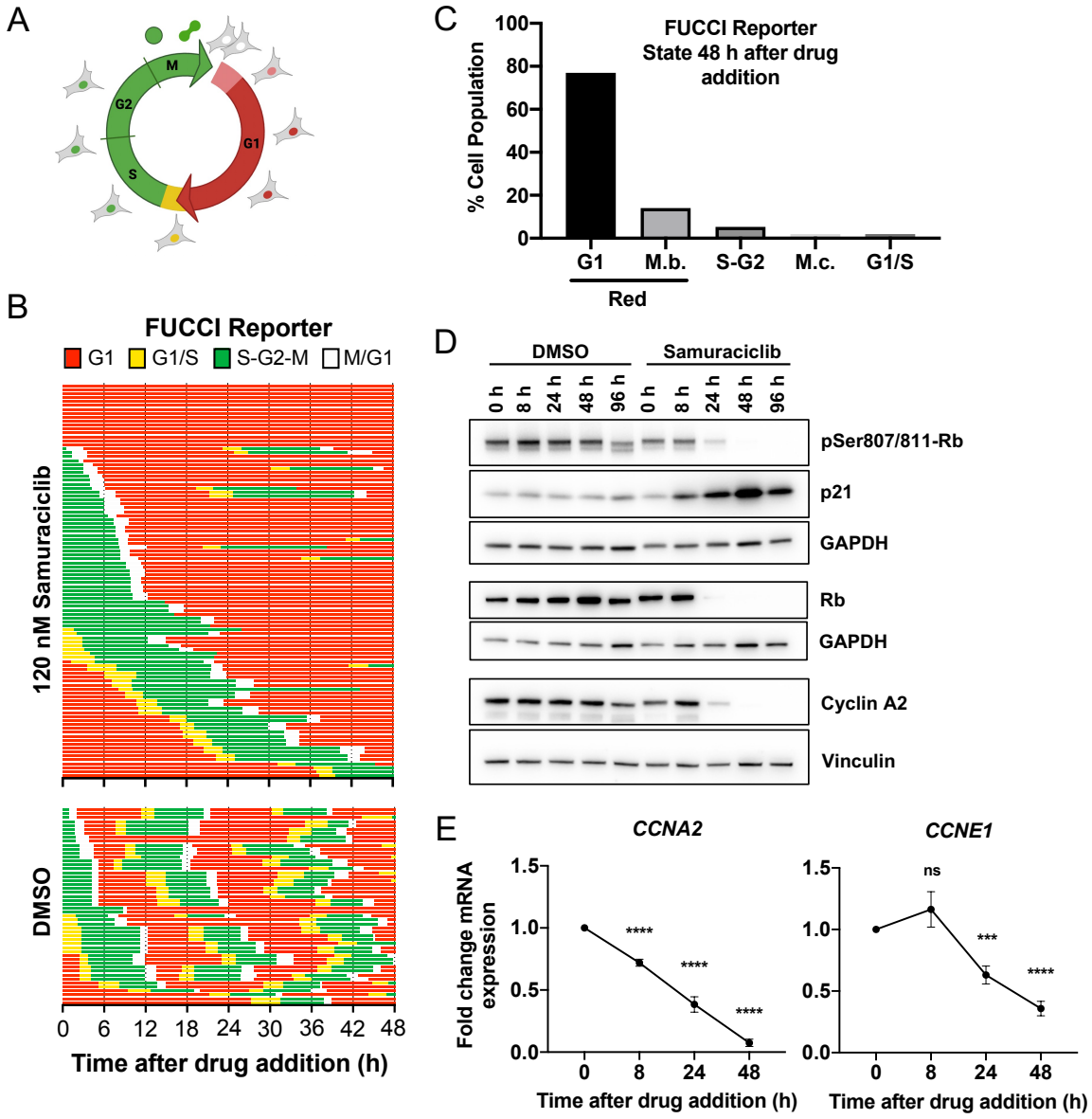

Figure 3.1: Samuraciclib induces a G1 cell cycle arrest.

Figure 3.1: (continued) **A)** Schematic of FUCCI reporter state. Illustration adapted from (Sakaue-Sawano *et al.*, 2008). Figure created with BioRender.com. **B)** RPE1 FUCCI cells were treated with vehicle control or 120 nM of samuraciclib and imaged for 48 hours. Cell cycle progression was monitored using the FUCCI reporter. State refers to cell cycle state based on tracking of FUCCI reporter where G1 is red, G1/S is yellow, S-G2-M is green and M/G1 is white (loss of signal). Representative tracks of 100 cells, at final time-point, are shown for samuraciclib treatment and 50 for vehicle control. **C)** Quantification of data of >200 cells tracked to determine cell cycle progression during 48 hours of samuraciclib treatment. State refers to cell cycle state at final time-point based on tracking of FUCCI reporter. G1 (red); M.b., mitotic bypass, where cells turn red without going through mitosis; S-G2 (green); M.c., mitotic catastrophe, where cells die after going through mitosis; and G1/S (yellow). **D)** Representative western blot of whole-cell extracts collected from RPE1 cells at indicated time-points after treatment with vehicle control or 120 nM of samuraciclib. GAPDH and vinculin: loading controls. **E)** RPE1 cells treated with 120 nM of samuraciclib were collected at indicated time-points and mRNA levels of *CCNA2* and *CCNE1* were analysed by RT-qPCR. Statistical significance was calculated using an unpaired two-tailed t test. Error bars are SD. Figure adapted from (Wilson *et al.*, 2023).

3.2. Samuraciclib does not induce a DNA damage response to cause a G1 arrest

The lack of cell death suggests that the samuraciclib-induced G1 arrest is cytostatic. However, I do observe a significant increase in the CDK inhibitor p21, which could be indicative of a role of the DNA damage response (DDR) in arresting cells in G1. ATM becomes activated in response to DNA damage and phosphorylates its downstream targets Chk2 and p53, which ultimately leads to an increased expression of p21 and a G1 cell cycle arrest (Matthews, Bertoli and de Bruin, 2022). I therefore checked whether samuraciclib treatment induces DNA damage signalling and thereby contributes to the robust G1 arrest. H2AX is a protein variant from the histone H2A family which becomes phosphorylated at serine residue 139 (γH2AX) by ATM upon DNA damage and formation of DNA double-strand breaks (Kinner *et al.*, 2008). I analysed the levels of γH2AX after samuraciclib treatment in both single cells using immunofluorescence (Figures 3.2A and 3.2B) and in whole-cell extracts using western blot (Figure 3.2C). Both revealed no significant increase in this DNA damage marker (Wilson *et al.*, 2023). As a positive control, I used camptothecin (CPT), a DNA topoisomerase I inhibitor, which is known to induce a DDR and therefore an increase in γH2AX (Berniak *et al.*, 2013). Moreover, I looked at the levels of Chk2 kinase

phosphorylated at threonine residue 68, which is phosphorylated by ATM in response to DNA damage. I used a DNA damage senescence-inducing topoisomerase II inhibitor, etoposide, as a positive control as it was previously shown to induce DNA damage and activate the DDR (te Poele *et al.*, 2002; Leontieva and Blagosklonny, 2010; Montecucco, Zanetta and Biamonti, 2015). In contrast to etoposide, 120 nM of samuraciclib does not lead to phosphorylated Chk2 (Figure 3.2D), which supports previous findings in a breast cancer MCF7 cell line at lower samuraciclib concentrations (Patel *et al.*, 2018). Overall, this data suggests that samuraciclib does not induce DNA damage nor activate the DNA damage signalling to arrest the cells in a G1 phase of the cell cycle.

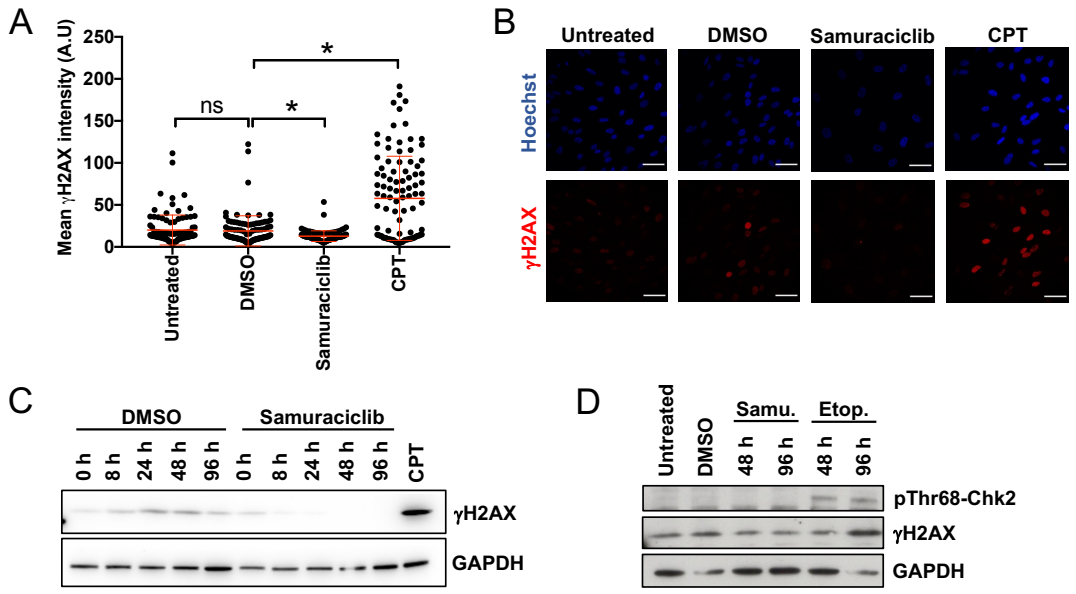

Figure 3.2: Samuraciclib treatment does not promote DNA damage signalling. **A)** RPE1 cells were treated with vehicle control or 120 nM of samuraciclib for 48 hours and 1 μM camptothecin (CPT) for 5 hours before cells were collected for immunofluorescent staining of γH2AX. Quantification of a representative experiment is shown where intensity of γH2AX was measured for 100 cells for each sample. Statistical significance was calculated using an unpaired two-tailed t test. Error bars are SD. **B)** Representative images of immunofluorescent staining of γH2AX from A. Scale bar represents 50 μm. **C)** Representative western blot of whole-cell extracts collected from RPE1 cells at the indicated time-points after treatment with vehicle control or 120 nM of samuraciclib. Cells treated with 2 μM CPT for 5 hours as a positive control. GAPDH: loading control. **D)** Western blot analysis from one experiment of whole-cell extracts collected from RPE1 cells, untreated or after treatment with vehicle control, 120 nM of samuraciclib (Samu., 48 and 96 hours) or 0.5 μg/ml etoposide (Etop., 48 and 96 hours). GAPDH: loading control. Figure adapted from (Wilson *et al.*, 2023).

3.3. Samuraciclib induces a permanent cell cycle exit via senescence

Previous work from Gemma Wilson indicated that the cell cycle exit induced by samuraciclib is via senescence, which I further confirm in the following section. An increase in senescence-associated β-galactosidase (SA β-gal) activity is traditionally the most frequently used senescence marker. This acidic lysosomal enzyme can be experimentally detected in senescent cells at suboptimal pH 6 due to its overexpression and increased lysosomal content (Kurz *et al.*, 2000; Campisi, 2013). Apart from the traditional cytochemical staining using X-gal as a β-gal substrate, SA β-gal activity can also be detected using another β-gal substrate, 5-dodecanoylaminofluorescein di-β-D-galactopyranoside (C_{12}FDG). This method is based on a fluorogenic substrate that can be detected using flow cytometry which yields a more quantitative result (Debacq-Chainiaux *et al.*, 2009; Cahu and Sola, 2013). Using this approach I show that after 96 hours of samuraciclib treatment, there is a statistically significant increase in SA β-gal activity, demonstrated by an increase in mean C_{12}FDG fluorescence (Figure 3.3A and 3.3B). However, increased SA β-gal activity, even though highly linked to senescence, can be caused by non-senescent reasons such as culturing cells at high confluence (Yang and Hu, 2005). Therefore, using several senescence markers is necessary.

Senescent cells change their morphology by increasing in size and volume, which can be measured using the Coulter counter. After 48 hours of samuraciclib treatment, cell volume is significantly increased compared to control cells (Figures 3.3C and 3.3D).

Moreover, the expression of a CDK inhibitor p21 is often increased in early senescence. As previously mentioned, p21 protein levels increase rapidly in response to samuraciclib treatment (Figure 3.1D). This is in line with a significant increase in mRNA levels of a p21 encoding gene, *CDKN1A*, after 48 hours (Figure 3.3E).

To further characterise senescence phenotypes, I analysed changes in both mRNA and protein levels of Lamin B1 in response to samuraciclib treatment (Figures 3.3E and 3.3F). Lamin B1 is a structural protein of the nuclear lamina and its levels have been shown to decrease in senescence as a result of its mRNA stability loss (Freund *et al.*, 2012). Western blot analysis of a timecourse of samuraciclib treatment showed a decrease of Lamin B1 levels after 24 hours (Figure 3.3F). I also checked *LMNB1*

mRNA levels after 48 hours of samuraciclib treatment and observed a significant decrease (Figure 3.3E), which is likely to contribute to the decrease in protein levels.

Finally, whilst counterintuitive, increased expression of cyclin D1 is also associated with senescence (Fukami *et al.*, 1995; Leontieva, Demidenko and Blagosklonny, 2013). I observed a significant increase in mRNA levels of *CCND1* after 48 hours of samuraciclib treatment (Figure 3.3E), providing another marker that indicates that samuraciclib treatment induces a senescent state.

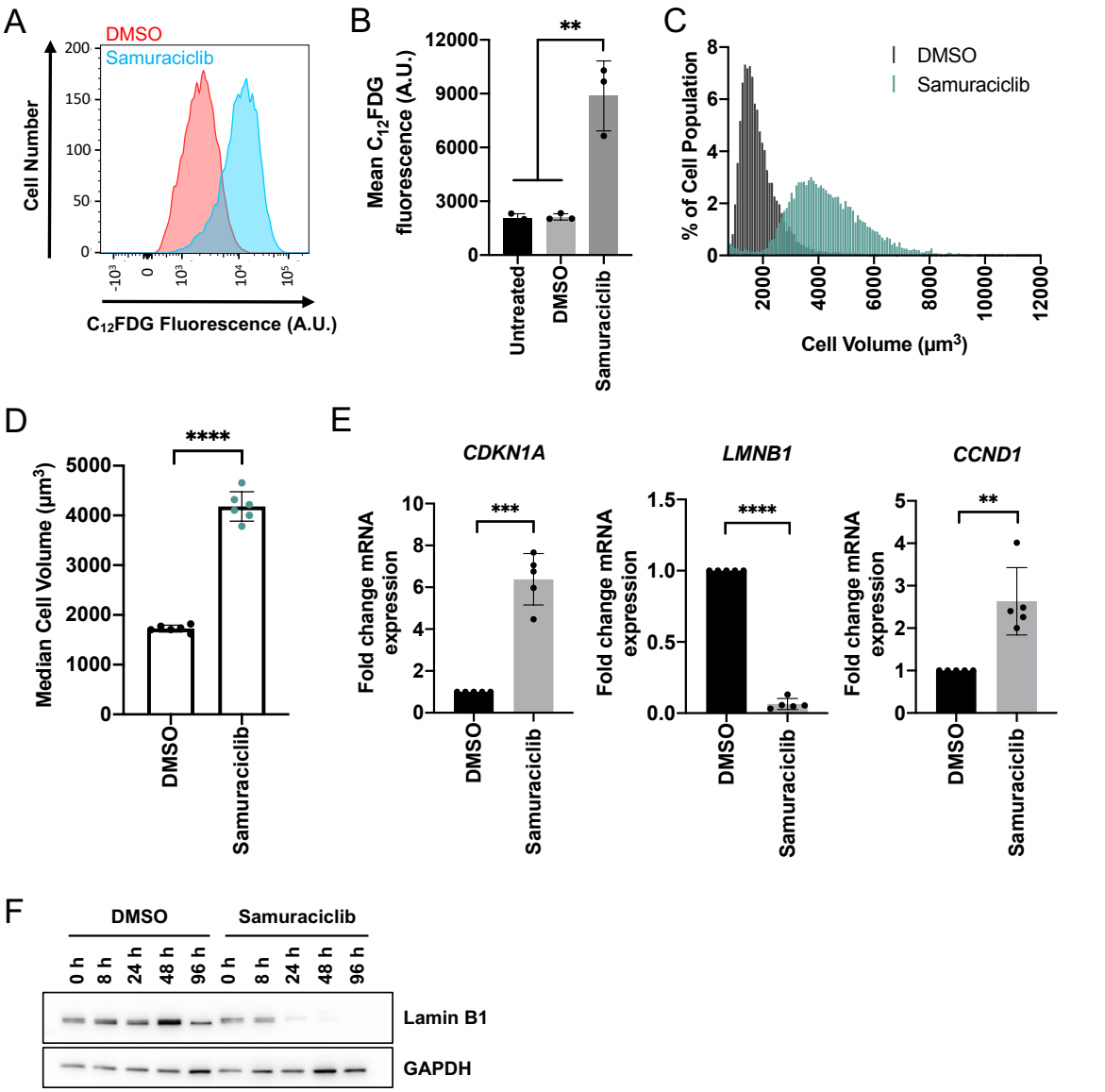

Figure 3.3: Samuraciclib induces senescence in RPE1 cells.

Figure 3.3: (continued) **A)** Flow cytometry data from a representative experiment, detecting SA β-gal activity with the fluorescent β-gal substrate, C_{12}FDG, in cells treated with vehicle control or 120 nM of samuraciclib for 96 hours. C_{12}FDG fluorescence is plotted against cell count. **B)** Quantification of the mean C_{12}FDG fluorescence from three independent experiments (representative shown in A). Statistical significance was calculated using an unpaired two-tailed t test. Error bars are SD. **C)** Coulter counter data from a representative experiment, with RPE1 cells treated with vehicle control or 120 nM samuraciclib for 48 hours. Percentage of cell population is plotted against various bins containing cells with different volumes in μm^3. **D)** Coulter counter data quantification of the median cell volume within the population from six independent experiments (representative shown in C). Statistical significance was calculated using an unpaired two-tailed t test. Error bars are SD. **E)** RPE1 cells that were treated with vehicle control or 120 nM of samuraciclib were collected after 48 hours and mRNA levels of *CDKN1A*, *LMNB1*, *CCND1* were analysed by RT-qPCR from five independent experiments. Statistical significance was calculated using an unpaired two-tailed t test. Error bars are SD. **F)** Representative western blot of whole-cell extracts collected from RPE1 cells at the indicated time-points after treatment with vehicle control or 120 nM of samuraciclib. GAPDH: loading control.

Altogether, the results from Figure 3.3 indicate that samuraciclib induces a senescent phenotype in RPE1 cells. However, the true hallmark of a senescent state is an irreversible exit from the cell cycle. Therefore, upon drug removal, senescent cells would not return to a proliferative state but remain arrested. Samuraciclib is a compound that is non-covalently bound and can therefore be washed away. To test the reversibility of samuraciclib, I treated RPE1 cells for 1 or 5 hours with samuraciclib and washed the drug away by doing five PBS washes. I then added fresh media and cultured cells without the drug for another 4 days as illustrated in Figure 3.4A schematic. After samuraciclib wash-out, p21 and phosphorylated Rb protein levels are comparable to cells treated with vehicle control (DMSO), indicating these cells are not arrested and are cycling as control cells (Figure 3.4B). Moreover, CDK1 phosphorylation at threonine residue 161, which is a residue phosphorylated by CDK7, is not reduced (Figure 3.4B). This suggests that samuraciclib and its effect on CDK7 inhibition is reversible and can be washed away from cells.

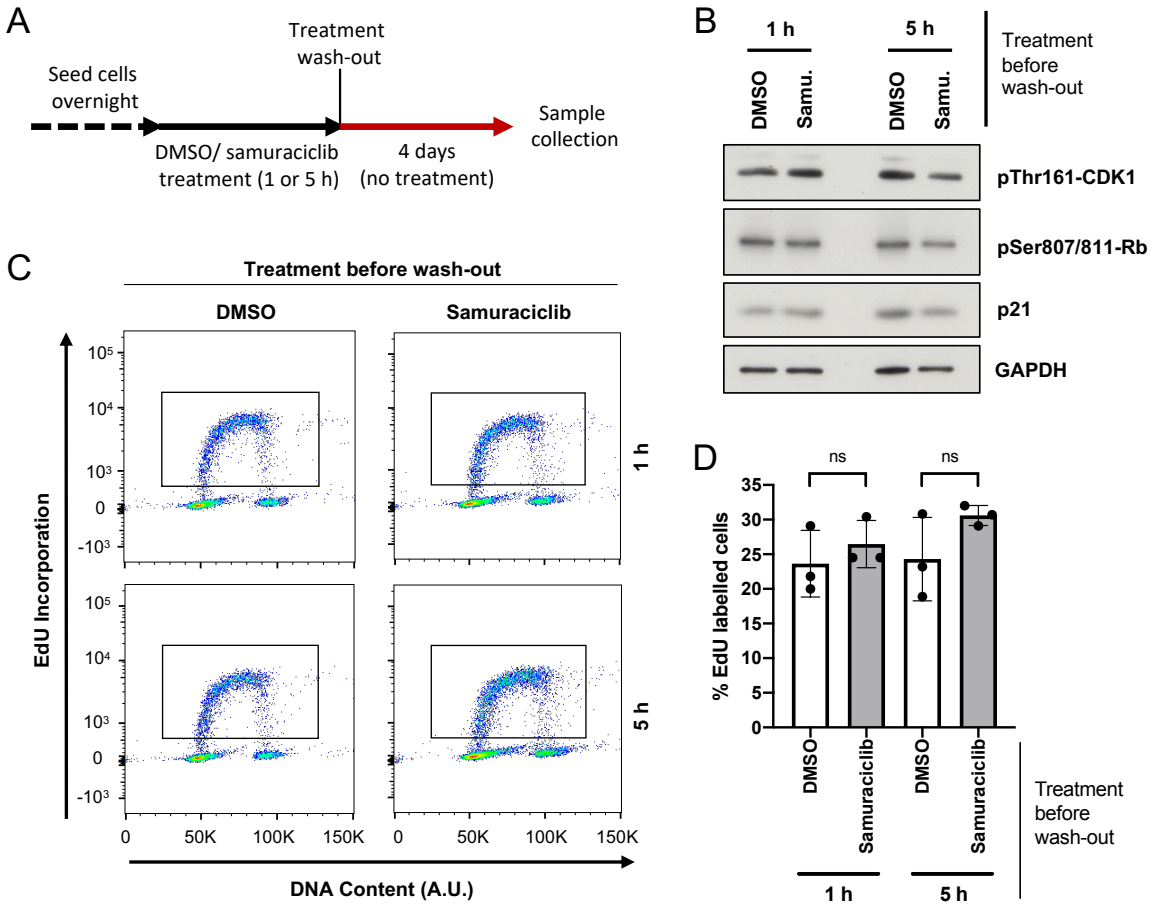

Figure 3.4: A non-covalent CDK7 inhibitor, samuraciclib, can be washed out from cells.
A) A schematic illustrating the experimental set up. RPE1 cells were seeded overnight and treated with vehicle control or 120 nM of samuraciclib for 1 or 5 hours. After the treatment, cells were washed five times with PBS to remove samuraciclib from cells, fresh media was added, and cells were cultured for another 4 days. Cells were then harvested for western blot analysis and EdU incorporation analysis by flow cytometry. **B)** Representative western blot of whole-cell extracts collected from RPE1 cells 4 days after drug wash-out following the indicated DMSO or 120 nM of samuraciclib (Samu.) treatment durations (n=3). GAPDH: loading control. **C)** RPE1 cells were treated with vehicle control or 120 nM of samuraciclib as indicated in schematic in panel A. 4 days after drug wash-out, cells were incubated with EdU for 1 hour before collection. Pseudocoloured plots of flow cytometry data from a representative experiment. DNA content is plotted against EdU incorporation. Inset gate drawn to include EdU-positive cells. **D)** Quantification of the percentage of EdU-positive cells from three independent experiments (representative shown in C). Statistical significance was calculated using an unpaired two-tailed t test. Error bars are SD.

To confirm this western blot analysis of proliferative markers, I analysed cell cycle dynamics using 5-ethynyl-2'-deoxyuridine (EdU) incorporation coupled with DAPI to measure DNA content by flow cytometry. EdU is a thymidine analogue that

incorporates into newly synthesized DNA during S phase which allows for quantification of the EdU-positive population, which represents actively replicating cells (Buck *et al.*, 2008). 4 days after washing-out samuraciclib, I incubated cells with EdU for 1 hour before harvesting the cells in order to obtain a snapshot of the population of proliferating cells. There is no significant decrease of EdU-positive cells following the drug removal compared to the DMSO control (Figures 3.4C and 3.4D). This confirms the western blot analysis and suggests that this non-covalent CDK7 inhibitor can be washed out from the cells using this protocol.

Gemma Wilson observed that the cell cycle arrest induced after 48 hours of samuraciclib treatment persists 5 days after drug wash-out in RPE1 cells, demonstrated by the lack of EdU incorporation (Wilson *et al.*, 2023). I confirmed this finding using a colony formation assay. Following a 48-hour treatment, I seeded cells at low numbers and left them in culture for approximately 10 days to test how many individual cells are able to form a colony. I use this read-out to assess the proliferative potential of cells in each condition. The results show that there is a significant decrease in proliferative potential after 48 hours of samuraciclib treatment compared to the DMSO control (Figures 3.5A and 3.5B). However, this assay does not specify whether the reduction in the ability to form colonies is due to an extended cell cycle arrest or cell death. To assess this, I carried out live-cell imaging using the FUCCI reporter system. I treated RPE1 FUCCI cells with samuraciclib for 72 hours, washed the drug away and started timelapse imaging for 72 hours. I marked FUCCI red cells at the first time-point which represent G1 arrested cells after samuraciclib treatment and monitored their cell cycle fate after drug wash-out. The majority of cells (~65%) remain arrested in G1, suggesting permanent cell cycle exit, likely via senescence, as the main outcome (Figures 3.5C and 3.5D). A much smaller number of cells (~11%) undergo cell death from G1 phase of the cell cycle (Figures 3.5C and 3.5D). Furthermore, around 24% of FUCCI red cells re-enter the cell cycle after samuraciclib arrest, which is determined by a yellow colour switch. Of those cells that enter a new cell cycle, around 40% undergo mitotic bypass, where cells turn red (enter the G1 state) without undergoing mitosis, and most likely also enter a senescent state. Taken together, the data from Figure 3.5 suggests that samuraciclib induces a permanent exit from the cell cycle, likely via senescence.

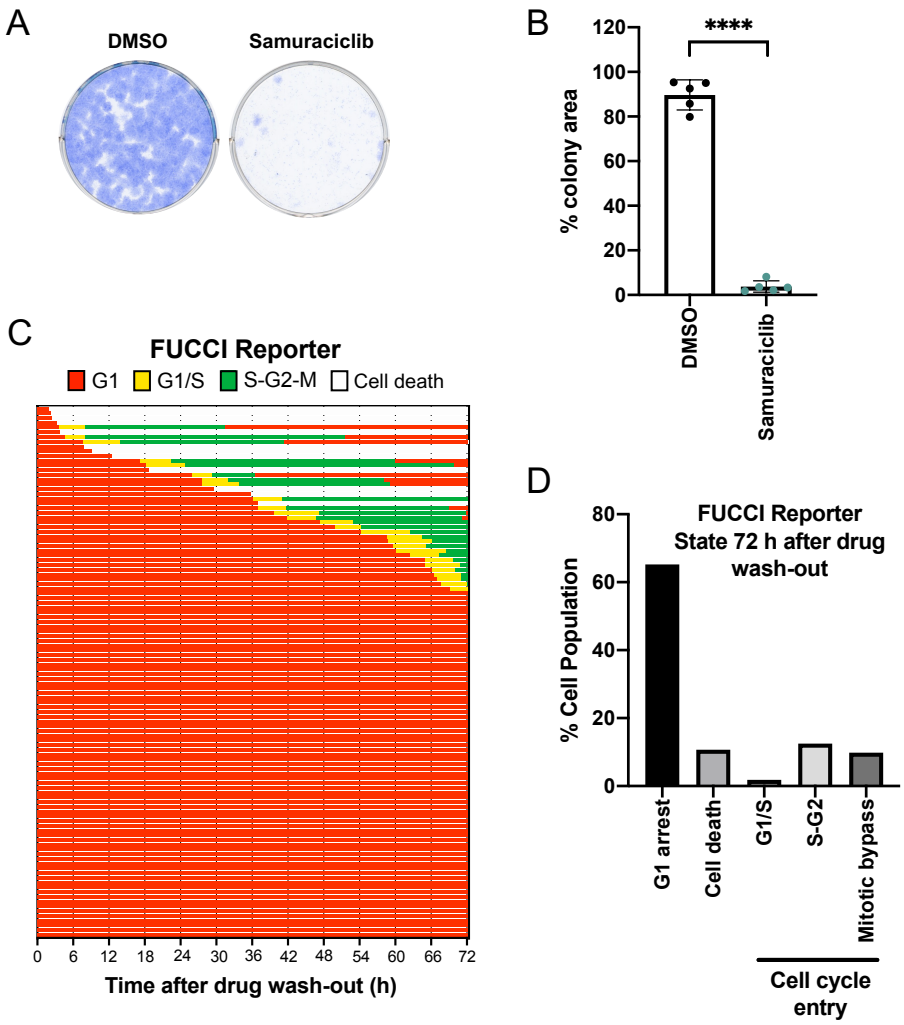

Figure 3.5: Samuraciclib induces a permanent cell cycle exit in RPE1 cells.
A) RPE1 cells were treated with vehicle control or 120 nM of samuraciclib for 48 hours. After 48 hours, cells were washed five times with PBS to remove samuraciclib from cells. Cells were re-seeded in the absence of drugs and allowed to grow for 9-11 days. Colonies were stained and visualised with Methylene Blue. **B)** Quantification of percentage of colony area from five independent experiments (representative shown in A). Statistical significance was calculated using an unpaired two-tailed t test. Error bars are SD. **C)** RPE1 FUCCI cells were treated with 120 nM of samuraciclib for 72 hours. After 72 hours, cells were washed five times with PBS to remove samuraciclib from the cells, and fresh media was added, after which live-cell imaging was started for 72 hours. Cell cycle progression was monitored using the FUCCI reporter. State refers to cell cycle state based on tracking of FUCCI reporter where G1 is red, G1/S is yellow, S-G2-M is green and cell death is white (loss of signal). Tracks of 112 cells are shown. **D)** Quantification of data from C. 112 FUCCI red cells (G1 arrest) were tracked to determine cell cycle progression during 72 hours of drug wash-out. State refers to cell cycle fate at final time-point based on tracking of FUCCI reporter. G1 arrest, where cells remain red; Cell death, where cells die in G1; G1/S, yellow; S-G2, green; and Mitotic bypass; where cells turn red without going through mitosis.

3.4. CDK7 knock-down increases sensitivity to samuraciclib

Samuraciclib was previously shown to selectively bind to CDK7, with some degree of binding affinity to other kinases, such as CDK2 and CDK9 at higher concentrations (Patel *et al.*, 2018; Constantin *et al.*, 2023). Therefore, I wanted to investigate whether samuraciclib has any off-target effects in RPE1 cells via a siRNA-mediated knock-down of CDK7.

I first checked whether transfection *per se* has an effect on RPE1 cells and treatments. I left cells untransfected or transfected with a non-targeting control siRNA (siCONT) and treated both conditions with either vehicle control (DMSO) or samuraciclib. I carried out EdU incorporation assay after 48 hours of treatment to test the effect on proliferation. There is no significant difference in the percentage of actively replicating cells between the untransfected and transfected conditions (Figures 3.6A and 3.6B). Western blot analysis of proliferative markers confirms these results (Figure 3.6C), demonstrating that transfection itself with non-targeting siRNA does not affect the phenotype observed upon samuraciclib treatment. I therefore continued using non-targeting control siRNA (siCONT) as a control condition in siRNA-mediated knock-down experiments.

I then tested whether knocking down CDK7 has a similar effect on cellular proliferation to samuraciclib treatment by carrying out EdU incorporation assay. Depletion of CDK7 using a siRNA-mediated knock-down does not recapitulate samuraciclib effects. There is no significant difference in the percentage of actively replicating cells between DMSO-treated control and CDK7-depleted RPE1 cells (Figures 3.7A and 3.7B). Depleting CDK7 does not arrest cellular proliferation as the CDK7 inhibitor. These cell cycle flow cytometry analyses are also supported by western blot analysis of proliferative markers, where there is no difference in cyclin A2, phosphorylated Rb or p21 levels (Figure 3.7C). Although I show that siRNA-mediated knock-down of CDK7 is efficient in this protocol and that CDK7 protein levels can be decreased in RPE1 cells, they are not fully reduced (Figure 3.7C). A small amount of CDK7 might still be able to carry out its function by phosphorylating and in turn activating its targets, the mitotic CDKs, and therefore allow proliferation in RPE1 cells. Whilst this needs to be tested, this is in line with previously published data that shows how siRNA-mediated

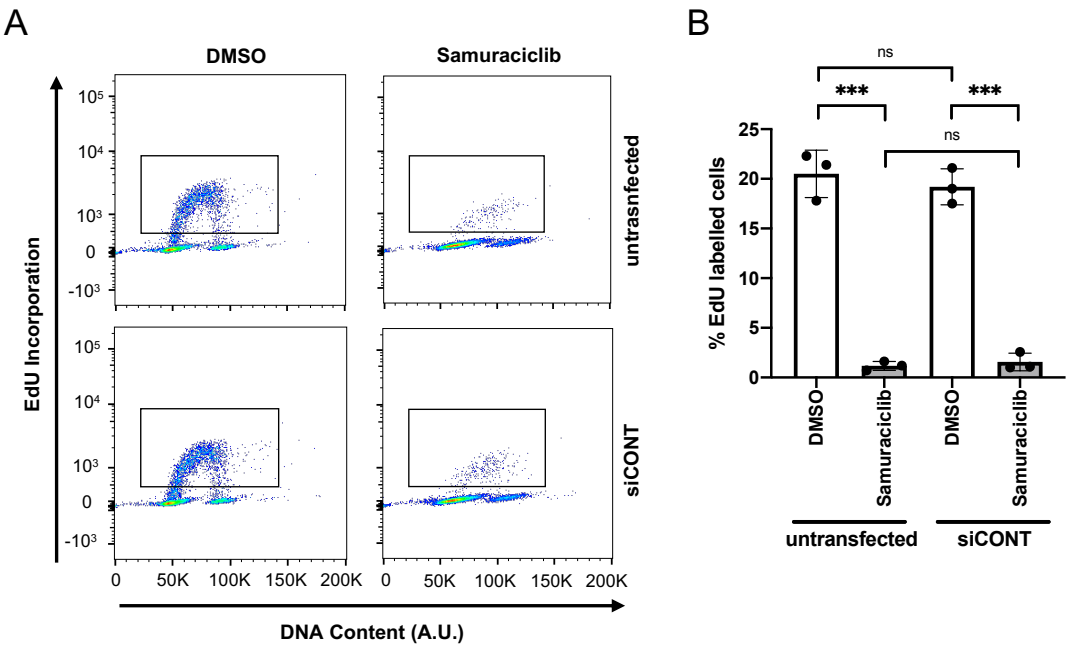

Figure 3.6: Transfection does not affect RPE1 cells and the effect of samuraciclib on proliferation.
A) RPE1 cells that were either left untransfected or transfected with a non-targeting siRNA (siCONT) were treated with vehicle control or 120 nM of samuraciclib for 48 hours. Cells were then incubated with EdU for 1 hour before collection. Pseudocoloured plots of flow cytometry data from a representative experiment. DNA content is plotted against EdU incorporation. Inset gate drawn to include EdU-positive cells. **B)** Quantification of the percentage of EdU-positive cells from three independent experiments (representative shown in A). Statistical significance was calculated using an unpaired two-tailed t test. Error bars are SD.

depletion of CDK7 levels by 50-75% only partially reduced CDK2 activation (Wohlbold *et al.*, 2006). Therefore, more efficient and acute CDK7 depletion approaches are necessary to investigate off-target effects of samuraciclib. This could be carried out by mutating the wild-type CDK7 in RPE1 cells to an analogue-sensitive CDK7 that can be inhibited by bulky adenine analogues as was carried out previously in a human colon cancer cell line (Larochelle *et al.*, 2007; Merrick *et al.*, 2008; Schachter *et al.*, 2013). Moreover, different selective CDK7 inhibitors, such as YKL-5-124 or LY3405105 could be tested and compared to samuraciclib phenotypes. Published data shows that YKL-5-124 includes cytostatic effects rather than cytotoxic, by arresting cells in a G1 phase of the cell cycle similarly to samuraciclib (Olson *et al.*,

2019). Further experiments should be done to test whether this cell cycle exit is irreversible via senescence.

Whilst RNAi-mediated knock-down of CDK7 does not recapitulate samuraciclib phenotypes, reducing CDK7 levels should make the cells more sensitive to samuraciclib. To test this, I treated control and CDK7-depleted cells with a range of lower concentrations of samuraciclib than the IC_{50} value (120 nM). CDK7 depletion causes a reduction of EdU-positive cells at lower samuraciclib concentrations than control-treated cells (Figure 3.7A and 3.7B). Specifically, at 15 nM of samuraciclib, CDK7-depleted cells are significantly more arrested compared to control-treated cells. This is further supported by a greater decrease in cyclin A2 and phosphorylated Rb levels at lower samuraciclib concentrations (15 and 30 nM) in CDK7-depleted cells compared to the control (Figure 3.7C). This suggests that reducing CDK7 protein levels increases sensitivity to samuraciclib.

In addition, cell size increases at a lower samuraciclib concentration in CDK7-depleted RPE1 cells compared to the control (Figures 3.7D and 3.7E). I measured cell size using the flow cytometry forward scatter (FSC) as it has been shown to correlate with cell volume and therefore can be used as a proxy of cell size (Shapiro, 2005; Berenson *et al.*, 2019; Neurohr *et al.*, 2019).

Taken together, CDK7 knock-down does not recapitulate the decrease in actively replicating cells observed with the CDK7 inhibitor samuraciclib, but this is likely due to the incomplete loss of CDK7 protein rather than more specific inhibition. However, CDK7 depletion renders cells more sensitive to lower doses of samuraciclib indicating that CDK7 knock-down does lower the cellular CDK7 activity.

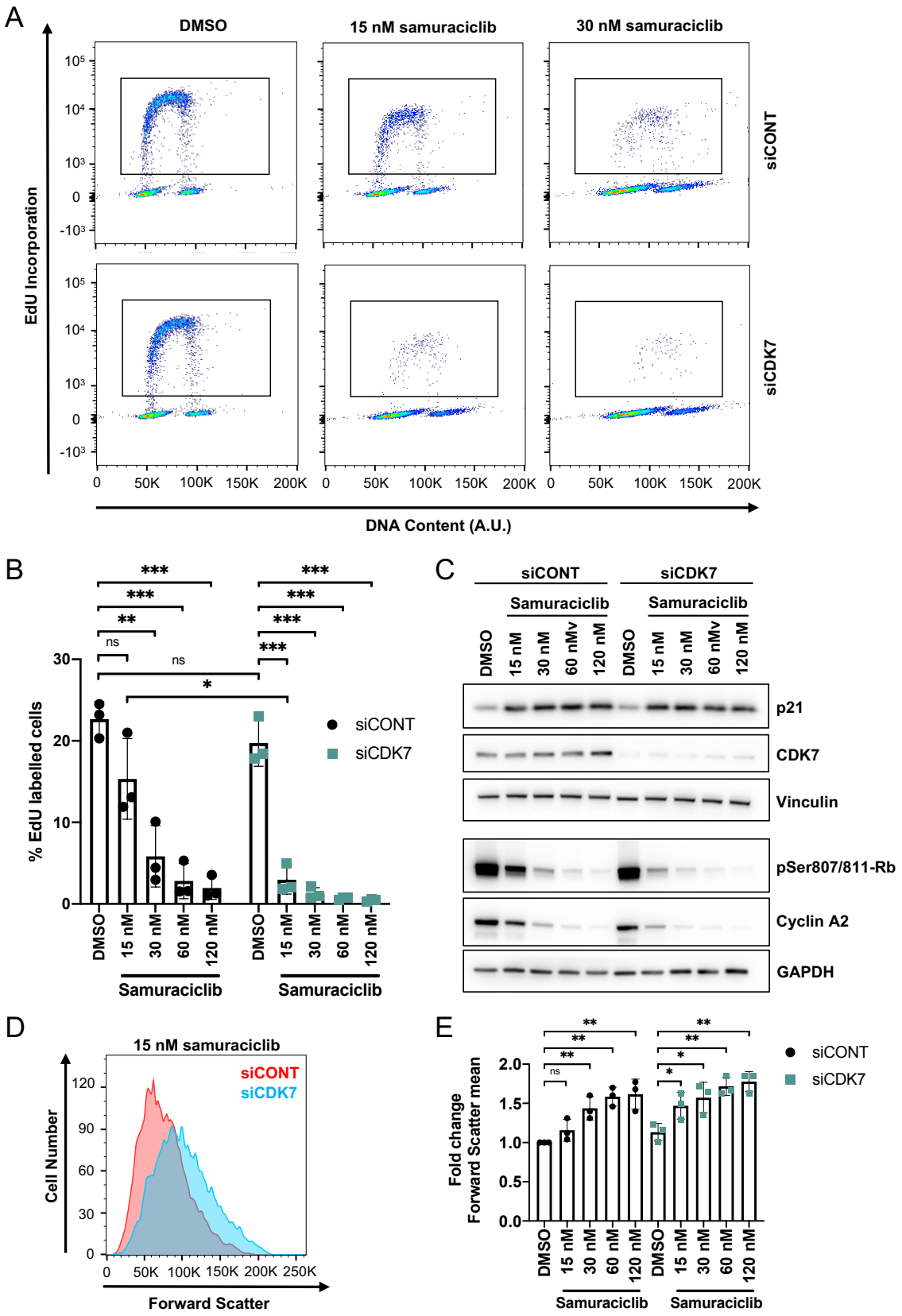

Figure 3.7: CDK7 knock-down increases sensitivity to samuraciclib in RPE1 cells.

Figure 3.7: (continued) RPE1 cells transfected with a non-targeting siRNA (siCONT) and siRNA targeting CDK7 (siCDK7) were treated with vehicle control or indicated concentrations of samuraciclib for 48 hours. **A)** Cells were incubated with EdU for 1 hour before collection. Pseudocoloured plots of flow cytometry data from a representative experiment. DNA content is plotted against EdU incorporation. Inset gate drawn to include EdU-positive cells. **B)** Quantification of the percentage of EdU-positive cells from three independent experiments (representative shown in A). Statistical significance was calculated using an unpaired two-tailed t test. Error bars are SD. **C)** Western blot analysis of whole-cell extracts. Vinculin: loading control. **D)** Flow cytometry data from a representative experiment. Forward scatter, a measure of cell size, is plotted against cell count. **E)** Flow cytometry data from D where fold change of mean forward scatter value, a measure of cell size, is calculated relative to siCONT DMSO control. Statistical significance was calculated using an unpaired two-tailed t test. Error bars are SD.

3.5. Genome-wide CRISPR KO chemogenetic screen identifies cellular growth, via mTOR signalling, as an important determinant of samuraciclib sensitivity

To identify processes required for sensitivity to samuraciclib treatment and thus to reveal mechanisms by which samuraciclib induces senescence, our collaborators, the laboratory of Mike Tyers at Montreal University, Canada, carried out a genome-wide CRISPR KO chemogenetic screen. They used a human B-cell precursor leukemia cell line, NALM-6. These cells grow in suspension culture, which makes synthetic genetic interaction screening quick and cost-efficient (Bertomeu et al., 2018). Gemma Wilson confirmed that NALM-6 cells are sensitive to samuraciclib, reducing proliferation by predominantly arresting cells in the G1 phase of the cell cycle (Wilson, 2020; Wilson *et al.*, 2023). However, their sensitivity is much lower than the sensitivity of RPE1 cells. At 350 nM of samuraciclib, there is around 30% reduction in the number of actively replicating cells after 48 hours. This concentration is around three times higher than the concentration at which, in RPE1 cells, there is almost a complete reduction in actively replicating cells. This lower sensitivity makes these cells a more suitable choice for the chemogenetic screen as it allows for identification of both positive and negative drug-gene interactors.

Our collaborators used a custom extended-knockout (EKO) library of 278754 single-guide RNAs (sgRNAs) which target 19084 RefSeq genes, 20852 alternatively spliced

exons and 3782 hypothetical genes (Bertomeu *et al.*, 2018). To calculate the relative abundance of each sgRNA, they developed a custom statistical tool called Robust Analytics and Normalization for Knock-out Screens (RANKS) (Bertomeu *et al.*, 2018). This analysis allows for identification of positive and negative interactors, when sgRNA abundance of drug-treated cells is compared to DMSO-control population. Positive interactors, which correspond to relative enrichment of sgRNAs, represent genes that when deleted make cells less sensitive and are therefore required for drug sensitivity. Their inactivation or depletion could result in potential resistance mechanisms. Negative interactors, which correspond to relative depletion of sgRNAs, on the other hand, represent genes that when deleted make cells more sensitive and therefore have a role in reducing sensitivity to the drug. Their inactivation or depletion could therefore increase drug sensitivity (Wilson *et al.*, 2023).

The initial screen was carried out with 350 nM of samuraciclib and based on the RANKS values provided by the Tyers lab, Gemma Wilson carried out Gene Ontology (GO) analysis and the screen results were published (Wilson, 2020; Wilson *et al.*, 2023). The analysis identified “TOR signalling” and “positive regulation of TOR signalling” among the top 20 positive interactors and “negative regulation of TOR signalling” among the top 20 negative interactors. This revealed that active mTOR signalling might be required for samuraciclib sensitivity.

Afterwards, the Tyers lab carried out three additional genome-wide CRISPR KO chemogenetic screens using samuraciclib: an additional one with 350 nM of samuraciclib, one screen with 180 nM and one with 501 nM of samuraciclib, and provided us with the RANKS values. These two additional concentrations are within the range of concentrations that were previously shown to significantly decrease percentage of S phase cells (Wilson, 2020; Wilson *et al.*, 2023). I then obtained an average RANKS score from the four screens. The top 20 positive and negative interactors with samuraciclib, based on the average RANKS score, are listed in Tables 3.1 and 3.2 respectively, and their functions are obtained from the UniProt database (The UniProt Consortium, 2023).

Table 3.1: Top 20 positive interactors with samuraciclib based on RANKS score.

Gene	RANKS score				Average RANKS score	Function
	180 nM	350 nM (exp.1)	350 nM (exp.2)	501 nM		
TP53	2.24	2.02	3.39	4.03	2.92	Tumour suppressor, transcription factor
MLST8	1.53	2.84	3.05	3.91	2.8325	Subunit of mTORC1 and mTORC2
MAPKAP1	1.19	3.46	3.58	3.09	2.83	Subunit of mTORC2
EIF4A1	1.95	3.12	2.9	2.69	2.665	ATP-dependent RNA helicase; subunit of the eIF4F complex
SPOP	1.45	3.38	2.09	2.82	2.435	Component of cullin-RING-based BCR E3 ubiquitin-protein ligase complex
YLPM1	3.14	2.47	2.57	1.35	2.3825	Regulation of telomere maintenance
RICTOR	1.2	2.82	3.86	1.55	2.3575	Subunit of mTORC2
PTPMT1	1.87	2.42	2.11	2.39	2.1975	Lipid phosphatase
UBE2G2	2.19	2.11	2.41	1.89	2.15	Member of E2 ubiquitin-conjugating enzyme family
GFM2	1.78	2.12	2.36	2.33	2.1475	Mitochondrial GTPase; one of the mitochondrial translation elongation factors
C15orf41	1.53	1.72	2.71	2.58	2.135	Role in erythroid cell differentiation
DARS2	2.19	2.3	1.89	2.14	2.13	Class-II aminoacyl-tRNA synthetase family
PIK3CD	2.51	1.32	2.2	2.2	2.0575	Phosphorylates phosphatidylinositol
INTS12	1.71	2.08	1.64	2.78	2.0525	Component of the Integrator complex
YARS2	2.91	1.9	2.02	1.36	2.0475	Catalyses attachment of tyrosine to tRNA

Table 3.1: (continued)

Gene	RANKS score				Average RANKS score	Function
	180 nM	350 nM (exp.1)	350 nM (exp.2)	501 nM		
DNLZ	2.38	1.96	2.34	1.44	2.03	Predicted to enable chaperone binding activity
SRM	2.75	1.88	1.48	1.86	1.9925	Catalyses production of spermidine
CD81	1.84	2.38	1.4	2.09	1.9275	Structural component of membrane tetraspanin-enrichment microdomains
ODC1	2.26	2.27	2.28	0.87	1.92	Catalyses rate-limiting step of polyamine biosynthesis
TNPO1	2.66	0.75	1.72	2.5	1.9075	Nuclear transport receptor
HEATR3	1.97	1.82	2.08	1.63	1.875	Role in ribosome biogenesis

Table 3.2: Top 20 negative interactors with samuraciclib based on RANKS score.

Gene	RANKS score				Average RANKS score	Function
	180 nM	350 nM (exp.1)	350 nM (exp.2)	501 nM		
GPR107	-3.45	-3.69	-5.01	-3.97	-4.03	Proposed to act as a receptor to neuronostatin
SLC5A3	-3.42	-4.09	-3.59	-2.59	-3.4225	Electrogenic Na^+-coupled sugar symporter
ARL1	-3.02	-4.08	-3.12	-2.7	-3.23	GTP-binding protein
YPEL5	-1.51	-2.91	-2.68	-3.56	-2.665	Component of CTLH E3 ubiquitin-protein ligase complex
UBE2H	-1.09	-2.2	-3.94	-3.3	-2.6325	Member of E2 ubiquitin-conjugating enzyme family

Table 3.2: (continued)

Gene	RANKS score				Average RANKS score	Function
	180 nM	350 nM (exp.1)	350 nM (exp.2)	501 nM		
ARMC5	-2.65	-3.12	-2.67	-1.83	-2.5675	Member of armadillo/beta-catenin-like repeat superfamily
NPRL3	-1.26	-3.47	-2.58	-2.94	-2.5625	Component of GATOR1 complex
ATP6V0A2	-2.61	-2.09	-2.19	-3.19	-2.52	Subunit of vacuolar ATPase
VPS25	-3.22	-2.53	-2.58	-1.73	-2.515	Component of ESCRT-II complex
CCNT1	-0.38	-2.7	-3.17	-3.34	-2.3975	Regulatory subunit of CDK9
TSSC1	-1.83	-2.48	-2.46	-2.26	-2.2575	Component of endosomal retrieval machinery
CCNB1	-1.59	-3.16	-2.48	-1.78	-2.2525	Control of cell cycle at G2/M transition
TCF4	-3.18	-2.53	-1.49	-1.7	-2.225	Transcription factor that binds to immunoglobulin enhancer Mu-E5/KE5-motif
SCYL1	-0.96	-2.64	-2.72	-2.54	-2.215	Regulates COPI-mediated retrograde protein traffic at the interface between Golgi and ER
GPX4	-1.28	-2.34	-2.37	-2.83	-2.205	Antioxidant peroxidase
MSI2	-2.51	-2.72	-1.98	-1.58	-2.1975	RNA binding protein; regulates expression of target mRNAs at translational level
JTB	-1.81	-2.25	-2.25	-2.42	-2.1825	Involved in mitotic cytokinesis

Table 3.2: (continued)

Gene	RANKS score				Average RANKS score	Function
	180 nM	350 nM (exp.1)	350 nM (exp.2)	501 nM		
DEPDC5	-1.59	-3.31	-1.82	-1.93	-2.1625	Component of GATOR1 complex
TOE1	-2.47	-1.91	-2.7	-1.55	-2.1575	Inhibits cell growth rate and cell cycle
ARFPR1	-2.21	-2.31	-1.93	-1.98	-2.1075	Trans-Golgi-associated GTPase; regulates protein sorting

I initially carried out GO analysis on these top 20 positive and negative interactors (Tables 3.1 and 3.2). However, the FDR q-values were equal to 1 for GO terms enriched within the negative interactors, making them insignificant. Therefore, I carried out GO analysis on the top 50 positive and negative interactors with samuraciclib using the GOrilla tool (Eden *et al.*, 2009) and processing by REVIGO (Supek *et al.*, 2011) to remove redundant GO terms (Figure 3.8). This analysis also indicates the importance of mTOR signalling in samuraciclib sensitivity. “TOR signalling” and “TORC2 signalling” are among the most enriched GO terms of positive interactors (Figure 3.8A) and “negative regulation of TOR signaling” and “regulation of TOR signaling” are among the most enriched GO terms of negative interactors (Figure 3.8B). The specific positive interactors found in GO terms related to mTOR signalling, which are necessary for samuraciclib sensitivity, are highlighted in magenta in the protein interaction network (Figures 3.9A). These genes are needed for active mTOR signalling. On the other hand, the specific negative interactors found in GO terms related to mTOR signalling, which might reduce samuraciclib activity, are highlighted in magenta in the protein interaction network (Figures 3.9B) and these include genes that inhibit mTOR signalling. Altogether, this data suggests that active mTOR signalling is an important factor in samuraciclib’s mechanism of action and for its sensitivity.

A

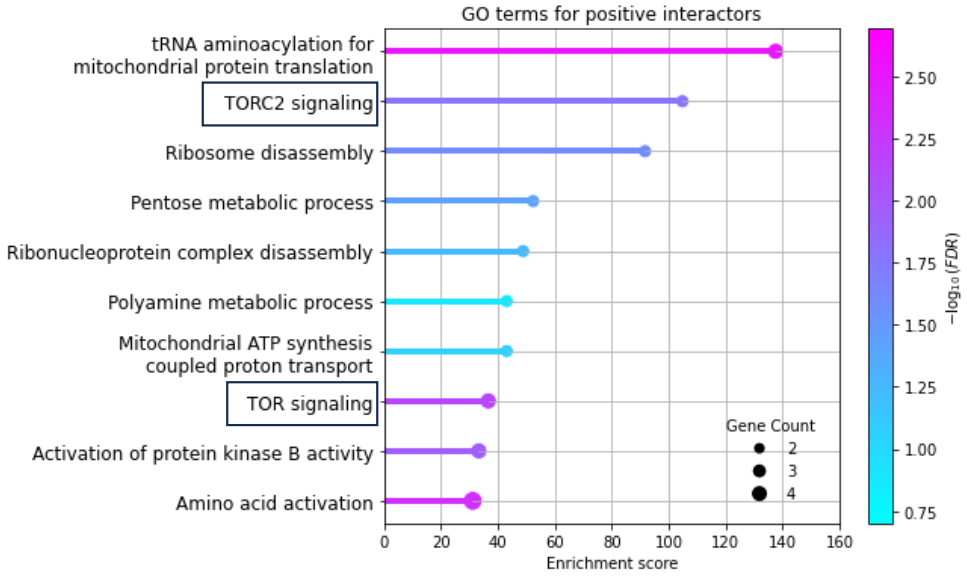

B

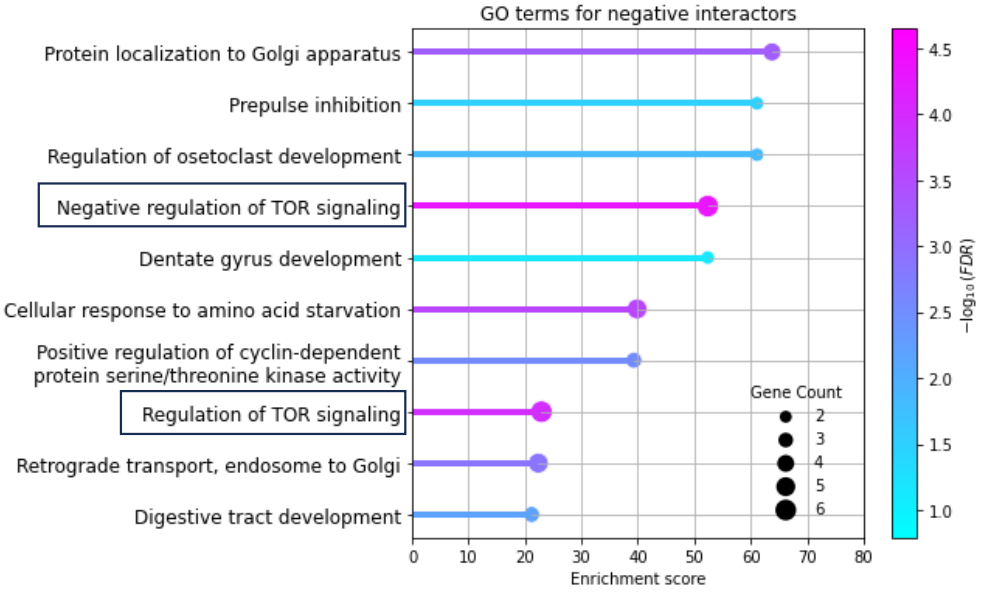

Figure 3.8: Genome-wide CRISPR KO chemogenetic screen identifies active mTOR signalling as an important determinant of samuraciclib sensitivity.
Pathway enrichment bubble plot representations of the most enriched GO terms among the top 50 interactors with samuraciclib, as determined using the GOrilla tool and processing by REVIGO. The GO terms are ordered by their enrichment score. Colour coding represents the -$\log_{10}$(false discovery rate [FDR] q-value), with the most statistically significant GO terms closer to the magenta end of the scale found on the right, and the least statistically significant GO terms closer to the light blue end of the scale. GO terms that include mTOR signalling are highlighted by the black boxes. Bubble size indicates number of genes associated with each GO term. Graphs were created using Matplotlib package in Python. **A)** Representation of the most enriched GO terms among the top 50 positive interactors with samuraciclib. **B)** Representation of the most enriched GO terms among the top 50 negative interactors with samuraciclib.

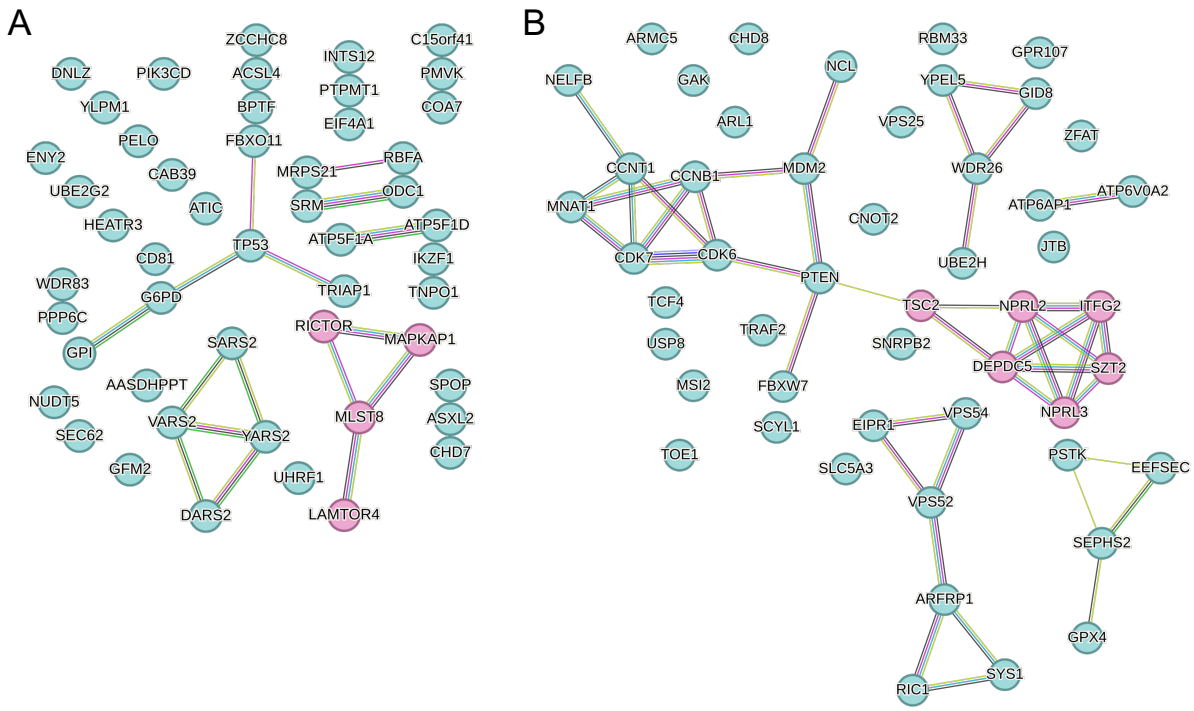

Figure 3.9: Components of the mTOR signalling pathway identified among the top 50 positive and negative interactors with samuraciclib.
A) Protein interaction network representation of the top 50 positive interactors with samuraciclib. Nodes of genes found in GO terms that include mTOR signalling (highlighted in boxes in Figure 3.8A) are coloured in magenta. Network was created in the STRING database (Szklarczyk *et al.*, 2023). **B)** Protein interaction network representation of the top 50 negative interactors with samuraciclib. Nodes of genes found in GO terms that include mTOR signalling (highlighted in boxes in Figure 3.8B) are coloured in magenta. Network was created in the STRING database (Szklarczyk *et al.*, 2023).

3.6. mTOR signalling inhibition reduces sensitivity to samuraciclib

Previous work from Gemma Wilson has validated that active mTOR signalling is required for samuraciclib sensitivity in RPE1 cells by using an ATP-competitive mTOR inhibitor, Torin1 (Wilson, 2020), and I further corroborated this in the following section. 25 nM of Torin1 was used as it does not lead to a significant inhibition of proliferation and it is sufficient to effectively inhibit mTOR (Wilson *et al.*, 2023). Inhibition of mTOR was assessed by checking protein levels of phosphorylated p70 S6 kinase at threonine residue 389, which is directly phosphorylated by mTOR (Chauvin *et al.*, 2014), as well as levels of phosphorylated 40S ribosomal subunit protein S6 at serine residues 235 and 236, which is downstream of p70 S6 kinase (Klingebiel, Dinekov and Köhler, 2017). A 48-hour co-treatment of samuraciclib and Torin1 significantly increases

percentage of proliferating cells compared to samuraciclib treatment alone, as demonstrated by EdU incorporation assay (Wilson *et al.*, 2023). This data suggests that active mTOR is necessary for the cell cycle arrest induced by samuraciclib. I then checked whether using a higher concentration of samuraciclib can overcome the effect of inhibiting mTOR signalling, but I observed a similar result where mTOR inhibition is still able to block the inhibition of proliferation induced by samuraciclib, as observed by an increase in EdU-positive, proliferating cells compared to samuraciclib treatment alone (Figures 3.10A and 3.10B). Although this experiment was carried out twice and so statistical analysis could not be carried out, I validated the EdU incorporation assay

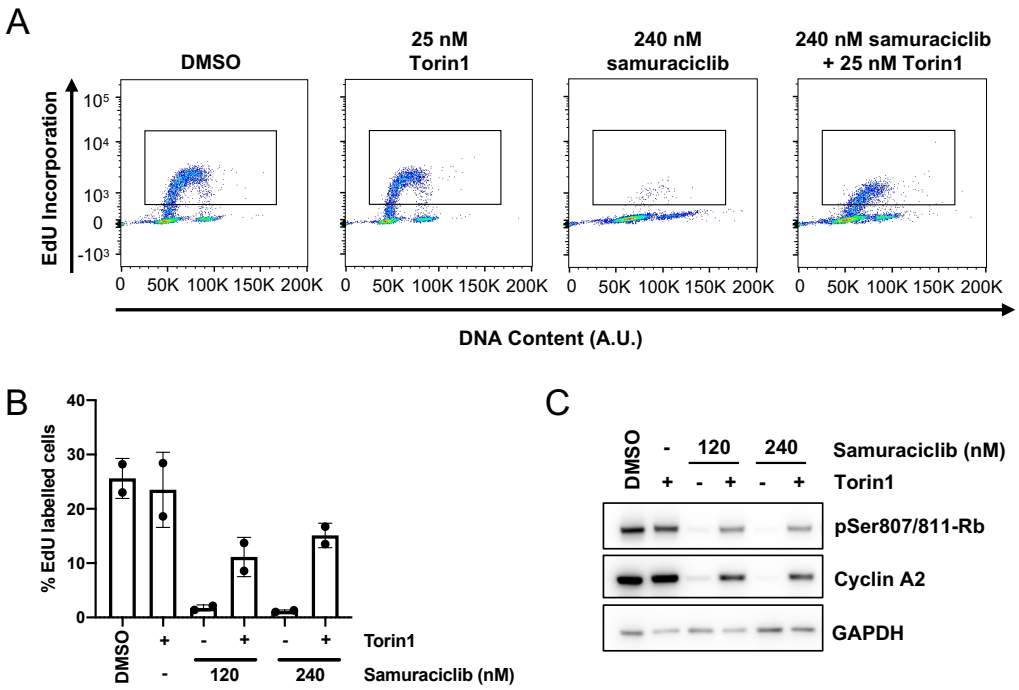

Figure 3.10: Pharmacological inhibition of mTOR reduces samuraciclib sensitivity in RPE1 cells.
RPE1 cells were treated with vehicle control, 25 nM of Torin1 alone, indicated concentrations of samuraciclib alone, or samuraciclib and 25 nM of Torin1 for 48 hours. **A)** Cells were incubated with EdU for 1 hour before collection. Pseudocolored plots of flow cytometry data from a representative experiment. DNA content is plotted against EdU incorporation. Inset gate drawn to include EdU-positive cells. **B)** Quantification of the percentage of EdU-positive cells from two independent experiments (representative shown in A). Error bars are SD. **C)** Representative western blot of whole-cell extracts collected from RPE1 cells. GAPDH: loading control.

results by western blot analysis of proliferative markers (Figure 3.10C). Both cyclin A2 and phosphorylated Rb levels increase upon a combined treatment of samuraciclib and Torin1 compared to samuraciclib alone (Figure 3.10C).

Analysis of EdU incorporation after 48 hours of treatment provides a snapshot analysis of a cell population. Whilst it indicates that a proportion of cells, simultaneously treated with samuraciclib and Torin1, are able to incorporate EdU, it does not show if this represents a subgroup of cells or are all cells less likely to arrest in G1. To address this, I carried out live-cell imaging using the FUCCI reporter system and compared it to samuraciclib treatment alone, for which cell cycle progression analysis is presented in Figure 3.1B. The single-cell timelapse analysis of the 48-hour co-treatment revealed a cell cycle profile more similar to samuraciclib treatment than DMSO-treated control. The majority of cells are able to complete one cell cycle during the 48 hours of samuraciclib and Torin1 co-treatment (Figure 3.11A), compared to 2 or 3 times during the DMSO treatment (Figure 3.1B). However, compared to samuraciclib treatment alone, where ~90% of the cells tracked are in a G1 state at the end of the treatment (marked by red nuclei), this is reduced to ~70% of the cells in samuraciclib and Torin1 co-treatment (Figure 3.11B). Moreover, there is a higher proportion of cells in S-G2 states (marked by green nuclei) and interestingly, unlike samuraciclib treatment alone, there are no events of mitotic bypass (Figure 3.11B). Mitotic bypass has previously been found important in senescence induction (Johmura *et al.*, 2014), which could be a mechanism by which a proportion of cells enter a senescent state during samuraciclib treatment. My data suggests that inhibiting mTOR signalling eliminates this effect (Figure 3.11B). Whilst FUCCI reporter states after 48 hours of samuraciclib treatment during a pharmacological inhibition of mTOR activity resemble flow cytometry DNA content analysis (Wilson *et al.*, 2023), tracking cell cycle progression indicates that the majority of cells does arrest in G1, but at a lower percentage than samuraciclib treatment alone. Those that are able to continue to proliferate spend more time in G1 than control cells. Interestingly, no mitotic bypass is observed in samuraciclib and Torin1 co-treated cells, suggesting that cells that continue to proliferate do so unimpeded.

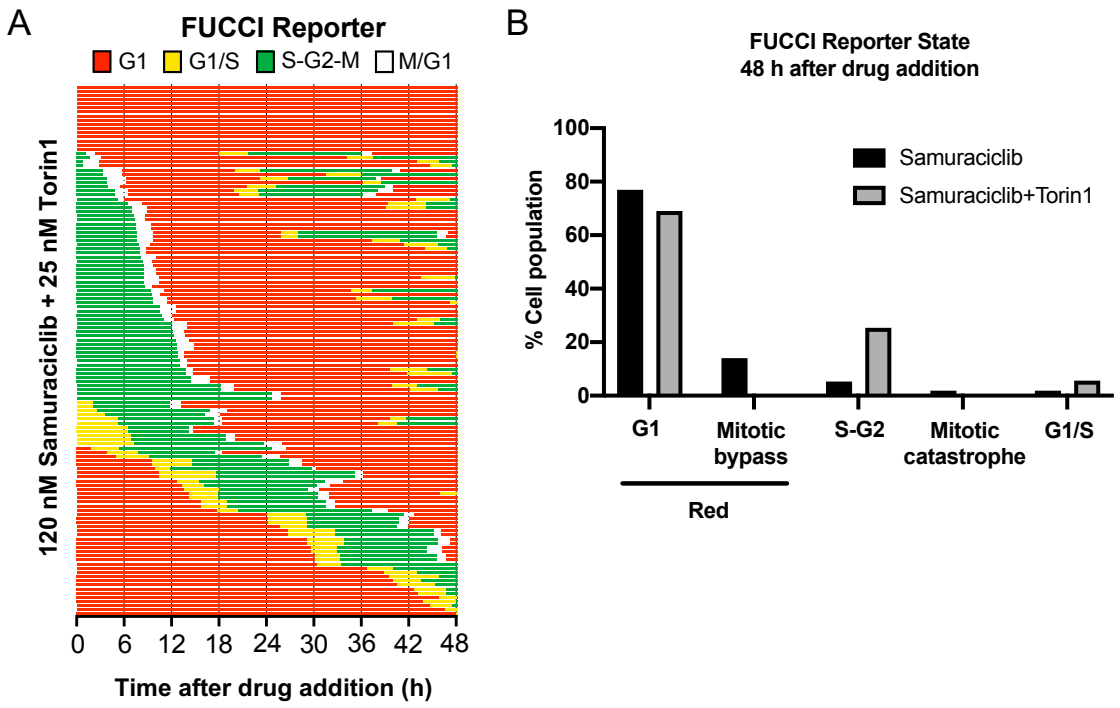

Figure 3.11: Pharmacological inhibition of mTOR reduces the percentage of G1 arrested cells during samuraciclib treatment.
A) RPE1 FUCCI cells were co-treated with 120 nM of samuraciclib and 25 nM of Torin1 and imaged for 48 hours. Cell cycle progression was monitored using the FUCCI reporter. State refers to cell cycle state based on tracking of FUCCI reporter where G1 is red, G1/S is yellow, S-G2-M is green and M/G1 is white (loss of signal). Tracks of 128 cells, at final time-point, are shown for samuraciclib and Torin1 co-treatment. **B)** Quantification of data of >200 cells and 96 cells tracked to determine cell cycle progression during 48 hours of samuraciclib treatment and samuraciclib and Torin1 co-treatment respectively. State refers to cell cycle state at final time-point based on tracking of FUCCI reporter. G1 (red); Mitotic bypass, where cells turn red without going through mitosis; S-G2 (green); Mitotic catastrophe, where cells die after going through mitosis; and G1/S (yellow).

The observation that the cell cycle profile of a co-treatment between samuraciclib and Torin1 resembles more the one of samuraciclib treatment alone rather than DMSO treatment indicates that these cells might arrest with a prolonged treatment. I therefore treated RPE1 cells with either samuraciclib alone or samuraciclib and Torin1 combined and collected protein lysates every 24 hours for 6 days for western blot analysis. The co-treatment causes levels of cyclin A2 and phosphorylated Rb to gradually start decreasing after 72 hours (Figures 3.12A and 3.12B respectively), which is matched by an increase in p21 levels (Figures 3.12A and 3.12B). The reduction in proliferation is not due to a prolonged Torin1 treatment as it does not lead to changes in

phosphorylated Rb or p21 levels (Figure 3.12B). This data suggests that a prolonged co-treatment of samuraciclib and Torin1 might eventually cause a cell cycle arrest. Further cell cycle analysis is, however, required to confirm this. I aim to carry out EdU incorporation assay to measure the number of proliferating cells after varying treatment durations. Moreover, colony formation during prolonged treatments (10 days) would evaluate the difference in the replicative potential of RPE1 cells that are able to resist the treatments and grow colonies.

Overall, this western blot analysis further confirms that inhibiting mTOR signalling while treating cells with samuraciclib reduces the effectiveness of this CDK7 inhibitor as samuraciclib treatment alone causes a drastic decrease in cyclin A2 and an increase in p21 levels after only 48 hours (Figure 3.12A). This response is delayed in samuraciclib and Torin1 co-treatment (Figure 3.12A).

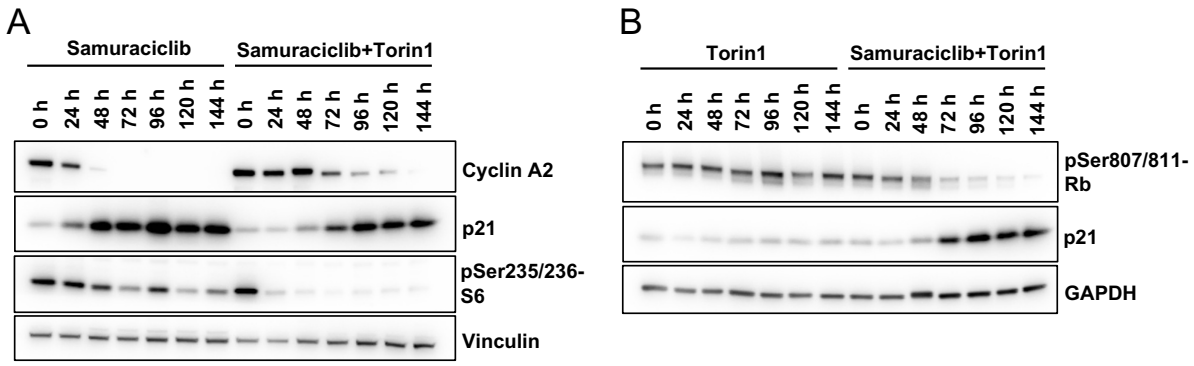

Figure 3.12: Prolonged co-treatment of samuraciclib and Torin1 decreases levels of proliferative markers in RPE1 cells.
A) B) Western blot analysis from one experiment of whole-cell extracts collected from RPE1 cells at indicated time-points after treatment with 25 nM of Torin1 alone, 120 nM of samuraciclib alone or 120 nM of samuraciclib and 25 nM of Torin1. GAPDH and Vinculin: loading controls.

Samuraciclib treatment during pharmacological inhibition of mTOR activity leads to a cell cycle progression profile more similar to samuraciclib than DMSO control (Figure 3.11). To test if these cells retain their proliferative potential or permanently exit the cell cycle, I carried out a colony formation assay after drug wash-out. RPE1 cells were treated with either samuraciclib or Torin1 alone or samuraciclib and Torin1 combined for 48 hours, after which cells were washed to remove the drugs. Cells were then re-

seeded at low numbers and allowed to grow and form colonies in drug-free medium for approximately 10 days. Colony area was measured as a read-out of survival and proliferative potential after specified treatments. After 48 hours of concurrent treatment, significantly greater proportion of cells is able to form colonies compared to samuraciclib treatment alone, which further extends the findings that inhibition of mTOR activity during samuraciclib treatment decreases sensitivity to this CDK7 inhibitor (Figures 3.13A and 3.13B). However, this colony formation is still significantly reduced compared to control DMSO treatment (Figure 3.13B). This indicates that some cells do permanently exit the cell cycle even with combined samuraciclib and Torin treatment. However, this assay cannot indicate which cells are able to continue proliferating and which exit the cell cycle, either via senescence or apoptosis. Tracking FUCCI reporter single cells following treatment wash-out would answer this question. Moreover, Torin1 treatment alone causes a minor yet significant decrease in the percentage of colony area compared to DMSO control, which suggests a part of this reduction in proliferative potential following the co-treatment of samuraciclib and Torin1 could be due to Torin1 treatment alone as well (Figure 3.13B).

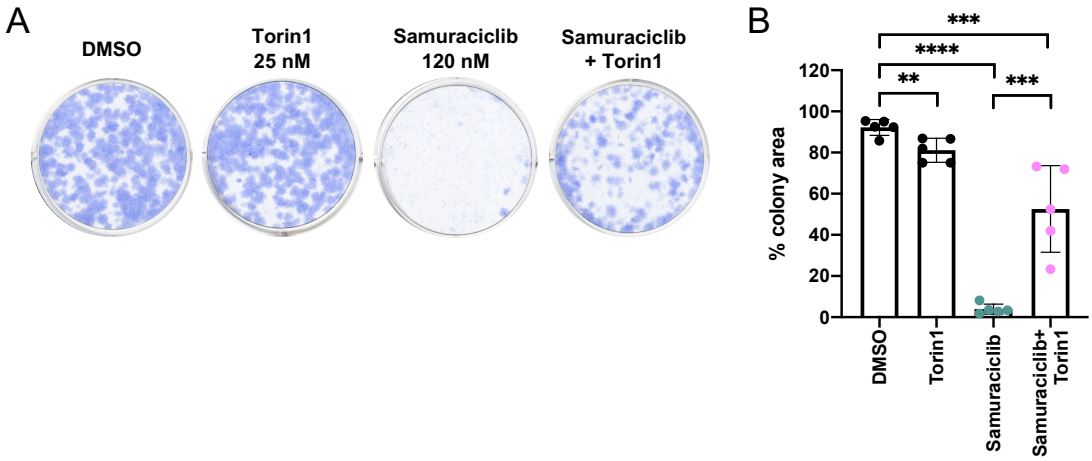

Figure 3.13: Pharmacological inhibition of mTOR during samuraciclib treatment increases proliferative potential following drug wash-out.
A) RPE1 cells were treated with vehicle control, 25 nM of Torin1 alone, 120 nM of samuraciclib alone or 120 nM of samuraciclib and 25 nM of Torin1 for 48 hours. After 48 hours, cells were washed five times with PBS to remove the drugs from cells. Cells were re-seeded in the absence of drugs and allowed to grow for 9-11 days. Colonies were stained and visualised with Methylene Blue. **B)** Quantification of percentage of colony area from five independent experiments (representative shown in A). Statistical significance was calculated using an unpaired two-tailed t test. Error bars are SD.

3.7. mTOR-dependent growth signalling promotes an increase in cell size and samuraciclib-induced senescence

The mTOR signalling pathway upregulates anabolic processes and downregulates catabolic processes, such as autophagy, in order to promote and drive cellular growth. It is therefore one of the key regulators of cellular growth. It has been found notable in senescence induction and an important determinant between a reversible quiescent state and a permanent senescent state (Demidenko and Blagosklonny, 2008; Blagosklonny, 2012; Terzi, Izmirli and Gogebakan, 2016). I therefore explored whether active mTOR signalling is necessary for samuraciclib-induced senescence phenotypes.

In the previous section I described how Torin1 treatment decreases sensitivity of RPE1 cells to samuraciclib. I further explored this sensitivity by establishing the effect of the co-treatment on senescence phenotypes previously observed upon samuraciclib treatment alone. This data is further confirmation of Gemma Wilson's work (Wilson, 2020). The activity of SA β-gal is significantly reduced upon samuraciclib and Torin1 co-treatment, compared to samuraciclib treatment alone (Figures 3.14A and 3.14B). In fact, the mean C_{12}FDG fluorescence, a measure of SA β-gal activity, is not significantly higher than the control treatments (Figure 3.14B). Moreover, combining samuraciclib treatment with Torin1 prevents an increase in *CDKN1A* and *CCND1* mRNA levels and a decrease in *LMNB1* mRNA levels (Figure 3.14C). These mRNA expression results are reflected in p21 and Lamin B1 protein levels (Figure 3.14D). Lastly, inhibiting mTOR signalling while treating the cells with samuraciclib leads to a decrease in cell volume (Figures 3.14E and 3.14F). Altogether, this shows that inhibiting mTOR activity using Torin1 reduces the ability of samuraciclib to induce senescence phenotypes, which suggests that active mTOR signalling is needed for samuraciclib-induced senescence in RPE1 cells.

A consequence of mTOR-driven cellular growth is an increase in cell size. During a permanent cell cycle arrest, cells continue increasing in cell size and accumulating biomass, which was previously thought to be a consequence of continued growth during a prolonged cell cycle arrest. However, this decoupling of proliferation and cellular growth could also be at the basis of senescence induction, rather than being

simply a consequence. Multiple studies have supported this notion recently (Neurohr *et al.*, 2019; Lanz *et al.*, 2022; Manohar *et al.*, 2023). Since samuraciclib increases cell size significantly, I wanted to investigate more closely the relationship between mTOR-dependent increase in cell size and senescence induction.

I used the flow cytometry analysis of SA β-gal activity from Figure 3.14A in order to study this relationship. I plotted C_{12}FDG fluorescence, as a measure of SA β-gal activity, against forward scatter (FSC), a proxy of cell size, and divided the plot into four quadrants to separate the small and large cells which are either C_{12}FDG positive (+) or negative (-) (Figure 3.15A). There is a higher percentage of cells that are large and have an increased SA β-gal activity (C_{12}FDG+) in samuraciclib treatment compared to control cells (Figure 3.15B). Upon pharmacological mTOR inhibition during samuraciclib treatment, this percentage is reduced. Moreover, the percentage of small cells that have low SA β-gal activity (C_{12}FDG-) is increased compared to samuraciclib treatment alone (Figure 3.15B) (Wilson *et al.*, 2023). This implies that increased SA β-gal activity relies on active mTOR signalling which correlates with an increased cell size. Altogether, this data suggests that there is a positive correlation between mTOR-dependent cell size increase and samuraciclib-induced senescence.

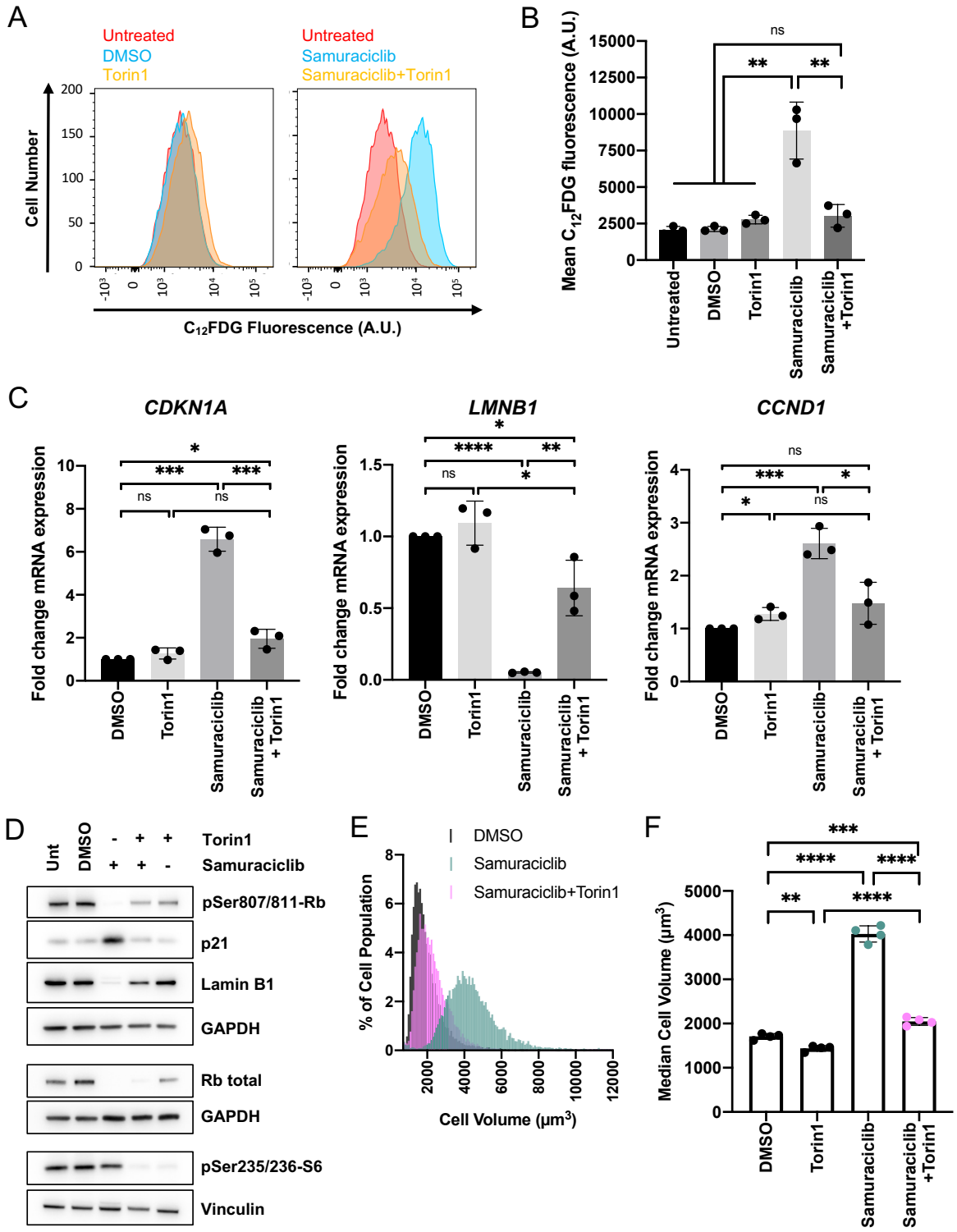

Figure 3.14: Samuraciclib-induced senescent phenotypes are dependent upon active mTOR signalling in RPE1 cells.

A) Flow cytometry data from a representative experiment, detecting SA β-gal activity with the fluorescent β-gal substrate, C_{12}FDG in RPE1 cells treated with vehicle control, 25 nM Torin1 of alone, 120 nM of samuraciclib alone or 120 nM of samuraciclib and 25 nM of Torin1 for 96 hours. C_{12}FDG fluorescence is plotted against cell count.

Figure 3.14: (continued) **B)** Quantification of the mean C_{12}FDG fluorescence from three independent experiments (representative shown in A). Statistical significance was calculated using an unpaired two-tailed t test. Error bars are SD. **C)** RPE1 cells that were left untreated or treated with vehicle control, 25 nM of Torin1 alone, 120 nM of samuraciclib alone or 120 nM of samuraciclib and 25 nM of Torin1 were collected after 48 hours and mRNA levels of *CDKN1A*, *LMNB1*, *CCND1* were analysed by RT-qPCR from three independent experiments. Statistical significance was calculated using an unpaired two-tailed t test. Error bars are SD. **D)** Western blot analysis of whole-cell extracts collected from RPE1 cells after 48 hours of treatment with vehicle control, 25 nM of Torin1 alone, 120 nM of samuraciclib alone or 120 nM of samuraciclib and 25 nM of Torin1. Vinculin and GAPDH: loading controls. **E)** Coulter counter data from a representative experiment, with RPE1 cells treated with vehicle control, 25 nM of Torin1 alone, 120 nM of samuraciclib alone, or 120 nM of samuraciclib and 25 nM of Torin1 for 48 hours. Percentage of cell population is plotted against various bins containing cells with different volumes in μm^3. **F)** Quantification of the median cell volume within the population from four independent experiments (representative shown in E). Statistical significance was calculated using an unpaired two-tailed t test. Error bars are SD.

SA β-gal activity is one of the most used senescence markers. However, determining if larger cells are more likely to stay arrested after samuraciclib treatment would be a more accurate way to establish a causative effect of size for inducing a senescent state. I therefore investigated the relationship between cell size and a samuraciclib-induced arrest using live-cell imaging of RPE1 FUCCI cells. I treated RPE1 FUCCI cells with either DMSO or samuraciclib for 72 hours, then washed the treatments away, re-added drug-free medium and initiated timelapse imaging for 72 hours. I marked FUCCI red cells (G1 state) at the first time-point (0 h), which is immediately after drug wash-out, and I considered these cells to be in a G1 arrest after 72 hours of samuraciclib treatment. I then measured nuclear area, which can be used as a proxy for cell size (Lanz *et al.*, 2022; Xie, Swaffer and Skotheim, 2022), of FUCCI red cells at the first time-point. As expected, comparing proliferating cell culture (DMSO) and samuraciclib-arrested cells (Arrest at 0 h) shows that cell size increases significantly during the arrest (Figure 3.15C). I then tracked these FUCCI red cells to determine which cells remain arrested in a G1 state over the period of 72 hours and which return to a proliferative state after samuraciclib wash-out. Cell cycle entry was determined by a nuclear yellow colour switch. Within the 72-hour wash-out, smaller cells on average re-enter the cell cycle after samuraciclib arrest whereas larger cells remain arrested (Figure 3.15C) (Wilson *et al.*, 2023). This data suggests that cell size is an important indicator of an irreversible arrest state and therefore also samuraciclib sensitivity.

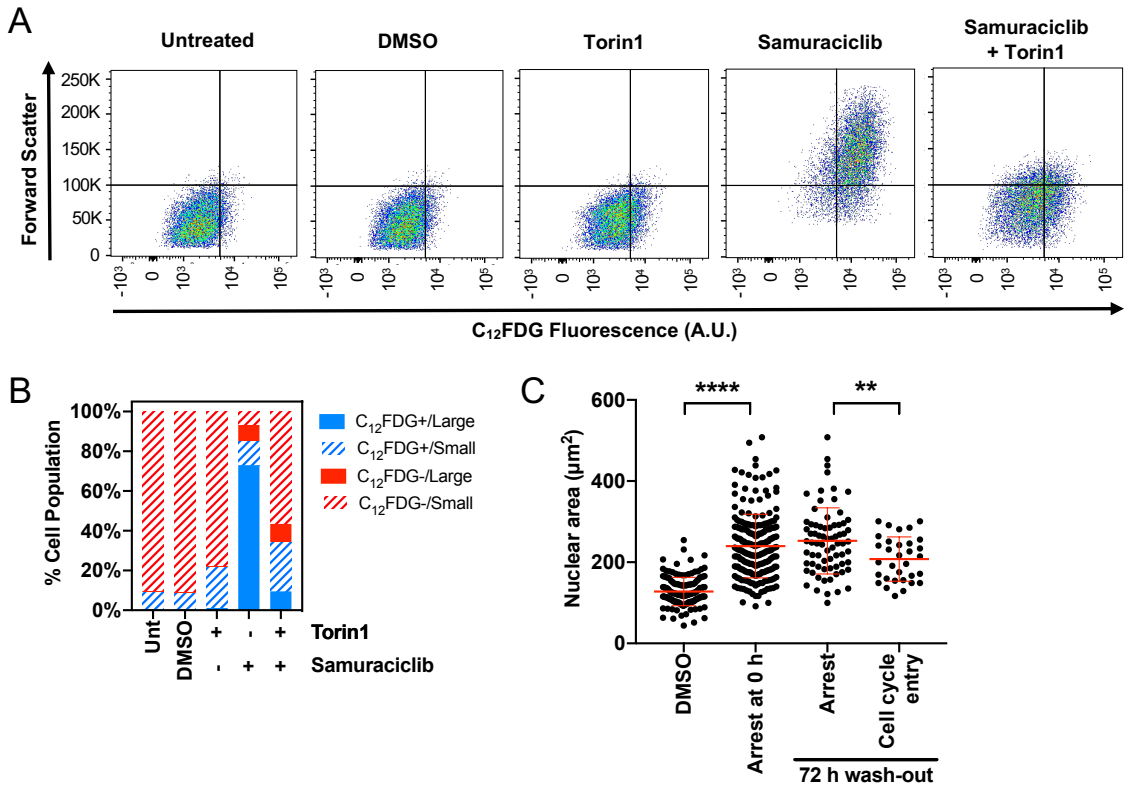

Figure 3.15: Cell size is an important indicator of samuraciclib sensitivity.
A) RPE1 cells were treated with vehicle control, 25 nM of Torin1 alone, 120 nM of samuraciclib alone, or 120 nM of samuraciclib and 25 nM of Torin1 for 96 hours. Pseudocoloured plots of flow cytometry data from a representative experiment. C_{12}FDG fluorescence is plotted against forward scatter, a measure of cell size. Quadrant drawn to distinguish between small, C_{12}FDG- cells, small, C_{12}FDG+ cells, large, C_{12}FDG- cells and large, C_{12}FDG+ cells. **B)** Quantification of data shown in panel A indicating the percentage of small, C_{12}FDG- cells, small, C_{12}FDG+ cells, large, C_{12}FDG- cells and large, C_{12}FDG+ cells. **C)** RPE1 FUCCI cells were treated with vehicle control or 120 nM of samuraciclib for 72 hours. After 72 hours, cells were washed with PBS five times to remove samuraciclib from the cells, and fresh media was added, after which live-cell imaging was started for 72 hours. Nuclear area was measured for red cells at the first time-point (0 h). 105 cells were tracked after samuraciclib wash-out to determine cells that remain arrested and cells that enter the cell cycle. Statistical significance was calculated using an unpaired two-tailed t test. Error bars are SD. Figure adapted from (Wilson *et al.*, 2023).

I observed that samuraciclib induces a robust and irreversible cell cycle arrest after 48 hours, and that this is largely dependent on an increase in cell size. I therefore wanted to investigate whether obstructing further biomass accumulation after CDK7 inhibitor wash-out could prevent this conversion from a cell cycle arrest to a permanent exit state. I treated RPE1 cells with samuraciclib for 48 hours after which I washed away

the drug and either re-incubated the cells with samuraciclib, allowed these cells to grow in drug-free media or treated the cells with Torin1 for 96 hours, as illustrated in Figure 3.16A. I observed that there is a minor increase, although non-significant, in the percentage of actively EdU incorporating cells when Torin1 is used to slow down cellular growth after samuraciclib wash-out (Figure 3.16B). During a samuraciclib wash-out there is a minor increase in phosphorylated Rb levels. However, during Torin1 treatment after a 48-hour treatment with samuraciclib, there is a greater increase in levels of phosphorylated Rb, indicating entry into the cell cycle (Figure 3.16C). This data suggests that, although this effect is minor, reducing mTOR activity and therefore cellular growth after samuraciclib wash-out increases the proportion of cells that are able to enter a proliferative state after a cell cycle arrest induced by CDK7 inhibition. Altogether, this indicates that mTOR activity, and therefore continued growth, during recovery from a samuraciclib-induced arrest contributes to cells exiting the cell cycle permanently.

In previous sections of this chapter, I demonstrated the importance of active mTOR signalling and the increase in cell volume in samuraciclib-induced senescence using Torin1 to pharmacologically inhibit mTOR. I next decided to evaluate these findings by manipulating mTOR levels and cell size via a more physiological method by reducing serum levels in the cell culture growth media. As a control, I used 10% serum-supplemented media, compared to 0.2% for serum depletion condition. I show that reducing serum levels to 0.2% for 48 hours reduces mTOR activity, as demonstrated by a reduction in levels of phosphorylated 40S ribosomal subunit protein S6 (Figure 3.17A). Moreover, lowering mTOR activity with serum depletion while treating RPE1 cells with samuraciclib significantly decreases the cell volume compared to samuraciclib treatment with active mTOR signalling (Figures 3.17B and 3.17C).

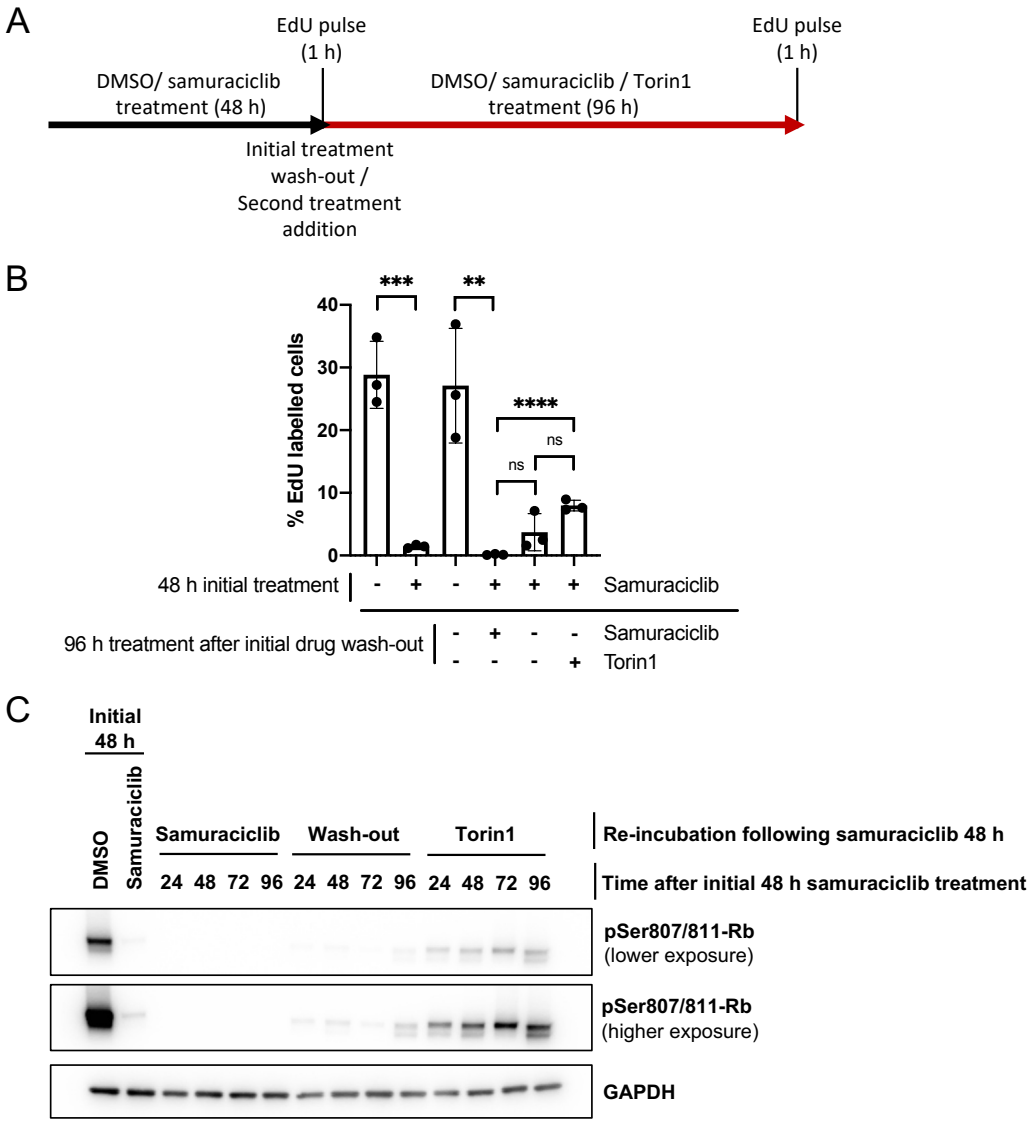

Figure 3.16: Preventing continued cellular growth after samuraciclib wash-out increases proliferative potential.
A) A schematic illustrating the experimental set up. RPE1 cells were treated with vehicle control or 120 nM of samuraciclib for 48 hours. After 48 hours of treatment some cells were labelled with EdU for 1 hour and then harvested. Other cells were washed five times with PBS to remove the drugs from cells and fresh media was added. New treatments (vehicle control, 120 nM of samuraciclib or 25 nM of Torin1) were added and cells were cultured for another 96 hours. After 96 hours of additional indicated treatments, cells were labelled with EdU for 1 hour and then harvested. **B)** Quantification of the percentage of EdU-positive cells from three independent experiments as described in A. Statistical significance was calculated using an unpaired two-tailed t test. Error bars are SD. **C)** Western blot analysis from whole-cell extracts collected from RPE1 cells. GAPDH: loading control.

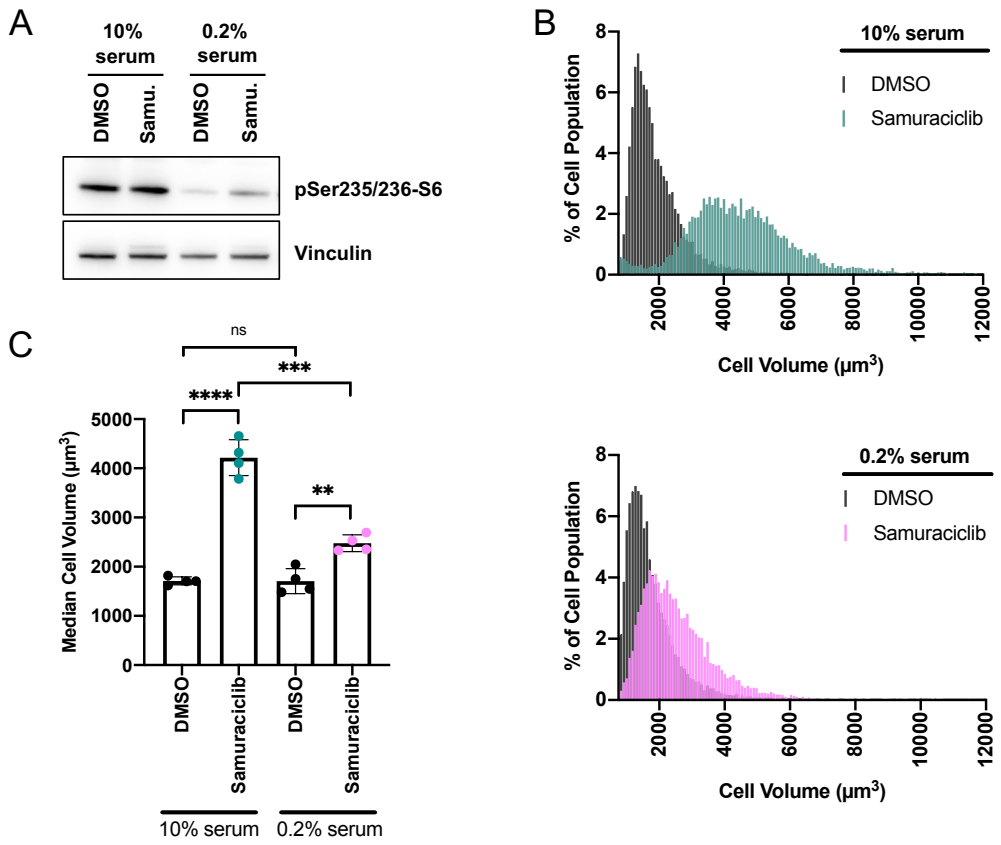

Figure 3.17: Serum depletion reduces mTOR activity and cell size of samuraciclib-treated RPE1 cells.
RPE1 cells were treated with vehicle control or 120 nM of samuraciclib for 48 hours while cultured in 10% or 0.2% serum (FBS)-supplemented media. **A)** Western blot analysis of whole-cell extracts. Vinculin: loading control. **B)** Coulter counter data from a representative experiment. Percentage of cell population is plotted against various bins containing cells with different volumes in μm^3. **C)** Quantification of the median cell volume within the population from four independent experiments (representative shown in B). Statistical significance was calculated using an unpaired two-tailed t test. Error bars are SD.

I then tested the effect of serum depletion on samuraciclib-induced arrest by carrying out cell cycle analysis using EdU incorporation assay. 48 hours of serum depletion *per se* causes a significant decrease in the percentage of actively replicating cells (Figures 3.18A and 3.18B). This conforms with the current understanding that serum withdrawal causes a G0 quiescent arrest in non-transformed cells and can be used as a G0/G1 synchronisation protocol (Demidenko and Blagosklonny, 2008; Zerjatke *et al.*, 2017). Since serum is not fully withdrawn from the cell culture medium, but considerably reduced, this could explain why there is a small proportion of cells proliferating (Figure

3.18B). Contrarily to pharmacological inhibition of mTOR by Torin1, serum depletion does not block samuraciclib-induced cell cycle arrest after 48 hours of treatment (Figures 3.17A and 3.18B). There is no significant difference in the percentage of cells incorporating EdU between samuraciclib treatment in control and serum depleted conditions (Figure 3.18B). The cell cycle analysis is mirrored by western blot analysis of proliferative markers, phosphorylated Rb and cyclin A2 (Figure 3.18C). A part of this effect could be due to serum depletion itself. Therefore, I tested protein levels of senescence markers, p21 and Lamin B1 previously observed to alter upon samuraciclib treatment. Serum depletion during samuraciclib treatment causes a slight increase in p21 and a smaller reduction in Lamin B1 levels (Figure 3.18C). This suggests that the senescence induction by samuraciclib might be less effective during serum depletion compared to the control condition. However, in order to investigate this further and determine the type of cell cycle exit that occurs during these treatments, I studied the proliferative potential of these cells following drug wash-out.

Samuraciclib-induced cell cycle arrest between control and serum depletion conditions is not significantly different. I therefore compared cell cycle entry and exit dynamics following samuraciclib wash-out. I treated RPE1 cells with DMSO or samuraciclib for 48 hours while being cultured in either control (10% serum) or serum depleted (0.2% serum) culture media. After 48 hours, I washed the cells to remove the treatments and I added fresh complete media containing 10% serum to all conditions to stimulate the cells to proliferate. Once the drugs were washed away and drug-free media was added, cells were incubated with EdU for 24 hours and then collected for flow cytometry analysis. The schematic of the experimental set up is illustrated in Figure 3.19A. RPE1 cells that were cultured in 0.2% serum-supplemented media incorporate significantly more EdU after samuraciclib wash-out compared to cells cultured in control 10% serum-supplemented media (Figures 3.19B and 3.19C). This suggests that inhibition of mTOR activity with serum depletion, which prevents excessive cell size increase, renders cells in part more likely to re-enter the cell cycle following samuraciclib-induced arrest. However, this rescue in proliferation during the first 24 hours after samuraciclib wash-out, although significant, is partial, as around 20% of the cell population is able to incorporate EdU compared to around 70% in the DMSO control (Figure 3.19C). This suggests that some cells might still undergo a persistent cell cycle arrest. This is aligned with the finding that, although senescence markers

are reduced compared to control samuraciclib treatment, there is a slight increase in p21 levels and a reduction in Lamin B1 in the serum depleted condition (Figure 3.18C).

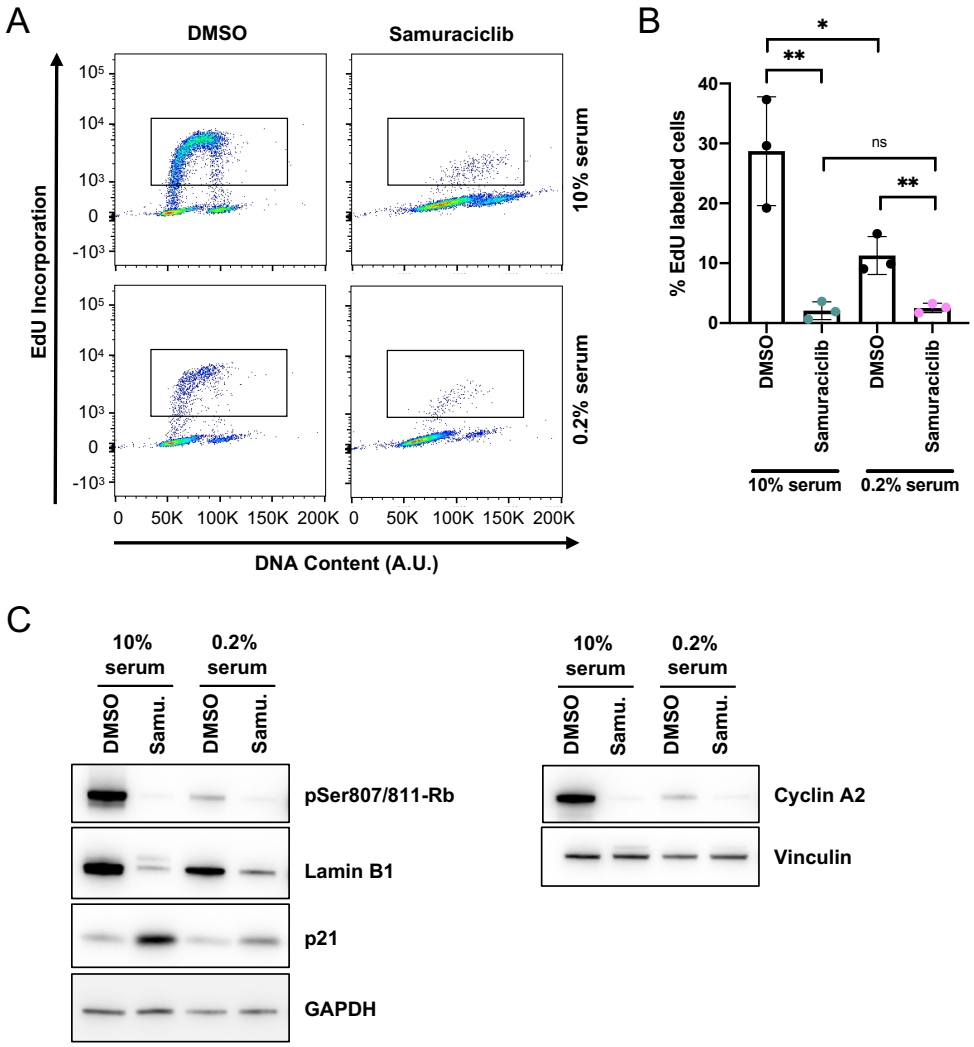

Figure 3.18: Samuraciclib induces a cell cycle arrest in a serum depleted condition.
RPE1 cells were treated with vehicle control or 120 nM of samuraciclib for 48 hours while cultured in 10% or 0.2% serum (FBS)-supplemented media. **A)** Cells were incubated with EdU for 1 hour before collection. Pseudocoloured plots of flow cytometry data from a representative experiment. DNA content is plotted against EdU incorporation. Inset gate drawn to include EdU-positive cells. **B)** Quantification of the percentage of EdU-positive cells from three independent experiments (representative shown in A). Statistical significance was calculated using an unpaired two-tailed t test. Error bars are SD. **C)** Representative western blot of whole-cell extracts collected from RPE1 cells. GAPDH and Vinculin: loading controls.

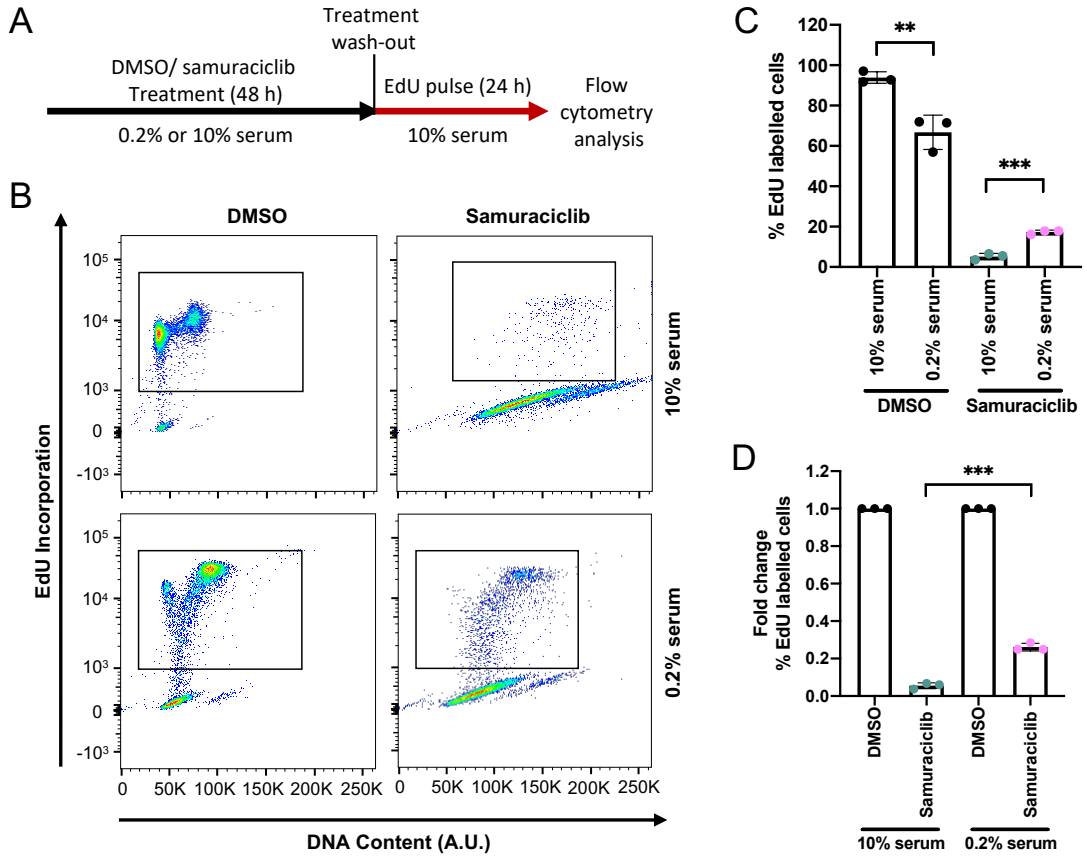

Figure 3.19: Serum depletion in RPE1 cells during samuraciclib treatment allows higher percentage of cells to re-enter the cell cycle after drug wash-out.
A) A schematic illustrating the experimental set up. RPE1 cells were treated with vehicle control or 120 nM of samuraciclib for 48 hours while cultured in 10% or 0.2% serum (FBS)-supplemented media. After 48 hours, cells were washed five times with PBS to remove the drugs from cells. Fresh drug-free 10% serum (FBS)-supplemented media was added to the cells. Cells were incubated with EdU for 24 hours after treatment wash-out. Cells were then harvested for flow cytometry analysis. **B)** Pseudocoloured plots of flow cytometry data from a representative experiment. DNA content is plotted against EdU incorporation. Inset gate drawn to include EdU-positive cells. **C)** Quantification of the percentage of EdU-positive cells from three independent experiments (representative shown in B). Statistical significance was calculated using an unpaired two-tailed t test. Error bars are SD. **D)** Quantification from C represented as fold change of the percentage of EdU labelled cells normalised to the corresponding DMSO treatments. Statistical significance was calculated using an unpaired two-tailed t test. Error bars are SD.

Furthermore, there is a significant difference in the percentage of EdU incorporation between control and serum depleted DMSO treatments (Figures 3.19B and 3.19C). Serum depletion *per se* causes a lower proportion of cells to enter the cell cycle following serum stimulation compared to an almost complete cell population in the control 10% serum condition (Figure 3.19C). The reason for this could be that these

cells might take longer to enter the proliferative state. To compensate for this difference in the DMSO treatments, I plotted the fold change of the EdU incorporation percentage normalising each samuraciclib treatment to its corresponding serum condition of DMSO treatment. This analysis showed a similar significant increase in the EdU labelled cells following samuraciclib wash-out after serum depletion (Figure 3.19D). Although this rescue in proliferation is partial, it is still a significant increase in proliferating cells that could potentially drive treatment resistance which reduces samuraciclib sensitivity.

Another way to study the sensitivity of samuraciclib treatment is by carrying out colony formation assays after treatment wash-out, exploring the proliferative potential of samuraciclib-arrested RPE1 cells. After 48 hours of treatment, I re-seeded the cells at low numbers and left in culture to grow and form colonies for approximately 10 days. DMSO-treated cells cultured initially in serum depleted media have a significantly lower colony formation potential than DMSO-treated cells cultured in control media, which could be due to a more delayed entry into the cell cycle (Figures 3.20A and 3.20B). Moreover, the colony formation assay shows that serum depletion during samuraciclib treatment significantly increases colony formation after treatment wash-out compared to control samuraciclib treatment (Figures 3.20A and 3.20B). This analysis confirms the previous results examining EdU incorporation during a 24-hour treatment wash-out (Figures 3.19B and 3.19C). Altogether these results suggests that inhibiting mTOR activity through serum depletion and in turn preventing an excessive cellular growth, increases the ability of samuraciclib-arrested cells to re-enter the cell cycle following drug wash-out, therefore decreasing samuraciclib sensitivity. This is further evidence of a correlation between mTOR-dependent increase in cell size and samuraciclib-induced senescence.

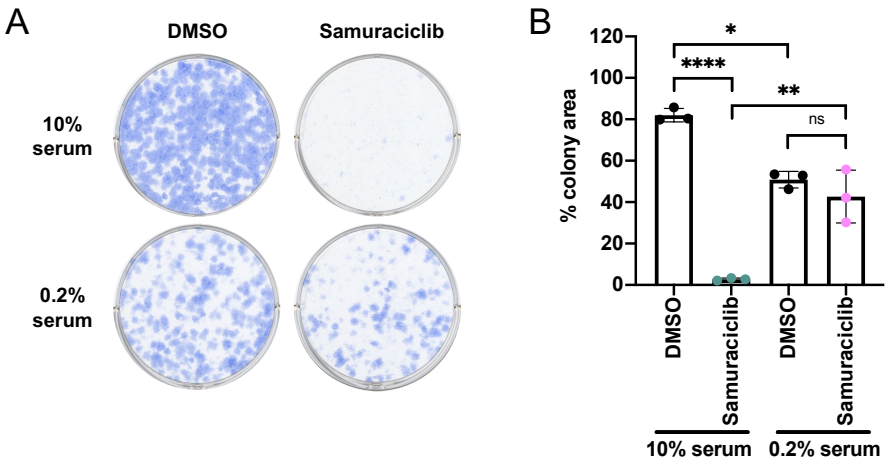

Figure 3.20: Serum depletion in RPE1 cells partially rescues permanent cell cycle exit induced by samuraciclib.
RPE1 cells were treated with vehicle control or 120 nM of samuraciclib for 48 hours while cultured in 10% or 0.2% serum (FBS)-supplemented media. **A)** After 48 hours, cells were washed five times with PBS to remove the drugs from cells. Cells were re-seeded in the absence of drugs and allowed to grow for 9-11 days in 10% serum (FBS)-supplemented media. Colonies were stained and visualised with Methylene Blue. **B)** Quantification of percentage of colony area from three independent experiments (representative shown in A). Statistical significance was calculated using an unpaired two-tailed t test. Error bars are SD.

3.8. Samuraciclib sensitivity positively correlates with mTOR activity in breast cancer cell lines

In previous sections, I showed that active mTOR signalling and an increase in cell size are an important indicator of samuraciclib senescence in non-transformed RPE1 cells. Since cellular growth signalling, via mTOR activity, is often upregulated in cancer, this could lead to the increased sensitivity of cancer cells to samuraciclib. I therefore investigated the correlation between mTOR activity and samuraciclib sensitivity in three breast cancer cell lines, as this is one of the cancers samuraciclib is in clinical trials for. These cell lines are MCF7 and T47D, both hormone receptor-dependent breast cancer cell lines, and BT549, a TNBC cell line. They have all been previously shown to be sensitive to samuraciclib treatment using IC_{50} analysis (Patel *et al.*, 2018). Moreover, they all have a growth-promoting mutation upstream of mTOR. Both MCF7 and T47D have a mutation in the *PIK3CA* gene; more precisely MCF7 has a *PIK3CA*: E545K and T47D a *PIK3CA*: H1047R mutation. BT549 is PTEN deficient, which is a

negative regulator of the mTOR signalling pathway (Hollestelle *et al.*, 2010; Smith *et al.*, 2017). Whilst all these cancer cell lines harbour a growth-activating mutation, I first established if mTOR activity levels vary to allow me to correlate this to samuraciclib sensitivity. I used p70 S6 kinase phosphorylation at threonine residue 389 as an mTOR activity read-out, as this is a direct downstream target of the mTOR kinase. I observed that MCF7 cells have considerably higher levels of p70 S6 kinase phosphorylation compared to T47D and BT549 (Figure 3.20A). T47D cells show slightly higher levels than BT549 (Figure 3.20A). These results are mirrored by total levels of p70 S6 kinase (Figure 3.20B) (Wilson *et al.*, 2023).

I then tested samuraciclib sensitivity in these three breast cancer cell lines by carrying out EdU incorporation analysis. IC_{50} values were previously determined for these cell lines using an assay based on cell mass, where MCF7 cells had the lowest IC_{50} value of 180 nM (Patel *et al.*, 2018). I therefore used this concentration of samuraciclib and three lower ones to test the effect on cellular proliferation of MCF7, T47D and BT549 cells. MCF7 cells show a marked decline in the percentage of actively replicating cells after 96 hours of samuraciclib treatment, which is dose-dependent. T47D cells are still sensitive to samuraciclib but with a smaller effect on the number of proliferating cells. Lastly, samuraciclib has no effect on BT549 cells at these concentrations as there is no reduction in the percentage of EdU incorporation (Figures 3.21C and 3.21D) (Wilson *et al.*, 2023). Therefore, level of mTOR activity positively correlates with samuraciclib sensitivity in these breast cancer cell lines.

Moreover, an increase in cell size after samuraciclib treatment positively correlates with mTOR activity levels and samuraciclib sensitivity (Figures 3.22A and 3.22B). The cell size is not significantly different between these three cell lines before treatment, as demonstrated by DMSO treatments (Figure 3.22B). However, during 96 hours of samuraciclib treatment, the most sensitive MCF7 cells exhibit the most pronounced increase in volume, whereas the least sensitive BT549 cells increase in size only slightly during treatment (Figures 3.22A and 3.22B) (Wilson *et al.*, 2023).

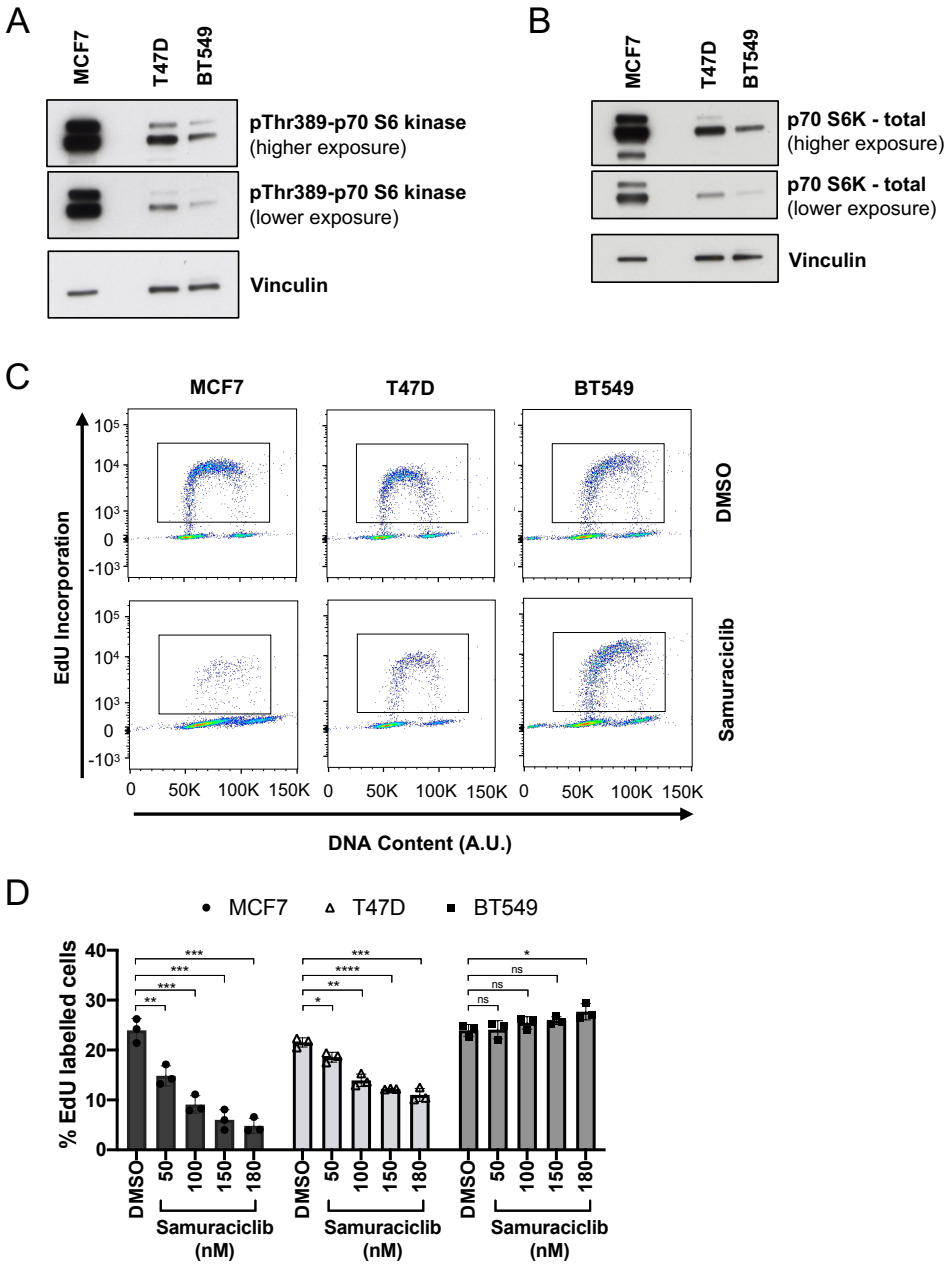

Figure 3.21: Samuraciclib sensitivity positively correlates with mTOR-dependent signalling in breast cancer cell lines.
A) Representative western blot of whole-cell extracts collected from MCF7, T47D, and BT549 cells (n=3). Vinculin: loading control. **B)** Representative western blot of whole-cell extracts collected from MCF7, T47D, and BT549 cells (n=3). Vinculin: loading control. **C)** MCF7, T47D, and BT549 cells were treated with vehicle control or 180 nM of samuraciclib for 96 hours. Cells were then incubated with EdU for 1 hour before collection. Pseudocoloured plots of flow cytometry data from one representative experiment. DNA content is plotted against EdU incorporation. Inset gate drawn to include EdU-positive cells. **D)** Quantification of the percentage of EdU-positive cells (representative shown in C) from three independent experiments. Statistical significance was calculated using an unpaired two-tailed t test. Error bars are SD. Figure adapted from (Wilson *et al.*, 2023).

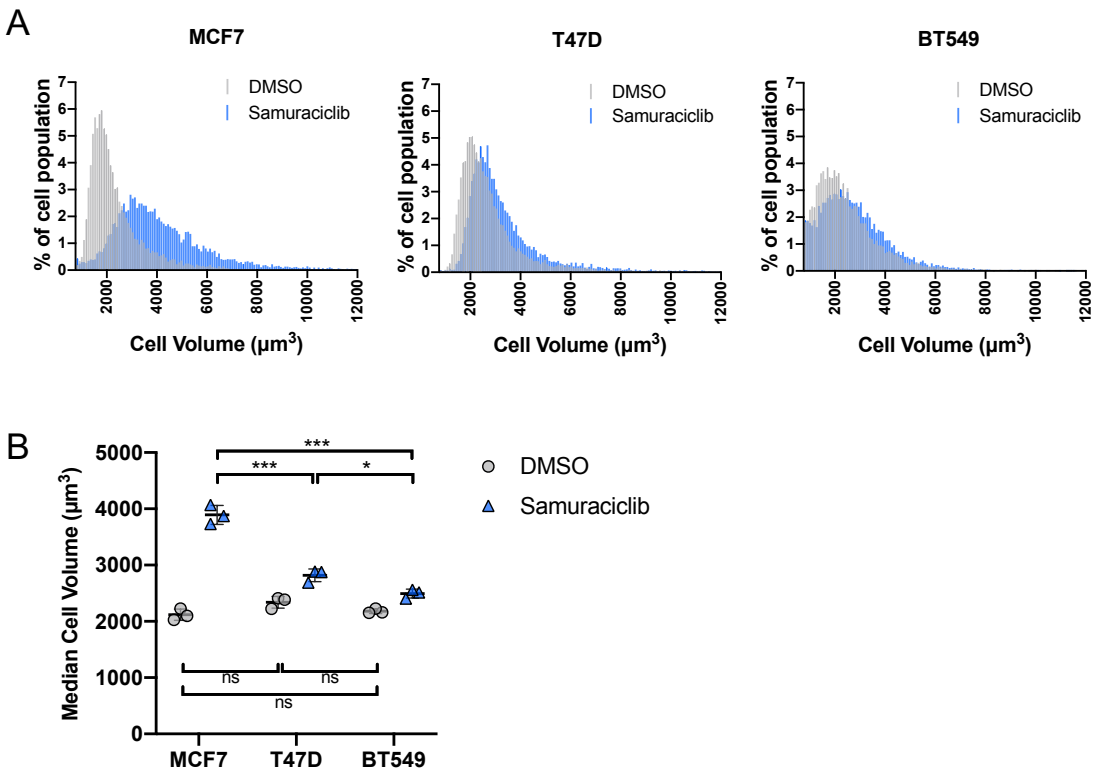

Figure 3.22: Samuraciclib-induced increase in cell size positively correlates with samuraciclib sensitivity in breast cancer cell lines.
MCF7, T47D and BT549 cells treated with vehicle control or 180 nM samuraciclib for 96 hours. **A)** Coulter counter data from one representative experiment. Percentage of cell population is plotted against various bins containing cells with different volumes in μm^3. **B)** Quantification of the median cell volume within the population from three independent experiments (representative shown in A). Statistical significance was calculated using an unpaired two-tailed t test. Error bars are SD. Figure adapted from (Wilson *et al.*, 2023).

Gemma Wilson has shown that MCF7 cells have an increased SA β-gal activity after 6 days of samuraciclib treatment, suggesting that also in cancer cells this treatment causes a senescent state (Wilson, 2020; Wilson *et al.*, 2023). I extended these findings by testing the protein levels of senescence markers that were previously observed upon samuraciclib treatment in RPE1 cells. After 96 hours of samuraciclib treatment, there is a marked increase in p21 levels and a reduction in Lamin B1 (Figure 3.23). Phosphorylated Rb levels, a cell cycle entry marker, are also reduced (Figure 3.23) (Wilson *et al.*, 2023). This suggests that samuraciclib is able to induce senescence in MCF7 cells.

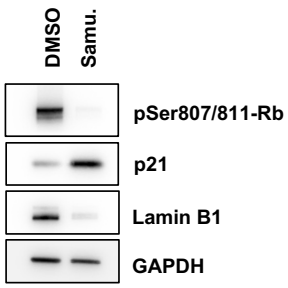

Figure 3.23: Samuraciclib induces senescence phenotypes in MCF7 cells. Western blot analysis from one experiment of whole-cell extract collected from MCF7 after 96 hours of treatment with vehicle control or 180 nM of samuraciclib (Samu.). GAPDH: loading control. Figure adapted from (Wilson *et al.*, 2023).

3.9. Growth-promoting mutation in MCF7 cells promotes samuraciclib sensitivity

MCF7 cell line is derived from an ER+ breast cancer and, as previously mentioned, has a growth-promoting mutation in the *PIK3CA* gene (E545K). *PIK3CA* gene encodes for p110α, which is a catalytic subunit of phosphatidylinositol 3-kinase (PI3K). This mutation is an activating mutation that leads to a hyperactivation of the mTOR signalling pathway (Beaver *et al.*, 2013; Liu *et al.*, 2018). The p110α-encoding gene has been found mutated in 20-50% of all breast cancers (Tian, Li and Zhang, 2019). Therefore, this is a clinically relevant cancer-associated mutation that promotes cellular growth. My data indicates that samuraciclib sensitivity positively correlates with mTOR activity in a small panel of breast cancer cell lines. To establish that growth signalling alone is causative of sensitivity, I used a pair of isogenic MCF7 cells, the parental MCF7 cell line with the native *PIK3CA* E545K mutation (*PIK3CA*^{mut}) and its isogenic pair where the E545K mutation in the *PIK3CA* gene has been reverted back to the wild-type sequence (*PIK3CA*^{wt}) (Beaver *et al.*, 2013). I tested levels of p70 S6 kinase phosphorylated at threonine residue 389, direct downstream target of mTOR, in these two cell lines and observed a small but significant increase in mTOR activity in the *PIK3CA*^{mut} cell line (Figures 3.24A and 3.24B) (Wilson *et al.*, 2023). This is in line with the previously published data, confirming there is an overactivation of the mTOR signalling pathway due to the *PIK3CA* E545K mutation (Beaver *et al.*, 2013; Liu *et al.*, 2018). These two cell lines are genetically identical apart from the *PIK3CA*

mutation, making them a suitable model to study the effect of this growth-promoting mutation and increased levels of mTOR activity on samuraciclib sensitivity.

Georgina Sava, a postdoc from our collaborators, the laboratory of Simak Ali at Imperial College London, tested the sensitivity of *PIK3CA*^{mut} and *PIK3CA*^{wt} MCF7 cell lines to samuraciclib. She treated these two isogenic cell lines with varying concentrations of samuraciclib for 30 days and counted cell number every 3 days using an IncuCyte. An IncuCyte measures cell confluency, however, as samuraciclib increases cell size, confluency measurement would not yield accurate readings. Therefore, she made the *PIK3CA*^{mut} and *PIK3CA*^{wt} MCF7 cell lines to stably express nuclear EGFP in order to accurately measure cell number using an IncuCyte. The analysis shows that samuraciclib reduces proliferation of both cell lines compared to a DMSO control (Figure 3.23D). However, *PIK3CA*^{mut} cells are more sensitive than *PIK3CA*^{wt} cells, as demonstrated by a significant difference between the cell number after 18 days for multiple concentrations of samuraciclib treatment (Figure 3.24C). The largest difference in cell number, and therefore sensitivity, is at 50 nM of samuraciclib, presenting the largest therapeutic window (Figure 3.24C). At 50 nM of samuraciclib, proliferation of *PIK3CA*^{mut} cells is completely inhibited as cell numbers remain very low throughout the 30 days of treatment, whereas *PIK3CA*^{wt} cells continue to proliferate (Figure 3.24D) (Wilson *et al.*, 2023). Moreover, I analysed protein levels of proliferative markers to further assess sensitivity differences between these two isogenic MCF7 cell lines. Since proliferation of *PIK3CA*^{mut} cells is fully inhibited at 50, 100 and 150 nM of samuraciclib, I tested these three concentrations. Levels of phosphorylated Rb and cyclin A2 reduce as a result of samuraciclib treatment in both *PIK3CA*^{mut} and *PIK3CA*^{wt} MCF7 cell lines compared to DMSO control, however, this decrease is more pronounced in *PIK3CA*^{mut} cells (Figure 3.24E). There is also a higher accumulation of p21 in *PIK3CA*^{mut} cells (Figure 3.24E). The western blot analysis further confirms IncuCyte cell number measurements suggesting that the growth-promoting mutation increases the sensitivity to samuraciclib.

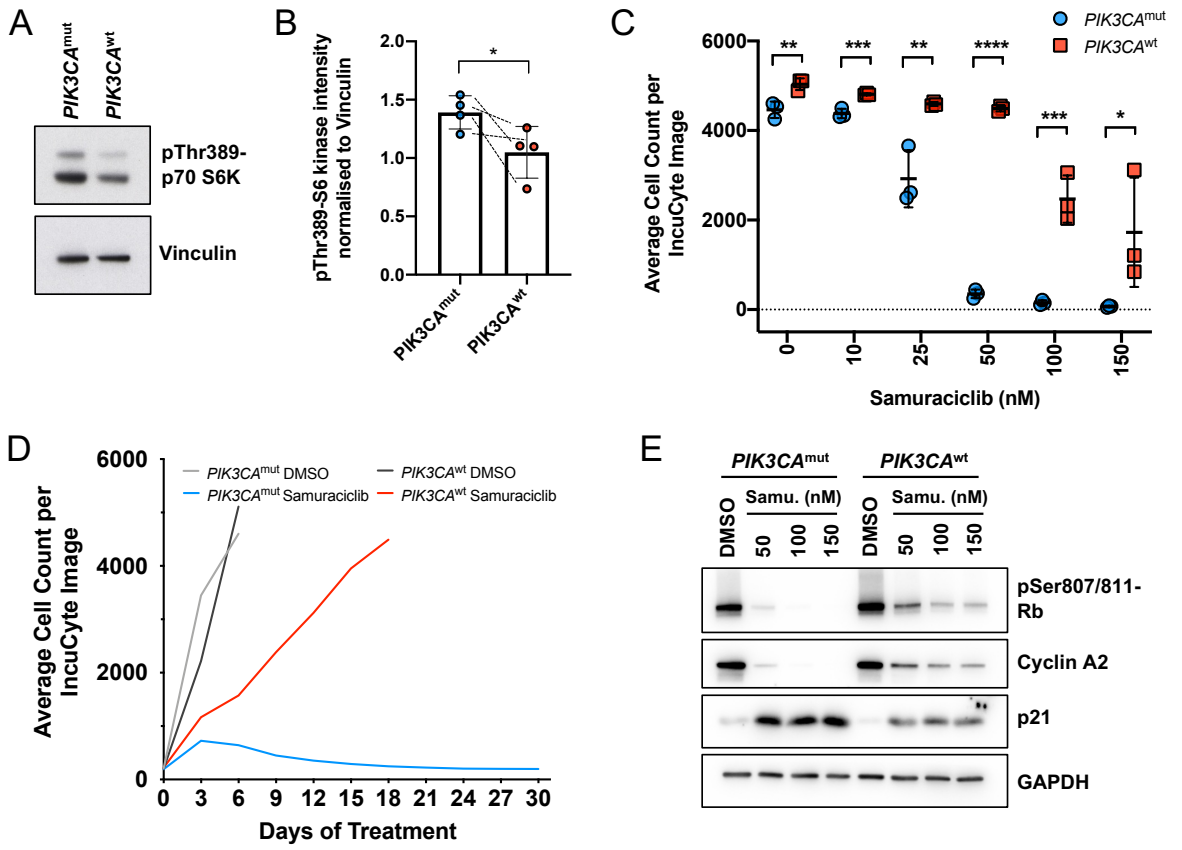

Figure 3.24: Growth-promoting mutation in MCF7 cells promotes samuraciclib sensitivity.

A) Representative western blot of whole-cell extracts collected from *PIK3CA*^{mut} and *PIK3CA*^{wt} MCF7 cells (n=4). Vinculin: loading control. **B)** Quantification of levels of p70 S6 kinase phosphorylated at residue Thr389 normalized to Vinculin as detected by western blots of whole-cell extracts from *PIK3CA*^{mut} and *PIK3CA*^{wt} MCF7 cells from four independent experiments. Statistical significance was calculated using an unpaired two-tailed t test. Error bars are SD. **C)** *PIK3CA*^{mut} and *PIK3CA*^{wt} MCF7 cells were treated with vehicle control or the indicated concentration of samuraciclib for 30 days. Cell numbers were assessed by IncuCyte every 3 days. Cell growth is plotted until day 30 or until cells reached confluency. Quantification of average cell numbers after 18 days of treatment from three independent experiments. Statistical significance was calculated using an FDR corrected unpaired t-test. (Experiment carried out by Georgina Sava). **D)** *PIK3CA*^{mut} and *PIK3CA*^{wt} MCF7 cells were treated with vehicle control or 50 nM of samuraciclib for 30 days. Cell numbers were assessed by IncuCyte every 3 days. Cell growth is plotted until day 30 or until cells reached confluency. Cell growth curves from a single representative experiment. (Experiment carried out by Georgina Sava). **E)** Western blot analysis from a representative experiment of whole-cell extracts collected from *PIK3CA*^{mut} and *PIK3CA*^{wt} MCF7 cells treated with vehicle control or indicated concentrations of samuraciclib (Samu.) for 96 hours. GAPDH: loading control. Figure adapted from (Wilson *et al.*, 2023).

The difference in sensitivity furthermore correlates with a larger increase in *PIK3CA*^{mut} cell size compared to *PIK3CA*^{wt} cells at lower samuraciclib concentrations (Figures 3.25A and 3.25B). The difference in cell volume is largest at 50 nM of samuraciclib; concentration at which there is the largest therapeutic window (Wilson *et al.*, 2023). This indicates that an increase in cellular growth positively correlates with increased cell size and sensitivity to samuraciclib. Altogether, these data support our model that samuraciclib is more effective in cells where growth signalling is hyperactivated through cancer-associated mutation.

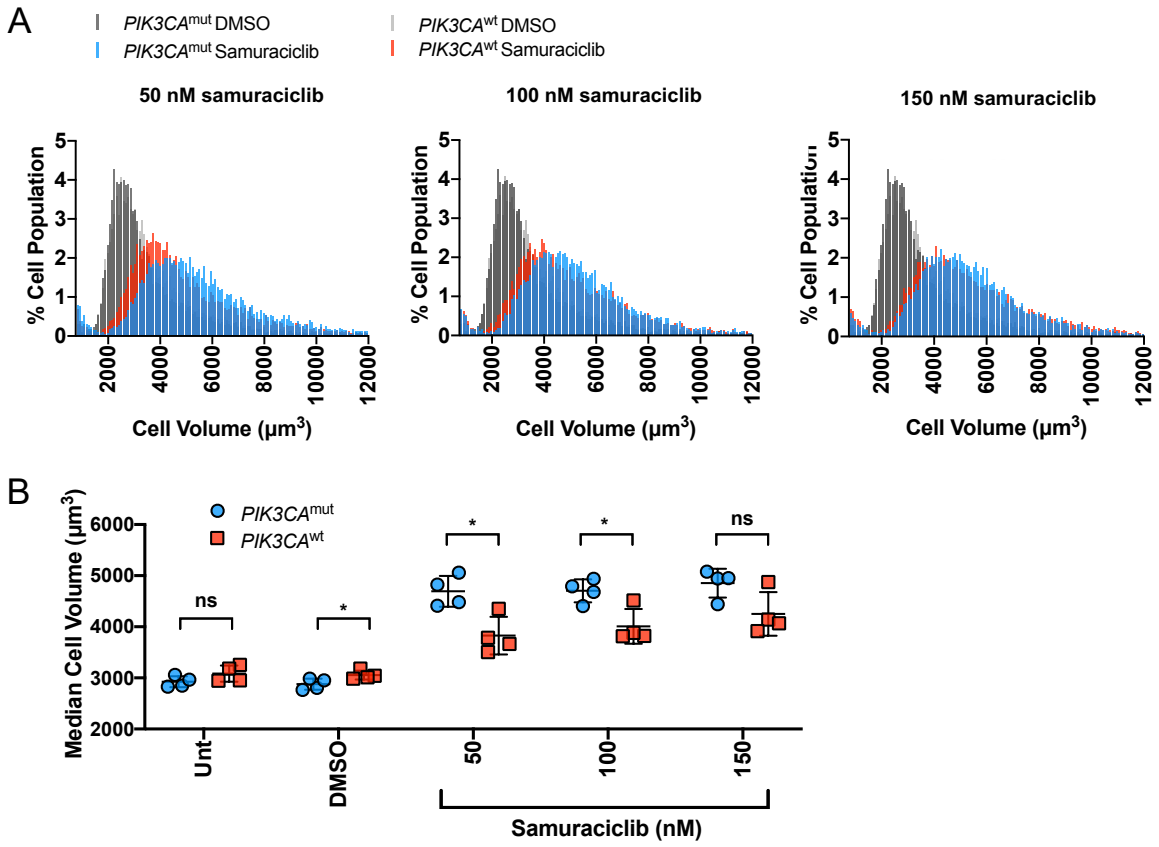

Figure 3.25: Increased levels of mTOR signalling correlates with increased cell size and sensitivity to samuraciclib.
PIK3CA^{mut} and *PIK3CA*^{wt} MCF7 cells were treated with vehicle control or the indicated concentrations of samuraciclib for 96 hours. **A)** Coulter counter data from a representative experiment. Percentage of cell population is plotted against various bins containing cells with different volumes in μm^3. **B)** Quantification of the median cell volume within the population from four independent experiments (representative shown in A). Statistical significance was calculated using an unpaired two-tailed t test. Error bars are SD. Figure adapted from (Wilson *et al.*, 2023).

3.10. Summary

The work presented in this chapter investigated the effect on cell cycle progression in response to the CDK7 inhibitor, samuraciclib, and the role of mTOR signalling in its mechanism of action. I showed that samuraciclib induces predominantly an arrest in a G1 state with a reduced G2 population. This arrest in G1 appears to be permanent via senescence as the vast majority of arrested cells do not re-enter the cell cycle upon samuraciclib removal. Those that enter a proliferative state after an arrest mainly undergo mitotic bypass which results in tetraploidy in the following G1 phase and is likely to lead to senescence.

To understand the mechanism by which samuraciclib induces a cell cycle exit as well as mechanisms that could cause treatment resistance, our collaborators from the Tyers lab carried out genome-wide CRISPR KO chemogenetic screen with samuraciclib to study drug-gene interactions. The screen revealed a potential role for active mTOR signalling in samuraciclib-induced cell cycle arrest, which I validated through multiple methods. Pharmacological inhibition of mTOR hampers samuraciclib-induced cell cycle arrest and senescence phenotypes previously observed upon samuraciclib treatment alone. Moreover, mTOR inhibition via serum depletion in non-transformed cells reduces the number of cells with a senescent phenotype, as a higher fraction of cells re-enter a proliferative state.

Cancer cells commonly harbour growth-promoting and mTOR signalling pathway-activating mutations. I showed that higher mTOR activity positively correlates with an increased sensitivity to samuraciclib in a small panel of breast cancer cell lines. Moreover, reverting a clinically relevant growth-promoting mutation in the *PIK3CA* gene to the WT sequence decreases samuraciclib sensitivity. Taken together, this shows that during a samuraciclib-dependent cell cycle arrest, cellular growth is needed to drive a permanent exit from the cell cycle, known as senescence.

The data in this chapter therefore revealed an important role for active growth signalling, via mTOR, in samuraciclib sensitivity. This insight could help explain not just the anti-cancer efficacy of samuraciclib and CDK7 inhibition, but maybe CDK inhibitors or cytostatic drugs in general. In addition, it also suggests that samuraciclib

should not be used in combination with mTOR inhibitors, since this could lead to treatment resistance.

4. CDK7 and CDK4/6 inhibition induce senescent phenotypes but cause long-term cell cycle withdrawal via different mechanisms

In the previous chapter, I demonstrated an important role for active growth signalling and an increase in cell size in the sensitivity to a CDK7 inhibitor samuraciclib and senescence induction (Wilson *et al.*, 2023). With CDK7's dual role in cell cycle regulation by activating all mitotic CDKs and transcription role in the RNA polymerase II-mediated transcriptional cycle, it is unclear through which mechanism samuraciclib mainly promotes a G1 arrest and a permanent loss in proliferative potential. A reason why samuraciclib predominantly induces a G1 cell cycle arrest, despite inhibiting the activity of CDK1, 2, 4 and 6, is likely due to the fact that CDK7 is not required for maintaining CDK2 and CDK1 activities but is required to maintain CDK4/6 activity (Schachter *et al.*, 2013). CDK7 inhibition therefore allows cells in the S-G2-M phases to progress through the cell cycle before arresting in a G1 state. As CDK7 is necessary for maintaining the activities of CDK4/6, inhibiting CDK7 would lead to an instant loss of activity of D-type cyclin-CDKs (Schachter *et al.*, 2013). Since CDK4/6 promote a proliferative G1 state, priming cells for a G1-to-S phase transition (Bertoli and de Bruin, 2014) acute loss of CDK4/6 activity upon CDK7 inhibition prevents G1 cells from entering S phase.

This suggests that the initial G1 cell cycle arrest induced by CDK7 inhibition is mediated through the inhibition of CDK4/6 activity, but with the added effect of loss of all mitotic CDK activities, most importantly CDK2. To investigate this, I compare the cytostatic effects of samuraciclib to a selective CDK4/6 inhibitor palbociclib, which induces a cell cycle exit with a G1 DNA content (Lanz *et al.*, 2022). Multiple pre-clinical studies observed senescence phenotypes upon palbociclib treatment (Leontieva and Blagosklonny, 2013; Wagner and Gil, 2020; Maskey *et al.*, 2021; Lanz *et al.*, 2022; Wang *et al.*, 2022) and demonstrated the role for excessive cellular hypertrophy in long-term cell cycle withdrawal (Leontieva and Blagosklonny, 2013; Neurohr *et al.*, 2019; Lanz *et al.*, 2022; Crozier *et al.*, 2023; Foy *et al.*, 2023; Manohar *et al.*, 2023).

These data suggest that there might be similarities between the cell cycle exit induced by CDK7 and CDK4/6 inhibition.

To investigate this, in this chapter, I compare cell cycle exit dynamics and expression of senescent phenotypes between samuraciclib and palbociclib in a non-transformed RPE1 cell line with intact cell cycle checkpoints. In addition, I compare the proliferative potential of samuraciclib- and palbociclib-arrested cells following drug wash-out. Finally, I analyse genome-wide CRISPR knock-out (KO) chemogenetic screen data for samuraciclib and palbociclib, carried out by our collaborators in the Tyers lab, to understand potential similarities and differences in the mechanisms of action of these two CDK inhibitors.

4.1. Palbociclib induces a G1 cell cycle arrest similar to samuraciclib, but at higher concentrations

To be able to compare the effects of palbociclib and samuraciclib treatment I first established the concentration at which these drugs induce a cell cycle arrest. Published research showed that the IC_{50} value of palbociclib in RPE1 cells is 150 nM (Crozier *et al.*, 2022). We have shown previously that the IC_{50} of samuraciclib (120 nM) is able to almost completely reduce the number of proliferating cells after 48 hours (Wilson *et al.*, 2023). I therefore assayed the amount of EdU incorporation after 48 hours of 150 nM of palbociclib treatment and observed a significant reduction in the percentage of EdU-positive cells (Figures 4.1A and 4.1B). However, the percentage of EdU-positive cells was significantly higher compared to samuraciclib treatment (Figure 4.1B). In fact, most studies that treat RPE1 cells with palbociclib to induce a complete G1 arrest use a concentration of 1000 nM or higher, which is more than six times the IC_{50} (Neurohr *et al.*, 2019; Crozier *et al.*, 2022, 2023; Lanz *et al.*, 2022; Manohar *et al.*, 2023). This indicates a more robust cell cycle arrest by samuraciclib at lower concentrations compared to palbociclib.

To find a palbociclib concentration that has a cell cycle arrest effect comparable to 120 nM of samuraciclib, I tested varying palbociclib concentrations between 150 nM and 1000 nM (not all shown). I observed that 400 nM of palbociclib is able to inhibit proliferation more similarly to 120 nM of samuraciclib. Moreover, 1000 nM of

palbociclib almost completely decreases the number of actively replicating cells after 48 hours (Figures 4.1C and 4.1D).

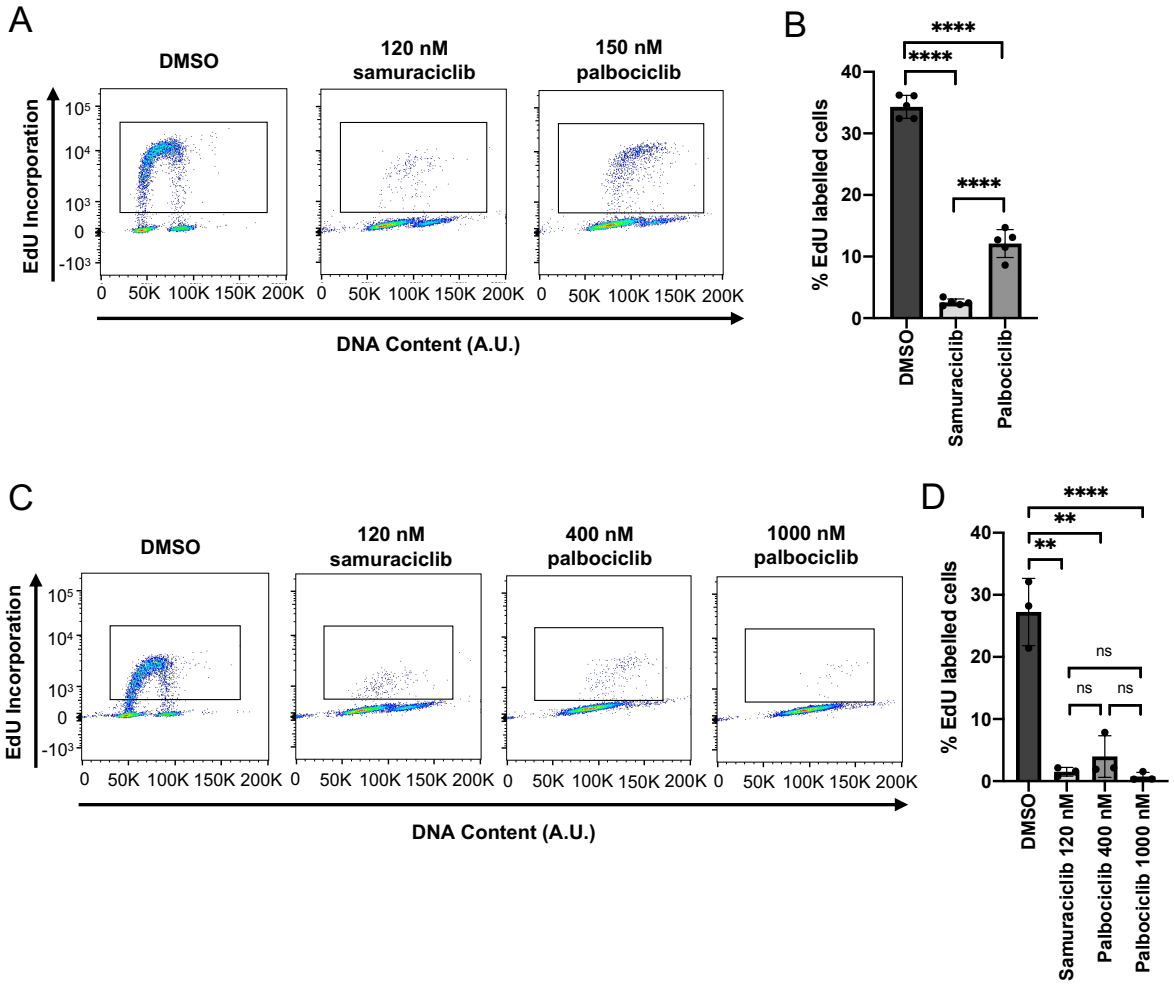

Figure 4.1: IC_{50} of palbociclib is not sufficient to completely reduce the number of proliferating cells.
A) RPE1 cells were treated with vehicle control, 120 nM of samuraciclib or 150 nM of palbociclib for 48 hours. Cells were incubated with EdU for 1 hour before collection. Pseudocoloured plots of flow cytometry data from a representative experiment. DNA content is plotted against EdU incorporation. Inset gate drawn to include EdU-positive cells. **B)** Quantification of the percentage of EdU-positive cells from three independent experiments (representative shown in A). Statistical significance was calculated using an unpaired two-tailed t test. Error bars are SD. **C)** RPE1 cells were treated with vehicle control, 120 nM of samuraciclib, 400 nM or 1000 nM of palbociclib for 48 hours. Cells were incubated with EdU for 1 hour before collection. Pseudocoloured plots of flow cytometry data from a representative experiment. DNA content is plotted against EdU incorporation. Inset gate drawn to include EdU-positive cells. **D)** Quantification of the percentage of EdU-positive cells from three independent experiments (representative shown in C). Statistical significance was calculated using an unpaired two-tailed t test. Error bars are SD.

Although there is no significant difference in the percentage of S phase cells after 48 hours of samuraciclib and 400 nM of palbociclib, the percentage of EdU-positive cells was slightly lower in samuraciclib treated cells. Therefore, to verify that the treatment with 400 nM of palbociclib is comparable to samuraciclib, I followed the cell cycle progression of S phase cells during a palbociclib treatment. I labelled S phase cells

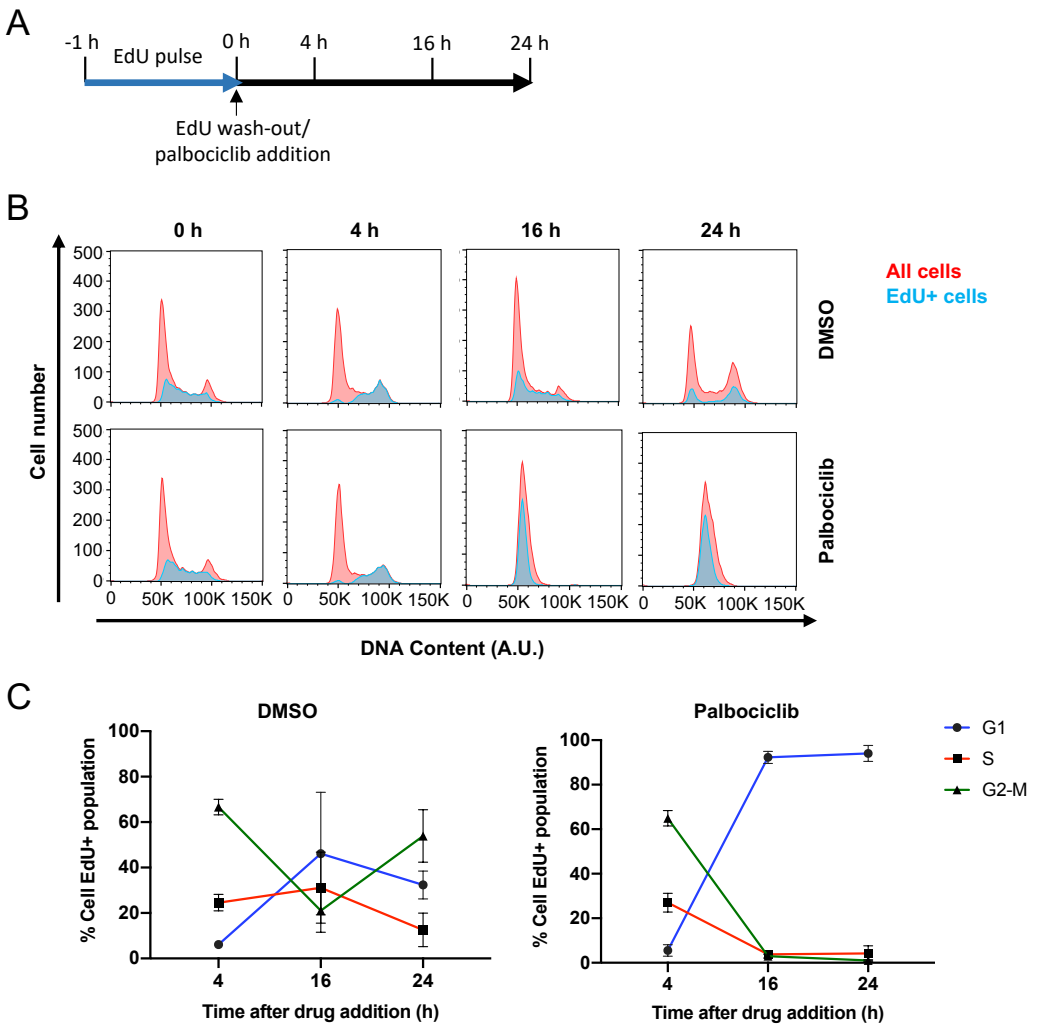

Figure 4.2: Palbociclib arrests RPE1 cells with a G1 DNA content.
A) A schematic illustrating the experimental set up. RPE1 cells were labelled with EdU for 1 hour. Unincorporated EdU was washed out of cells and the cells were treated with vehicle control or 400 nM of palbociclib. Cells were collected at the indicated time-points after drug addition and then analysed using flow cytometry. **B)** Flow cytometry data from a representative experiment. DNA content is plotted against cell count. In red are all cells in the sample and overlaid in blue are the EdU-positive cells. **C)** Quantifications from three independent experiments (representative shown in B) showing the percentage of EdU-positive cells in the different phases of the cell cycle. Error bars are SD.

with EdU for 1 hour prior to the treatment and followed them through the cell cycle for 24 hours as illustrated in the schematic in Figure 4.2A. I observed that palbociclib-treated S phase cells complete S-G2-M phases and arrest in the following G1 phase of the cell cycle (Figure 4.2B). As CDK2 and CDK1 are still active during a palbociclib treatment, regulating the progression through proliferative stages, this explains how CDK4/6 inhibition arrests the cells with a G1 DNA content after 16 hours. These results confirm that 400 nM of palbociclib causes a similar increase in G1 cell population to samuraciclib, as more than 90% of EdU-labelled cells arrest in a G1 phase after 24 hours of treatment (Figure 4.2C). This is comparable to a samuraciclib-induced G1 cell cycle arrest (Wilson *et al.*, 2023), and justifies the use of 400 nM and 1000 nM of palbociclib in further experiments.

4.2. Robust induction of senescent phenotypes by palbociclib treatment

Samuraciclib treatment induces senescent phenotypes, such as an elevated SA β-gal activity and an increase in cell size (Wilson *et al.*, 2023). I compared these to palbociclib treatment and observed that palbociclib induces these phenotypes more profoundly. SA β-gal activity, as determined by C_{12}FDG fluorescence, increases to a greater extent during a 96-hour palbociclib treatment (Figures 4.3A and 4.3B). As I have observed before, higher SA β-gal activity correlates with larger cell size during samuraciclib treatment, as described in the previous chapter (Figures 3.15A and 3.15B). This suggests that palbociclib might cause greater cellular hypertrophy. Cell volume is indeed significantly larger after treating the cells for 48 hours with the CDK4/6 inhibitor than with the CDK7 inhibitor (Figures 4.3C and 4.3D).

Furthermore, I investigated whether palbociclib induces a rapid increase in p21 levels as was observed for samuraciclib. Palbociclib is able to induce p21 accumulation; however, this occurs at a later time-point compared to samuraciclib (Figure 4.4). p21 accumulation in response to samuraciclib occurs already after 24 hours of treatment, which coincides with the reduction in phosphorylated Rb levels. However, in response to palbociclib, an increase in p21 levels occurs only after 72 hours of treatment (Figure 4.4). Interestingly, the increase in p21 levels occurs almost 48 hours after the reduction

in levels of phosphorylated Rb. This suggests that samuraciclib-induced rapid accumulation of p21 coincides with the cell cycle arrest, whilst in response to palbociclib treatment, p21 levels increase after the cell cycle arrest is induced at 24 hours.

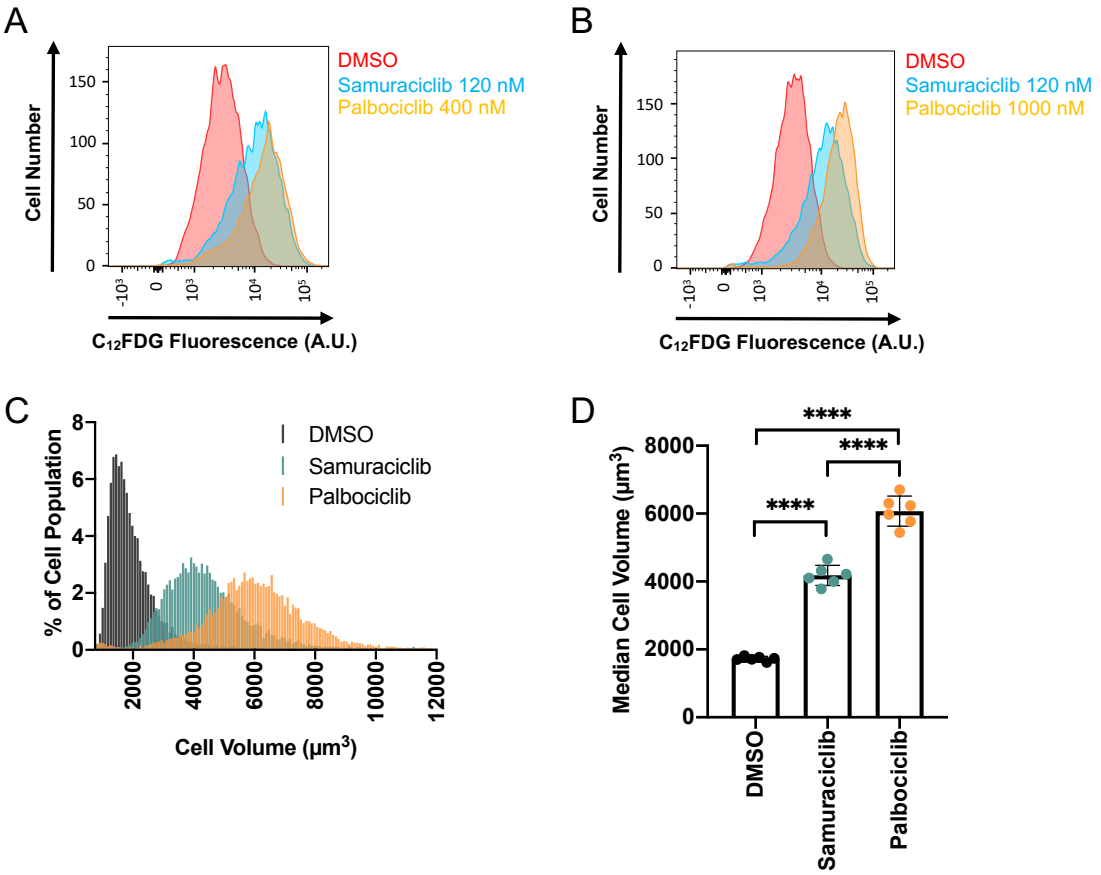

Figure 4.3: Palbociclib induces senescence phenotypes to a greater extent than samuraciclib.
A) Flow cytometry data from a representative experiment (n=2), detecting SA β-gal activity with the fluorescent β-gal substrate, C_{12}FDG, in cells treated with vehicle control, 120 nM of samuraciclib or 400 nM of palbociclib for 96 hours. C_{12}FDG fluorescence is plotted against cell count. **B)** Flow cytometry data from a representative experiment (n=2), detecting SA β-gal activity with the fluorescent β-gal substrate, C_{12}FDG, in cells treated with vehicle control, 120 nM of samuraciclib or 1000 nM of palbociclib for 96 hours. C_{12}FDG fluorescence is plotted against cell count. **C)** Coulter counter data from a representative experiment, with RPE1 cells treated with vehicle control, 120 nM of samuraciclib or 1000 nM of palbociclib for 48 hours. Percentage of cell population is plotted against various bins containing cells with different volumes in µm^3. **D)** Coulter counter data quantification of the median cell volume within the population from six independent experiments (representative shown in C). Statistical significance was calculated using an unpaired two-tailed t test. Error bars are SD.

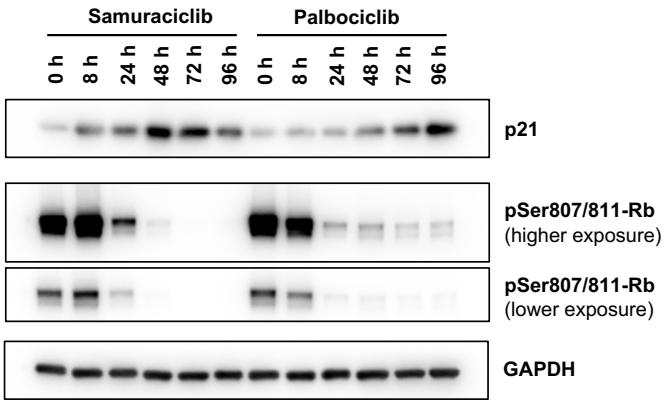

Figure 4.4: Samuraciclib leads to a more rapid increase in a CDK inhibitor p21 compared to palbociclib.
Representative western blot of whole-cell extracts collected from RPE1 cells at indicated time-points after treatment with 120 nM of samuraciclib or 1000 nM of palbociclib. GAPDH: loading control.

4.3. Palbociclib induces a less robust cell cycle arrest than samuraciclib

The data presented in the last section showed that samuraciclib- and palbociclib-induced arrests, although both cytostatic, differ in the extent to which they induce specific senescent phenotypes in RPE1 cells. Palbociclib treatment induces a great increase in cell size and SA β-gal activity, whereas samuraciclib treatment causes much quicker p21 accumulation. Next, I tested how these differences relate to the main feature of a senescent state, the inability to return to a proliferative state. Samuraciclib was shown to induce a persistent cell cycle exit after 48 hours of treatment, most clearly observed via a colony formation assay. I therefore compared this to the ability of palbociclib-arrested cells to form colonies after drug wash-out. Palbociclib is a non-covalent CDK4/6 inhibitor and previous research showed it can be washed out from cells, suggesting this inhibition is reversible (Crozier *et al.*, 2022). I observed that after 48 hours of palbociclib treatment, although there is a significant decrease in colony formation compared to DMSO control, this is significantly higher than colony formation following samuraciclib treatment (Figures 4.5A and 4.5B). This is in line with published results which show that a significant fraction of G1 arrested cells are able to re-enter the cell cycle 24 hours after a 48- or 72-hour palbociclib treatment (Crozier *et al.*, 2022). The published data indicates that it requires at least a

96-hour palbociclib treatment to prevent cell cycle re-entry, suggesting that palbociclib requires a longer treatment duration to induce a stronger reduction of proliferative potential. This indicates that samuraciclib induces a more robust cell cycle exit than palbociclib (Figure 4.5B), despite palbociclib treatment causing a larger increase in cell size and SA β-gal activity (Figure 4.3). This suggests that cell size *per se* cannot explain the differences in cell cycle exit dynamics between these two CDK inhibitors. A potential reason for samuraciclib causing a more robust cell cycle exit could be due to the rapid increase in p21 levels (Figure 4.4). This will be discussed further in chapter 5.

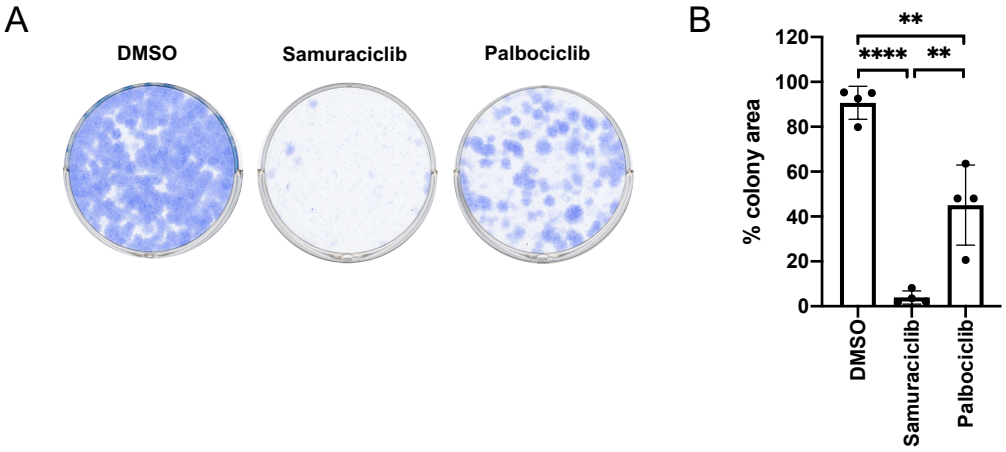

Figure 4.5: Samuraciclib induces a more robust cell cycle arrest compared to palbociclib.
RPE1 cells were treated with vehicle control, 120 nM of samuraciclib or 1000 nM of palbociclib for 48 hours. **A)** After 48 hours of treatment, cells were washed five times with PBS to remove the drugs from cells. Cells were re-seeded in the absence of drugs and allowed to grow for 9-11 days. Colonies were stained and visualised with Methylene Blue. **B)** Quantification of percentage of colony area from four independent experiments (representative shown in A). Statistical significance was calculated using an unpaired two-tailed t test. Error bars are SD.

4.4. Genome-wide CRISPR KO chemogenetic screen suggests palbociclib and samuraciclib mechanisms of action differ

A genome-wide CRISPR KO chemogenetic screens can identify genes important for drug sensitivity and resistance mechanisms. This approach was essential in uncovering the role of active cellular growth via mTOR signalling in samuraciclib sensitivity. Since there are both similarities and differences in the effect of samuraciclib

and palbociclib treatment, I decided to compare our samuraciclib chemogenetic screen data with that for palbociclib to further investigate these two CDK inhibitors. Our collaborators from the Tyers lab carried out two genome-wide CRISPR KO chemogenetic screens in NALM-6 cells, one with 335 nM and the second with 1000 nM of palbociclib. NALM-6 cells were previously shown to be sensitive to a palbociclib treatment, with 1000 nM greatly increasing the fraction of G1 cells (Manohar *et al.*, 2023). Testing a lower concentration as well, 335 nM, might allow for a better identification of positive and negative interactors. I therefore calculated an average RANKS score between the two screens and ordered them based on their RANKS scores.

To obtain a better understanding of the similarities and differences between the mechanisms of action of palbociclib and samuraciclib, I listed the top 50 positive and negative interactors with palbociclib based on their RANKS scores and carried out GO analysis using GOrilla tool (Eden *et al.*, 2009) and processing by REVIGO to remove any redundant GO terms (Supek *et al.*, 2011), as I described for samuraciclib in chapter 3. The GO terms for positive and negative interactors with palbociclib are ordered by their enrichment score (Figures 4.6A and 4.6B). Interestingly, “negative regulation of TOR signalling” and “regulation of TOR signalling” are among the most enriched GO terms for positive interactors (Figure 4.6A). This is opposite to samuraciclib, where these GO terms are found within the negative interactors (Figure 3.8B). Out of 8 positive gene interactors with palbociclib found in these two mTOR-related GO terms, 6 were in common with negative gene interactors with samuraciclib (Table 4.1). I listed the individual hits that were found within the GO terms related to mTOR signalling in the samuraciclib screen and compared the RANKS scores found in the palbociclib chemogenetic screen (Table 4.1). I observed that positive regulators of mTOR signalling, which are among the top positive interactors with samuraciclib, have RANKS scores close to 0 (depicting no interaction) in response to palbociclib. Negative regulators of mTOR signalling, which are among the top negative interactors with samuraciclib, show positive average RANKS scores in the palbociclib screens. This suggests that mTOR signalling might have different effects on CDK7 and CDK4/6 inhibition where on the contrary to samuraciclib, inactive mTOR signalling might increase sensitivity to palbociclib treatment.

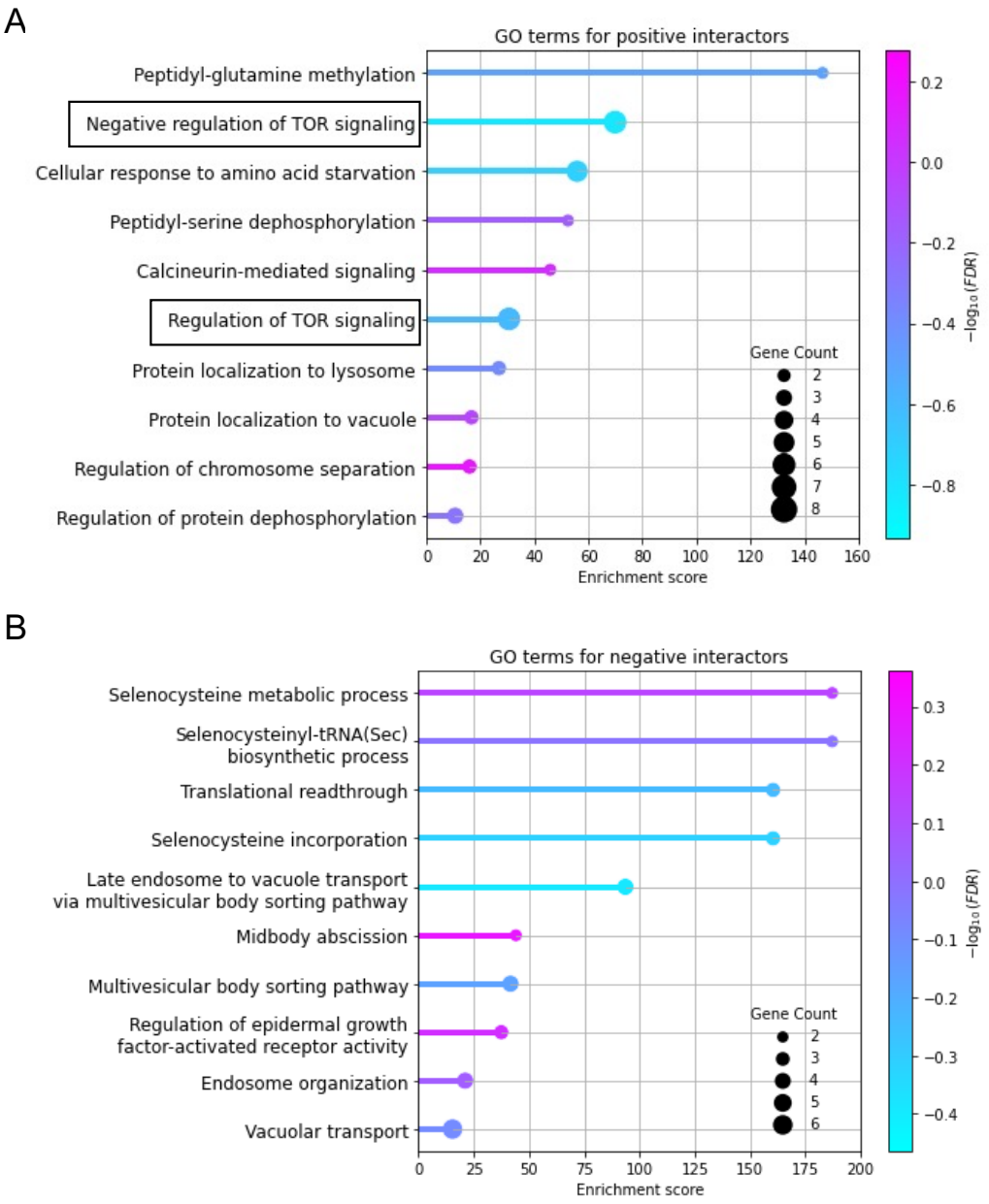

Figure 4.6: Genome-wide CRISPR KO chemogenetic screen reveals negative regulation of mTOR signalling might be required for palbociclib sensitivity. Pathway enrichment bubble plot representations of the most enriched GO terms among the top 50 interactors with palbociclib, as determined using the GOrilla tool and processing by REVIGO. The GO terms are ordered by their enrichment score. Colour coding represents the -$\log_{10}$(false discovery rate [FDR] q-value), with the most statistically significant GO terms closer to the magenta end of the scale found on the right, and the least statistically significant GO terms closer to the light blue end of the scale. GO terms that include mTOR signalling are highlighted by the black boxes. Bubble size indicates number of genes associated with each GO term. Graphs were created using Matplotlib package in Python. **A)** Representation of the most enriched GO terms among the top 50 positive interactors with palbociclib. **B)** Representation of the most enriched GO terms among the top 50 negative interactors with palbociclib.

Table 4.1: Gene interactors with samuraciclib found in the GO terms related to mTOR signalling pathway compared to their interaction with palbociclib.

Gene	Samuraciclib (RANKS score)					Palbociclib (RANKS score)		
	180 nM	350 nM	350 nM	501 nM	Average	335 nM	1 μM	Average
MLST8	1.53	2.84	3.05	3.91	**2.8325**	-0.21	1.31	0.55
MAPKAP1	1.19	3.46	3.58	3.09	**2.83**	0.06	1.33	0.695
RICTOR	1.2	2.82	3.86	1.55	**2.3575**	0.91	0.55	0.73
LAMTOR4	0.5	1.04	2.6	2.41	**1.6375**	-0.02	1.49	0.735
NPRL3	-1.26	-3.47	-2.58	-2.94	**-2.5625**	5.6	0.95	3.275
DEPDC5	-1.59	-3.31	-1.82	-1.93	**-2.1625**	5.33	2.01	3.67
ITFG2	-1.9	-1.36	-1.86	-2.95	**-1.685**	3.87	0.14	2.005
NPRL2	-1.22	-2.47	-2.23	-1.22	**-1.785**	6.91	2.15	4.53
SZT2	-0.67	-2.41	-1.91	-2.04	**-1.7575**	4.37	0.56	2.465
TSC2	-1.44	-2.24	-1.73	-1.33	**-1.685**	2.07	1.94	2.005

4.5. Inhibition of mTOR signalling increases sensitivity to palbociclib during treatment

To validate the results obtained from the chemogenetic screens in RPE1 cells, I used a pharmacological inhibition of mTOR via Torin1, as was done for samuraciclib in chapter 3. 25 nM of Torin1 does not have a significant effect on proliferation of RPE1 cells (Figures 4.7A and 4.7B) and it leads to a strong mTOR inhibition, as demonstrated by the reduction in phosphorylation of the p70 S6 kinase at threonine residue 389 (Figure 4.7C). When I combined palbociclib and Torin1 treatments for 48 hours, I observed a stronger inhibition of proliferation compared to palbociclib treatment alone. Although this difference is not significant, the cell cycle analysis is corroborated by western blot analysis of a proliferative marker, phosphorylated Rb, with a greater reduction in the palbociclib and Torin1 co-treatment compared to palbociclib alone (Figure 4.7C). Of note, I treated cells with palbociclib concentrations that induce a strong cell cycle arrest. Therefore, to assess the difference between the single treatment and co-treatment, in my future experiments I should use lower palbociclib concentrations, such as the IC_{50} value (150 nM), at which this effect might be more apparent. In fact, the RANKS scores from the chemogenetic screen show that the lower palbociclib concentration (335 nM) had stronger positive interactions

with the negative mTOR signalling regulators compared to the higher palbociclib concentration (1000 nM) (Table 4.1).

Taken together, this data in RPE1 cells confirms the results from the screen. Pharmacological mTOR inhibition decreases samuraciclib sensitivity and slightly increases the sensitivity to palbociclib treatment in RPE1 cells. In line with this data, several studies found synergistic effects of inhibition of the PI3K-Akt-mTOR signalling axis with palbociclib (Herrera-Abreu *et al.*, 2015; Bonelli *et al.*, 2017). This might be due to the suppression of cyclin D1 levels that could otherwise reduce sensitivity to this CDK4/6 inhibition.

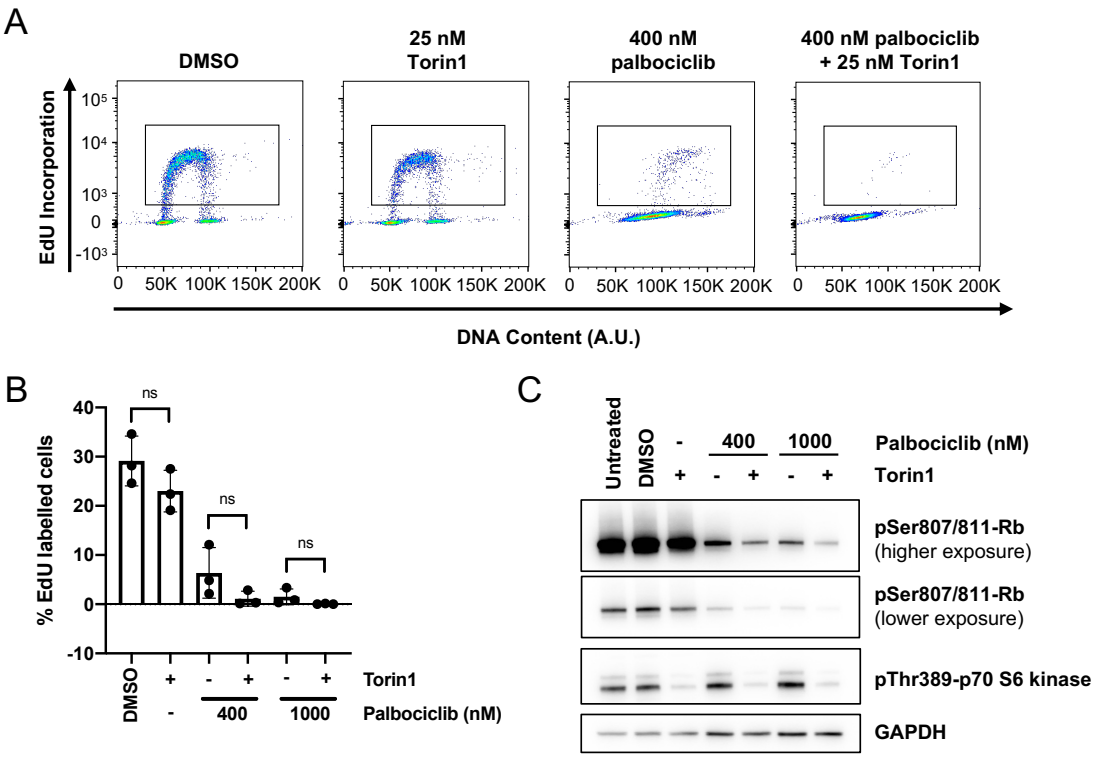

Figure 4.7: Pharmacological inhibition of mTOR slightly increases palbociclib sensitivity in RPE1 cells.
RPE1 cells were treated with vehicle control, 25 nM of Torin1 alone, indicated concentrations of palbociclib alone, or palbociclib and 25 nM of Torin1 for 48 hours. **A)** Cells were incubated with EdU for 1 hour before collection. Pseudocoloured plots of flow cytometry data from a representative experiment. DNA content is plotted against EdU incorporation. Inset gate drawn to include EdU-positive cells. **B)** Quantification of the percentage of EdU-positive cells from three independent experiments (representative shown in A). Statistical significance was calculated using an unpaired two-tailed t test. Error bars are SD. **C)** Representative western blot of whole-cell extracts collected from RPE1 cells. GAPDH: loading control.

4.6. Inhibition of mTOR signalling during palbociclib treatment increases proliferative potential following drug removal

Even though the data from the previous sections suggests that mTOR inhibition increases the efficacy of palbociclib, multiple studies have shown that preventing cellular growth and biomass accumulation during the G1 arrest induced by palbociclib renders cells more likely to re-enter the proliferative state following drug removal (Neurohr *et al.*, 2019; Lanz *et al.*, 2022; Crozier *et al.*, 2023; Manohar *et al.*, 2023). I therefore decided to test this in my system to be able to make better comparisons with the role of cellular growth in samuraciclib sensitivity. I used 1000 nM of palbociclib as it is able to potently induce a G1 arrest in both palbociclib single treatment and palbociclib combined with Torin1 (Figure 4.7B). Pharmacologically inhibiting mTOR during a 48-hour palbociclib treatment decreases cell volume significantly compared to palbociclib treatment alone (Figures 4.8A and 4.8B). After 48 hours of treatments, I washed the drugs away and re-seeded the cells at low numbers and cultured them for approximately 10 days to allow colony formation and assess proliferative potential. The release experiment showed that reducing cellular growth during a G1 arrest increases the number of cells able to re-enter the cell cycle and form colonies, as demonstrated by the significantly higher colony formation compared to enlarged palbociclib arrested cells where mTOR signalling is active (Figures 4.8C and 4.8D).

Similar results, as with the pharmacological inhibition of the mTOR kinase, are observed when cellular growth and mTOR activity is negatively regulated by serum depletion (Figure 4.9). Serum depletion prevents cell size increase during palbociclib treatment (Figures 4.9A and 4.9B). When both growth-restricted and enlarged palbociclib-arrested RPE1 cells are released from the 48-hour CDK4/6 inhibitor arrest, enlarged cells have a lower proliferative potential compared to cells that had reduced cellular growth prior to drug wash-out (Figures 4.9C and 4.9D).

The data from both the pharmacological inhibition of mTOR and serum depletion support previously published studies and demonstrate an important role for mTOR-dependent cellular growth and an increase in cell size in inducing a more robust permanent cell cycle exit (Neurohr *et al.*, 2019; Lanz *et al.*, 2022; Crozier *et al.*, 2023;

Foy *et al.*, 2023; Manohar *et al.*, 2023). This data therefore demonstrates different

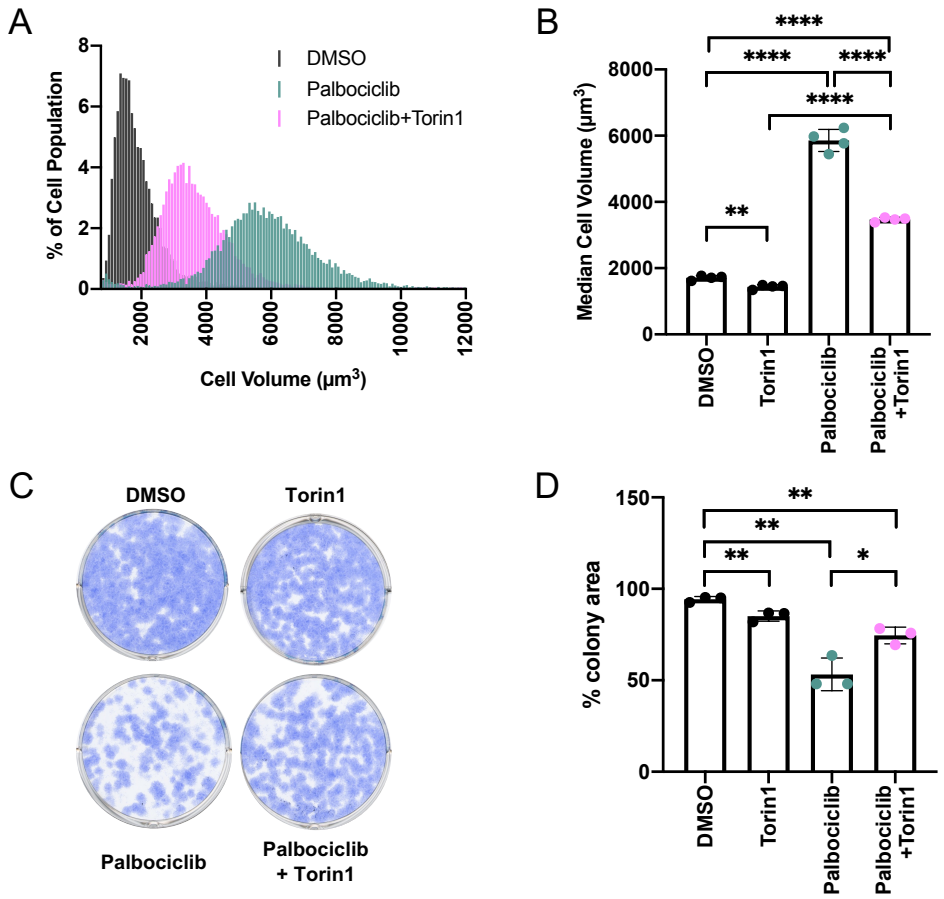

Figure 4.8: Pharmacological inhibition of mTOR activity during palbociclib treatment reduces cell size and increases proliferative potential after drug wash-out.

RPE1 cells were treated with vehicle control, 25 nM of Torin1 alone, 1000 nM of palbociclib alone or 1000 nM of palbociclib and 25 nM of Torin1 for 48 hours. **A)** Coulter counter data from a representative experiment. Percentage of cell population is plotted against various bins containing cells with different volumes in μm^3. **B)** Quantification of the median cell volume within the population from four independent experiments (representative shown in A). Statistical significance was calculated using an unpaired two-tailed t test. Error bars are SD. **C)** After 48 hours of treatment, cells were washed five times with PBS to remove the drugs from cells. Cells were re-seeded in the absence of drugs and allowed to grow for 9-11 days. Colonies were stained and visualised with Methylene Blue. **D)** Quantification of percentage of colony area from three independent experiments (representative shown in C). Statistical significance was calculated using an unpaired two-tailed t test. Error bars are SD.

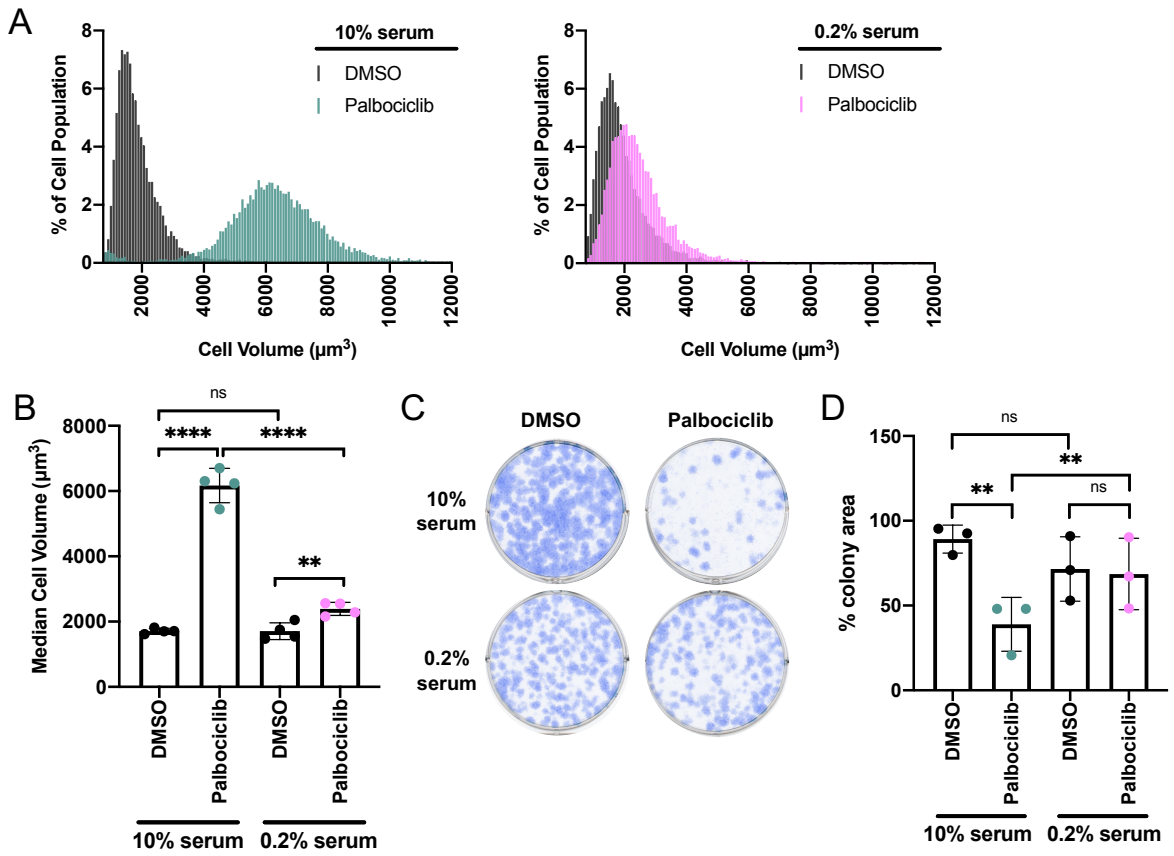

Figure 4.9: Serum depletion-driven reduction in cell size during palbociclib treatment increases proliferative potential after drug wash-out.
RPE1 cells were treated with vehicle control or 1000 nM of palbociclib for 48 hours while cultured in 10% or 0.2% serum (FBS)-supplemented media. **A)** Coulter counter data from a representative experiment. Percentage of cell population is plotted against various bins containing cells with different volumes in μm^3. **B)** Quantification of the median cell volume within the population from four independent experiments (representative shown in A). Statistical significance was calculated using an unpaired two-tailed t test. Error bars are SD. **C)** After 48 hours of treatment, cells were washed five times with PBS to remove the drugs from cells. Cells were re-seeded in the absence of drugs and allowed to grow for 9-11 days in 10% serum (FBS)-supplemented media. Colonies were stained and visualised with Methylene Blue. **D)** Quantification of percentage of colony area from three independent experiments (representative shown in C). Statistical significance was calculated using an unpaired two-tailed t test. Error bars are SD.

roles of cellular growth in CDK4/6 inhibitor-mediated cell cycle arrest and exit. On one hand, inhibiting mTOR signalling increases the efficacy of palbociclib to arrest the cell cycle in a G1 state (Figures 4.7A and 4.7B), and on the other, hinders the ability of palbociclib to induce a permanent cell cycle exit. This is likely due to the fact that inhibiting mTOR signalling lowers CDK4/6 activity, but also inhibits an increase in cell

size and the accumulation of cell mass, allowing more cells to re-enter the cell cycle after palbociclib removal (Figures 4.8 and 4.9).

Although I show the effects after 48 hours of treatment which does not induce a robust cell cycle exit as samuraciclib, comparable conclusions were made with longer palbociclib treatment durations, such as 6 or 7 days (Lanz *et al.*, 2022; Foy *et al.*, 2023; Manohar *et al.*, 2023).

4.7. Prolonged G1 arrest causes replication stress upon treatment release

I showed that a 48-hour treatment with samuraciclib causes a more significant loss in proliferative potential compared to palbociclib, mainly due to senescence induction where cells remain arrested and do not re-enter the cell cycle, as described in chapter 3. However, my data does not explain what causes a partial loss in proliferative potential after release from palbociclib treatment.

I was involved in another recently published study that was investigating the role of cell size enlargement in a permanent cell cycle exit after a prolonged G1 cell cycle arrest (Manohar *et al.*, 2023). They treated RPE1 cells with palbociclib for 7 days and observed that after drug wash-out, 1/3 of the cell population remains arrested, indicating a senescent state. From the remaining cell population that re-enters the cell cycle, a fraction undergoes mitotic bypass where a G2 cell skips mitosis and enters a G1 state, and the majority reaches mitosis but with a high frequency of mitotic abnormalities, such as binucleation or nuclear fragmentation. Furthermore, they observed that a large fraction of enlarged cells displays DNA damage after G1-release. When they blocked an increase in cell size during a prolonged palbociclib-mediated G1 arrest by treating the cells with a high concentration of Torin1 (500 nM), they observed the majority of cells re-entering the cell cycle and normally progressing to mitosis, as well as reduced levels of DNA damage. This suggested that preventing excessive cellular growth during a G1 arrest protects the cells from a permanent cell cycle arrest or mitotic defects after cell cycle re-entry (Manohar *et al.*, 2023).

A previous study has suggested that a prolonged G1 arrest by CDK4/6 inhibitors induces a long-term cell cycle withdrawal because of downregulation of origin licensing components, which they postulated would cause replication stress when cell re-entered the cell cycle (Crozier *et al.*, 2022). In this study they did not establish if these conditions do indeed cause replication stress. Since replication stress is defined as slowing down or stalling of active replication forks, the standard technique for measuring replication stress levels are DNA fibre assays, which measure the speed of replication forks (Zeman and Cimprich, 2014). In a collaboration with the laboratory of Gabriel Neurohr at ETH Zurich, I carried out DNA fibre assay on G1-released enlarged and growth-restricted cells, as illustrated in a schematic in Figure 4.10A, to investigate whether this could explain defects observed upon cell cycle re-entry after drug removal. In a DNA fibre assay, cells are sequentially incubated with two nucleotide analogues, CIdU and IdU, which incorporate into the replicating DNA during S phase. These analogues can then be visualised by immunofluorescence (Petermann, Woodcock and Helleday, 2010). I was interested in the replicative fork speed, which can be estimated by measuring replicative track lengths of ongoing fibres, represented by two consecutive analogue signals. Shorter track lengths indicate stalled forks and in turn replication stress. I therefore measured replicative track length of G1-released cells to determine whether these cells undergo DNA replication stress. Compared to cycling cells, enlarged G1-released cells undergo mild replication stress levels, demonstrated by shorter DNA fibres (Figures 4.10C and 4.10D) (Manohar *et al.*, 2023). This was observed by another recent study (Crozier *et al.*, 2023). This is slightly rescued by limiting biomass accumulation during the G1 arrest. However, compared to cycling cells, both enlarged and growth-restricted cells have slightly, but significantly, shorter DNA fibres (Figures 4.10C and 4.10D). This suggests a prolonged G1 arrest *per se* causes mild levels of replication stress. One possible explanation for why enlarged cells upon re-entry into the cell cycle after a prolonged G1 arrest experience higher levels of DNA damage than smaller cells might be their inability to cope with replication stress and DNA damage. Our collaborator's work shows that larger cells do indeed have a dampened DNA damage response (DDR) to repair the DNA lesions. Overall, they show that the cell cycle defects observed after a prolonged G1 arrest is cell size-dependent (Manohar *et al.*, 2023).

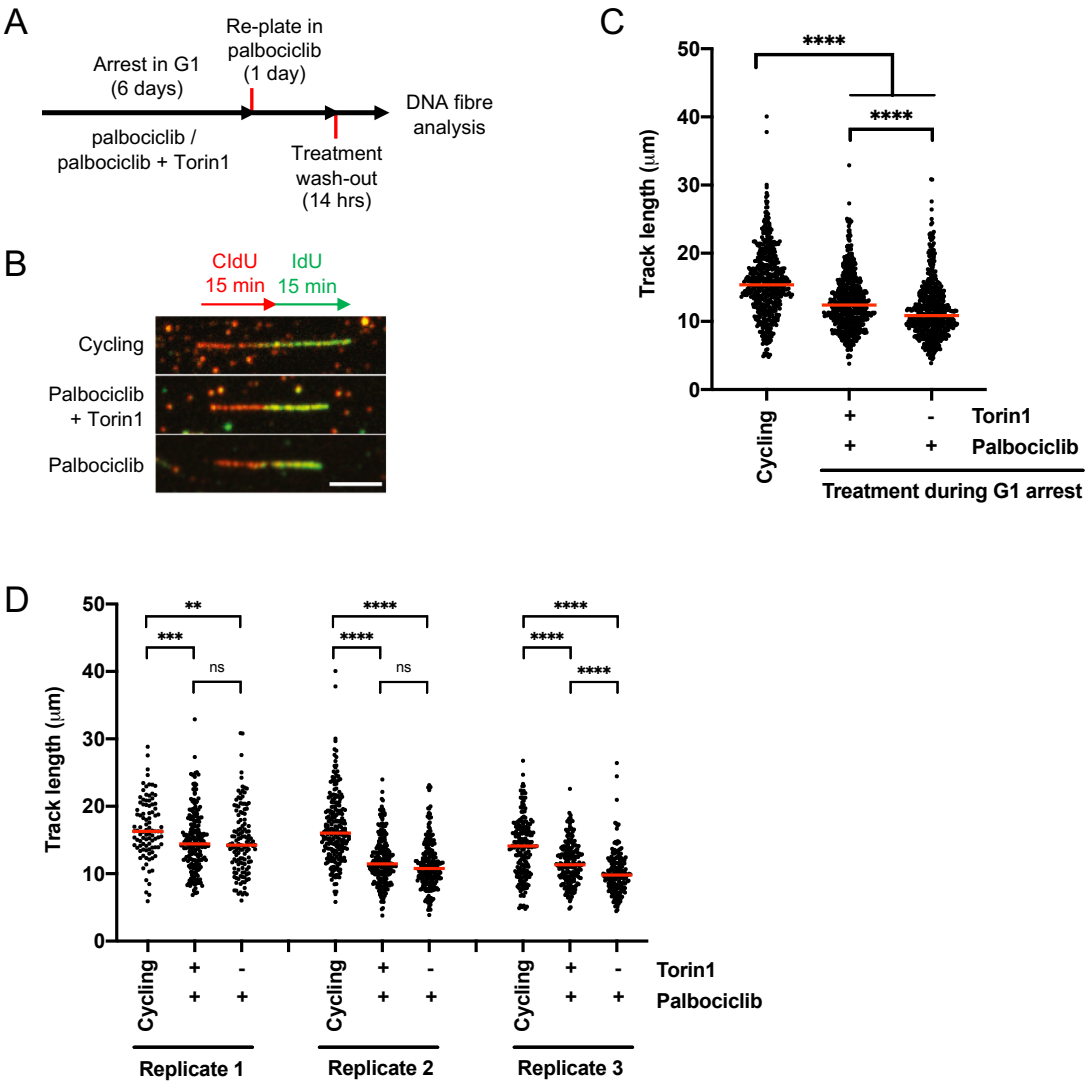

Figure 4.10: Prolonged G1 arrest causes a modest replication stress upon release to a new cell cycle.

A) A schematic illustrating experimental set up. RPE1 cells were treated with 1 μM of palbociclib alone or 1 μM of palbociclib and 500 nM of Torin1 for 6 days. Cells were then re-plated in presence of 1 μM of palbociclib. After 24 hours, cells were washed three time with PBS to remove palbociclib from cells, fresh media was added, and cells were culture for another 14 hours after which cells were pulse-labelled as shown in B and collected for DNA fibre analysis. **B)** A schematic illustrating pulse labelling with two nucleotides, CIdU and IdU for 15 min each. Immunofluorescence images of representative fibres of cycling cells or cells released from palbociclib or palbociclib and Torin1 arrest for 14 hours. Scale bar represents 5 μm. **C)** Quantification of B, track length of >480 fibres from three independent experiments were scored. Statistical significance was calculated using Kruskal-Wallis test (one-way ANOVA on ranks). Bars show median track length. **D)** Data from C re-plotted with the three replicates separated. Statistical significance was calculated using Kruskal-Wallis test (one-way ANOVA on ranks). Bars show median track length. Figure adapted from (Manohar *et al.*, 2023).

Whilst this work was carried out after 7 days of palbociclib treatment, I observed that even a shorter 48-hour palbociclib treatment causes some mitotic abnormalities. I treated cells with palbociclib for 48 hours, washed the drug away and cultured the cells for another 96 hours in drug-free media. 96 hours after drug release, I stained the nuclei and imaged nuclear shape using immunofluorescence. Although not quantified as the experiment was carried out once and requires repeating, I observed multiple events of nuclear fragmentation and micronuclei, which are all marks of DNA damage (Figure 4.11). This suggests that an increase in cell size after 48 hours might already cause some cell cycle defects observed in our collaborative study (Manohar *et al.*, 2023). However, 96 hours after samuraciclib treatment, there are almost no events of nuclear fragmentation (Figure 4.11). It needs to be established if this is the result of the more robust cell cycle arrest caused by a CDK7 inhibition, where only a few cells enter the cell cycle, or cells re-entering the cell cycle never enter mitosis.

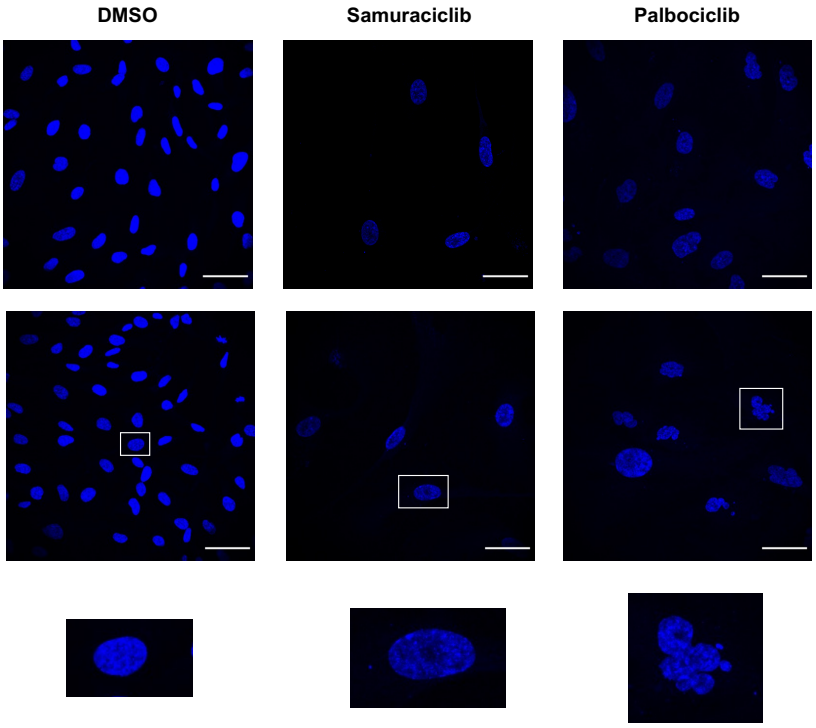

Figure 4.11: Palbociclib release leads to irregularities in nuclear morphology. RPE1 cells were treated with vehicle control, 120 nM of samuraciclib or 1000 nM of palbociclib for 48 hours. After 48 hours, cells were washed five times with PBS to remove samuraciclib from cells. Fresh drug-free media was added, and cells were cultured for another 96 hours. After a 96-hour wash-out, cells were collected for immunofluorescence staining and analysis. Shown are representative images from one experiment of Hoechst nuclear staining. Scale bar represents 50 μm. Areas labelled by the boxes are enlarged below.

4.8. Summary

The experiments in this chapter compared cell cycle exit dynamics between a CDK7 inhibitor, samuraciclib, and a CDK4/6 inhibitor, palbociclib. I showed that palbociclib concentrations that are higher than IC_{50} are required to inhibit proliferation of RPE1 cells to a similar extent as IC_{50} of samuraciclib. Although palbociclib induces senescent phenotypes, such as an increased SA β-gal and excess cell size, to a greater extent than samuraciclib, it induces a delayed increase in p21 levels and causes a less robust permanent cell cycle exit compared to samuraciclib. This was observed by a greater percentage of colony formation after palbociclib wash-out compared to samuraciclib indicating a large proportion of palbociclib-arrested cells retain their proliferative potential during a 48-hour arrest. This suggests that CDK4/6 and CDK7 inhibition might differ in their mechanisms of action.

A genome-wide CRISPR KO screen indicated that, in contrast to samuraciclib, negative regulation of mTOR signalling might lead to increased palbociclib efficacy. I validated this through pharmacological inhibition of mTOR, via Torin1 treatment in RPE1 cells. This indicated that mTOR signalling has opposing effects on cell cycle arrest induction during palbociclib and samuraciclib treatment. Nevertheless, similarly to samuraciclib, an mTOR signalling-dependent increase in cell size during palbociclib treatment renders cells more likely to exit the cell cycle permanently after palbociclib treatment. This suggests that although mTOR inhibition might render cells more sensitive to initial palbociclib treatment, these cells might re-enter the cell cycle after drug removal to a greater extent than a palbociclib mono-treatment.

Work I contributed to shows that larger cells that re-enter the cell cycle after palbociclib treatment are likely to undergo mitotic defects and harbour increased levels of DNA damage (Manohar *et al.*, 2023). I observed that these cells undergo mild levels of replication stress, which can partially be rescued by Torin1-mediated size containment. However, as both enlarged and growth-restricted cells display shorter DNA fibres indicating mild replication stress, this suggests that smaller cells are able to cope with this stress level better by having a functional DDR (Manohar *et al.*, 2023).

Taken together, the data in this chapter indicates that an increase in cell size during palbociclib treatment is an important indicator of a reduced proliferative potential,

which is in line with the data presented in chapter 3 for samuraciclib. However, the results suggest that the dynamics by which samuraciclib and palbociclib cause long-term cell cycle withdrawal is different. Samuraciclib treatment predominantly induces a robust irreversible cell cycle arrest, which is closely linked to the increase in cell size during the arrest. On one hand, palbociclib treatment can induce a robust cell cycle arrest, which is enhanced by limiting growth, but this is only irreversible in the minority of cells with most cells re-entering the cell cycle. On the other hand, excessive cellular growth during a palbociclib-induced arrest causes replication-acquired DNA damage upon cell cycle re-entry, which can cause cells to exit the cell cycle (Manohar *et al.*, 2023).

5. p53 and p21, but not Rb, are required for samuraciclib sensitivity

In the previous two chapters, I explored the role of cellular growth in the anti-cancer efficacy of both a CDK7 inhibitor samuraciclib and a CDK4/6 inhibitor palbociclib. Together with our collaborators I showed that active growth signalling and cell size enlargement are important indicators of a permanent cell cycle exit induced by samuraciclib and palbociclib following a CDK inhibitor wash-out (Manohar *et al.*, 2023; Wilson *et al.*, 2023). However, cell volume *per se* cannot explain the differences in the degree of proliferative potential reduction during these two CDK inhibitors as palbociclib-arrested RPE1 cells become more enlarged than samuraciclib-arrested cells but are able to return to a proliferative state to a greater extent after inhibitor removal. This suggests that other mechanisms must account for this difference, and I decided to explore one of these in this chapter.

The CDK inhibitor p21 accumulates rapidly in response to samuraciclib treatment, whereas accumulation in response to palbociclib takes much longer. This could be one potential reason for the difference observed in cell cycle exit dynamics. p21 is a target of the transcription factor p53, which is a tumour suppressor and its encoding gene *TP53* is most commonly mutated in cancer (Chen *et al.*, 2022). Therefore, understanding their role in CDK inhibitor-induced cell cycle arrest is therapeutically relevant. Previous research showed that neither p21 (Pennycook and Barr, 2021) nor p53 (Crozier *et al.*, 2022) are required for the initial cell cycle arrest induced by palbociclib. However, it is still unclear whether they are required for samuraciclib efficacy. The first results from a modular phase I clinical trial study with samuraciclib suggested a potentially better prognosis in the p53 wild-type (WT) breast cancers (Coombes *et al.*, 2023). Moreover, the analysis of the genome-wide CRISPR knock-out (KO) chemogenetic screens presented in chapter 3 revealed p53 as the top positive interactor with samuraciclib. This indicates that p53 might be required for samuraciclib-induced cell cycle arrest. I use p21 KO and p53 KO RPE1 cell lines to investigate this in this chapter.

In addition, to further understand the effect of clinically relevant cancer alterations in samuraciclib efficacy, I explore the roles of a loss of tumour suppressor Rb and an overexpression of cyclin E, which are one of the key mutations that render cancer cells resistant to palbociclib and both play important roles in cell cycle entry. I investigate this using an siRNA targeting Rb and an RPE1 cell line with a doxycycline-inducible cyclin E1.

5.1. p21 is required for samuraciclib sensitivity

As described in the previous two chapters, samuraciclib induces a more robust cell cycle arrest after 48 hours in RPE1 cells, which persists after inhibitor wash-out, compared to palbociclib. CDK4/6 inhibition reduces the proliferative potential of RPE1 cells but allows a greater fraction of cells to re-enter the cell cycle once inhibition is removed. One of the differences observed between these two CDK inhibitors is that samuraciclib induces a rapid accumulation of p21, whereas during palbociclib treatment, this response is delayed (Figure 4.4). Below I show a western blot that confirms the timecourse analysis previously presented in chapter 4 (Figure 4.4). After 48 hours of samuraciclib treatment, p21 levels increase; however, there is no change in p21 expression after 48 hours of palbociclib treatment (Figure 5.1).

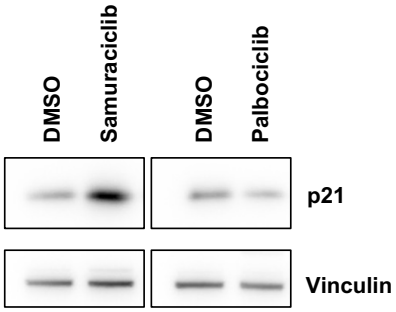

Figure 5.1: Samuraciclib induces a rapid accumulation of p21.
Representative western blot of whole-cell extracts collected from RPE1 cells treated with vehicle control, 120 nM of samuraciclib or 1000 nM of palbociclib for 48 hours. Vinculin: loading control. These images are from the same western blot but are cut to present only the necessary results.

To investigate whether p21 is required for the initial robust cell cycle arrest induced by samuraciclib, I tested cellular proliferation after samuraciclib treatment in RPE1 p21 KO cells using EdU incorporation assay. RPE1 p21 KO cells were generated by the

laboratory of Alexis Barr (Barr *et al.*, 2017; Pennycook and Barr, 2021). As shown

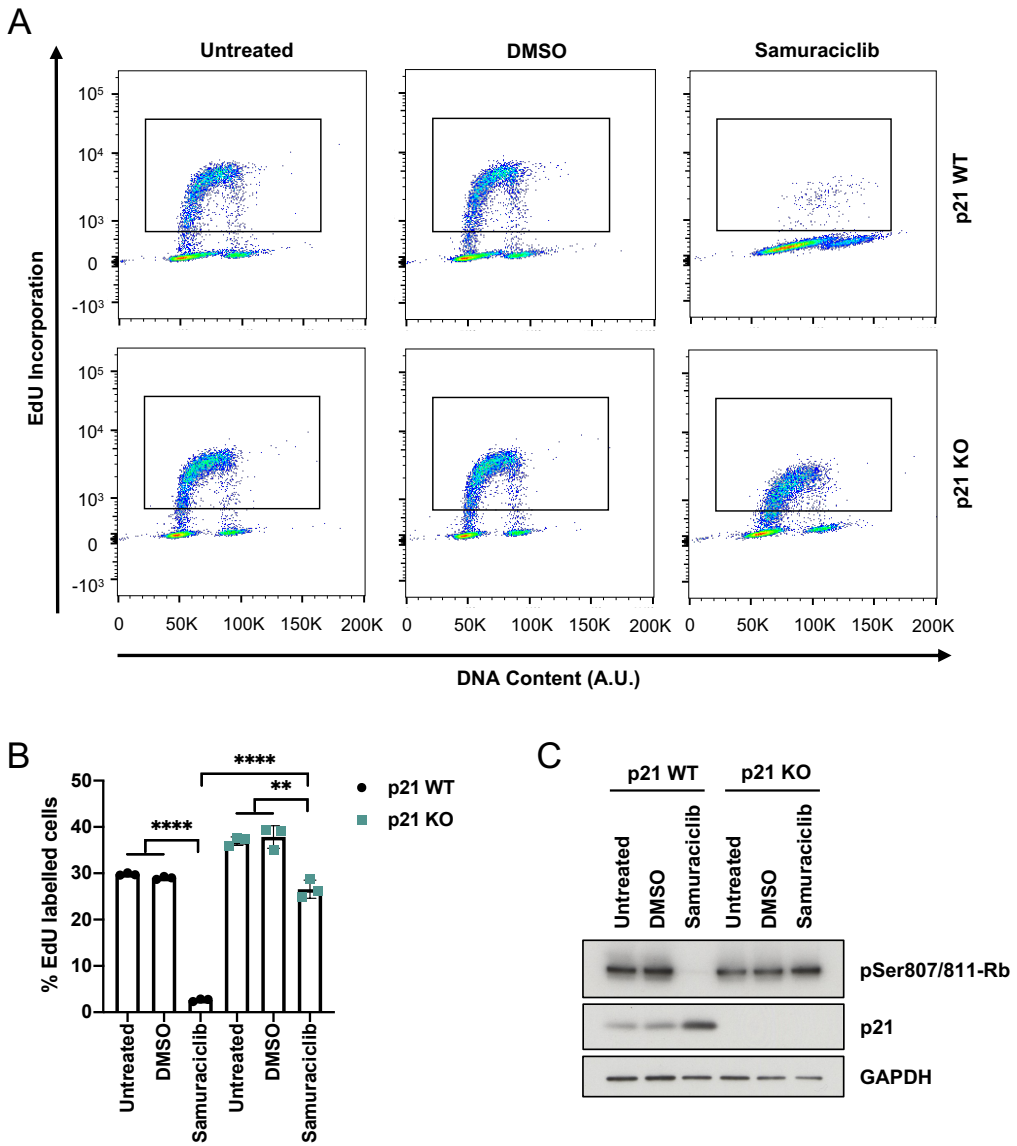

Figure 5.2: p21 is required for samuraciclib-induced cell cycle arrest.
RPE1 wild-type (WT) and p21 knock-out (KO) cells were left untreated, treated with vehicle control or 120 nM of samuraciclib for 48 hours. **A)** Cells were incubated with EdU for 1 hour before collection. Pseudocoloured plots of flow cytometry data from a representative experiment. DNA content is plotted against EdU incorporation. Inset gate drawn to include EdU-positive cells. **B)** Quantification of the percentage of EdU-positive cells from three independent experiments (representative shown in A). Statistical significance was calculated using an unpaired two-tailed t test. Error bars are SD. **C)** Representative western blot of whole-cell extracts collected from RPE1 cells. GAPDH: loading control.

before, 48 hours of samuraciclib treatment is able to almost completely prevent EdU incorporating in a p21 WT RPE1 cell line. However, there is a significantly higher percentage of cells incorporating EdU, so actively replicating, in p21 KO cells compared to p21 WT (Figures 5.2A and 5.2B). This is confirmed by high levels of phosphorylated Rb, after a 48-hour samuraciclib treatment in p21 KO cells (Figure 5.2B).

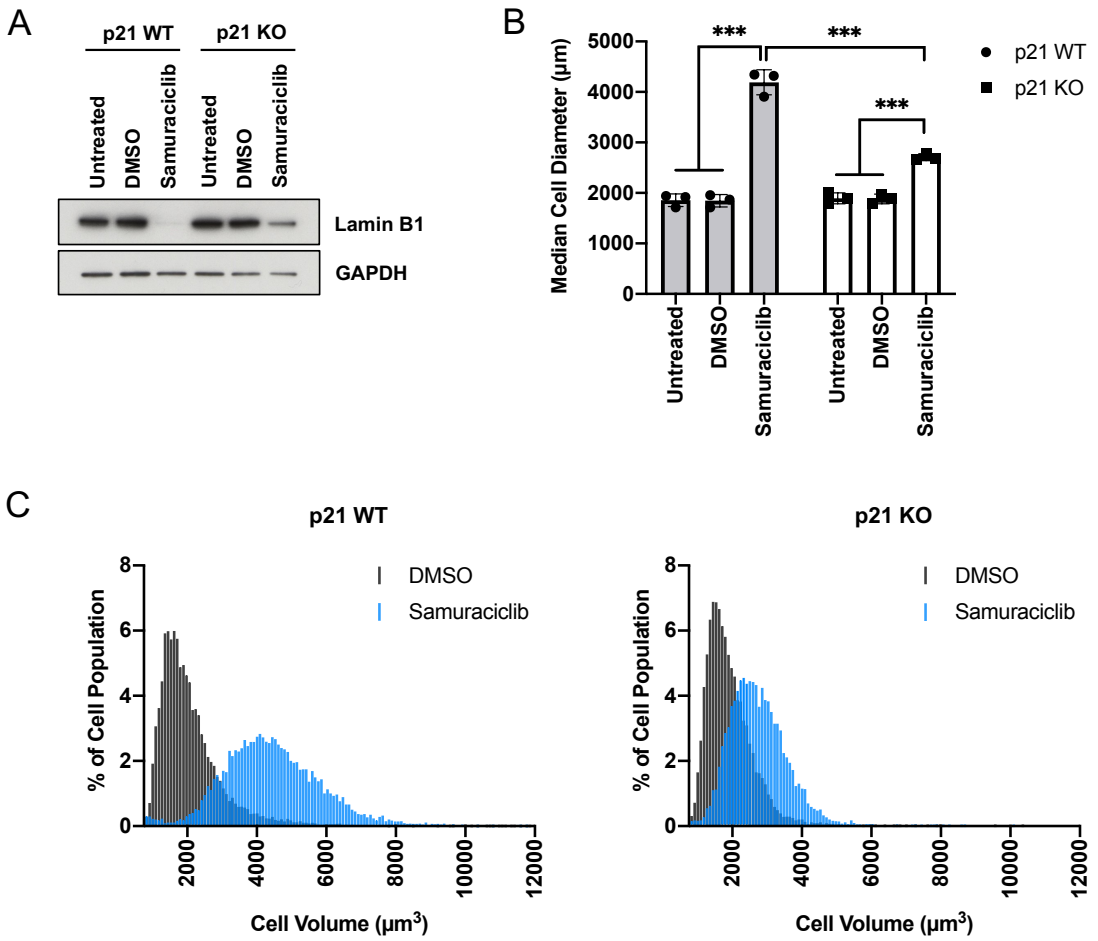

Figure 5.3: Loss of p21 reduces senescent phenotypes previously observed upon samuraciclib treatment.
RPE1 wild-type (WT) and p21 knock-out (KO) cells were left untreated, treated with vehicle control or 120 nM of samuraciclib for 48 hours. **A)** Representative western blot of whole-cell extracts collected from RPE1 cells. GAPDH: loading control. **B)** Coulter counter data quantification of the median cell volume within the population from three independent experiments (representative shown in C). Statistical significance was calculated using an unpaired two-tailed t test. Error bars are SD. **C)** Coulter counter data from a representative experiment. Percentage of cell population is plotted against various bins containing cells with different volumes in μm^3.

In addition, senescent phenotypes previously observed upon samuraciclib treatment are reduced in a p21 KO cell line. The loss of Lamin B1 is hindered in p21 KO cells during CDK7 inhibition compared to the control cells (Figure 5.3A). Moreover, an increase in cell size is significantly inhibited (Figures 5.3B and 5.3C).

I further validated the results comparing the effect of samuraciclib on p21 WT and p21 KO RPE1 cell lines with an siRNA-mediated knock-down. I transfected RPE1 cells with either non-targeting control siRNA (siCONT) or siRNA targeting *CDKN1A*, a p21-encoding gene (sip21) and treated the cells with either DMSO or samuraciclib. After 48 hours, both phosphorylated Rb and Lamin B1 are drastically reduced in a control samuraciclib condition. However, in p21-depleted cells, there is no difference in phosphorylated Rb levels between DMSO and samuraciclib treatments, suggesting these cells are proliferating despite CDK7 inhibition. Moreover, Lamin B1 reduction is inhibited by p21 depletion (Figure 5.4). siRNA-mediated p21 knock-down confirms the results observed in a p21 KO cell line. Taken together, these data suggest that p21 is required for CDK7 inhibitor-induced cell cycle arrest and senescence.

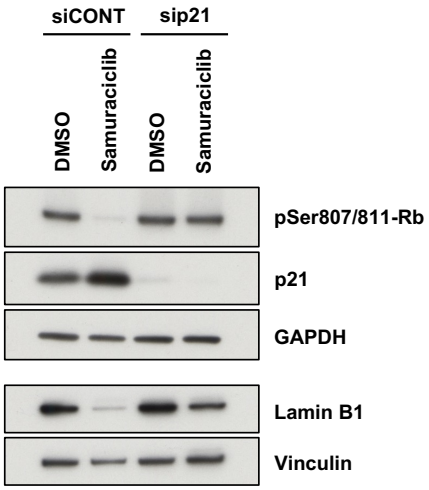

Figure 5.4: p21 knock-down reduces samuraciclib efficacy.
RPE1 cells transfected with a non-targeting siRNA (siCONT) and siRNA targeting p21 (sip21) were treated with vehicle control or 120 nM of samuraciclib for 48 hours. Representative western blot of whole-cell extracts collected from RPE1 cells. GAPDH and Vinculin: loading controls.

5.2. Samuraciclib induces p53 upregulation

I previously observed that an increase in p21 protein levels in response to samuraciclib treatment coincides with an increase in mRNA levels of a p21-encoding gene *CDKN1A* (Figure 3.3). This suggests gene expression of p21 is actively upregulated. The tumour suppressor, p53 is the key transcriptional activator of p21 (Abbas and Dutta, 2009). I therefore investigated whether p53 levels become upregulated in response to samuraciclib. Western blot analysis revealed that the levels of total p53 protein start increasing after 24 hours of treatment (Figure 5.5A).

To further explore the potential activation of p53, I assayed the levels of mouse double minute 2 (MDM2) in response to samuraciclib treatment. MDM2 is an oncogene and frequently mutated in cancer and it is a key negative regulator of p53. It is an E3 ubiquitin ligase that mediates ubiquitination of p53, targeting it for proteasomal degradation (Kung and Weber, 2022). Among other transcriptional activators, transcription of MDM2-encoding gene was found to be induced by p53, creating a negative feedback loop in order to regulate p53 activity (Barak *et al.*, 1993; Kung and Weber, 2022). A samuraciclib treatment timecourse reveals an increase in MDM2 protein levels, which could be due to upregulation of p53 (Figure 5.5B). This data, together with the transcriptional activation of *CDKN1A* gene, suggest that p53 activity increases in response to samuraciclib.

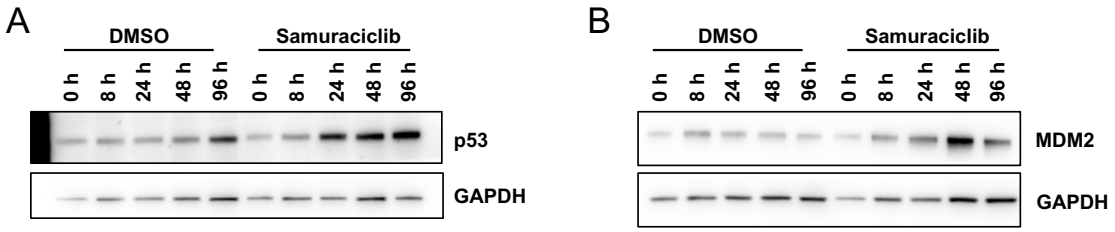

Figure 5.5: Samuraciclib treatment leads to p53 upregulation.
A) B) Representative western blot of whole-cell extracts collected from RPE1 cells at indicated time-points after treatment with vehicle control or 120 nM of samuraciclib. GAPDH: loading control.

In fact, *TP53* gene is the top positive interactor with samuraciclib based on the average RANKS score from four genome-wide CRISPR KO chemogenetic screens presented in chapter 3. A positive interactor represents a gene that is required for drug sensitivity,

and its depletion might lead to resistance. The screen data therefore suggests that p53 might be required for samuraciclib efficacy. Interestingly, the highest samuraciclib concentration (501 nM) used to treat NALM-6 cells in the chemogenetic screen, puts p53 as the highest RANKS score suggesting a strong dependency (Table 5.1).

Moreover, the *MDM2* gene is among the top 50 negative interactors with samuraciclib (Table 5.1). A negative interactor represents a gene that reduces drug efficacy, and their depletion could increase it. As MDM2 is a negative regulator of p53, its depletion would result in increased levels of p53. Therefore, these findings suggest that p53 might be an important indicator of samuraciclib sensitivity. On the contrary, these genes are not among the top hits in the two chemogenetic screens with palbociclib. Their average RANKS scores are close to 0, which indicates almost no interaction with the CDK4/6 inhibitor. This is in line with published results (Pennycook and Barr, 2021; Crozier *et al.*, 2022).

Table 5.1: Comparison of RANKS scores reveals importance of stabilisation of p53 in samuraciclib sensitivity but not for palbociclib.

Gene	Samuraciclib (RANKS score)					Palbociclib (RANKS score)		
	180 nM	350 nM	350 nM	501 nM	Average	335 nM	1000 nM	Average
TP53	2.24	2.02	3.39	4.03	**2.92**	0.55	0.11	0.33
MDM2	-1.69	-1.4	-1.86	-2.18	**-1.7825**	0.01	-0.29	-0.14

5.3. p53 is required for samuraciclib sensitivity

To test the role of p53 in samuraciclib-induced cell cycle arrest, I used an RPE1 cell line where p53 is knocked-out and compared it to the control p53 WT RPE1 cells. RPE1 p53 KO cells were generated by the laboratory of Adrian Saurin (Crozier *et al.*, 2022). EdU incorporation assay revealed that p53 KO significantly reduces efficacy of samuraciclib (Figures 5.6A and 5.6B). At 120 nM of samuraciclib, a concentration at which the p53 WT cells almost fully arrest, p53 KO cells incorporate EdU similarly to the control cycling conditions (Figure 5.6B). There is no significant difference in the percentage of EdU labelled cells after 48 hours of DMSO and samuraciclib treatments (Figure 5.6B). Only a minor reduction in phosphorylated Rb and cyclin A2 levels after

samuraciclib treatment of p53 KO cells confirm the cell cycle analysis (Figure 5.6C). Altogether these findings suggest that p53 is necessary for the samuraciclib-induced cell cycle arrest.

It is important to note that knocking-out p53 results in almost complete loss of p21 (Figure 5.6C). Overexposure of the western blot reveals a very low level of p21. However, there is no increase in p21 in response to samuraciclib treatment suggesting that p21 accumulation during CDK7 inhibition is p53-dependent (Figure 5.6C).

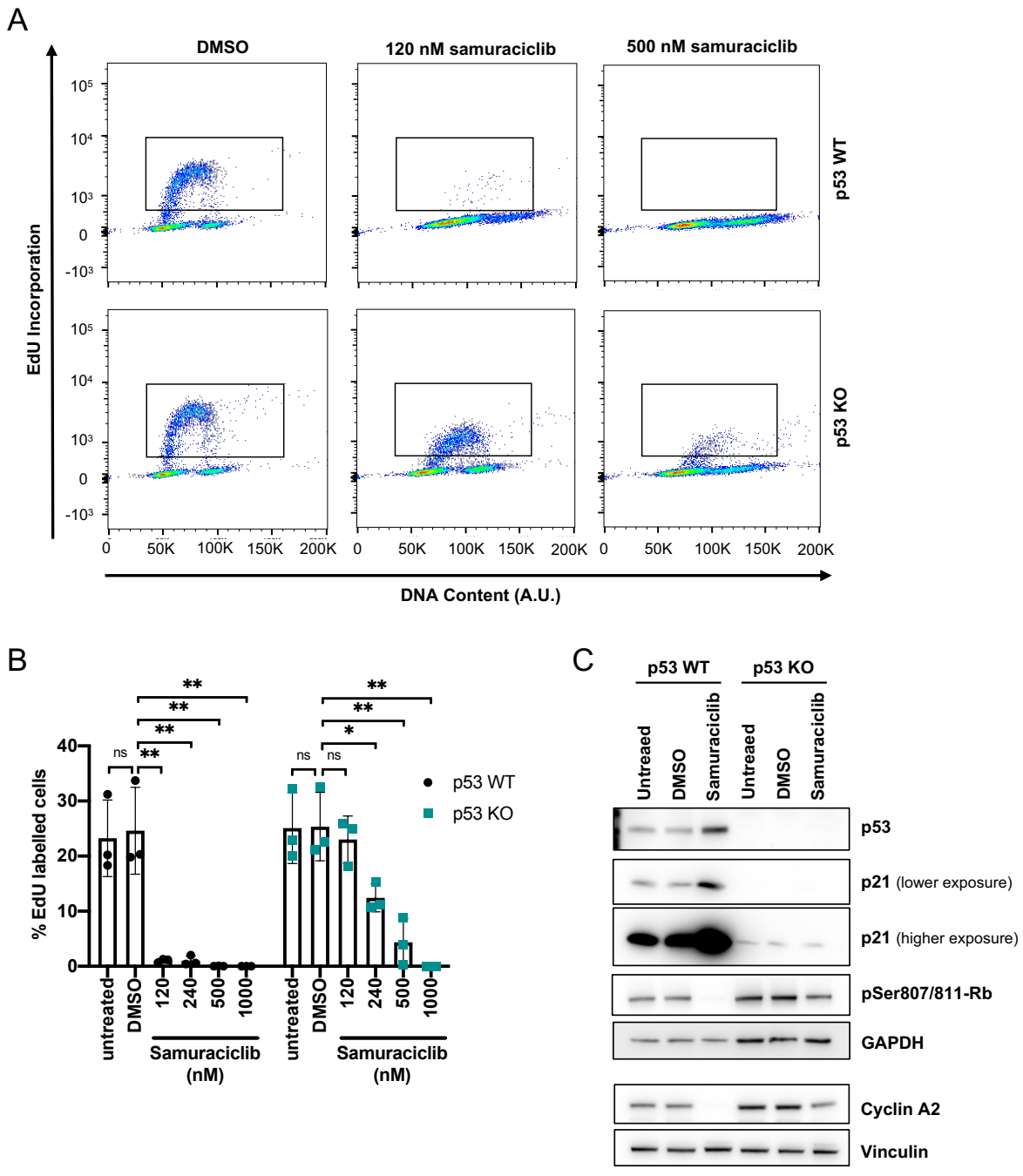

Figure 5.6: Loss of p53 reduces samuraciclib efficacy.

Figure 5.6: (continued) RPE1 wild-type (WT) and p53 knock-out (KO) cells were left untreated, treated with vehicle control or indicated concentrations of samuraciclib for 48 hours. **A)** Cells were incubated with EdU for 1 hour before collection. Pseudocoloured plots of flow cytometry data from a representative experiment. DNA content is plotted against EdU incorporation. Inset gate drawn to include EdU-positive cells. **B)** Quantification of the percentage of EdU-positive cells from three independent experiments (representative shown in A). Statistical significance was calculated using an unpaired two-tailed t test. Error bars are SD. **C)** Representative western blot of whole-cell extracts collected from RPE1 cells. GAPDH and Vinculin: loading controls.

Although 120 nM of samuraciclib is unable to inhibit proliferation of p53 KO cells, increasing samuraciclib concentration could sensitise them. In fact, higher samuraciclib concentrations are able to induce a significant reduction in EdU incorporating cells, creating a dose-dependent effect (Figures 5.6A and 5.6B). 1000 nM of samuraciclib completely inhibits proliferation in p53 KO cells (Figure 5.6B). This suggests that although p53 loss reduces samuraciclib efficacy, higher concentrations of samuraciclib are able to arrest the cell cycle.

I observed that upon samuraciclib treatment in p53 KO cells, even though there is a higher frequency of EdU incorporating cells, there is an overall lower EdU intensity (Figure 5.6A). This could suggest that these cells are encountering issues during DNA replication and could potentially eventually be arrested in response to prolonged samuraciclib treatment. An explanation for this observation could be that CDK7 inhibition in this case leads to DNA replication stress or stalling of the replication forks. I therefore investigated whether the replication stress checkpoint is activated in p53 KO cells in response to samuraciclib treatment by analysing the levels of replication stress markers, phosphorylated Chk1 and replication protein A (RPA). Exposed ssDNA is bound and shielded by RPA, which becomes phosphorylated in response to replication stress. Serine residues 4 and 8 of RPA are not direct targets of ATR and are phosphorylated mainly by DNA-PK but can be used as a replication stress marker (Liu *et al.*, 2012; Ashley *et al.*, 2014). ssDNA coated by RPA is recognised by the kinase ATR activating the replication stress checkpoint. ATR in turn phosphorylates Chk1 at serine residue 345 (Zeman and Cimprich, 2014). As a positive control, I used a topoisomerase I inhibitor CPT, which is known to induce replication stress and activate the checkpoint signalling cascade (Vesela *et al.*, 2017). Compared to CPT, samuraciclib treatment does not lead to an increase in either phosphorylated RPA or

Chk1, suggesting no activation of the replication stress checkpoint (Figure 5.7). Therefore, this decrease in EdU intensity in p53 KO cells that are incorporating EdU during DNA synthesis cannot be explained by replication stress. It could occur due to under-licencing of the origins, but this requires further investigation.

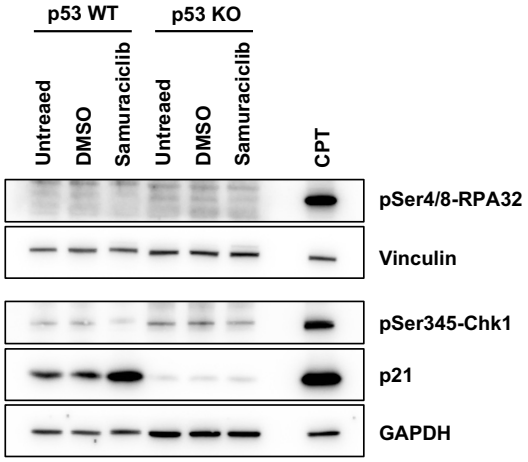

Figure 5.7: Reduced amount of EdU incorporation per cell cannot be explained by DNA replication stress.
RPE1 wild-type (WT) and p53 knock-out (KO) cells were left untreated, treated with vehicle control or 120 nM of samuraciclib for 48 hours. RPE1 WT cells were treated with 2 μM of camptothecin (CPT) for 5 hours as a positive control. Western blot analysis from one experiment of whole-cell extracts collected from RPE1 cells. GAPDH and Vinculin: loading controls.

As palbociclib does not induce p21 accumulation at earlier time-points, and p53 is not among the top hits found in the chemogenetic screen, p53 is likely not required for the initial cell cycle arrest. This is supported by published work which shows that palbociclib is able to increase the percentage of G1 cells to a similar extent in both p53 WT and p53 KO RPE1 cells (Crozier *et al.*, 2022). Moreover, p21 loss was also shown not to affect palbociclib-induced cell cycle arrest (Pennycook and Barr, 2021). Using EdU incorporation to assay cellular proliferation, I confirmed that palbociclib does not require p53 to the same extent as samuraciclib to induce a cell cycle arrest. Although there is a small increase in the fraction of actively replicating p53 KO cells after a 48-hour treatment of 400 nM of palbociclib, this difference is non-significant. At higher palbociclib concentration of 1000 nM there is no significant difference in the percentage of EdU labelled p53 WT and p53 KO cells treated with samuraciclib for 48 hours (Figures 5.8A ad 5.8B). This suggests that p53 loss might slightly reduce

palbociclib sensitivity at lower concentrations, but this effect is much greater in samuraciclib-treated cells.

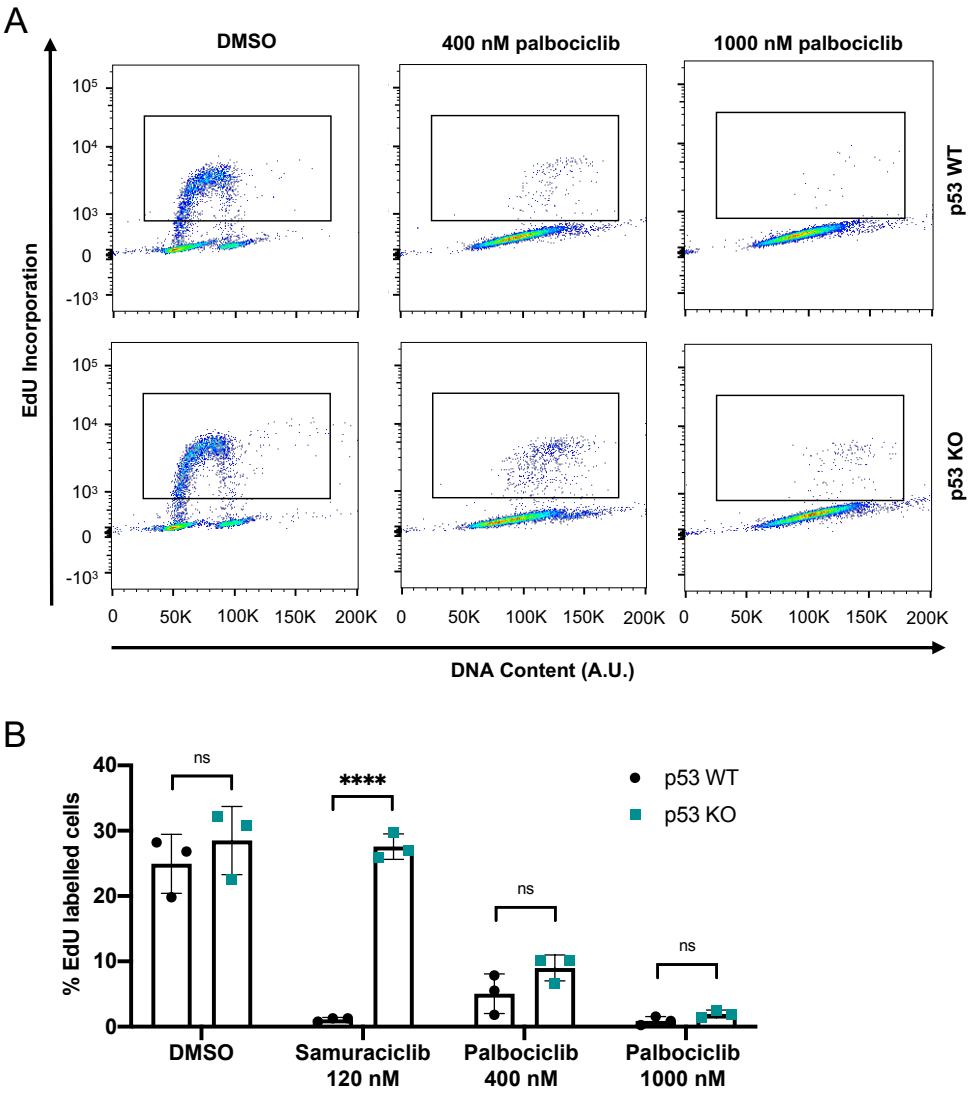

Figure 5.8: p53 level is not a crucial indicator of a palbociclib-induced cell cycle arrest.
RPE1 wild-type (WT) and p53 knock-out (KO) cells were left untreated, treated with vehicle control, 120 nM of samuraciclib, 400 nM or 1000 nM of palbociclib for 48 hours. **A)** Cells were incubated with EdU for 1 hour before collection. Pseudocoloured plots of flow cytometry data from a representative experiment. DNA content is plotted against EdU incorporation. Inset gate drawn to include EdU-positive cells. **B)** Quantification of the percentage of EdU-positive cells from three independent experiments (representative shown in A). Statistical significance was calculated using an unpaired two-tailed t test. Error bars are SD.

Furthermore, sensitivity to palbociclib and samuraciclib correlates with an increase in cell size (Figure 5.9). As observed in p21 KO RPE1 cells, samuraciclib leads to a smaller increase in cell size in p53 KO compared to WT cells (Figures 5.9A and 5.9B). Palbociclib instead causes a similar increase in cell size in both p53 WT and KO cells, which correlates with the sensitivity to these CDK inhibitors (Figures 5.9A and 5.9B).

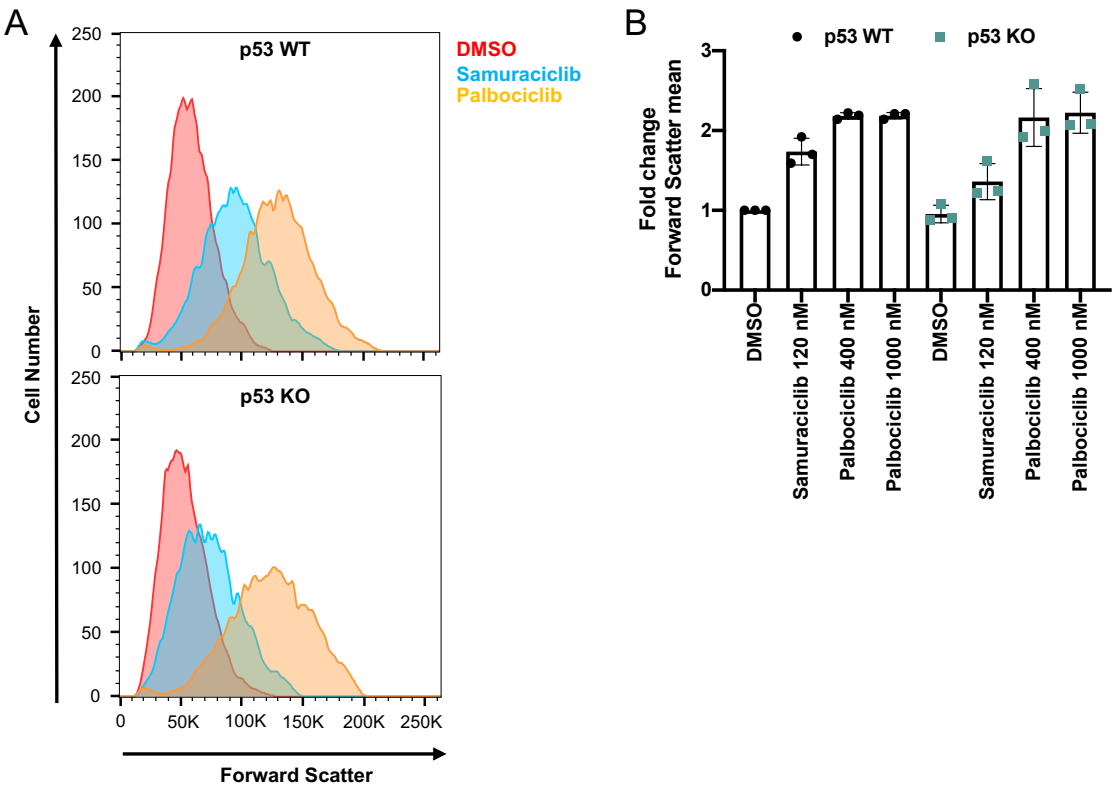

Figure 5.9: Cell size increase correlates with samuraciclib and palbociclib sensitivity in RPE1 p53 KO cells.
RPE1 wild-type (WT) and p53 knock-out (KO) cells were treated with vehicle control, 120 nM of samuraciclib, 400 nM or 1000 nM of palbociclib for 48 h. **A)** Flow cytometry data from a representative experiment. 1000 nM of palbociclib treatment shown only. Forward scatter, a measure of cell size, is plotted against cell count. **B)** Flow cytometry data from A where fold change of mean forward scatter value, a measure of cell size, is calculated relative to p53 WT DMSO control. Error bars are SD.

5.4. Samuraciclib sensitivity positively correlates with p21 levels in breast cancer cell lines

The work presented so far shows that p53 and p21 are both required for a samuraciclib-induced cell cycle arrest in a non-transformed RPE1 cell line. Loss-of-

function mutations in *TP53* gene are very common in cancer and therefore it is important to understand its role in samuraciclib's mechanism of action. A phase I clinical trial study recently revealed that p53 status might be a useful indicator of CDK7 inhibitor efficacy (Coombes *et al.*, 2023). I tested this using the three breast cancer cell lines in which I previously assessed samuraciclib sensitivity in chapter 3. MCF7 cells, which are the most sensitive among the three cell lines, have a WT *TP53* sequence and therefore a functional p53 (Leroy *et al.*, 2014; Elwakeel *et al.*, 2021). After 96 hours of samuraciclib treatment, there is an increase in both p21 (Figure 5.10A) and p53 levels (Figure 5.10B). T47D cells with medium sensitivity and BT549 with the lowest sensitivity to samuraciclib both have a loss-of-function *TP53* mutation. T47D harbours a L194F missense mutation in the *TP53* gene, which results in the loss of p53 ability to bind to DNA and induce transcription of its downstream target genes. BT549 harbours a R249S mutation in the *TP53* gene (Leroy *et al.*, 2014; Elwakeel *et al.*, 2021). Although both of these cell lines have loss-of-function p53 mutations and have an overall weaker response to samuraciclib than MCF7 cells with WT p53, T47D still partially inhibit proliferation during samuraciclib treatment. However, their basal p21 levels differ, with T47D having a higher p21 expression in comparison to BT549 cells (Figure 5.10A). This suggests that p21 levels positively correlate with samuraciclib sensitivity in these three breast cancer cell lines. p21 itself is not commonly mutated in cancer but it is often deregulated by p53 status (Kreis, Louwen and Yuan, 2019; Matthews, Bertoli and de Bruin, 2022).

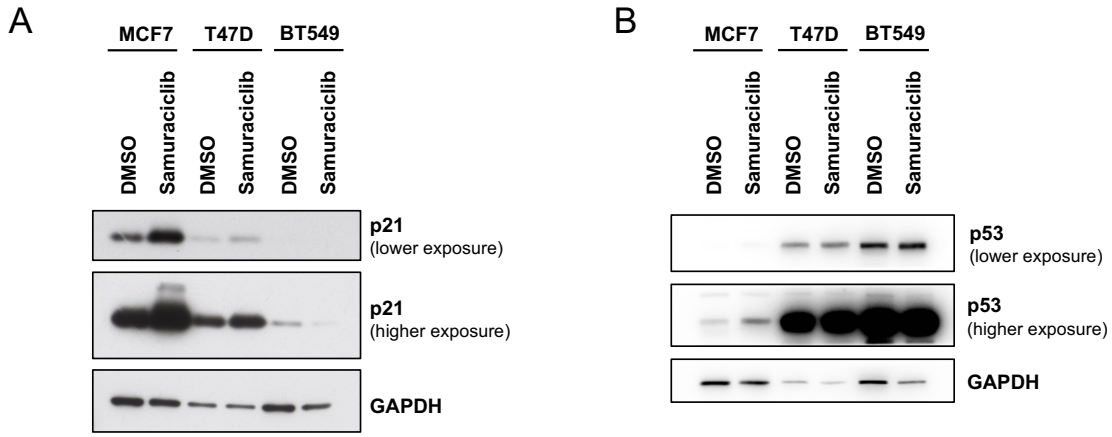

Figure 5.10: p21 levels positively correlate with samuraciclib sensitivity in breast cancer cell lines.
A) B) Western blot analysis from one experiment of whole-cell extracts collected from MCF7, T47D and BT549 cells treated with vehicle control or 180 nM of samuraciclib for 96 hours. GAPDH: loading control.

Even though this analysis indicates that p53 status does indeed correlate with samuraciclib sensitivity, as the p53 WT cells are more sensitive than the p53 mutant, this requires further investigation by increasing the panel of breast cancer cell lines. Moreover, within the two p53 mutant cell lines, there is a difference in samuraciclib sensitivity suggesting that examining only p53 status might omit some potentially sensitive cancers to this CDK7 inhibitor. However, levels of CDK inhibitor p21 correlate with the samuraciclib sensitivity in this small panel of cancer cell lines.

Taken together, the experiments in RPE1 cells with either p53 and p21 KO as well as the analysis of the three breast cancer cell lines suggest that samuraciclib sensitivity correlates with the cell's ability to upregulate p21 expression and mediate cell cycle arrest, which could therefore be used as a drug response read-out.

5.5. p21 is required for maintaining samuraciclib-induced cell cycle arrest

In the previous sections I demonstrated the importance of p21 in the initial samuraciclib response and its ability to induce a cell cycle arrest. However, it is unclear whether p21 is required for inducing a permanent cell cycle exit. To explore this, I treated RPE1 cells with samuraciclib for 48 hours, which was shown to cause a persistent cell cycle exit following drug wash-out. After 48 hours I washed the inhibitor away and transfected the cells with either a non-targeting control siRNA (siCONT) or siRNA targeting p21-encoding gene (sip21). Following drug wash-out and siRNA transfection, I either re-treated the cells with samuraciclib or left the cells in a drug-free media. The experimental set up is illustrated in a schematic in Figure 5.11A. Depleting p21 after 48 hours of samuraciclib-induced arrest increases levels of proliferative markers, phosphorylated Rb and cyclin A2 compared to the control (Figure 5.11B). This rescue in cell cycle progression is slightly more apparent in samuraciclib wash-out (48 h after release: Samu. release) than in continued samuraciclib treatment (48 h after release: Samu.), which is likely due to samuraciclib wash-out *per se* as even in the control cells (siCONT) there is a faintly higher expression of cyclin A2 and phosphorylated Rb (Figure 5.11B).

This western blot analysis of proliferative markers requires further confirmation using cell cycle assays, but it does suggest that p21 is required to maintain a cell cycle arrest, or drive a permanent cell cycle exit, after samuraciclib treatment. Moreover, it indicates that after 48 hours of samuraciclib treatment, RPE1 cells are not yet in a senescent state, as the cell cycle arrest can be reversed using p21 depletion, but they are in a senescence-promoting state.

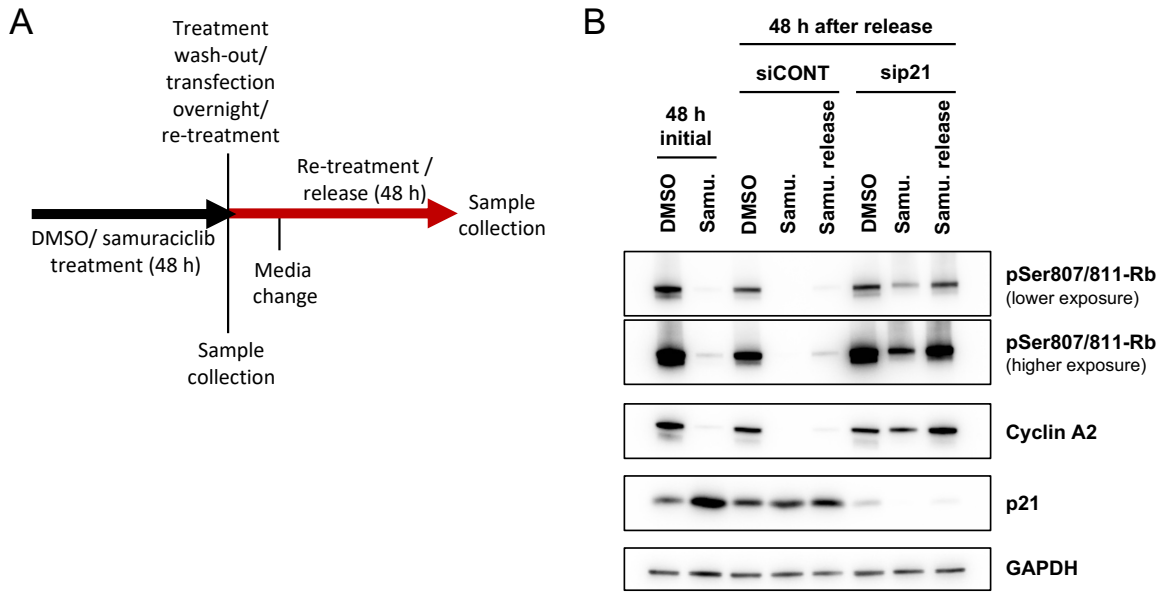

Figure 5.11: p21 is required for maintaining samuraciclib-induced cell cycle arrest.
A) A schematic illustrating the experimental set up. RPE1 cells were treated with vehicle control or 120 nM of samuraciclib for 48 hours. After 48 hours of treatment, cells were washed five times with PBS to remove the drugs from cells. Cells were then transfected with a non-targeting siRNA (siCONT) or siRNA targeting p21 (sip21) and either re-treated with corresponding treatments or left untreated (release condition) overnight. The following morning, cells were washed with PBS and fresh media was added and cells were left in culture for another 48 hours with samuraciclib re-treatment or left untreated (wash-out/ release condition). **B)** Representative western blot of whole-cell extracts collected as described in A (n=3). The initial vehicle control or samuraciclib (Samu.) treatment is labelled as “48 h initial”. GAPDH: loading control.

5.6. Rb is required for palbociclib efficacy but not in the case of samuraciclib

In 2021 samuraciclib received FDA-approved fast track designations, in combination with fulvestrant, for the treatment of CDK4/6 inhibitor resistant HR+, HER2- advanced

breast cancer (Carrick Therapeutics, 2021). This suggests that it could re-sensitise cancers that progressed on palbociclib treatment due to resistance. One of the most frequent palbociclib resistance mechanisms occurs due to the loss of tumour suppressor Rb encoded by the *RB1* gene, which is commonly mutated in cancer. Rb is an E2F repressor, which when mutated, allows activation of E2F-dependent transcription promoting cell cycle entry. Since during palbociclib treatment CDK2 and CDK1 activities are not inhibited, activation of E2F-dependent transcription results in cyclin E and A accumulation which can drive cell cycle entry, explaining why Rb loss results in palbociclib resistance. This is confirmed by the two genome-wide CRISPR KO chemogenetic screens, which identified *RB1* as one of the two top positive interactors with palbociclib (Table 5.2). Interestingly, *RB1* is not a hit in the samuraciclib screens as the average RANKS score is close to 0, suggesting a mutation in *RB1* potentially does not affect samuraciclib sensitivity (Table 5.2).

Table 5.2: Top positive interactors with palbociclib compared to their interaction with samuraciclib.

Gene	Samuraciclib (RANKS score)					Palbociclib (RANKS score)		
	180 nM	350 nM	350 nM	501 nM	Average	335 nM	1000 nM	Average
AMBRA1	0.31	0.76	-0.17	0.26	0.29	8.16	8.38	**8.27**
RB1	0.61	0.53	-0.28	-0.6	0.065	8.52	7.97	**8.245**

To investigate this, I depleted Rb levels in RPE1 cells using a siRNA-mediated knock-down. I demonstrated that I can successfully reduce Rb levels using this method (Figure 5.12D). Assaying cellular proliferation after 48 hours revealed that samuraciclib can significantly arrest the cell cycle in Rb-depleted cells as in control cells (Figures 5.12A and 5.12B). This suggests that Rb is not required for a samuraciclib-induced cell cycle arrest. As a control, I treated Rb-depleted cells with palbociclib and observed a significantly higher percentage of proliferating cells compared to palbociclib-treated control cells (Figures 5.12A and 5.12C). Moreover, I validated the cell cycle analysis with western blots of cyclin A2 and p21 (Figure 5.12D). Rb depletion does not affect loss of cyclin A2 levels during samuraciclib treatment as

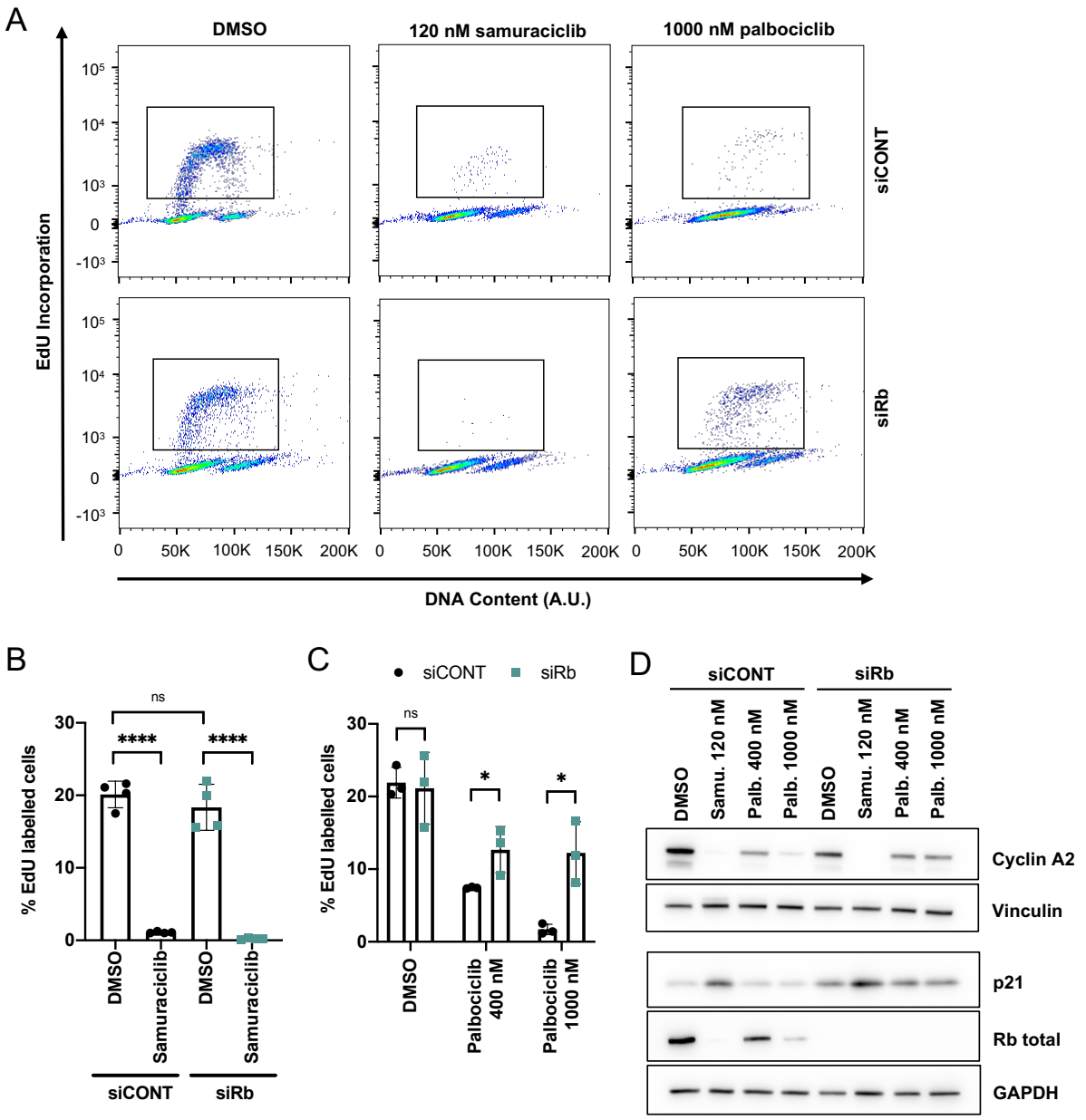

Figure 5.12: Palbociclib, but not samuraciclib, requires Rb for its activity. RPE1 cells transfected with a non-targeting siRNA (siCONT) and siRNA targeting Rb (siRb) were treated with vehicle control, 120 nM of samuraciclib, 400 nM or 1000 nM of palbociclib for 48 hours. **A)** Cells were incubated with EdU for 1 hour before collection. Pseudocoloured plots of flow cytometry data from a representative experiment. DNA content is plotted against EdU incorporation. Inset gate drawn to include EdU-positive cells. **B)** Quantification of the percentage of EdU-positive cells from four independent experiments (representative shown in A). Statistical significance was calculated using an unpaired two-tailed t test. Error bars are SD. **C)** Quantification of the percentage of EdU-positive cells from three independent experiments (representative shown in A). Statistical significance was calculated using an unpaired two-tailed t test. Error bars are SD. **D)** Western blot analysis of whole-cell extracts. Vinculin and GAPDH: loading controls.

they remain low, but it leads to an increased expression in response to palbociclib treatment. Moreover, p21 accumulates due to CDK7 inhibition to a similar extent in both control and Rb-depleted cells. Taken together, this data shows that Rb loss rescues cell cycle progression during palbociclib treatment but not during samuraciclib.

In addition to *RB1*, the chemogenetic screen data indicates that *AMBRA1* is the top positive interactor for palbociclib (Table 5.2). AMBRA1 is an important regulator of the cyclin D ubiquitination and therefore proteasomal degradation. Loss of AMBRA1 would therefore lead to higher levels of cyclin D. It was recently shown that AMBRA1 depletion reduces sensitivity to palbociclib (Simoneschi *et al.*, 2021), which confirms the results from the chemogenetic screen. Interestingly, *AMBRA1* was not found among the top interactors with samuraciclib in the chemogenetic screen (Table 5.2). Its role in samuraciclib sensitivity requires further investigation but altogether this indicates that these two CDK4/6 and CDK7 inhibitors depend on different mechanisms to induce a cell cycle arrest.

5.7. Cyclin E overexpression causes samuraciclib resistance to a lower extent compared to palbociclib

Apart from Rb mutations, another cancer-associated alteration that has been found in cell lines resistant to palbociclib treatment is cyclin E amplification (Herrera-Abreu *et al.*, 2016; Guarducci *et al.*, 2018). Moreover, analysing patient tumour samples revealed that high expression of *CCNE1* mRNA encoding for cyclin E1 correlated with poorer palbociclib efficacy (Turner *et al.*, 2019). This resistance mechanism arises due to higher activity of CDK2, which is able to bypass CDK4/6 inactivation. In fact, CDK2 inhibitors have been shown to re-sensitise CDK4/6 inhibitor resistant cell lines (Herrera-Abreu *et al.*, 2016; Pandey *et al.*, 2020; Yap *et al.*, 2023; Dietrich *et al.*, 2024). As CDK7 is required for activation of all mitotic CDKs, its inhibition reduces both CDK4/6 and CDK2 activity. Therefore, I investigated whether cyclin E overexpression affects the sensitivity to palbociclib and samuraciclib. I used an RPE1 cell line expressing doxycycline-inducible (“TetON”) cyclin E1, developed by the laboratory of John Diffley (Zeng *et al.*, 2023). Upon doxycycline treatment, *CCNE1* transcription is

overexpressed, leading to increased cyclin E1 protein levels. I treated the cells with doxycycline overnight in order to induce cyclin E expression before treating with samuraciclib or palbociclib for another 48 hours. I observed that cyclin E expression is significantly upregulated in doxycycline conditions compared to untreated cells (Figure 5.13C). Using this model, I then tested the sensitivity of cells to samuraciclib and palbociclib using EdU incorporation assay and western blot analysis.

As expected, cyclin E overexpression drives cells into the cell cycle and therefore there is a significant increase in cells displaying EdU incorporation (Figures 5.13A and 5.13B). An increase is also observed upon palbociclib and samuraciclib treatments, indicating that upregulation of cyclin E reduces sensitivity to both CDK4/6 and CDK7 inhibition. However, this effect seems greater in the palbociclib condition (Figures 5.13A and 5.13B) suggesting that this might be a more important resistance mechanism for palbociclib. This is in line with the finding that 1000 nM of palbociclib, which fully arrests RPE1 WT cells, is much less effective in RPE1 TetON cyclin E cells even in repressed conditions (Figure 5.13B). This suggests that this system might be leaky and even a small increase in cyclin E levels can cause resistance to palbociclib. This hypothesis requires further confirmation by comparing *CCNE1* mRNA levels in RPE1 WT and RPE1 TetON cyclin E cells. In contrast, samuraciclib is able to effectively induce a cell cycle arrest in repressed conditions (Figure 5.13B). Interestingly, although there is a partial rescue in proliferation during samuraciclib treatment in cyclin E overexpressed cells, based on EdU incorporation and an increased levels of phosphorylated Rb, the increase in p21 levels is unaffected (Figure 5.13C). This suggests that samuraciclib could still be effective during cyclin E overexpression due to an accumulation of p21 and a decreased activity of CDK2, but further experiments comparing a panel of cancer cell lines with different cyclin E levels need to be carried out to confirm this.

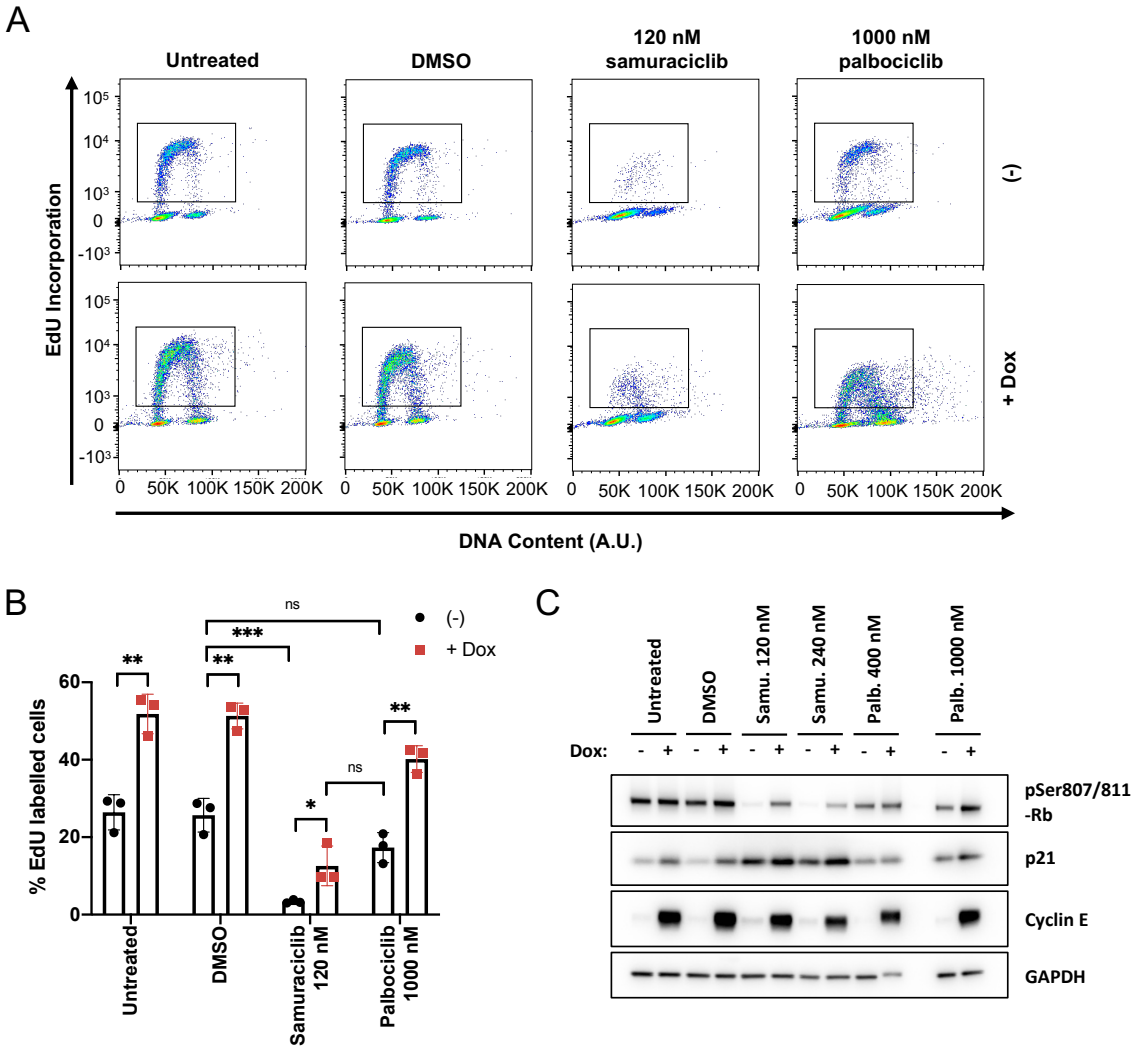

Figure 5.13: Cyclin E overexpression greatly reduces sensitivity to palbociclib and to a smaller extent to samuraciclib.
RPE1 TetON Cyclin E cells were left untreated or treated with doxycycline overnight to induce cyclin E expression. The following day, cells were treated with vehicle control, 120 nM or 240 nM of samuraciclib (Samu.) and 400 nM or 1000 nM of palbociclib (Palb.) for 48 hours. **A)** Cells were incubated with EdU for 1 hour before collection. Pseudocoloured plots of flow cytometry data from a representative experiment. DNA content is plotted against EdU incorporation. Inset gate drawn to include EdU-positive cells. **B)** Quantification of the percentage of EdU-positive cells from three independent experiments (representative shown in A). Statistical significance was calculated using an unpaired two-tailed t test. Error bars are SD. **C)** Western blot analysis from one experiment of whole-cell extracts. GAPDH: loading control.

5.8. Summary

This chapter focused on exploring the roles of other fundamental cell cycle processes apart from cellular growth in the sensitivity to samuraciclib and compared it to

palbociclib treatment. This way I explored potential sensitivity and resistance mechanisms that can affect the drug response.

The genome-wide CRISPR KO chemogenetic screen, carried out by our collaborators from the Tyers lab, revealed a potential role for p53 in samuraciclib sensitivity. Samuraciclib robustly upregulates p21 and MDM2, both targets of a transcription factor p53. Moreover, p53 levels themselves are increased in response to CDK7 inhibition. This suggests that p21 accumulation is an active response to this treatment. Both p53 and p21 depletions greatly reduce the sensitivity to samuraciclib, indicating they are required to induce the initial cell cycle arrest. These data align with the published phase I clinical trial results that suggest p53 status might be important for samuraciclib efficacy and therefore for patient stratification (Coombes *et al.*, 2023). Interestingly, from the three breast cancer cell lines I previously tested for samuraciclib sensitivity in chapter 3, T47D cells with a p53 loss-of-function mutation still display a degree of sensitivity at a concentration lower than its IC_{50} value. This suggests that some p53 mutant cell lines might still respond to samuraciclib treatment, but testing this on a greater panel of cancer cell lines is required to investigate this further. I observed a positive correlation with samuraciclib sensitivity and basal p21 levels in these three breast cancer cell lines, which could suggest that p21 might be a clearer read-out of samuraciclib response. Apart from being an important indicator of a cell cycle arrest, p21 is also required to maintain a samuraciclib-induced cell cycle arrest to allow cells to enter a senescent state.

Furthermore, the top positive interactors for palbociclib, Rb and AMBRA1, are not among the top hits in the samuraciclib screen, suggesting they are not required for samuraciclib sensitivity. Depleting Rb in RPE1 cells indeed does not affect the ability of samuraciclib to inhibit proliferation. However, overexpression of cyclin E appears to reduce sensitivity to samuraciclib, but to a much lower extent than to palbociclib.

These experiments reveal potentially different resistance mechanisms in samuraciclib and palbociclib treatment, providing insight into why samuraciclib might be effective in palbociclib-resistant cancers.

6. Discussion

The aim of my PhD project was to understand the anti-cancer efficacy of CDK inhibitors, focusing on clinically relevant CDK4/6 and CDK7 inhibitors, palbociclib and samuraciclib respectively. Three CDK4/6 inhibitors are FDA approved and currently used as standard of care treatments for metastatic HR+, HER2- breast cancer in combination with ET (Beaver *et al.*, 2015; US Food and Drug Administration, 2017; Shah *et al.*, 2018; Morrison, Loibl and Turner, 2024). The CDK7 inhibitor samuraciclib is in several phase I/II clinical trials and has obtained fast track designations from FDA for treating CDK4/6 inhibitor-resistant HR+, HER2- advanced breast cancer in combination with fulvestrant and also in combination with chemotherapy for treating locally advanced TNBC (Carrick Therapeutics, 2021; Coombes *et al.*, 2023). Despite their anti-tumour efficacy, the exact mechanisms of action are not well understood, especially for samuraciclib being a more novel small molecule inhibitor. Palbociclib, despite being well-tolerated and inducing an effective initial response, patients commonly acquire resistance and eventually succumb to the disease (Rinnerthaler, Gampenrieder and Greil, 2018; Xu *et al.*, 2021; Fassl, Geng and Sicinski, 2022).

The work in my thesis shows that samuraciclib and palbociclib are both cytostatic drugs that induce a senescent phenotype. It establishes an important role for active cellular growth, and the consequent increase in cell size during the arrest, in determining sensitivity to both CDK inhibitors. However, it also reveals that samuraciclib and palbociclib have distinct sensitivity and resistance mechanisms. Overall, it provides a better understanding of the mechanisms of their anti-cancer efficacy that can help identify biomarkers of treatment response, guide their clinical use, and therefore potentially improve patient stratification and outcome.

6.1. Samuraciclib and palbociclib arrest cells in a G1 state by inducing senescent phenotypes

CDK4/6 are involved in priming the cells for G1-to-S transition, whereas CDK2 is necessary for cell cycle entry and S phase progression and CDK1 for M phase entry

and progression (Matthews, Bertoli and de Bruin, 2022). Palbociclib, leading to CDK4/6 activity loss, is known to induce a G1 cell cycle arrest (Pennycook and Barr, 2021; Lanz *et al.*, 2022), which I confirmed in chapter 4. Palbociclib treatment leads to unphosphorylated Rb and promotes cell cycle exit from the G1 phase. In chapter 3 together with our published data, I demonstrated that samuraciclib also induces a cell cycle arrest predominantly in a G1 state with a significantly reduced G2 population (Wilson *et al.*, 2023). Whilst CDK7 is the CAK, the G1 arrest is likely due to the requirement of CDK7 to maintain the activities of CDK4/6, but not that of CDK2 and CDK1 (Schachter and Fisher, 2013; Schachter *et al.*, 2013; Fisher, 2019). This would explain why cells, when treated with a CDK7 inhibitor, are able to progress through S-G2-M phases, completing the cell cycle and arrest in the subsequent G1 phase. In addition, and contrary to palbociclib, p21, a CDK2/4/6 inhibitor, rapidly accumulates in response to samuraciclib, reinforcing a G1 cell cycle arrest.

These two CDK inhibitors, samuraciclib and palbociclib, have cytostatic effects *in vitro*, where they inhibit proliferation without inducing cell death (Fry *et al.*, 2004; Wilson, 2020; Crozier *et al.*, 2022; Wilson *et al.*, 2023). Previous work using the covalent CDK7 inhibitor THZ1 suggested that CDK7 inhibition is largely cytotoxic, but a previous PhD student in the de Bruin lab, Gemma Wilson, established that a samuraciclib-induced reduction in cell number cannot be attributed to cell death (Wilson, 2020), which I confirmed by the live-cell imaging of the FUCCI reporter cells (Wilson *et al.*, 2023). More recently, THZ1 was found to also inhibit CDK12 and CDK13, both involved in the RNAPII-mediated transcriptional cycle (Kwiatkowski *et al.*, 2014). This suggests that the cytotoxic phenotype could be due to the inhibition of CDK7/12/13 simultaneously, affecting global transcription to a greater extent. Interestingly, YKL-5-124, a selective covalent CDK7 inhibitor, induces a cytostatic phenotype by arresting the cell cycle in a G1 phase (Olson *et al.*, 2019). This is in line with samuraciclib-induced proliferative arrest, and further supports the findings that selective CDK7 inhibition induces cytostasis (Wilson *et al.*, 2023).

The cytostatic effect induced by samuraciclib and palbociclib is accompanied by multiple senescent phenotypes, suggesting a permanent arrest state (Crozier *et al.*, 2023; Manohar *et al.*, 2023; Wilson *et al.*, 2023). However, there is currently no single biomarker of a senescent state. The expression of these markers is heterogeneous

and highly depends on a cell type, treatment duration and a senescence inducer (Kumari and Jat, 2021). What all senescent cells have in common is the permanent loss of a proliferative potential and the inability to return to a proliferative state despite growth- and proliferation-promoting stimuli (Herranz and Gil, 2018; Kumari and Jat, 2021). Therefore, studying the cell's inability to re-enter the cell cycle upon removal of a senescence inducer would more clearly detect a senescent state. Although this poses difficulty in patient samples, it can be studied in *in vitro* cell culture models. Using colony formation assay I showed that both samuraciclib and palbociclib reduce the proliferative potential of non-transformed near-diploid RPE1 cells after inhibitor wash-out; however, samuraciclib does this more robustly than palbociclib after 48 hours of treatment. Tracking cell cycle progression of single RPE1 cells using the FUCCI reporter system, revealed more clearly that the majority of cells remain arrested in G1 rather than undergo cell death following samuraciclib wash-out. This further confirms the predominant cytostatic effect of this inhibitor and indicates a robust senescence induction. Other studies have shown that palbociclib can induce long-term cell cycle exit after a prolonged treatment, but only a minority of cells remain arrested in G1, with the majority being able to re-enter the cell cycle. These, however, are more likely to subsequently exit the cell cycle due to replication-acquired DNA damage and an impaired DNA damage response (DDR) resulting in mitotic bypass or mitotic abnormalities (Crozier *et al.*, 2022, 2023; Manohar *et al.*, 2023). After samuraciclib wash-out, I observed only a small percentage return to a proliferative state. However, many of these also undergo mitotic bypass events, which suggests that replication-acquired DNA damage might play a role in permanent cell cycle exit of those cells that do not arrest in response to CDK7 inhibition itself. To test this, DNA fibre assay should be carried out on samuraciclib treatment-released cells to measure levels of replication stress as I carried out for palbociclib (Manohar *et al.*, 2023). Moreover, levels of γH2AX and 53BP1 foci should be tested as markers of DNA damage. Although, more work is required to comprehensively compare cell cycle fate in samuraciclib and palbociclib release experiments, my data altogether indicate that samuraciclib induces a more robust permanent cell cycle arrest during treatment.

6.2. Genome-wide CRISPR KO chemogenetic screens reveal distinct sensitivity and resistance mechanisms between samuraciclib and palbociclib

Samuraciclib and palbociclib treatments demonstrated different cell cycle exit dynamics following treatment release, and they likely require distinct mechanisms to promote a long-lasting anti-cancer response. Analysing the data from our genome-wide CRISPR KO chemogenetic screens, carried out by our collaborators from the Tyers lab, confirmed this as it revealed no GO terms shared within the top 50 hits between these two CDK inhibitors, suggesting they have different sensitivity and resistance mechanisms.

The chemogenetic screens with palbociclib indicated *RB1* and *AMBRA1* as the top positive interactors, which confirms previously published data (Fry *et al.*, 2004; Simoneschi *et al.*, 2021). On the contrary, samuraciclib showed almost no interaction with these genes. My work validates these findings by showing that a knock-down of Rb results in resistance to palbociclib, but has no effect on samuraciclib efficacy in RPE1 cells.

Furthermore, when I averaged the RANKS scores from four chemogenetic screens with different concentrations of samuraciclib, *TP53* came up as the top positive interactor, whereas two chemogenetic screens with palbociclib revealed little interaction. I validated this result using p53 KO RPE1 cells which are significantly less sensitive to samuraciclib. In fact, p53 and its targets p21 and MDM2 are upregulated in response to samuraciclib treatment, suggesting an active role of the p53-p21 signalling in a samuraciclib-induced arrest. Despite the overall loss of sensitivity in p53 depleted cells, higher samuraciclib concentrations are able to inhibit proliferation. However, higher doses can potentially cause off-target effects and increase toxicity in healthy cells. Therefore, future work should investigate if increasing treatment duration could eventually arrest the cell cycle of p53 KO cells. If this is the case, it would also be interesting to test the proliferative potential of samuraciclib-arrested p53 KO cells after a treatment wash-out to test whether this arrest leads to an irreversible cell cycle exit or a temporary one allowing cells to re-enter the cell cycle and continue proliferating.

A positive correlation between *TP53* WT and treatment response was observed in a modular phase I clinical study using samuraciclib as an anti-cancer therapy (Coombes *et al.*, 2023). When I analysed three breast cancer cell lines, it showed that the *TP53* WT MCF7 cell line is the most sensitive to samuraciclib treatment, whereas *TP53* mutant T47D and BT549 cell lines are less sensitive. However, *TP53* mutation cannot fully explain the reduction in the sensitivity as T47D cells still respond to lower concentrations of samuraciclib. Basal levels of a p53 target p21 correlate with samuraciclib sensitivity in these three breast cancer cell lines, therefore the response to samuraciclib could be measured by assessing the ability of cells to accumulate p21. However, cancer cell lines have multiple mutations that could affect their response to CDK7 inhibition, and we have identified another signalling pathway required for samuraciclib efficacy, via active mTOR signalling (Wilson *et al.*, 2023). Therefore, a larger panel of breast cancer cell lines should be tested, which is listed in Table 6.1, and mutations in p53 regulators, such as MDM2 or ARF, an upstream regulator of MDM2, should be assessed as well as they could impact the p53 response in p53-proficient cells.

Depletion of p53, on the other hand, appears to have only a small effect on palbociclib-induced initial cell cycle arrest as demonstrated in chapter 4 and by a previously published study (Crozier *et al.*, 2022). Though palbociclib was able to arrest these cells in G1, they had a higher proliferative potential following treatment release (Crozier *et al.*, 2022). Moreover, sequencing of patient sample biopsies revealed that *TP53* mutations were more prevalent in the palbociclib-resistant tumours. However, when they carried out further pre-clinical studies, it suggested that p53 mutation or loss itself is not sufficient to drive the treatment resistance (Wander *et al.*, 2020). Whilst palbociclib, like samuraciclib, induces an upregulation of p53 and p21 (Crozier *et al.*, 2023; Foy *et al.*, 2023; Manohar *et al.*, 2023), I show that the increase in p21 levels occurs at a later timepoint and is preceded by the G1 arrest. This could explain why p53 does not have a significant role in the initial arrest but might contribute to driving a permanent arrest. This is in line with recent studies that show that p53-dependent p21 accumulation during a palbociclib treatment is important for driving a long-term cell cycle exit (Crozier *et al.*, 2023; Manohar *et al.*, 2023). p21 upregulation is not due to DNA damage as palbociclib does not induce DNA damage and p21 cannot be lowered using an inhibitor of ATM, a kinase upstream of Chk2 that becomes activated

in response to DNA damage and mediates the DDR (Crozier *et al.*, 2022; Wang *et al.*, 2022; Manohar and Neurohr, 2023; Manohar *et al.*, 2023). Instead, during the arrest, p21 expression is induced in response to osmotic stress and p38 mitogen-activated protein kinase (MAPK)-mediated activation of p53 (Crozier *et al.*, 2023).

In comparison, samuraciclib treatment induces p53-dependent p21 accumulation much earlier than palbociclib and I show that p21 accumulation significantly contributes to the initial cell cycle arrest, as depleting p21 levels in RPE1 cells significantly reduces samuraciclib sensitivity. It remains unclear what causes this rapid p21 upregulation, but it is unlikely to be due to DNA damage as I observe no increase in γH2AX, a marker of DNA damage, throughout samuraciclib treatment or an activation of the DNA damage checkpoint indicated by the absence of phosphorylated Chk2. This should also be tested more directly using an ATM inhibitor KU-55933 to confirm whether p21 upregulation is dependent on ATM. However, p53-dependent p21 accumulation can occur due to different stimuli, such as osmotic stress, as was observed for palbociclib treatment (Crozier *et al.*, 2023), or oxidative stress, which has been found as a potential inducer of premature senescence (Gorgoulis *et al.*, 2019). These should be investigated in order to identify the source of p53-p21 activation. Activation of p38 MAPK signalling in response to samuraciclib should be tested by measuring levels of phosphorylated p38 MAPK at threonine residue 180 and tyrosine residue 189. Moreover, a co-treatment of samuraciclib and a p38 MAPK inhibitor should be carried out to assess whether p21 levels can be lowered as was observed with palbociclib (Crozier *et al.*, 2023). Furthermore, senescent cells often display altered mitochondrial phenotypes and dysfunction, as well as produce higher levels of reactive oxygen species (ROS), which can lead to macromolecular damage, such as proteins and lipids (Gorgoulis *et al.*, 2019). ROS was previously observed to accumulate in response to palbociclib treatment in MCF7 and T47D breast cancer cells (Vijayaraghavan *et al.*, 2017). Future work can test cellular ROS levels in response to samuraciclib using the CellROX assay. Even though high levels of ROS do not appear to be the source of p21 accumulation during the palbociclib treatment, as antioxidant activity does not lower p21 levels (Crozier *et al.*, 2023), this should be tested for samuraciclib. Potential accumulation of ROS can be inhibited using N-acetyl cysteine (NAC) molecule (Vijayaraghavan *et al.*, 2017; Crozier *et al.*, 2023).

Importantly, the rapid accumulation of p21 in response to samuraciclib could potentially explain why samuraciclib induces a more robust cell cycle exit compared to palbociclib after 48 hours. I observed that after 48 hours, there is little to no increase in p21 levels in response to palbociclib and these cells are able to re-enter the cell cycle following treatment release to a greater extent than samuraciclib-treated cells. p21 inhibits CDK2 activity, which prevents cell cycle entry. Therefore, in the case of samuraciclib, high levels of p21 and therefore additional CDK2 inhibition, could prevent or delay cell cycle entry even after CDK7 inhibition is removed resulting in greater loss of proliferative potential compared to palbociclib. In fact, depleting p21 levels after 48 hours of samuraciclib treatment increases levels of proliferative markers, which suggests that p21 is required for maintaining samuraciclib-induced cell cycle arrest. This requires further validation by assessing the cell cycle progression using EdU incorporation assay and comparing it to palbociclib treatment. Moreover, wash-out experiments can be carried out in RPE1 cells with endogenously tagged p21 and PCNA to correlate levels of p21 and the ability to enter S phase (Barr *et al.*, 2017). Whilst p21 accumulation seems to be important for the initial arrest during samuraciclib treatment and maintaining the arrest after wash-out of both CDK inhibitors my data and that of others show that excessive cellular growth during the cell cycle arrest is central for the induction of an irreversible cell cycle exit (Lanz *et al.*, 2022; Crozier *et al.*, 2023; Foy *et al.*, 2023; Manohar *et al.*, 2023; Wilson *et al.*, 2023).

The important role of growth signalling via mTOR pathway in samuraciclib sensitivity was first revealed through our unbiased chemogenetic screen (Wilson, 2020; Wilson *et al.*, 2023). This was validated by pharmacologically inhibiting mTOR activity with Torin1, which reduces samuraciclib-induced cell cycle arrest and senescent phenotypes. However, pharmacological inhibition of mTOR increases sensitivity to palbociclib. This indicates that mTOR signalling increases samuraciclib's but decreases palbociclib's ability to inhibit cellular proliferation, which points to potentially distinct sensitivity mechanisms.

6.3. Active cellular growth during samuraciclib- and palbociclib-mediated cell cycle arrest is important for a permanent cell cycle exit

Whilst downregulation of mTOR signalling increases sensitivity and cytostatic effects of palbociclib, recent studies have shown that active cellular growth during palbociclib-mediated cell cycle arrest is important for a permanent cell cycle exit after drug wash-out (Lanz *et al.*, 2022; Crozier *et al.*, 2023; Foy *et al.*, 2023; Manohar *et al.*, 2023). Understanding what happens to cells following removal of a cytostatic drug is essential as a temporary cytostatic effect could lead to cancer relapse in the future. The idea that cellular growth and active mTOR signalling are required for senescence induction was proposed around 15 years ago (Demidenko and Blagosklonny, 2008; Blagosklonny, 2012, 2014). Cellular hypertrophy, a hallmark of senescence, during a cell cycle arrest was found to be important for converting this arrest to the irreversible arrested state of senescence, which was referred to as geroconversion (Blagosklonny, 2014).

I demonstrated the importance of active growth signalling and an increase in cell size for driving an irreversible cell cycle exit, through treatment wash-out experiments for both palbociclib and samuraciclib. Downregulation of mTOR activity during samuraciclib and palbociclib treatment using both pharmacological and serum depletion approaches leads to an increased re-entry into a proliferative state compared to arrested cells with active mTOR signalling. This indicates that cell cycle arrest induced by samuraciclib and palbociclib during inhibition of mTOR activity is more reversible, which supports the idea of geroconversion.

I further demonstrated that samuraciclib-induced senescent phenotypes and a permanent cell cycle exit correlate with mTOR-dependent increase in cell size. Moreover, I showed that reducing mTOR activity in samuraciclib-arrested cells after treatment wash-out slightly increases the fraction of proliferating cells, suggesting that active mTOR signalling and therefore continued cellular growth during the recovery from a samuraciclib-induced arrest contributes to cells exiting the cell cycle permanently. Lastly, I showed more directly that larger cells on average remain permanently arrested whereas smaller cells are more likely to re-enter the proliferative state after samuraciclib treatment. This was recently shown for palbociclib-mediated

cell cycle arrest as well (Lanz *et al.*, 2022). However, in both cases there is no clear threshold in cell size that leads to an irreversible arrest state. This might suggest that to some extent cellular growth signalling might drive senescence independently of cell size, but also that other types of stress stimuli might cause smaller cells to remain arrested (Wilson *et al.*, 2023).

To more clearly understand the relationship between cell size and a proliferative potential, RPE1 cells treated with samuraciclib should be sorted based on cell size using fluorescence-activated cell sorting (FACS) and forward scatter (FSC) and cultured further in drug-free media to investigate whether smaller cells have a higher proliferative potential. This can be tested using colony formation or EdU incorporation assays. Furthermore, cell cycle fates of differently sized samuraciclib-arrested cells should be investigated after treatment wash-out using the FUCCI reporter system. Different sizes can be controlled using pharmacological mTOR inhibition with Torin1 and serum depletion. Tracking FUCCI reporter red cells after different treatment combinations can give better insight into relationship between cellular growth and cell size and samuraciclib-induced cell cycle arrest.

Interestingly, palbociclib-arrested cells increase in cell size more significantly than samuraciclib-arrested cells, yet samuraciclib induces a more robust cell cycle exit after 48 hours of treatment. Whilst this suggests that the absolute cell size *per se* is not the main determinant of a permanent cell cycle exit, it does not exclude that increasing cell size beyond a proliferative limit, or so called ‘point of no return’, is key to inducing a senescent state. A likely contributing factor to the difference observed between samuraciclib- and palbociclib-arrested cells is the time it takes for cells to accumulate enough CDK activity to drive cell cycle entry once the inhibitors have been removed. After samuraciclib treatment the cell needs to overcome not just loss of CDK4/6, as with palbociclib-arrested cells, but also loss of CDK2 activity and the p21-dependent CDK2/4/6 inhibition. This could delay S phase entry, during which cells continue to increase in size allowing them to reach the ‘point of no return’. Future work should establish if samuraciclib-treated cells take longer to re-enter the cell cycle after wash-out and if their size increases during recovery beyond that observed for palbociclib-arrested cells. In addition, the ‘point of no return’, and the corresponding cell size,

could be investigated by establishing at what point loss of p53 or p21 cannot reverse a samuraciclib- or palbociclib-induced arrest.

The molecular mechanisms of geroconversion remain unknown, but recent work has suggested potential mechanisms by which cellular hypertrophy leads to a permanent cell cycle exit. It was recently suggested that it could be linked to limitation in gene expression scaling with size (Neurohr *et al.*, 2019). It was shown in budding yeast that when cells increase in cell size beyond a certain point DNA becomes limiting and both RNA and protein biosynthesis fail to scale with cell volume, which ultimately leads to cytoplasmic dilution and reduced cell fitness. This study also showed that in human fibroblasts, prolonged palbociclib treatment leads to a reduced macromolecular crowding in the cytoplasm (Neurohr *et al.*, 2019). Macromolecular crowding, an indirect measure for cytoplasmic density, was measured using genetically encoded multimeric nanoparticles (GEMs). These GEMs are 20 nm and 40 nm large and fused to a fluorescent protein (Delarue *et al.*, 2018). By tracking these nanoparticles through the cytoplasm, one can obtain an understanding of cytoplasmic macromolecular crowding. Future work should investigate this in samuraciclib-treated cells and compare it to palbociclib. Gemma Wilson observed that samuraciclib reduces global RNA transcription (Wilson, 2020). This inhibitory effect on transcription could lead to a reduced gene expression and therefore cytoplasmic dilution occurring at a smaller size compared to palbociclib. GEMs should also be tracked in samuraciclib- and palbociclib-treated cells that had downregulated mTOR signalling and therefore restricted cell size increase.

Alternatively, measuring cell mass rather than cellular volume could give us a better understanding of the relationship between macromolecular biosynthesis and permanent cell cycle exit. Future work could measure cell dry mass with quantitative phase microscopy approach using a Phasics SID4Bio shearing interferometer. A phase shift is quantified when light waves pass through a cell and this is directly related to cell dry mass, which is everything that makes up a cell apart from water (Park, Depeursinge and Popescu, 2018). However, a challenging step in quantifying dry mass using this approach is accurate cell segmentation. Once optimised, this could provide a powerful tool to further explore the role of cellular growth in guiding a cell cycle exit in response to palbociclib and samuraciclib as this method can be used for

live-cell imaging and coupled with fluorescence signals of proliferative markers, using either RPE1 FUCCI cells or RPE1 cells with endogenously tagged p21 and PCNA (Barr *et al.*, 2017).

Furthermore, excessive cellular growth was found to be accompanied by an imbalance in the proteome scaling, with some proteins subscaling and some superscaling as a function of cell size (Lanz *et al.*, 2022, 2023; Zatulovskiy *et al.*, 2022; Crozier *et al.*, 2023). In fact, large cycling cells have proteome changes similar to senescent cells, and they were found to permanently exit the cell cycle earlier than smaller cycling cells (Lanz *et al.*, 2022). Future work should explore and compare proteome changes in response to samuraciclib and palbociclib using mass spectrometry to understand better whether this imbalance occurs at a smaller size in response to samuraciclib or there is a change in distinct proteins that guide a more robust cell cycle exit in response to samuraciclib.

In palbociclib-mediated cell cycle exit, size-dependent accumulation of p21 played an important role (Crozier *et al.*, 2023; Manohar *et al.*, 2023). It is likely that this is the case for samuraciclib as well as samuraciclib-treated cells which have active mTOR signalling accumulate p21 rapidly, whereas those that have inhibited mTOR-dependent cellular growth, which prevents an increase in cell size, do not increase p21 levels as quickly. However, this requires further investigation and establishing the mechanism of p21 accumulation will provide a better understanding of its role.

6.4. mTOR-dependent growth signalling positively correlates with samuraciclib efficacy in breast cancer cells

Samuraciclib is the most clinically advanced CDK7 inhibitor. Therefore, it is necessary to expand the investigation from a non-transformed cell line with intact cell cycle checkpoints to cancer cell lines. Despite all three tested breast cancer cell lines having growth-promoting mutations, they display different mTOR activity levels, which I observed positively correlate with samuraciclib sensitivity. However, this is a relatively small panel of breast cancer cell lines and I have also observed a positive correlation with basal p21 levels. Therefore, to further explore the relationship between cellular

growth and p53-dependent p21 accumulation and samuraciclib sensitivity, future work should test a larger panel of breast cancer cell lines including non-transformed mammary cells, such as MCF10A and HMEC, which were previously found to be less sensitive to samuraciclib than transformed cell lines (Patel *et al.*, 2018). The panel proposed is listed in Table 6.1. When testing sensitivity to samuraciclib, traditional sensitivity assays that are based on ATP activity or protein mass, such as CellTiterGlo or SRB assays respectively, should not be used. It was recently shown that these assays can underestimate the sensitivity of cell lines that are able to increase their cellular volume in response to cytostatic CDK inhibitors, more precisely palbociclib (Foy, Lew and Saurin, 2024). As they increase in cell size, they accumulate protein mass and also have an increased metabolic activity, which can result in inaccurate IC_{50} values. Therefore, when testing sensitivity of the breast cancer cell lines listed in Table 6.1 to samuraciclib, cell number should be measured.

Table 6.1: Panel of mammary cell lines to test samuraciclib sensitivity.

Cell lines	Breast cancer subtype	mTOR signalling activation	*TP53* status
MCF10A	Non-transformed	-	WT
HMEC	Non-transformed	-	WT
MCF7	HR+, HER2-	*PIK3CA* E545K	WT
T47D	HR+, HER2-	*PIK3CA* H1047R	L194F
BT549	TNBC	PTEN-	R249S
CAL51	TNBC	PTEN-	WT
MDA-MB-231	TNBC	-	R280K
MDA-MB-361	HR+, HER2+	*PIK3CA* E545K *PIK3CA* K567R	WT
MDA-MB-468	TNBC	p85α-/PTEN-	R273H
HCC1806	TNBC	p85α-	p53-

Although correlative findings can be obtained from these studies, cancer cell lines harbour multiple genetic mutations that could lead to treatment resistance. It is therefore difficult to delineate a causal relationship from such experiments. To investigate a role of a single growth-promoting mutation in the *PIK3CA* gene, I used a pair of isogenic MCF7 cell lines where this mutation was reverted back to the WT sequence (Beaver *et al.*, 2013). In chapter 3, I demonstrated that the *PIK3CA* E545K mutation in MCF7 cells increases mTOR activity and together with our collaborators

from the Ali lab, we observed that this increases sensitivity to samuraciclib (Wilson *et al.*, 2023). This work showed more clearly the role of a cancer-associated growth-promoting mutation in driving a samuraciclib-induced cell cycle arrest. A recent study found that the MCF7 cells harbouring the WT sequence of the *PIK3CA* gene are more likely to return to a proliferative state following palbociclib wash-out (Foy *et al.*, 2023). They also demonstrated that inserting cancer-associated growth-promoting mutations into a non-transformed mammary cell line, MCF10A, increases its sensitivity to palbociclib by increasing cell size and upregulating p21 to a greater extent than the WT MCF10A cell line, which correlates with a more delayed cell cycle entry (Foy *et al.*, 2023). Future work can investigate samuraciclib efficacy in the MCF10A cells with the *PIK3CA* oncogenic mutations compared to the WT MCF10A (Gustin *et al.*, 2009).

Furthermore, to investigate the interplay more clearly between p53 and cellular growth in samuraciclib sensitivity, future experiments should deplete p53 levels using an siRNA-mediated knock-down or knocking-out p53 in the two MCF7 isogenic cell lines mentioned earlier. This would reveal whether a growth-promoting mutation that increases samuraciclib sensitivity can overcome the resistance caused by loss of p53 and in turn p21.

6.5. Future research opportunities

To fully understand samuraciclib's mechanism of action, it is important to understand its selectivity and any potential off-target effects. For instance, palbociclib was chosen as the CDK4/6 inhibitor to compare the effects on the cell cycle to samuraciclib because of its high selectivity (Klein *et al.*, 2018) and numerous data available on its anti-proliferative effect in RPE1 cells (Crozier *et al.*, 2022, 2023; Lanz *et al.*, 2022; Manohar *et al.*, 2023). High selectivity of palbociclib towards CDK4 and CDK6 was demonstrated in *in vitro* kinase assays. It has a similar affinity towards both CDK4 and CDK6 and the IC_{50} for other kinases was more than 600-fold greater (Fry *et al.*, 2004). Palbociclib's selectivity was more recently confirmed in live cells as well (Wells *et al.*, 2020) and using a dual siRNA-mediated knock-down of CDK4 and CDK6 (Vijayaraghavan *et al.*, 2017). Samuraciclib was also shown to be selective towards CDK7, having a higher affinity towards CDK7 than other kinases in cell-free kinase

assays (Patel *et al.*, 2018). On the other hand, studying target binding in live cells demonstrated engagement with CDK4 in addition to CDK7 (Wells *et al.*, 2020). However, more recently a study investigating target specificity in prostate cancer cell line published data more similar to the *in vitro* kinase assay, where samuraciclib was selective for CDK7 but had some degree of binding affinity towards CDK2 and CDK9 (Constantin *et al.*, 2023). In chapter 3, I attempted to study potential off-target effects in RPE1 cells using a CDK7 knock-down but could not recapitulate the effects of samuraciclib. This could be due to the incomplete loss of CDK7 levels and therefore its activity, but the effects of a CDK7 knock-down should be further investigated by testing levels of T loop phosphorylations in mitotic CDKs during a longer CDK7 depletion timecourse. A potential indication of an off-target effect of samuraciclib was revealed in the CRISPR KO chemogenetic screen in NALM-6 cells. The screen results identified CDK7 as a negative interactor of samuraciclib, which indicates that samuraciclib affects an activity independent of CDK7. What this potential off-target effect of samuraciclib is should be further investigated. For this, more efficient approaches inducing an acute loss of CDK7 activity should be used. One way is to mutate the WT CDK7 in RPE1 cells to an analogue-sensitive CDK7 that can be inhibited by bulky adenine analogues (Shah *et al.*, 1997). This has successfully been done in a human colon cancer cell line and used for studying CDK7's role as a CAK (Larochelle *et al.*, 2007; Merrick *et al.*, 2008; Schachter *et al.*, 2013). The effect of CDK7 depletion in RPE1 cells can also be studied using degron tagging for rapid and inducible protein degradation (Hégarat *et al.*, 2020).

The work presented in this thesis compared cell cycle exit dynamics of a CDK7 and CDK4/6 inhibitor, and I observed that palbociclib is less effective in driving a permanent cell cycle exit compared to samuraciclib. Since CDK7 acts as a CAK to activate all mitotic CDKs and also the transcriptional CDK9 it is likely that inhibition of CDK2 and/or CDK9, in addition to CDK4/6 contributes to this increased efficacy. To dissect this, samuraciclib-mediated cell cycle exit could be compared to combinatorial treatments of CDK4/6, CDK2 and CDK9 inhibition. Recently, a novel CDK2 inhibitor, INX-315, that has entered clinical trials displayed a cytostatic effect via senescence (Dietrich *et al.*, 2024). Moreover, a CDK9 inhibitor, enitociclib, is also in clinical trials (Lücking *et al.*, 2021; Diamond *et al.*, 2022). Using different combinations of these

clinically relevant CDK inhibitors could help delineate the mechanism of samuraciclib efficacy as well as inform on potential off-target effects.

This work and that of others, has established an important role for cellular growth in driving a permanent exit from the cell cycle (Neurohr *et al.*, 2019; Lanz *et al.*, 2022; Crozier *et al.*, 2023; Foy *et al.*, 2023; Manohar *et al.*, 2023; Wilson *et al.*, 2023). However, these studies were all carried out in 2D cell culture models, and the role of cellular growth and cell size in regulating response to these cytostatic CDK inhibitors *in vivo* remains to be established. Growth is likely much more restricted in tissue, both mechanically and by contact inhibition, which decreases mTOR signalling (Leontieva, Demidenko and Blagosklonny, 2014; Foy *et al.*, 2023). However, cancer cells often experience both increased growth signalling and loss of contact inhibition which could exacerbate the difference in a cell size increase between cancer and healthy cells and therefore the therapeutic window for samuraciclib and palbociclib treatment. To investigate this, future work should test the efficacy of these CDK inhibitors in 3D tumour structures spheroids. Using cross-sectional imaging, nuclear area can be measured in the centre of a spheroid and on the edge to investigate whether samuraciclib and palbociclib can increase the cell size and induce senescence in a 3D setting.

A CDK inhibitor implicated in senescence induction that I did not explore in this thesis is p16, encoded by the *CDKN2A* gene, which is a CDK4/6 inhibitor. Although it was observed that samuraciclib does not increase p16 levels in RPE1 cells (Wilson, 2020; Wilson *et al.*, 2023), these cells harbour a missense mutation in the *CDKN2A* gene (Libouban *et al.*, 2017). However, MCF7 cells, which are sensitive to samuraciclib, do not express p16 (Todd, Langan and Sclafani, 2017) and p16 was not identified in our chemogenetic screen, suggesting it is unlikely it plays an important role in sensitivity. However, a potential role of p16 in driving and maintaining a senescent state in response to samuraciclib needs further investigation.

Apart from the senescence phenotypes I tested, one important characteristic that I did not explore is the presence of the senescence-associated secretory phenotype (SASP). Senescent cells, despite being permanently arrested, are metabolically active and release a number of cytokines, chemokines and growth factors (Coppé *et al.*, 2010). SASP can have anti-tumorigenic properties, such as immune system activation

to clear the damaged cells or senescence reinforcement and induction of senescence in the neighbouring cells (Gorgoulis *et al.*, 2019; Takasugi *et al.*, 2023). Nevertheless, it can also have pro-tumorigenic properties, such as metastasis or angiogenesis, and it is therefore essential to study the presence, as well as the composition, of the SASP in therapy-induced senescence (TIS) to better understand the treatment response. This is likely to vary in different cell types and as a result should be investigated in RPE1 cells and a panel of cancer cell lines. Future work should explore the potential SASP induction by samuraciclib treatment and compare it to palbociclib, which was previously found to induce several components of the SASP (Ruscetti *et al.*, 2018; Crozier *et al.*, 2023; Wang *et al.*, 2023). Recently, an unbiased proteomic approach revealed SASP signatures in two different cell types and several senescence stimuli, including Ras overexpression and X-ray irradiation, publishing it as the SASP Atlas (Basisty *et al.*, 2020). The core SASP components overlapping in different conditions, such as growth/differentiation factor 15 (GDF15), could be tested in response to samuraciclib. This list of SASP proteins that should be tested was described in a recently published protocol for studying senescence in experimental samples, and their presence in the conditioned cell growth media can be tested using an enzyme-linked immunosorbent assay (ELISA) (Kohli *et al.*, 2021).

Moreover, potential combination of samuraciclib or palbociclib and a senolytic, drugs that eliminate senescent cells, should be explored. Targeting senescent cells for cell death could eliminate the potential harmful effects of senescent phenotypes, such as the SASP. To do so, senolytic-dependent mechanisms need to be studied in samuraciclib and palbociclib-mediated cell cycle arrest. For instance, navitoclax is a Bcl-2 inhibitor and acts as a senolytic by targeting the anti-apoptotic feature of senescent cells (Zhu *et al.*, 2016). Therefore, upregulation of Bcl-2 and the anti-apoptotic pathways need to be explored in response to samuraciclib and palbociclib treatment.

Lastly, as samuraciclib and palbociclib depend on distinct sensitivity and resistance mechanisms, it would be interesting to test the effect of a combinatorial treatment of these two inhibitors. Can the combinatorial treatment overcome samuraciclib's resistance to loss of p53-p21 signalling and palbociclib's resistance to loss of Rb and overexpression of cyclin E? Similar experiments carried out for single treatments in

chapter 5 can be conducted for the combinatorial or sequential treatment of samuraciclib and palbociclib.

6.6. Summary

To summarise, my PhD work demonstrated an important role for mTOR-dependent cellular growth and an increase in cell size in sensitivity to two clinically relevant CDK inhibitors, CDK4/6 inhibitor palbociclib and CDK7 inhibitor samuraciclib. They act by inducing senescence phenotypes, which can be reduced by inhibiting mTOR activity and cellular size. Although cellular growth is important in driving a cell cycle exit during both a samuraciclib and palbociclib treatment, these two CDK inhibitors have distinct sensitivity and resistance mechanisms.

Our current understanding of how excessive cellular growth drives a permanent cell cycle exit is illustrated in Figure 6.1. Cellular proliferation and growth are two fundamental processes coupled to regulate an accurate cell size important for cellular function. When these two processes are decoupled, and cells excessively increase in size during a prolonged CDK inhibitor-induced cell cycle arrest, this leads to senescence (Davies *et al.*, 2022; Manohar and Neurohr, 2023). What drives this cellular growth-dependent cell cycle exit remains unclear and requires further investigation. Two mechanisms likely to be involved are dilution of cytoplasmic components and proteome imbalance which reduce cellular fitness (Neurohr *et al.*, 2019; Lanz *et al.*, 2022; Crozier *et al.*, 2023). Moreover, size-dependent upregulation of p21 was found important in both samuraciclib- and palbociclib-mediated cell cycle exit (Crozier *et al.*, 2023; Manohar *et al.*, 2023). Importantly, even if CDK inhibitor-arrested cells do not permanently exit the cell cycle, which represents the first mode of action, they are more likely to undergo replication-acquired DNA damage during cell cycle re-entry upon CDK inhibitor removal, due to their increased size. This leads to mitotic abnormalities or mitotic bypass that can induce an irreversible cell cycle exit in the subsequent cell cycle (Crozier *et al.*, 2022, 2023; Foy *et al.*, 2023; Manohar *et al.*, 2023) representing a second mode of action for CDK inhibitor anti-cancer efficacy. A detailed fundamental understanding of how these two modes of action contribute to their anti-cancer efficacy can guide their clinical use and new drug development.

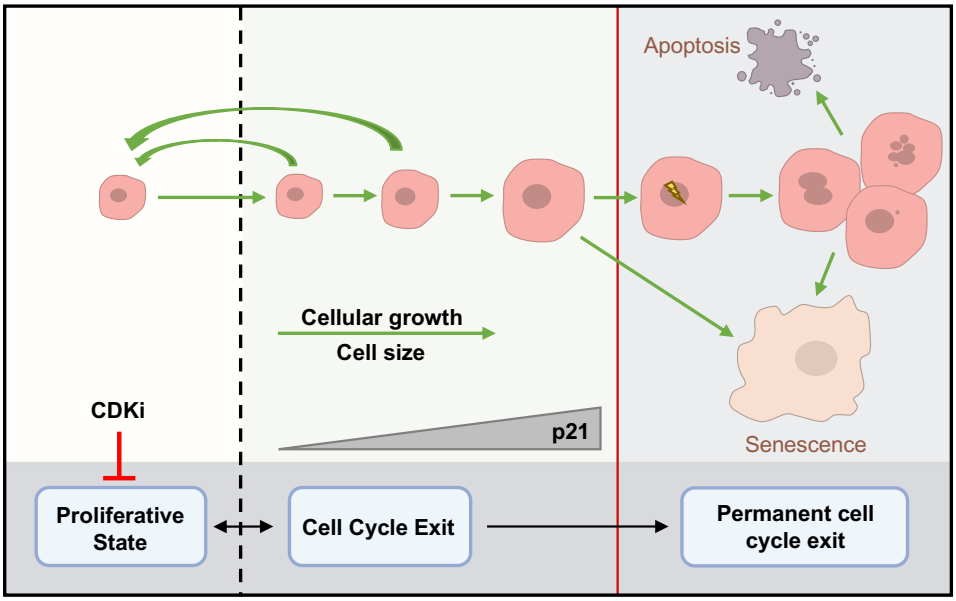

Figure 6.1: Working model on how excessive cellular growth drives permanent cell cycle exit. Figure adapted from (Wilson *et al.*, 2023).

7. Bibliography

Abbas, T. and Dutta, A. (2009). 'p21 in cancer: intricate networks and multiple activities'. *Nature Reviews Cancer*, 9 (6), pp. 400–414. doi: 10.1038/nrc2657.

Aird, K. M. and Zhang, R. (2013). 'Detection of Senescence-Associated Heterochromatin Foci (SAHF)'. in, pp. 185–196. doi: 10.1007/978-1-62703-239-1_12.

Alfieri, C., Chang, L., Zhang, Z., Yang, J., Maslen, S., Skehel, M. and Barford, D. (2016). 'Molecular basis of APC/C regulation by the spindle assembly checkpoint'. *Nature*, 536 (7617), pp. 431–436. doi: 10.1038/nature19083.

Ali, S., Heathcote, D. A., Kroll, S. H. B., Jogalekar, A. S., Scheiper, B., Patel, H., Brackow, J., Siwicka, A., Fuchter, M. J., Periyasamy, M., Tolhurst, R. S., Kanneganti, S. K., Snyder, J. P., Liotta, D. C., Aboagye, E. O., Barrett, A. G. M. and Coombes, R. C. (2009). 'The Development of a Selective Cyclin-Dependent Kinase Inhibitor That Shows Antitumor Activity'. *Cancer Research*, 69 (15), pp. 6208–6215. doi: 10.1158/0008-5472.CAN-09-0301.

Ashley, A. K., Shrivastav, M., Nie, J., Amerin, C., Troksa, K., Glanzer, J. G., Liu, S., Opiyo, S. O., Dimitrova, D. D., Le, P., Sishc, B., Bailey, S. M., Oakley, G. G. and Nickoloff, J. A. (2014). 'DNA-PK phosphorylation of RPA32 Ser4/Ser8 regulates replication stress checkpoint activation, fork restart, homologous recombination and mitotic catastrophe'. *DNA Repair*, 21, pp. 131–139. doi: 10.1016/j.dnarep.2014.04.008.

Barak, Y., Juven, T., Haffner, R. and Oren, M. (1993). 'mdm2 expression is induced by wild type p53 activity.' *The EMBO Journal*, 12 (2), pp. 461–468. doi: 10.1002/j.1460-2075.1993.tb05678.x.

Barr, A. R., Cooper, S., Heldt, F. S., Butera, F., Stoy, H., Mansfeld, J., Novák, B. and Bakal, C. (2017). 'DNA damage during S-phase mediates the proliferation-quiescence decision in the subsequent G1 via p21 expression'. *Nature Communications*, 8 (1), p. 14728. doi: 10.1038/ncomms14728.

Barr, A. R., Heldt, F. S., Zhang, T., Bakal, C. and Novák, B. (2016). 'A Dynamical Framework for the All-or-None G1/S Transition'. *Cell Systems*, 2 (1), pp. 27–37. doi: 10.1016/j.cels.2016.01.001.

Barr, A. R. and McClelland, S. E. (2022). 'Cells on lockdown: long-term consequences of CDK4/6 inhibition'. *The EMBO Journal*, 41 (6). doi: 10.15252/embj.2022110764.

Bartkova, J., Zemanova, M. and Bartek, J. (1996). 'Expression of CDK7/CAK in normal and tumour cells of diverse histogenesis, cell-cycle position and differentiation'. *International Journal of Cancer*, 66 (6), pp. 732–737. doi: 10.1002/(SICI)1097-0215(19960611)66:6<732::AID-IJC4>3.0.CO;2-0.

Basisty, N., Kale, A., Jeon, O. H., Kuehnemann, C., Payne, T., Rao, C., Holtz, A., Shah, S., Sharma, V., Ferrucci, L., Campisi, J. and Schilling, B. (2020). 'A proteomic atlas of senescence-associated secretomes for aging biomarker development'. *PLOS Biology*, 18 (1), p. e3000599. doi: 10.1371/journal.pbio.3000599.

Beach, D., Durkacz, B. and Nurse, P. (1982). 'Functionally homologous cell cycle control genes in budding and fission yeast'. *Nature*, 300 (5894), pp. 706–709. doi: 10.1038/300706a0.

Beaver, J. A., Amiri-Kordestani, L., Charlab, R., Chen, W., Palmby, T., Tilley, A., Zirkelbach, J. F., Yu, J., Liu, Q., Zhao, L., Crich, J., Chen, X. H., Hughes, M., Bloomquist, E., Tang, S., Sridhara, R., Kluetz, P. G., Kim, G., Ibrahim, A., Pazdur, R. and Cortazar, P. (2015). 'FDA Approval: Palbociclib for the Treatment of Postmenopausal Patients with Estrogen Receptor–Positive, HER2-Negative Metastatic Breast Cancer'. *Clinical Cancer Research*, 21 (21), pp. 4760–4766. doi: 10.1158/1078-0432.CCR-15-1185.

Beaver, J. A., Gustin, J. P., Yi, K. H., Rajpurohit, A., Thomas, M., Gilbert, S. F., Rosen, D. M., Ho Park, B. and Lauring, J. (2013). 'PIK3CA and AKT1 mutations have distinct effects on sensitivity to targeted pathway inhibitors in an isogenic luminal breast cancer model system'. *Clinical cancer research : an official journal of the American Association for Cancer Research*. 2013/07/25, 19 (19), pp. 5413–5422. doi: 10.1158/1078-0432.CCR-13-0884.

Benjamini, Y. and Hochberg, Y. (1995). 'Controlling the False Discovery Rate: A Practical and Powerful Approach to Multiple Testing'. *Journal of the Royal Statistical Society: Series B (Methodological)*, 57 (1), pp. 289–300. doi: 10.1111/j.2517-6161.1995.tb02031.x.

Berenson, D. F., Zatulovskiy, E., Xie, S. and Skotheim, J. M. (2019). 'Constitutive expression of a fluorescent protein reports the size of live human cells'. *Molecular Biology of the Cell*, 30 (24), pp. 2985–2995. doi: 10.1091/mbc.E19-03-0171.

Berniak, K., Rybak, P., Bernas, T., Zarębski, M., Biela, E., Zhao, H., Darzynkiewicz, Z. and Dobrucki, J. W. (2013). 'Relationship between DNA damage response, initiated by camptothecin or oxidative stress, and DNA replication, analyzed by quantitative 3D image analysis'. *Cytometry Part A*, 83 (10), pp. 913–924. doi: 10.1002/cyto.a.22327.

Beroukhim, R., Mermel, C. H., Porter, D., Wei, G., Raychaudhuri, S., Donovan, J., Barretina, J., Boehm, J. S., Dobson, J., Urashima, M., Mc Henry, K. T., Pinchback, R. M., Ligon, A. H., Cho, Y.-J., Haery, L., Greulich, H., Reich, M., Winckler, W., Lawrence, M. S., Weir, B. A., Tanaka, K. E., Chiang, D. Y., Bass, A. J., Loo, A., Hoffman, C., Prensner, J., Liefeld, T., Gao, Q., Yecies, D., Signoretti, S., Maher, E., Kaye, F. J., Sasaki, H., Tepper, J. E., Fletcher, J. A., Tabernero, J., Baselga, J., Tsao, M.-S., Demichelis, F., Rubin, M. A., Janne, P. A., Daly, M. J., Nucera, C., Levine, R. L., Ebert, B. L., Gabriel, S., Rustgi, A. K., Antonescu, C. R., Ladanyi, M., Letai, A., Garraway, L. A., Loda, M., Beer, D. G., True, L. D., Okamoto, A., Pomeroy, S. L., Singer, S., Golub, T. R., Lander, E. S., Getz, G., Sellers, W. R. and Meyerson, M. (2010). 'The landscape of somatic copy-number alteration across human cancers'. *Nature*, 463 (7283), pp. 899–905. doi: 10.1038/nature08822.

Bertoli, C. and de Bruin, R. A. M. (2014). 'Cell Division: Turning cell cycle entry on its head'. *eLife*, 3, p. e03475.

Bertoli, C., Skotheim, J. M. and de Bruin, R. A. M. (2013). 'Control of cell cycle transcription during G1 and S phases'. *Nature Reviews Molecular Cell Biology*, 14 (8), pp. 518–528. doi: 10.1038/nrm3629.

Bertomeu, T., Coulombe-Huntington, J., Chatr-aryamontri, A., Bourdages, K. G., Coyaud, E., Raught, B., Xia, Y. and Tyers, M. (2018). 'A High-Resolution Genome-Wide CRISPR/Cas9 Viability Screen Reveals Structural Features and Contextual Diversity of the Human Cell-Essential Proteome'. *Molecular and Cellular Biology*, 38 (1). doi: 10.1128/MCB.00302-17.

Blagosklonny, M. V. (2012). 'Cell cycle arrest is not yet senescence, which is not just cell cycle arrest: terminology for TOR-driven aging'. *Aging*, 4 (3), pp. 159–165. doi: 10.18632/aging.100443.

Blagosklonny, M. V. (2014). 'Geroconversion: irreversible step to cellular senescence'. *Cell Cycle*, 13 (23), pp. 3628–3635. doi: 10.4161/15384101.2014.985507.

Blethrow, J. D., Glavy, J. S., Morgan, D. O. and Shokat, K. M. (2008). 'Covalent capture of kinase-specific phosphopeptides reveals Cdk1-cyclin B substrates'. *Proceedings of the National Academy of Sciences*, 105 (5), pp. 1442–1447. doi: 10.1073/pnas.0708966105.

Bonelli, M. A., Digiacomo, G., Fumarola, C., Alfieri, R., Quaini, F., Falco, A., Madeddu, D., La Monica, S., Cretella, D., Ravelli, A., Ulivi, P., Tebaldi, M., Calistri, D., Delmonte, A., Ampollini, L., Carbognani, P., Tiseo, M., Cavazzoni, A. and Petronini, P. G. (2017). 'Combined Inhibition of CDK4/6 and PI3K/AKT/mTOR Pathways Induces a Synergistic Anti-Tumor Effect in Malignant Pleural Mesothelioma Cells'. *Neoplasia*, 19 (8), pp. 637–648. doi: 10.1016/j.neo.2017.05.003.

Buck, S. B., Bradford, J., Gee, K. R., Agnew, B. J., Clarke, S. T. and Salic, A. (2008). 'Detection of S-phase cell cycle progression using 5-ethynyl-2′-deoxyuridine incorporation with click chemistry, an alternative to using 5-bromo-2′-deoxyuridine antibodies'. *BioTechniques*, 44 (7), pp. 927–929. doi: 10.2144/000112812.

Cahu, J. and Sola, B. (2013). 'A Sensitive Method to Quantify Senescent Cancer Cells'. *Journal of Visualized Experiments*, (78). doi: 10.3791/50494.

Campisi, J. (1997). 'The biology of replicative senescence'. *European Journal of Cancer*, 33 (5), pp. 703–709. doi: 10.1016/S0959-8049(96)00058-5.

Campisi, J. (2013). 'Aging, Cellular Senescence, and Cancer'. *Annual Review of Physiology*, 75 (1), pp. 685–705. doi: 10.1146/annurev-physiol-030212-183653.

Cappell, S. D., Chung, M., Jaimovich, A., Spencer, S. L. and Meyer, T. (2016). 'Irreversible APC (Cdh1) Inactivation Underlies the Point of No Return for Cell-Cycle Entry'. *Cell*, 166 (1), pp. 167–180. doi: 10.1016/j.cell.2016.05.077.

Cappell, S. D., Mark, K. G., Garbett, D., Pack, L. R., Rape, M. and Meyer, T. (2018). 'EMI1 switches from being a substrate to an inhibitor of APC/C^{CDH1} to start the cell cycle'. *Nature*, 558 (7709), pp. 313–317. doi: 10.1038/s41586-018-0199-7.

Carrick Therapeutics. (2021). *Carrick Therapeutics Receives FDA Fast Track Designations for Two Samuraciclib Combinations for the Treatment of HR+, HER2lJ Advanced Breast Cancer and Locally Advanced or Metastatic Triple Negative Breast Cancer*. Available at: https://www.carricktherapeutics.com/news-media/press-releases/detail/10/carrick-therapeutics-receives-fda-fast-track-designations (Accessed: 19 April 2024).

Chapman, R. D., Heidemann, M., Hintermair, C. and Eick, D. (2008). 'Molecular evolution of the RNA polymerase II CTD'. *Trends in Genetics*, 24 (6), pp. 289–296. doi: 10.1016/j.tig.2008.03.010.

Chauvin, C., Koka, V., Nouschi, A., Mieulet, V., Hoareau-Aveilla, C., Dreazen, A., Cagnard, N., Carpentier, W., Kiss, T., Meyuhas, O. and Pende, M. (2014). 'Ribosomal protein S6 kinase activity controls the ribosome biogenesis transcriptional program'. *Oncogene*, 33 (4), pp. 474–483. doi: 10.1038/onc.2012.606.

Chehab, N. H., Malikzay, A., Appel, M. and Halazonetis, T. D. (2000). 'Chk2/hCds1 functions as a DNA damage checkpoint in G1 by stabilizing p53'. *Genes & Development*, 14 (3), pp. 278–288. doi: 10.1101/gad.14.3.278.

Chen, X., Zhang, T., Su, W., Dou, Z., Zhao, D., Jin, X., Lei, H., Wang, J., Xie, X., Cheng, B., Li, Q., Zhang, H. and Di, C. (2022). 'Mutant p53 in cancer: from molecular mechanism to therapeutic modulation'. *Cell Death & Disease*, 13 (11), p. 974. doi: 10.1038/s41419-022-05408-1.

Chen, Z., Trotman, L. C., Shaffer, D., Lin, H.-K., Dotan, Z. A., Niki, M., Koutcher, J. A., Scher, H. I., Ludwig, T., Gerald, W., Cordon-Cardo, C. and Paolo Pandolfi, P. (2005). 'Crucial role of p53-dependent cellular senescence in suppression of Pten-deficient tumorigenesis'. *Nature*, 436 (7051), pp. 725–730. doi: 10.1038/nature03918.

Choi, Y. J. and Anders, L. (2014). 'Signaling through cyclin D-dependent kinases'. *Oncogene*, 33 (15), pp. 1890–1903. doi: 10.1038/onc.2013.137.

Cicenas, J., Kalyan, K., Sorokinas, A., Stankunas, E., Levy, J., Meskinyte, I., Stankevicius, V., Kaupinis, A. and Valius, M. (2015). 'Roscovitine in cancer and other diseases'. *Ann Transl Med.*, 3 (10).

Constantin, T. A., Varela-Carver, A., Greenland, K. K., de Almeida, G. S., Olden, E., Penfold, L., Ang, S., Ormrod, A., Leach, D. A., Lai, C.-F., Ainscow, E. K., Bahl, A. K., Carling, D., Fuchter, M. J., Ali, S. and Bevan, C. L. (2023). 'The CDK7 inhibitor CT7001 (Samuraciclib) targets proliferation pathways to inhibit advanced prostate cancer'. *British Journal of Cancer*, 128 (12), pp. 2326–2337. doi: 10.1038/s41416-023-02252-8.

Coombes, R. C., Howell, S., Lord, S. R., Kenny, L., Mansi, J., Mitri, Z., Palmieri, C., Chap, L. I., Richards, P., Gradishar, W., Sardesai, S., Melear, J., O'Shaughnessy, J.,

Ward, P., Chalasani, P., Arkenau, T., Baird, R. D., Jeselsohn, R., Ali, S., Clack, G., Bahl, A., McIntosh, S. and Krebs, M. G. (2023). 'Dose escalation and expansion cohorts in patients with advanced breast cancer in a Phase I study of the CDK7-inhibitor samuraciclib'. *Nature Communications*, 14 (1), p. 4444. doi: 10.1038/s41467-023-40061-y.

Coppé, J.-P., Desprez, P.-Y., Krtolica, A. and Campisi, J. (2010). 'The Senescence-Associated Secretory Phenotype: The Dark Side of Tumor Suppression'. *Annual Review of Pathology: Mechanisms of Disease*, 5 (1), pp. 99–118. doi: 10.1146/annurev-pathol-121808-102144.

Core, L. and Adelman, K. (2019). 'Promoter-proximal pausing of RNA polymerase II: a nexus of gene regulation'. *Genes & Development*, 33 (15–16), pp. 960–982. doi: 10.1101/gad.325142.119.

Crncec, A. and Hochegger, H. (2019). 'Triggering mitosis'. *FEBS Letters*, 593 (20), pp. 2868–2888. doi: 10.1002/1873-3468.13635.

Crozier, L., Foy, R., Adib, R., Kar, A., Holt, J. A., Pareri, A. U., Valverde, J. M., Rivera, R., Weston, W. A., Wilson, R., Regnault, C., Whitfield, P., Badonyi, M., Bennett, L. G., Vernon, E. G., Gamble, A., Marsh, J. A., Staples, C. J., Saurin, A. T., Barr, A. R. and Ly, T. (2023). 'CDK4/6 inhibitor-mediated cell overgrowth triggers osmotic and replication stress to promote senescence'. *Molecular Cell*, 83 (22), pp. 4062-4077.e5. doi: 10.1016/j.molcel.2023.10.016.

Crozier, L., Foy, R., Mouery, B. L., Whitaker, R. H., Corno, A., Spanos, C., Ly, T., Gowen Cook, J. and Saurin, A. T. (2022). 'CDK4/6 inhibitors induce replication stress to cause long-term cell cycle withdrawal'. *The EMBO Journal*, 41 (6). doi: 10.15252/embj.2021108599.

Davies, D. M., van den Handel, K., Bharadwaj, S. and Lengefeld, J. (2022). 'Cellular enlargement - A new hallmark of aging?' *Frontiers in Cell and Developmental Biology*, 10. doi: 10.3389/fcell.2022.1036602.

Debacq-Chainiaux, F., Erusalimsky, J. D., Campisi, J. and Toussaint, O. (2009). 'Protocols to detect senescence-associated beta-galactosidase (SA-βgal) activity, a biomarker of senescent cells in culture and in vivo'. *Nature Protocols*, 4 (12), pp. 1798–1806. doi: 10.1038/nprot.2009.191.

Delarue, M., Brittingham, G. P., Pfeffer, S., Surovtsev, I. V., Pinglay, S., Kennedy, K. J., Schaffer, M., Gutierrez, J. I., Sang, D., Poterewicz, G., Chung, J. K., Plitzko, J. M., Groves, J. T., Jacobs-Wagner, C., Engel, B. D. and Holt, L. J. (2018). 'mTORC1 Controls Phase Separation and the Biophysical Properties of the Cytoplasm by Tuning Crowding'. *Cell*, 174 (2), pp. 338-349.e20. doi: 10.1016/j.cell.2018.05.042.

Demidenko, Z. N. and Blagosklonny, M. V. (2008). 'Growth stimulation leads to cellular senescence when the cell cycle is blocked'. *Cell Cycle*. Taylor & Francis, 7 (21), pp. 3355–3361. doi: 10.4161/cc.7.21.6919.

Demidenko, Z. N., Zubova, S. G., Bukreeva, E. I., Pospelov, V. A., Pospelova, T. V. and Blagosklonny, M. V. (2009). 'Rapamycin decelerates cellular senescence'. *Cell Cycle*, 8 (12), pp. 1888–1895. doi: 10.4161/cc.8.12.8606.

Dephoure, N., Zhou, C., Villén, J., Beausoleil, S. A., Bakalarski, C. E., Elledge, S. J. and Gygi, S. P. (2008). 'A quantitative atlas of mitotic phosphorylation'. *Proceedings of the National Academy of Sciences*, 105 (31), pp. 10762–10767. doi: 10.1073/pnas.0805139105.

Deshpande, A., Sicinski, P. and Hinds, P. W. (2005). 'Cyclins and cdks in development and cancer: a perspective'. *Oncogene*, 24 (17), pp. 2909–2915. doi: 10.1038/sj.onc.1208618.

Diamond, J. R., Boni, V., Lim, E., Nowakowski, G., Cordoba, R., Morillo, D., Valencia, R., Genvresse, I., Merz, C., Boix, O., Frigault, M. M., Greer, J. M., Hamdy, A. M., Huang, X., Izumi, R., Wong, H. and Moreno, V. (2022). 'First-in-Human Dose-Escalation Study of Cyclin-Dependent Kinase 9 Inhibitor VIP152 in Patients with Advanced Malignancies Shows Early Signs of Clinical Efficacy'. *Clinical Cancer Research*, 28 (7), pp. 1285–1293. doi: 10.1158/1078-0432.CCR-21-3617.

Dietrich, C., Trub, A., Ahn, A., Taylor, M., Ambani, K., Chan, K. T., Lu, K.-H., Mahendra, C. A., Blyth, C., Coulson, R., Ramm, S., Watt, A. C., Matsa, S. K., Bisi, J., Strum, J., Roberts, P. and Goel, S. (2024). 'INX-315, a Selective CDK2 Inhibitor, Induces Cell Cycle Arrest and Senescence in Solid Tumors'. *Cancer Discovery*, 14 (3), pp. 446–467. doi: 10.1158/2159-8290.CD-23-0954.

Dimri, G. P., Lee, X., Basile, G., Acosta, M., Scott, G., Roskelley, C., Medrano, E. E., Linskens, M., Rubelj, I. and Pereira-Smith, O. (1995). 'A biomarker that identifies senescent human cells in culture and in aging skin in vivo.' *Proceedings of the National Academy of Sciences*, 92 (20), pp. 9363–9367. doi: 10.1073/pnas.92.20.9363.

Ebmeier, C. C., Erickson, B., Allen, B. L., Allen, M. A., Kim, H., Fong, N., Jacobsen, J. R., Liang, K., Shilatifard, A., Dowell, R. D., Old, W. M., Bentley, D. L. and Taatjes, D. J. (2017). 'Human TFIIH Kinase CDK7 Regulates Transcription-Associated Chromatin Modifications'. *Cell Reports*, 20 (5), pp. 1173–1186. doi: 10.1016/j.celrep.2017.07.021.

Eden, E., Lipson, D., Yogev, S. and Yakhini, Z. (2007). 'Discovering Motifs in Ranked Lists of DNA Sequences'. *PLoS Computational Biology*, 3 (3), p. e39. doi: 10.1371/journal.pcbi.0030039.

Eden, E., Navon, R., Steinfeld, I., Lipson, D. and Yakhini, Z. (2009). 'GOrilla: a tool for discovery and visualization of enriched GO terms in ranked gene lists'. *BMC Bioinformatics*, 10 (1), p. 48. doi: 10.1186/1471-2105-10-48.

Elwakeel, A., Sari, A. N., Dhanjal, J. K., Meidinna, H. N., Sundar, D., Kaul, S. C. and Wadhwa, R. (2021). 'Mutant $p53^{L194F}$ Harboring Luminal-A Breast Cancer Cells Are Refractory to Apoptosis and Cell Cycle Arrest in Response to Mortaparib^{Plus}, a Multimodal Small Molecule Inhibitor'. *Cancers*, 13 (12), p. 3043. doi: 10.3390/cancers13123043.

Evans, T., Rosenthal, E. T., Youngblom, J., Distel, D. and Hunt, T. (1983). 'Cyclin: A protein specified by maternal mRNA in sea urchin eggs that is destroyed at each cleavage division'. *Cell*, 33 (2), pp. 389–396. doi: 10.1016/0092-8674(83)90420-8.

Ewald, J. A., Desotelle, J. A., Wilding, G. and Jarrard, D. F. (2010). 'Therapy-Induced Senescence in Cancer'. *JNCI: Journal of the National Cancer Institute*, 102 (20), pp. 1536–1546. doi: 10.1093/jnci/djq364.

Ewald, J. A., Peters, N., Desotelle, J. A., Hoffmann, F. M. and Jarrard, D. F. (2009). 'A High-Throughput Method to Identify Novel Senescence-Inducing Compounds'. *SLAS Discovery*, 14 (7), pp. 853–858. doi: 10.1177/1087057109340314.

Faheem, M. M., Seligson, N. D., Ahmad, S. M., Rasool, R. U., Gandhi, S. G., Bhagat, M. and Goswami, A. (2020). 'Convergence of therapy-induced senescence (TIS) and EMT in multistep carcinogenesis: current opinions and emerging perspectives'. *Cell Death Discovery*, 6 (1), p. 51. doi: 10.1038/s41420-020-0286-z.

Fassl, A., Geng, Y. and Sicinski, P. (2022). 'CDK4 and CDK6 kinases: From basic science to cancer therapy'. *Science*, 375 (6577). doi: 10.1126/science.abc1495.

Fisher, R. P. (2019). 'Cdk7: a kinase at the core of transcription and in the crosshairs of cancer drug discovery'. *Transcription*, 10 (2), pp. 47–56. doi: 10.1080/21541264.2018.1553483.

Foy, R., Crozier, L., Pareri, A. U., Valverde, J. M., Park, B. H., Ly, T. and Saurin, A. T. (2023). 'Oncogenic signals prime cancer cells for toxic cell overgrowth during a G1 cell cycle arrest'. *Molecular Cell*, 83 (22), pp. 4047-4061.e6. doi: 10.1016/j.molcel.2023.10.020.

Foy, R., Lew, K. X. and Saurin, A. T. (2024). 'The search for CDK4/6 inhibitor biomarkers has been hampered by inappropriate proliferation assays'. *npj Breast Cancer*, 10 (1), p. 19. doi: 10.1038/s41523-024-00624-8.

Freeman-Cook, K. D., Hoffman, R. L., Behenna, D. C., Boras, B., Carelli, J., Diehl, W., Ferre, R. A., He, Y.-A., Hui, A., Huang, B., Huser, N., Jones, R., Kephart, S. E., Lapek, J., McTigue, M., Miller, N., Murray, B. W., Nagata, A., Nguyen, L., Niessen, S., Ninkovic, S., O'Doherty, I., Ornelas, M. A., Solowiej, J., Sutton, S. C., Tran, K., Tseng, E., Visswanathan, R., Xu, M., Zehnder, L., Zhang, Q., Zhang, C. and Dann, S. (2021). 'Discovery of PF-06873600, a CDK2/4/6 Inhibitor for the Treatment of Cancer'. *Journal of Medicinal Chemistry*, 64 (13), pp. 9056–9077. doi: 10.1021/acs.jmedchem.1c00159.

Freeman-Cook, K., Hoffman, R. L., Miller, N., Almaden, J., Chionis, J., Zhang, Q., Eisele, K., Liu, C., Zhang, C., Huser, N., Nguyen, L., Costa-Jones, C., Niessen, S., Carelli, J., Lapek, J., Weinrich, S. L., Wei, P., McMillan, E., Wilson, E., Wang, T. S., McTigue, M., Ferre, R. A., He, Y.-A., Ninkovic, S., Behenna, D., Tran, K. T., Sutton, S., Nagata, A., Ornelas, M. A., Kephart, S. E., Zehnder, L. R., Murray, B., Xu, M., Solowiej, J. E., Visswanathan, R., Boras, B., Looper, D., Lee, N., Bienkowska, J. R., Zhu, Z., Kan, Z., Ding, Y., Mu, X. J., Oderup, C., Salek-Ardakani, S., White, M. A., VanArsdale, T. and Dann, S. G. (2021). 'Expanding control of the tumor cell cycle

with a CDK2/4/6 inhibitor'. *Cancer Cell*, 39 (10), pp. 1404-1421.e11. doi: 10.1016/j.ccell.2021.08.009.

Freund, A., Laberge, R.-M., Demaria, M. and Campisi, J. (2012). 'Lamin B1 loss is a senescence-associated biomarker'. *Molecular Biology of the Cell*, 23 (11), pp. 2066–2075. doi: 10.1091/mbc.e11-10-0884.

Fry, D. W., Harvey, P. J., Keller, P. R., Elliott, W. L., Meade, M., Trachet, E., Albassam, M., Zheng, X., Leopold, W. R., Pryer, N. K. and Toogood, P. L. (2004). 'Specific inhibition of cyclin-dependent kinase 4/6 by PD 0332991 and associated antitumor activity in human tumor xenografts'. *Molecular Cancer Therapeutics*, 3 (11), pp. 1427–1438. doi: 10.1158/1535-7163.1427.3.11.

Fukami, J., Anno, K., Ueda, K., Takahashi, T. and Ide, T. (1995). 'Enhanced expression of cyclin D1 in senescent human fibroblasts'. *Mechanisms of Ageing and Development*, 81 (2–3), pp. 139–157. doi: 10.1016/0047-6374(95)93703-6.

Gasek, N. S., Kuchel, G. A., Kirkland, J. L. and Xu, M. (2021). 'Strategies for targeting senescent cells in human disease'. *Nature Aging*, 1 (10), pp. 870–879. doi: 10.1038/s43587-021-00121-8.

Ginzberg, M. B., Kafri, R. and Kirschner, M. (2015). 'On being the right (cell) size'. *Science*, 348 (6236). doi: 10.1126/science.1245075.

Gorgoulis, V., Adams, P. D., Alimonti, A., Bennett, D. C., Bischof, O., Bishop, C., Campisi, J., Collado, M., Evangelou, K., Ferbeyre, G., Gil, J., Hara, E., Krizhanovsky, V., Jurk, D., Maier, A. B., Narita, M., Niedernhofer, L., Passos, J. F., Robbins, P. D., Schmitt, C. A., Sedivy, J., Vougas, K., von Zglinicki, T., Zhou, D., Serrano, M. and Demaria, M. (2019). 'Cellular Senescence: Defining a Path Forward'. *Cell*, 179 (4), pp. 813–827. doi: 10.1016/j.cell.2019.10.005.

Guarducci, C., Bonechi, M., Benelli, M., Biagioni, C., Boccalini, G., Romagnoli, D., Verardo, R., Schiff, R., Osborne, C. K., De Angelis, C., Di Leo, A., Malorni, L. and Migliaccio, I. (2018). 'Cyclin E1 and Rb modulation as common events at time of resistance to palbociclib in hormone receptor-positive breast cancer'. *npj Breast Cancer*, 4 (1), p. 38. doi: 10.1038/s41523-018-0092-4.

Guarducci, C., Nardone, A., Russo, D., Nagy, Z., Heraud, C., Grinshpun, A., Zhang, Q., Freelander, A., Leventhal, M. J., Feit, A., Cohen Feit, G., Feiglin, A., Liu, W., Hermida-Prado, F., Kesten, N., Ma, W., De Angelis, C., Morlando, A., O'Donnell, M., Naumenko, S., Huang, S., Nguyen, Q.-D., Huang, Y., Malorni, L., Bergholz, J. S., Zhao, J. J., Fraenkel, E., Lim, E., Schiff, R., Shapiro, G. I. and Jeselsohn, R. (2024). 'Selective CDK7 Inhibition Suppresses Cell Cycle Progression and MYC Signaling While Enhancing Apoptosis in Therapy-resistant Estrogen Receptor–positive Breast Cancer'. *Clinical Cancer Research*, pp. OF1–OF17. doi: 10.1158/1078-0432.CCR-23-2975.

Gustin, J. P., Karakas, B., Weiss, M. B., Abukhdeir, A. M., Lauring, J., Garay, J. P., Cosgrove, D., Tamaki, A., Konishi, H., Konishi, Y., Mohseni, M., Wang, G., Rosen, D. M., Denmeade, S. R., Higgins, M. J., Vitolo, M. I., Bachman, K. E. and Park, B. H. (2009). 'Knockin of mutant PIK3CA activates multiple oncogenic pathways'.

Proceedings of the National Academy of Sciences, 106 (8), pp. 2835–2840. doi: 10.1073/pnas.0813351106.

Guzmán, C., Bagga, M., Kaur, A., Westermarck, J. and Abankwa, D. (2014). 'ColonyArea: An ImageJ Plugin to Automatically Quantify Colony Formation in Clonogenic Assays'. *PLoS ONE*, 9 (3), p. e92444. doi: 10.1371/journal.pone.0092444.

Hanahan, D. and Weinberg, R. A. (2011). 'Hallmarks of Cancer: The Next Generation'. *Cell*, 144 (5), pp. 646–674. doi: 10.1016/j.cell.2011.02.013.

Hartwell, L. H., Culotti, J., Pringle, J. R. and Reid, B. J. (1974). 'Genetic Control of the Cell Division Cycle in Yeast'. *Science*, 183 (4120), pp. 46–51. doi: 10.1126/science.183.4120.46.

Hartwell, L. H., Culotti, J. and Reid, B. (1970). 'Genetic Control of the Cell-Division Cycle in Yeast, I. Detection of Mutants'. *Proceedings of the National Academy of Sciences*, 66 (2), pp. 352–359. doi: 10.1073/pnas.66.2.352.

Hartwell, L. H., Mortimer, R. K., Culotti, J. and Culotti, M. (1973). 'Genetic Control of the Cell Division Cycle in Yeast: V. Genetic Analysis of cdc Mutants'. *Genetics*, 74 (2), pp. 267–286. doi: 10.1093/genetics/74.2.267.

Hayflick, L. and Moorhead, P. S. (1961). 'The serial cultivation of human diploid cell strains'. *Experimental Cell Research*, 25 (3), pp. 585–621. doi: 10.1016/0014-4827(61)90192-6.

Hégarat, N., Crncec, A., Suarez Peredo Rodriguez, M. F., Echegaray Iturra, F., Gu, Y., Busby, O., Lang, P. F., Barr, A. R., Bakal, C., Kanemaki, M. T., Lamond, A. I., Novak, B., Ly, T. and Hochegger, H. (2020). 'Cyclin A triggers Mitosis either via the Greatwall kinase pathway or Cyclin B'. *The EMBO Journal*, 39 (11). doi: 10.15252/embj.2020104419.

Henley, S. A. and Dick, F. A. (2012). 'The retinoblastoma family of proteins and their regulatory functions in the mammalian cell division cycle'. *Cell Division*, 7 (1), p. 10. doi: 10.1186/1747-1028-7-10.

Hernandez-Segura, A., Nehme, J. and Demaria, M. (2018). 'Hallmarks of Cellular Senescence'. *Trends in Cell Biology*, 28 (6), pp. 436–453. doi: 10.1016/j.tcb.2018.02.001.

Herranz, N. and Gil, J. (2018). 'Mechanisms and functions of cellular senescence'. *Journal of Clinical Investigation*, 128 (4), pp. 1238–1246. doi: 10.1172/JCI95148.

Herrera-Abreu, M. T., Asghar, U. S., Elliot, R., Pearson, A., Nannini, M. A., Young, A., Sampath, D., Dowsett, M., Martin, L. A. and Turner, N. (2015). 'PI3 kinase/mTOR inhibition increases sensitivity of ER positive breast cancers to CDK4/6 inhibition by blocking cell cycle re-entry driven by cyclinD1 and inducing apoptosis'. *Annals of Oncology*, 26, p. iii29. doi: 10.1093/annonc/mdv120.01.

Herrera-Abreu, M. T., Palafox, M., Asghar, U., Rivas, M. A., Cutts, R. J., Garcia-Murillas, I., Pearson, A., Guzman, M., Rodriguez, O., Grueso, J., Bellet, M., Cortés,

J., Elliott, R., Pancholi, S., Lord, C. J., Baselga, J., Dowsett, M., Martin, L.-A., Turner, N. C. and Serra, V. (2016). 'Early Adaptation and Acquired Resistance to CDK4/6 Inhibition in Estrogen Receptor–Positive Breast Cancer'. *Cancer Research*, 76 (8), pp. 2301–2313. doi: 10.1158/0008-5472.CAN-15-0728.

Hirao, A., Kong, Y.-Y., Matsuoka, S., Wakeham, A., Ruland, J., Yoshida, H., Liu, D., Elledge, S. J. and Mak, T. W. (2000). 'DNA Damage-Induced Activation of p53 by the Checkpoint Kinase Chk2'. *Science*, 287 (5459), pp. 1824–1827. doi: 10.1126/science.287.5459.1824.

Hollestelle, A., Nagel, J. H. A., Smid, M., Lam, S., Elstrodt, F., Wasielewski, M., Ng, S. S., French, P. J., Peeters, J. K., Rozendaal, M. J., Riaz, M., Koopman, D. G., ten Hagen, T. L. M., de Leeuw, B. H. C. G. M., Zwarthoff, E. C., Teunisse, A., van der Spek, P. J., Klijn, J. G. M., Dinjens, W. N. M., Ethier, S. P., Clevers, H., Jochemsen, A. G., den Bakker, M. A., Foekens, J. A., Martens, J. W. M. and Schutte, M. (2010). 'Distinct gene mutation profiles among luminal-type and basal-type breast cancer cell lines'. *Breast Cancer Research and Treatment*, 121 (1), pp. 53–64. doi: 10.1007/s10549-009-0460-8.

Hu, S., Marineau, J. J., Rajagopal, N., Hamman, K. B., Choi, Y. J., Schmidt, D. R., Ke, N., Johannessen, L., Bradley, M. J., Orlando, D. A., Alnemy, S. R., Ren, Y., Ciblat, S., Winter, D. K., Kabro, A., Sprott, K. T., Hodgson, J. G., Fritz, C. C., Carulli, J. P., di Tomaso, E. and Olson, E. R. (2019). 'Discovery and Characterization of SY-1365, a Selective, Covalent Inhibitor of CDK7'. *Cancer Research*, 79 (13), pp. 3479–3491. doi: 10.1158/0008-5472.CAN-19-0119.

Huang, R. and Zhou, P.-K. (2021). 'DNA damage repair: historical perspectives, mechanistic pathways and clinical translation for targeted cancer therapy'. *Signal Transduction and Targeted Therapy*, 6 (1), p. 254. doi: 10.1038/s41392-021-00648-7.

Huang, W., Hickson, L. J., Eirin, A., Kirkland, J. L. and Lerman, L. O. (2022). 'Cellular senescence: the good, the bad and the unknown'. *Nature Reviews Nephrology*, 18 (10), pp. 611–627. doi: 10.1038/s41581-022-00601-z.

Jiang, L., Huang, R., Wu, Y., Diao, P., Zhang, W., Li, J., Li, Z., Wang, Y., Cheng, J. and Yang, J. (2019). 'Overexpression of CDK7 is associated with unfavourable prognosis in oral squamous cell carcinoma'. *Pathology*, 51 (1), pp. 74–80. doi: 10.1016/j.pathol.2018.10.004.

Johmura, Y., Shimada, M., Misaki, T., Naiki-Ito, A., Miyoshi, H., Motoyama, N., Ohtani, N., Hara, E., Nakamura, M., Morita, A., Takahashi, S. and Nakanishi, M. (2014). 'Necessary and Sufficient Role for a Mitosis Skip in Senescence Induction'. *Molecular Cell*, 55 (1), pp. 73–84. doi: 10.1016/j.molcel.2014.05.003.

Kim, J. and Guan, K.-L. (2019). 'mTOR as a central hub of nutrient signalling and cell growth'. *Nature Cell Biology*, 21 (1), pp. 63–71. doi: 10.1038/s41556-018-0205-1.

Kinner, A., Wu, W., Staudt, C. and Iliakis, G. (2008). 'γ-H2AX in recognition and signaling of DNA double-strand breaks in the context of chromatin'. *Nucleic Acids Research*, 36 (17), pp. 5678–5694. doi: 10.1093/nar/gkn550.

Klein, M. E., Kovatcheva, M., Davis, L. E., Tap, W. D. and Koff, A. (2018). 'CDK4/6 Inhibitors: The Mechanism of Action May Not Be as Simple as Once Thought'. *Cancer Cell*, 34 (1), pp. 9–20. doi: 10.1016/j.ccell.2018.03.023.

Klingebiel, M., Dinekov, M. and Köhler, C. (2017). 'Analysis of ribosomal protein S6 baseline phosphorylation and effect of tau pathology in the murine brain and human hippocampus'. *Brain Research*, 1659, pp. 121–135. doi: 10.1016/j.brainres.2017.01.016.

Kohli, J., Wang, B., Brandenburg, S. M., Basisty, N., Evangelou, K., Varela-Eirin, M., Campisi, J., Schilling, B., Gorgoulis, V. and Demaria, M. (2021). 'Algorithmic assessment of cellular senescence in experimental and clinical specimens'. *Nature Protocols*, 16 (5), pp. 2471–2498. doi: 10.1038/s41596-021-00505-5.

Kreis, Louwen and Yuan. (2019). 'The Multifaceted p21 (Cip1/Waf1/CDKN1A) in Cell Differentiation, Migration and Cancer Therapy'. *Cancers*, 11 (9), p. 1220. doi: 10.3390/cancers11091220.

Kumari, R. and Jat, P. (2021). 'Mechanisms of Cellular Senescence: Cell Cycle Arrest and Senescence Associated Secretory Phenotype'. *Frontiers in Cell and Developmental Biology*, 9. doi: 10.3389/fcell.2021.645593.

Kung, C.-P. and Weber, J. D. (2022). 'It's Getting Complicated—A Fresh Look at p53-MDM2-ARF Triangle in Tumorigenesis and Cancer Therapy'. *Frontiers in Cell and Developmental Biology*, 10. doi: 10.3389/fcell.2022.818744.

Kurz, D. J., Decary, S., Hong, Y. and Erusalimsky, J. D. (2000). 'Senescence-associated β-galactosidase reflects an increase in lysosomal mass during replicative ageing of human endothelial cells'. *Journal of Cell Science*, 113 (20), pp. 3613–3622. doi: 10.1242/jcs.113.20.3613.

Kwiatkowski, N., Zhang, T., Rahl, P. B., Abraham, B. J., Reddy, J., Ficarro, S. B., Dastur, A., Amzallag, A., Ramaswamy, S., Tesar, B., Jenkins, C. E., Hannett, N. M., McMillin, D., Sanda, T., Sim, T., Kim, N. D., Look, T., Mitsiades, C. S., Weng, A. P., Brown, J. R., Benes, C. H., Marto, J. A., Young, R. A. and Gray, N. S. (2014). 'Targeting transcription regulation in cancer with a covalent CDK7 inhibitor'. *Nature*, 511 (7511), pp. 616–620. doi: 10.1038/nature13393.

Langmead, B. and Salzberg, S. L. (2012). 'Fast gapped-read alignment with Bowtie 2'. *Nature Methods*, 9 (4), pp. 357–359. doi: 10.1038/nmeth.1923.

Lanz, M. C., Fuentes Valenzuela, L., Elias, J. E. and Skotheim, J. M. (2023). 'Cell Size Contributes to Single-Cell Proteome Variation'. *Journal of Proteome Research*, 22 (12), pp. 3773–3779. doi: 10.1021/acs.jproteome.3c00441.

Lanz, M. C., Zatulovskiy, E., Swaffer, M. P., Zhang, L., Ilerten, I., Zhang, S., You, D. S., Marinov, G., McAlpine, P., Elias, J. E. and Skotheim, J. M. (2022). 'Increasing cell size remodels the proteome and promotes senescence'. *Molecular Cell*, 82 (17), pp. 3255-3269.e8. doi: 10.1016/j.molcel.2022.07.017.

Laplante, M. and Sabatini, D. M. (2012). 'mTOR signaling in growth control and disease'. *Cell*, 149 (2), pp. 274–293. doi: 10.1016/j.cell.2012.03.017.

Larochelle, S., Batliner, J., Gamble, M. J., Barboza, N. M., Kraybill, B. C., Blethrow, J. D., Shokat, K. M. and Fisher, R. P. (2006). 'Dichotomous but stringent substrate selection by the dual-function Cdk7 complex revealed by chemical genetics'. *Nature Structural & Molecular Biology*, 13 (1), pp. 55–62. doi: 10.1038/nsmb1028.

Larochelle, S., Merrick, K. A., Terret, M.-E., Wohlbold, L., Barboza, N. M., Zhang, C., Shokat, K. M., Jallepalli, P. V. and Fisher, R. P. (2007). 'Requirements for Cdk7 in the Assembly of Cdk1/Cyclin B and Activation of Cdk2 Revealed by Chemical Genetics in Human Cells'. *Molecular Cell*, 25 (6), pp. 839–850. doi: 10.1016/j.molcel.2007.02.003.

Lengefeld, J., Cheng, C.-W., Maretich, P., Blair, M., Hagen, H., McReynolds, M. R., Sullivan, E., Majors, K., Roberts, C., Kang, J. H., Steiner, J. D., Miettinen, T. P., Manalis, S. R., Antebi, A., Morrison, S. J., Lees, J. A., Boyer, L. A., Yilmaz, Ö. H. and Amon, A. (2021). 'Cell size is a determinant of stem cell potential during aging'. *Science Advances*, 7 (46). doi: 10.1126/sciadv.abk0271.

Leontieva, O. V. and Blagosklonny, M. V. (2010). 'DNA damaging agents and p53 do not cause senescence in quiescent cells, while consecutive re-activation of mTOR is associated with conversion to senescence'. *Aging*, 2 (12), pp. 924–935. doi: 10.18632/aging.100265.

Leontieva, O. V. and Blagosklonny, M. V. (2013). 'CDK4/6-inhibiting drug substitutes for p21 and p16 in senescence: Duration of cell cycle arrest and MTOR activity determine geroconversion'. *Cell Cycle*, 12 (18), pp. 3063–3069. doi: 10.4161/cc.26130.

Leontieva, O. V, Demidenko, Z. N. and Blagosklonny, M. V. (2013). 'MEK drives cyclin D1 hyperelevation during geroconversion'. *Cell Death & Differentiation*, 20 (9), pp. 1241–1249. doi: 10.1038/cdd.2013.86.

Leontieva, O. V., Demidenko, Z. N. and Blagosklonny, M. V. (2014). 'Contact inhibition and high cell density deactivate the mammalian target of rapamycin pathway, thus suppressing the senescence program'. *Proceedings of the National Academy of Sciences*, 111 (24), pp. 8832–8837. doi: 10.1073/pnas.1405723111.

Leroy, B., Girard, L., Hollestelle, A., Minna, J. D., Gazdar, A. F. and Soussi, T. (2014). 'Analysis of TP53 Mutation Status in Human Cancer Cell Lines: A Reassessment'. *Human Mutation*, 35 (6), pp. 756–765. doi: 10.1002/humu.22556.

Libouban, M. A. A., de Roos, J. A. D. M., Uitdehaag, J. C. M., Willemsen-Seegers, N., Mainardi, S., Dylus, J., de Man, J., Tops, B., Meijerink, J. P. P., Storchová, Z., Buijsman, R. C., Medema, R. H. and Zaman, G. J. R. (2017). 'Stable aneuploid tumors cells are more sensitive to TTK inhibition than chromosomally unstable cell lines'. *Oncotarget*, 8 (24), pp. 38309–38325. doi: 10.18632/oncotarget.16213.

Liu, G. Y. and Sabatini, D. M. (2020). 'mTOR at the nexus of nutrition, growth, ageing and disease'. *Nature Reviews Molecular Cell Biology*, 21 (4), pp. 183–203. doi: 10.1038/s41580-019-0199-y.

Liu, S., Opiyo, S. O., Manthey, K., Glanzer, J. G., Ashley, A. K., Amerin, C., Troksa, K., Shrivastav, M., Nickoloff, J. A. and Oakley, G. G. (2012). 'Distinct roles for DNA-PK, ATM and ATR in RPA phosphorylation and checkpoint activation in response to replication stress'. *Nucleic Acids Research*, 40 (21), pp. 10780–10794. doi: 10.1093/nar/gks849.

Liu, S., Tang, Y., Yan, M. and Jiang, W. (2018). 'PIK3CA mutation sensitizes breast cancer cells to synergistic therapy of PI3K inhibition and AMPK activation'. *Investigational New Drugs*, 36 (5), pp. 763–772. doi: 10.1007/s10637-018-0563-3.

Liu, X., Ding, J. and Meng, L. (2018). 'Oncogene-induced senescence: a double edged sword in cancer'. *Acta Pharmacologica Sinica*, 39 (10), pp. 1553–1558. doi: 10.1038/aps.2017.198.

Lloyd, A. C. (2013). 'The Regulation of Cell Size'. *Cell*, 154 (6), pp. 1194–1205. doi: https://doi.org/10.1016/j.cell.2013.08.053.

Lücking, U., Kosemund, D., Böhnke, N., Lienau, P., Siemeister, G., Denner, K., Bohlmann, R., Briem, H., Terebesi, I., Bömer, U., Schäfer, M., Ince, S., Mumberg, D., Scholz, A., Izumi, R., Hwang, S. and von Nussbaum, F. (2021). 'Changing for the Better: Discovery of the Highly Potent and Selective CDK9 Inhibitor VIP152 Suitable for Once Weekly Intravenous Dosing for the Treatment of Cancer'. *Journal of Medicinal Chemistry*, 64 (15), pp. 11651–11674. doi: 10.1021/acs.jmedchem.1c01000.

Lundberg, A. S. and Weinberg, R. A. (1998). 'Functional Inactivation of the Retinoblastoma Protein Requires Sequential Modification by at Least Two Distinct Cyclin-cdk Complexes'. *Molecular and Cellular Biology*, 18 (2), pp. 753–761. doi: 10.1128/MCB.18.2.753.

Malumbres, M. and Barbacid, M. (2009). 'Cell cycle, CDKs and cancer: a changing paradigm'. *Nature Reviews Cancer*, 9 (3), pp. 153–166. doi: 10.1038/nrc2602.

Manohar, S., Estrada, M. E., Uliana, F., Vuina, K., Alvarez, P. M., de Bruin, R. A. M. and Neurohr, G. E. (2023). 'Genome homeostasis defects drive enlarged cells into senescence'. *Molecular Cell*, 83 (22), pp. 4032-4046.e6. doi: 10.1016/j.molcel.2023.10.018.

Manohar, S. and Neurohr, G. E. (2023). 'Too big not to fail: emerging evidence for size-induced senescence'. *The FEBS Journal*. doi: 10.1111/febs.16983.

Maskey, R. S., Wang, F., Lehman, E., Wang, Y., Emmanuel, N., Zhong, W., Jin, G., Abraham, R. T., Arndt, Kim. T., Myers, J. S. and Mazurek, A. (2021). 'Sustained mTORC1 activity during palbociclib-induced growth arrest triggers senescence in ER+ breast cancer cells'. *Cell Cycle*, 20 (1), pp. 65–80.

Matthews, H. K., Bertoli, C. and de Bruin, R. A. M. (2022). 'Cell cycle control in cancer'. *Nature Reviews Molecular Cell Biology*, 23 (1), pp. 74–88. doi: 10.1038/s41580-021-00404-3.

Merrick, K. A., Larochelle, S., Zhang, C., Allen, J. J., Shokat, K. M. and Fisher, R. P. (2008). 'Distinct Activation Pathways Confer Cyclin-Binding Specificity on Cdk1 and Cdk2 in Human Cells'. *Molecular Cell*, 32 (5), pp. 662–672. doi: 10.1016/j.molcel.2008.10.022.

Di Micco, R., Fumagalli, M., Cicalese, A., Piccinin, S., Gasparini, P., Luise, C., Schurra, C., Garre', M., Giovanni Nuciforo, P., Bensimon, A., Maestro, R., Giuseppe Pelicci, P. and d'Adda di Fagagna, F. (2006). 'Oncogene-induced senescence is a DNA damage response triggered by DNA hyper-replication'. *Nature*, 444 (7119), pp. 638–642. doi: 10.1038/nature05327.

Mitsui, Y. and Schneider, E. L. (1976). 'Increased nuclear sizes in senescent human diploid fibroblast cultures'. *Experimental Cell Research*, 100 (1), pp. 147–152. doi: 10.1016/0014-4827(76)90336-0.

Mittnacht, S., Lees, J. A., Desai, D., Harlow, E., Morgan, D. O. and Weinberg, R. A. (1994). 'Distinct sub-populations of the retinoblastoma protein show a distinct pattern of phosphorylation.' *The EMBO Journal*, 13 (1), pp. 118–127. doi: 10.1002/j.1460-2075.1994.tb06241.x.

Montecucco, A., Zanetta, F. and Biamonti, G. (2015). 'Molecular mechanisms of etoposide'. *EXCLI J.*, 14, pp. 95–108.

Morrison, L., Loibl, S. and Turner, N. C. (2024). 'The CDK4/6 inhibitor revolution — a game-changing era for breast cancer treatment'. *Nature Reviews Clinical Oncology*, 21 (2), pp. 89–105. doi: 10.1038/s41571-023-00840-4.

Musacchio, A. and Salmon, E. D. (2007). 'The spindle-assembly checkpoint in space and time'. *Nature Reviews Molecular Cell Biology*, 8 (5), pp. 379–393. doi: 10.1038/nrm2163.

Narasimha, A. M., Kaulich, M., Shapiro, G. S., Choi, Y. J., Sicinski, P. and Dowdy, S. F. (2014). 'Cyclin D activates the Rb tumor suppressor by mono-phosphorylation'. *eLife*, 3. doi: 10.7554/eLife.02872.

Narita, Masashi, Nuñez, S., Heard, E., Narita, Masako, Lin, A. W., Hearn, S. A., Spector, D. L., Hannon, G. J. and Lowe, S. W. (2003). 'Rb-Mediated Heterochromatin Formation and Silencing of E2F Target Genes during Cellular Senescence'. *Cell*, 113 (6), pp. 703–716. doi: 10.1016/S0092-8674(03)00401-X.

Neurohr, G. E., Terry, R. L., Lengefeld, J., Bonney, M., Brittingham, G. P., Moretto, F., Miettinen, T. P., Vaites, L. P., Soares, L. M., Paulo, J. A., Harper, J. W., Buratowski, S., Manalis, S., van Werven, F. J., Holt, L. J. and Amon, A. (2019). 'Excessive Cell Growth Causes Cytoplasm Dilution And Contributes to Senescence'. *Cell*. 2019/02/07. Cell Press, 176 (5), pp. 1083-1097.e18. doi: 10.1016/j.cell.2019.01.018.

Nilson, K. A., Guo, J., Turek, M. E., Brogie, J. E., Delaney, E., Luse, D. S. and Price, D. H. (2015). 'THZ1 Reveals Roles for Cdk7 in Co-transcriptional Capping and Pausing'. *Molecular Cell*, 59 (4), pp. 576–587. doi: 10.1016/j.molcel.2015.06.032.

Nurse, P. and Bissett, Y. (1981). ‘Gene required in G1 for commitment to cell cycle and in G2 for control of mitosis in fission yeast’. *Nature*, 292 (5823), pp. 558–560. doi: 10.1038/292558a0.

Nurse, P. and Thuriaux, P. (1980). ‘Regulatory genes controlling mitosis in the fission yeast *Schizosaccharomyces pombe*’. *Genetics*, 96 (3), pp. 627–637. doi: 10.1093/genetics/96.3.627.

Nurse, P., Thuriaux, P. and Nasmyth, K. (1976). ‘Genetic control of the cell division cycle in the fission yeast *Schizosaccharomyces pombe*’. *Molecular and General Genetics MGG*, 146 (2), pp. 167–178. doi: 10.1007/BF00268085.

O’Farrell, P. H. (2001). ‘Triggering the all-or-nothing switch into mitosis’. *Trends in Cell Biology*, 11 (12), pp. 512–519. doi: 10.1016/S0962-8924(01)02142-0.

Olson, C. M., Liang, Y., Leggett, A., Park, W. D., Li, L., Mills, C. E., Elsarrag, S. Z., Ficarro, S. B., Zhang, T., Düster, R., Geyer, M., Sim, T., Marto, J. A., Sorger, P. K., Westover, K. D., Lin, C. Y., Kwiatkowski, N. and Gray, N. S. (2019). ‘Development of a Selective CDK7 Covalent Inhibitor Reveals Predominant Cell-Cycle Phenotype’. *Cell Chemical Biology*, 26 (6), pp. 792-803.e10. doi: 10.1016/j.chembiol.2019.02.012.

Pandey, K., Park, N., Park, K.-S., Hur, J., Cho, Y. Bin, Kang, M., An, H.-J., Kim, S., Hwang, S. and Moon, Y. W. (2020). ‘Combined CDK2 and CDK4/6 Inhibition Overcomes Palbociclib Resistance in Breast Cancer by Enhancing Senescence’. *Cancers*, 12 (12), p. 3566. doi: 10.3390/cancers12123566.

Paplomata, E. and O’Regan, R. (2014). ‘The PI3K/AKT/mTOR pathway in breast cancer: targets, trials and biomarkers’. *Therapeutic Advances in Medical Oncology*, 6 (4), pp. 154–166. doi: 10.1177/1758834014530023.

Park, Y., Depeursinge, C. and Popescu, G. (2018). ‘Quantitative phase imaging in biomedicine’. *Nature Photonics*, 12 (10), pp. 578–589. doi: 10.1038/s41566-018-0253-x.

Parua, P. K. and Fisher, R. P. (2020). ‘Dissecting the Pol II transcription cycle and derailing cancer with CDK inhibitors’. *Nature Chemical Biology*, 16 (7), pp. 716–724. doi: 10.1038/s41589-020-0563-4.

Patel, H., Abduljabbar, R., Lai, C.-F., Periyasamy, M., Harrod, A., Gemma, C., Steel, J. H., Patel, N., Busonero, C., Jerjees, D., Remenyi, J., Smith, S., Gomm, J. J., Magnani, L., Győrffy, B., Jones, L. J., Fuller-Pace, F., Shousha, S., Buluwela, L., Rakha, E. A., Ellis, I. O., Coombes, R. C. and Ali, S. (2016). ‘Expression of CDK7, Cyclin H, and MAT1 Is Elevated in Breast Cancer and Is Prognostic in Estrogen Receptor–Positive Breast Cancer’. *Clinical Cancer Research*, 22 (23), pp. 5929–5938. doi: 10.1158/1078-0432.CCR-15-1104.

Patel, H., Periyasamy, M., Sava, G. P., Bondke, A., Slafer, B. W., Kroll, S. H. B., Barbazanges, M., Starkey, R., Ottaviani, S., Harrod, A., Aboagye, E. O., Buluwela, L., Fuchter, M. J., Barrett, A. G. M., Coombes, R. C. and Ali, S. (2018). ‘ICEC0942, an Orally Bioavailable Selective Inhibitor of CDK7 for Cancer Treatment’. *Molecular*

cancer therapeutics. 2018/03/15, 17 (6), pp. 1156–1166. doi: 10.1158/1535-7163.MCT-16-0847.

Pennycook, B. R. and Barr, A. R. (2020). 'Restriction point regulation at the crossroads between quiescence and cell proliferation'. *FEBS Letters*, 594 (13). doi: 10.1002/1873-3468.13867.

Pennycook, B. R. and Barr, A. R. (2021). 'Palbociclib-mediated cell cycle arrest can occur in the absence of the CDK inhibitors p21 and p27'. *Open Biology*, 11 (11). doi: 10.1098/rsob.210125.

Petermann, E., Woodcock, M. and Helleday, T. (2010). 'Chk1 promotes replication fork progression by controlling replication initiation'. *Proceedings of the National Academy of Sciences*, 107 (37), pp. 16090–16095. doi: 10.1073/pnas.1005031107.

te Poele, R. H., Okorokov, A. L., Jardine, L., Cummings, J. and Joel, S. P. (2002). 'DNA Damage Is Able to Induce Senescence in Tumor Cells in Vitro and in Vivo'. *Cancer Research*, 62 (6), pp. 1876–1883.

Potapova, T. A., Daum, J. R., Byrd, K. S. and Gorbsky, G. J. (2009). 'Fine Tuning the Cell Cycle: Activation of the Cdk1 Inhibitory Phosphorylation Pathway during Mitotic Exit'. *Molecular Biology of the Cell*, 20 (6), pp. 1737–1748. doi: 10.1091/mbc.e08-07-0771.

Prasanna, P. G., Citrin, D. E., Hildesheim, J., Ahmed, M. M., Venkatachalam, S., Riscuta, G., Xi, D., Zheng, G., Deursen, J. van, Goronzy, J., Kron, S. J., Anscher, M. S., Sharpless, N. E., Campisi, J., Brown, S. L., Niedernhofer, L. J., O'Loghlen, A., Georgakilas, A. G., Paris, F., Gius, D., Gewirtz, D. A., Schmitt, C. A., Abazeed, M. E., Kirkland, J. L., Richmond, A., Romesser, P. B., Lowe, S. W., Gil, J., Mendonca, M. S., Burma, S., Zhou, D. and Coleman, C. N. (2021). 'Therapy-Induced Senescence: Opportunities to Improve Anticancer Therapy'. *JNCI: Journal of the National Cancer Institute*, 113 (10), pp. 1285–1298. doi: 10.1093/jnci/djab064.

Rader, J., Russell, M. R., Hart, L. S., Nakazawa, M. S., Belcastro, L. T., Martinez, D., Li, Y., Carpenter, E. L., Attiyeh, E. F., Diskin, S. J., Kim, S., Parasuraman, S., Caponigro, G., Schnepp, R. W., Wood, A. C., Pawel, B., Cole, K. A. and Maris, J. M. (2013). 'Dual CDK4/CDK6 Inhibition Induces Cell-Cycle Arrest and Senescence in Neuroblastoma'. *Clinical Cancer Research*, 19 (22), pp. 6173–6182. doi: 10.1158/1078-0432.CCR-13-1675.

Reinhardt, H. C. and Yaffe, M. B. (2009). 'Kinases that control the cell cycle in response to DNA damage: Chk1, Chk2, and MK2'. *Current Opinion in Cell Biology*, 21 (2), pp. 245–255. doi: 10.1016/j.ceb.2009.01.018.

Rinnerthaler, G., Gampenrieder, S. P. and Greil, R. (2018). 'ASCO 2018 highlights: metastatic breast cancer'. *memo - Magazine of European Medical Oncology*, 11 (4), pp. 276–279. doi: 10.1007/s12254-018-0450-9.

Rodier, F., Muñoz, D. P., Teachenor, R., Chu, V., Le, O., Bhaumik, D., Coppé, J.-P., Campeau, E., Beauséjour, C. M., Kim, S.-H., Davalos, A. R. and Campisi, J. (2011). 'DNA-SCARS: distinct nuclear structures that sustain damage-induced senescence

growth arrest and inflammatory cytokine secretion'. *Journal of Cell Science*, 124 (1), pp. 68–81. doi: 10.1242/jcs.071340.

Roger, L., Tomas, F. and Gire, V. (2021). 'Mechanisms and Regulation of Cellular Senescence'. *International Journal of Molecular Sciences*, 22 (23), p. 13173. doi: 10.3390/ijms222313173.

Ruscetti, M., Leibold, J., Bott, M. J., Fennell, M., Kulick, A., Salgado, N. R., Chen, C.-C., Ho, Y., Sanchez-Rivera, F. J., Feucht, J., Baslan, T., Tian, S., Chen, H.-A., Romesser, P. B., Poirier, J. T., Rudin, C. M., de Stanchina, E., Manchado, E., Sherr, C. J. and Lowe, S. W. (2018). 'NK cell–mediated cytotoxicity contributes to tumor control by a cytostatic drug combination'. *Science*, 362 (6421). doi: 10.1126/science.aas9090.

Sakaue-Sawano, A., Kurokawa, H., Morimura, T., Hanyu, A., Hama, H., Osawa, H., Kashiwagi, S., Fukami, K., Miyata, T., Miyoshi, H., Imamura, T., Ogawa, M., Masai, H. and Miyawaki, A. (2008). 'Visualizing Spatiotemporal Dynamics of Multicellular Cell-Cycle Progression'. *Cell*, 132 (3), pp. 487–498. doi: 10.1016/j.cell.2007.12.033.

Sarkisian, C. J., Keister, B. A., Stairs, D. B., Boxer, R. B., Moody, S. E. and Chodosh, L. A. (2007). 'Dose-dependent oncogene-induced senescence in vivo and its evasion during mammary tumorigenesis'. *Nature Cell Biology*, 9 (5), pp. 493–505. doi: 10.1038/ncb1567.

Sava, G. P., Fan, H., Coombes, R. C., Buluwela, L. and Ali, S. (2020). 'CDK7 inhibitors as anticancer drugs'. *Cancer metastasis reviews*. Springer US, 39 (3), pp. 805–823. doi: 10.1007/s10555-020-09885-8.

Saxton, R. A. and Sabatini, D. M. (2017). 'mTOR Signaling in Growth, Metabolism, and Disease'. *Cell*, 168 (6), pp. 960–976. doi: 10.1016/j.cell.2017.02.004.

Schachter, M. M. and Fisher, R. P. (2013). 'The CDK-activating kinase Cdk7'. *Cell Cycle*, 12 (20), pp. 3239–3240. doi: 10.4161/cc.26355.

Schachter, M. M., Merrick, K. A., Larochelle, S., Hirschi, A., Zhang, C., Shokat, K. M., Rubin, S. M. and Fisher, R. P. (2013). 'A Cdk7-Cdk4 T-Loop Phosphorylation Cascade Promotes G1 Progression'. *Molecular Cell*, 50 (2), pp. 250–260. doi: 10.1016/j.molcel.2013.04.003.

Serrano, M., Lin, A. W., McCurrach, M. E., Beach, D. and Lowe, S. W. (1997). 'Oncogenic ras Provokes Premature Cell Senescence Associated with Accumulation of p53 and p16INK4a'. *Cell*, 88 (5), pp. 593–602. doi: 10.1016/S0092-8674(00)81902-9.

Shah, A., Bloomquist, E., Tang, S., Fu, W., Bi, Y., Liu, Q., Yu, J., Zhao, P., Palmby, T. R., Goldberg, K. B., Chang, C. J. G., Patel, P., Alebachew, E., Tilley, A., Pierce, W. F., Ibrahim, A., Blumenthal, G. M., Sridhara, R., Beaver, J. A. and Pazdur, R. (2018). 'FDA Approval: Ribociclib for the Treatment of Postmenopausal Women with Hormone Receptor–Positive, HER2-Negative Advanced or Metastatic Breast Cancer'. *Clinical Cancer Research*, 24 (13), pp. 2999–3004. doi: 10.1158/1078-0432.CCR-17-2369.

Shah, K., Liu, Y., Deirmengian, C. and Shokat, K. M. (1997). 'Engineering unnatural nucleotide specificity for Rous sarcoma virus tyrosine kinase to uniquely label its direct substrates'. *Proceedings of the National Academy of Sciences*, 94 (8), pp. 3565–3570. doi: 10.1073/pnas.94.8.3565.

Shapiro, H. M. (2005). *Practical Flow Cytometry*. John Wiley & Sons.

Shiloh, Y. and Ziv, Y. (2013). 'The ATM protein kinase: regulating the cellular response to genotoxic stress, and more'. *Nature Reviews Molecular Cell Biology*, 14 (4), pp. 197–210. doi: 10.1038/nrm3546.

Simoneschi, D., Rona, G., Zhou, N., Jeong, Y.-T., Jiang, S., Milletti, G., Arbini, A. A., O'Sullivan, A., Wang, A. A., Nithikasem, S., Keegan, S., Siu, Y., Cianfanelli, V., Maiani, E., Nazio, F., Cecconi, F., Boccalatte, F., Fenyö, D., Jones, D. R., Busino, L. and Pagano, M. (2021). 'CRL4^{AMBRA1} is a master regulator of D-type cyclins'. *Nature*, 592 (7856), pp. 789–793. doi: 10.1038/s41586-021-03445-y.

Smith, S. E., Mellor, P., Ward, A. K., Kendall, S., McDonald, M., Vizeacoumar, F. S., Vizeacoumar, F. J., Napper, S. and Anderson, D. H. (2017). 'Molecular characterization of breast cancer cell lines through multiple omic approaches'. *Breast Cancer Research*, 19 (1), p. 65. doi: 10.1186/s13058-017-0855-0.

Supek, F., Bošnjak, M., Škunca, N. and Šmuc, T. (2011). 'REVIGO Summarizes and Visualizes Long Lists of Gene Ontology Terms'. *PLoS ONE*, 6 (7), p. e21800. doi: 10.1371/journal.pone.0021800.

Szklarczyk, D., Kirsch, R., Koutrouli, M., Nastou, K., Mehryary, F., Hachilif, R., Gable, A. L., Fang, T., Doncheva, N. T., Pyysalo, S., Bork, P., Jensen, L. J. and von Mering, C. (2023). 'The STRING database in 2023: protein–protein association networks and functional enrichment analyses for any sequenced genome of interest'. *Nucleic Acids Research*, 51 (D1), pp. D638–D646. doi: 10.1093/nar/gkac1000.

Takasugi, M., Yoshida, Y., Hara, E. and Ohtani, N. (2023). 'The role of cellular senescence and SASP in tumour microenvironment'. *The FEBS Journal*, 290 (5), pp. 1348–1361. doi: 10.1111/febs.16381.

Tassan, J. P., Jaquenoud, M., Fry, A. M., Frutiger, S., Hughes, G. J. and Nigg, E. A. (1995). 'In vitro assembly of a functional human CDK7-cyclin H complex requires MAT1, a novel 36 kDa RING finger protein.' *The EMBO Journal*, 14 (22), pp. 5608–5617. doi: 10.1002/j.1460-2075.1995.tb00248.x.

Terzi, M. Y., Izmirli, M. and Gogebakan, B. (2016). 'The cell fate: senescence or quiescence'. *Molecular Biology Reports*, 43 (11), pp. 1213–1220. doi: 10.1007/s11033-016-4065-0.

The UniProt Consortium. (2023). 'UniProt: the Universal Protein Knowledgebase in 2023'. *Nucleic Acids Research*, 51 (D1), pp. D523–D531. doi: 10.1093/nar/gkac1052.

Tian, T., Li, X. and Zhang, J. (2019). 'mTOR Signaling in Cancer and mTOR Inhibitors in Solid Tumor Targeting Therapy'. *International Journal of Molecular Sciences*, 20 (3), p. 755. doi: 10.3390/ijms20030755.

Timmins, J. (2023). ‘Recognition of DNA Lesions’. *International Journal of Molecular Sciences*, 24 (11), p. 9682. doi: 10.3390/ijms24119682.

Todd, M. C., Langan, T. A. and Sclafani, R. A. (2017). ‘Doxycycline-Regulated p16 MTS1 Expression Suppresses the Anchorage-Independence and Tumorigenicity of Breast Cancer Cell Lines that Lack Endogenous p16’. *Journal of Cancer*, 8 (2), pp. 190–198. doi: 10.7150/jca.15481.

Turner, N. C., Liu, Y., Zhu, Z., Loi, S., Colleoni, M., Loibl, S., DeMichele, A., Harbeck, N., André, F., Bayar, M. A., Michiels, S., Zhang, Z., Giorgetti, C., Arnedos, M., Huang Bartlett, C. and Cristofanilli, M. (2019). ‘Cyclin E1 Expression and Palbociclib Efficacy in Previously Treated Hormone Receptor–Positive Metastatic Breast Cancer’. *Journal of Clinical Oncology*, 37 (14), pp. 1169–1178. doi: 10.1200/JCO.18.00925.

US Food and Drug Administration. (2017). *FDA approves abemaciclib for HR-positive, HER2-negative breast cancer*. *FDA*. Available at: https://www.fda.gov/drugs/resources-information-approved-drugs/fda-approves-abemaciclib-hr-positive-her2-negative-breast-cancer (Accessed: 1 May 2024).

Vesela, E., Chroma, K., Turi, Z. and Mistrik, M. (2017). ‘Common Chemical Inductors of Replication Stress: Focus on Cell-Based Studies’. *Biomolecules*, 7 (4), p. 19. doi: 10.3390/biom7010019.

Vijayaraghavan, S., Karakas, C., Doostan, I., Chen, X., Bui, T., Yi, M., Raghavendra, A. S., Zhao, Y., Bashour, S. I., Ibrahim, N. K., Karuturi, M., Wang, J., Winkler, J. D., Amaravadi, R. K., Hunt, K. K., Tripathy, D. and Keyomarsi, K. (2017). ‘CDK4/6 and autophagy inhibitors synergistically induce senescence in Rb positive cytoplasmic cyclin E negative cancers’. *Nature Communications*, 8 (1), p. 15916. doi: 10.1038/ncomms15916.

Wagner, V. and Gil, J. (2020). ‘Senescence as a therapeutically relevant response to CDK4/6 inhibitors’. *Oncogene*, 39 (29), pp. 5165–5176. doi: 10.1038/s41388-020-1354-9.

Wander, S. A., Cohen, O., Gong, X., Johnson, G. N., Buendia-Buendia, J. E., Lloyd, M. R., Kim, D., Luo, F., Mao, P., Helvie, K., Kowalski, K. J., Nayar, U., Waks, A. G., Parsons, S. H., Martinez, R., Litchfield, L. M., Ye, X. S., Yu, C., Jansen, V. M., Stille, J. R., Smith, P. S., Oakley, G. J., Chu, Q. S., Batist, G., Hughes, M. E., Kremer, J. D., Garraway, L. A., Winer, E. P., Tolaney, S. M., Lin, N. U., Buchanan, S. G. and Wagle, N. (2020). ‘The Genomic Landscape of Intrinsic and Acquired Resistance to Cyclin-Dependent Kinase 4/6 Inhibitors in Patients with Hormone Receptor–Positive Metastatic Breast Cancer’. *Cancer Discovery*, 10 (8), pp. 1174–1193. doi: 10.1158/2159-8290.CD-19-1390.

Wang, A. S., Ong, P. F., Chojnowski, A., Clavel, C. and Dreesen, O. (2017). ‘Loss of lamin B1 is a biomarker to quantify cellular senescence in photoaged skin’. *Scientific Reports*, 7 (1), p. 15678. doi: 10.1038/s41598-017-15901-9.

Wang, B., Varela-Eirin, M., Brandenburg, S. M., Hernandez-Segura, A., van Vliet, T., Jongbloed, E. M., Wilting, S. M., Ohtani, N., Jager, A. and Demaria, M. (2022).

‘Pharmacological CDK4/6 inhibition reveals a p53-dependent senescent state with restricted toxicity’. *The EMBO Journal*, 41 (6). doi: 10.15252/embj.2021108946.

Wang, C., Vegna, S., Jin, H., Benedict, B., Lieftink, C., Ramirez, C., de Oliveira, R. L., Morris, B., Gadiot, J., Wang, W., du Chatinier, A., Wang, L., Gao, D., Evers, B., Jin, G., Xue, Z., Schepers, A., Jochems, F., Sanchez, A. M., Mainardi, S., te Riele, H., Beijersbergen, R. L., Qin, W., Akkari, L. and Bernards, R. (2019). ‘Inducing and exploiting vulnerabilities for the treatment of liver cancer’. *Nature*, 574 (7777), pp. 268–272. doi: 10.1038/s41586-019-1607-3.

Wang, E. (1995). ‘Senescent human fibroblasts resist programmed cell death, and failure to suppress bcl2 is involved.’ *Cancer research*, 55 (11), pp. 2284–92.

Wang, L., Lankhorst, L. and Bernards, R. (2022). ‘Exploiting senescence for the treatment of cancer’. *Nature Reviews Cancer*, 22 (6), pp. 340–355. doi: 10.1038/s41568-022-00450-9.

Wang, Xianzhe, Shi, W., Wang, Xumei, Lu, J.-J., He, P., Zhang, H. and Chen, X. (2023). ‘Nifuroxazide boosts the anticancer efficacy of palbociclib-induced senescence by dual inhibition of STAT3 and CDK2 in triple-negative breast cancer’. *Cell Death Discovery*, 9 (1), p. 355. doi: 10.1038/s41420-023-01658-w.

Wells, C. I., Vasta, J. D., Corona, C. R., Wilkinson, J., Zimprich, C. A., Ingold, M. R., Pickett, J. E., Drewry, D. H., Pugh, K. M., Schwinn, M. K., Hwang, B., Zegzouti, H., Huber, K. V. M., Cong, M., Meisenheimer, P. L., Willson, T. M. and Robers, M. B. (2020). ‘Quantifying CDK inhibitor selectivity in live cells’. *Nature Communications*, 11 (1), p. 2743. doi: 10.1038/s41467-020-16559-0.

Wilson, G. A. (2020). *Exploring the potential of CDK7 inhibition to permanently arrest cancer cells*. UCL.

Wilson, G. A., Vuina, K., Sava, G., Huard, C., Meneguello, L., Coulombe-Huntington, J., Bertomeu, T., Maizels, R. J., Lauring, J., Kriston-Vizi, J., Tyers, M., Ali, S., Bertoli, C. and de Bruin, R. A. M. (2023). ‘Active growth signaling promotes senescence and cancer cell sensitivity to CDK7 inhibition’. *Molecular Cell*, 83 (22), pp. 4078-4092.e6. doi: 10.1016/j.molcel.2023.10.017.

Wohlbold, L., Larochelle, S., Liao, J. C.-F., Livshits, G., Singer, J., Shokat, K. M. and Fisher, R. P. (2006). ‘The Cyclin-Dependent Kinase (CDK) Family Member PNQALRE/CCRK Supports Cell Proliferation but has no Intrinsic CDK-Activating Kinase (CAK) Activity’. *Cell Cycle*, 5 (5), pp. 546–554. doi: 10.4161/cc.5.5.2541.

Xie, S., Swaffer, M. and Skotheim, J. M. (2022). ‘Eukaryotic Cell Size Control and Its Relation to Biosynthesis and Senescence’. *Annual Review of Cell and Developmental Biology*, 38 (1), pp. 291–319. doi: 10.1146/annurev-cellbio-120219-040142.

Xu, X., Pan, X., Wang, T., Wang, J., Yang, B., He, Q. and Ding, L. (2021). ‘Intrinsic and acquired resistance to CDK4/6 inhibitors and potential overcoming strategies’. *Acta Pharmacologica Sinica*, 42 (2), pp. 171–178. doi: 10.1038/s41401-020-0416-4.

Yang, N.-C. and Hu, M.-L. (2005). 'The limitations and validities of senescence associated-β-galactosidase activity as an aging marker for human foreskin fibroblast Hs68 cells'. *Experimental Gerontology*, 40 (10), pp. 813–819. doi: 10.1016/j.exger.2005.07.011.

Yap, T. A., Elhaddad, A. M., Grisham, R. N., Hamm, J. T., Marks, D. K., Shapiro, G., Le Corre, C., Li, J., Lin, T. T., Liu, F., Malky, L., Moreau, A. R., Neumann, H., Juric, D. and Sharma, M. (2023). 'First-in-human phase 1/2a study of a potent and novel CDK2-selective inhibitor PF-07104091 in patients (pts) with advanced solid tumors, enriched for CDK4/6 inhibitor resistant HR+/HER2- breast cancer.' *Journal of Clinical Oncology*, 41 (16_suppl), pp. 3010–3010. doi: 10.1200/JCO.2023.41.16_suppl.3010.

Yoshida, A., Lee, E. K. and Diehl, J. A. (2016). 'Induction of Therapeutic Senescence in Vemurafenib-Resistant Melanoma by Extended Inhibition of CDK4/6'. *Cancer Research*, 76 (10), pp. 2990–3002. doi: 10.1158/0008-5472.CAN-15-2931.

Zatulovskiy, E., Lanz, M. C., Zhang, S., McCarthy, F., Elias, J. E. and Skotheim, J. M. (2022). 'Delineation of proteome changes driven by cell size and growth rate'. *Frontiers in Cell and Developmental Biology*, 10. doi: 10.3389/fcell.2022.980721.

Zatulovskiy, E., Zhang, S., Berenson, D. F., Topacio, B. R. and Skotheim, J. M. (2020). 'Cell growth dilutes the cell cycle inhibitor Rb to trigger cell division'. *Science*, 369 (6502). doi: 10.1126/science.aaz6213.

Zeman, M. K. and Cimprich, K. A. (2014). 'Causes and consequences of replication stress'. *Nature Cell Biology*, 16 (1), pp. 2–9. doi: 10.1038/ncb2897.

Zeng, J., Hills, S. A., Ozono, E. and Diffley, J. F. X. (2023). 'Cyclin E-induced replicative stress drives p53-dependent whole-genome duplication'. *Cell*, 186 (3), pp. 528-542.e14. doi: 10.1016/j.cell.2022.12.036.

Zerjatke, T., Gak, I. A., Kirova, D., Fuhrmann, M., Daniel, K., Gonciarz, M., Müller, D., Glauche, I. and Mansfeld, J. (2017). 'Quantitative Cell Cycle Analysis Based on an Endogenous All-in-One Reporter for Cell Tracking and Classification'. *Cell Reports*, 19 (9), pp. 1953–1966. doi: 10.1016/j.celrep.2017.05.022.

Zhang, L., Pitcher, L. E., Yousefzadeh, M. J., Niedernhofer, L. J., Robbins, P. D. and Zhu, Y. (2022). 'Cellular senescence: a key therapeutic target in aging and diseases'. *Journal of Clinical Investigation*, 132 (15). doi: 10.1172/JCI158450.

Zhang, M., Zhang, L., Hei, R., Li, X., Cai, H., Wu, X., Zheng, Q. and Cai, C. (2021). 'CDK inhibitors in cancer therapy, an overview of recent development.' *American journal of cancer research*, 11 (5), pp. 1913–1935.

Zhang, Y. and Hunter, T. (2014). 'Roles of Chk1 in cell biology and cancer therapy'. *International Journal of Cancer*, 134 (5), pp. 1013–1023. doi: 10.1002/ijc.28226.

Zhu, Y., Tchkonia, T., Fuhrmann-Stroissnigg, H., Dai, H. M., Ling, Y. Y., Stout, M. B., Pirtskhalava, T., Giorgadze, N., Johnson, K. O., Giles, C. B., Wren, J. D., Niedernhofer, L. J., Robbins, P. D. and Kirkland, J. L. (2016). 'Identification of a

novel senolytic agent, navitoclax, targeting the Bcl-2 family of anti-apoptotic factors'. *Aging Cell*, 15 (3), pp. 428–435. doi: 10.1111/acel.12445.